



Universität Hamburg
DER FORSCHUNG | DER LEHRE | DER BILDUNG

DISSERTATION

Prothrombotic Variants of von Willebrand Factor (VWF)

with the aim of obtaining a doctoral degree (Dr. rer. nat.)

at the Department of Chemistry

Faculty of Mathematics, Informatics and Natural Sciences

University of Hamburg

submitted by

Angelika Anja Mojzisch

Hamburg, 2024

Reviewers of the dissertation:

Prof. Dr. rer. nat. Dr. Sc. Christian Betzel

University of Hamburg
Department of Chemistry
Institute of Biochemistry and Molecular Biology
Research Group Betzel
Martin-Luther-King-Platz 6
20146 Hamburg

Prof. Dr. rer. nat. Maria A. Brehm

University of Siegen
Department of Digital Biomedical and Health Sciences
Artur-Woll-Haus (AE-Campus)
Am Eichenhang 50
57076 Siegen

Date of disputation: 15.11.2024

Date of print approval: 04.12.2024

The dissertation was executed at the:

University Medical Center Hamburg-Eppendorf | UKE

Center for Internal Medicine

Department of Dermatology and Venereology

Martinistraße 52

20246 Hamburg, Germany

from 01.10.2020 to 28.07.2024

INSERM Unit 1176 Hemostasis Inflammation Thrombosis

Centre Hospitalier Universitaire de Bicêtre

80 rue du Général Leclerc

Bâtiment Grégory Pincus

94276 Le Kremlin Bicêtre, France

from 13.03.2023 to 05.05.2023

LIST OF PUBLICATIONS

Mojzisch A, Brehm MA. 2021. The Manifold Cellular Functions of von Willebrand Factor. *Cells*. 10(9):2351.

Chen PC, Kutzki F, Mojzisch A, Simon B, Xu ER, Aponte-Santamaría C, Horny K, Jeffries C, Schneppenheim R, Wilmanns M, Brehm MA, Gräter F, Hennig J. 2022. Structure and dynamics of the von Willebrand Factor C6 domain. *J. Struct. Biol.* 214(4), 107923.

LIST OF ORAL AND POSTER PRESENTATIONS AT NATIONAL AND INTERNATIONAL CONGRESSES

1. Structure of the von Willebrand Factor C6 domain and effect of variant p.Gly2705Arg

Po-chia Chen, Fabian Kutzki, Emma-Ruoqi Xu, Angelika Mojzisch, Kai Horny, Bernd Simon, Reinhard Schneppenheim, Maria A. Brehm, Matthias Wilmanns, Frauke Graeter and Janosch Hennig. **2021**, International Society for Thrombosis and Hemostasis (ISTH), Philadelphia, USA. (oral presentation) **2022**, Gesellschaft für Thrombose- und Hämostaseforschung (GTH), Leipzig, Germany. (poster presentation)

2. Analysis of single nucleotide polymorphisms in the C4 domain of VWF reveals the novel gain-of-function variant p.Ser2564Arg

Angelika Mojzisch, Stefan W. Schneider, Maria A. Brehm. **2023**, Gesellschaft für Thrombose- und Hämostaseforschung (GTH), Frankfurt, Germany. (poster presentation)

3. Identification of a novel gain-of-function variant p.Ser2564Arg by analysis of single nucleotide polymorphisms in the C4 domain of von Willebrand Factor

Angelika Mojzisch, Sonja Schneppenheim, Stefan W. Schneider, Maria A. Brehm. **2023**, Hamburger Hämophilie Symposion (HHS), Hamburg, Germany. (poster presentation)

4. Relevance of the VWF C4 domain for gain-of-function variants

Angelika Mojzisch, Nico Remmert, Sonja Schneppenheim, Stefan W. Schneider, Maria A. Brehm. **2024**, Gesellschaft für Thrombose- und Hämostaseforschung (GTH), Vienna, Austria. (poster presentation)

TABLE OF CONTENTS

1. Zusammenfassung.....	1
2. Abstract	3
3. Introduction	5
3.1. Vessel anatomy and function.....	5
3.2. Hemostasis	6
3.2.1. Vasoconstriction.....	7
3.2.2. Primary hemostasis	8
3.2.3. Secondary hemostasis.....	9
3.2.4. Clot resorption	10
3.3. Thrombosis.....	11
3.3.1. Virchow's Triad.....	11
3.3.2. Venous and arterial thrombi	12
3.4. Von Willebrand Factor	13
3.4.1. Biosynthesis and structure of VWF	13
3.4.2. Function and activity of VWF	16
3.4.2.1. Shear sensitivity of VWF.....	16
3.4.2.1. Size of VWF determines its activity.....	17
3.4.2.2. Adhesion and activation of platelets.....	17
3.4.2.3. Evaluation of VWF function in laboratory testing.....	19
3.4.3. Pathogenicity of VWF	20
3.4.3.1. Von Willebrand Disease	20
3.4.3.2. Role of VWF in thrombosis.....	22
3.4.3.3. Gain-of-function variants of VWF with mutations in the C4 domain	23
4. Aim of this thesis.....	27
5. Material and Methods.....	29
5.1. Material	29
5.1.1. Animals.....	29
5.1.2. Patient samples	29
5.1.3. Bacteria	29
5.1.4. Cell lines	29
5.1.5. Instruments	30
5.1.6. Consumables	31
5.1.7. Chemicals	32
5.1.8. Buffers and Media	34

5.1.9. Peptides.....	35
5.1.10. Oligonucleotides.....	36
5.1.11. Plasmids.....	39
5.1.12. Kit systems and enzymes.....	40
5.1.13. Antibodies	41
5.1.14. Software	41
5.2. Methods.....	42
5.2.1. Cell biological methods	42
5.2.1.1. Culturing cell lines	42
5.2.1.2. Plasmid transfection with Lipofectamine LTX.....	42
5.2.1.3. VWF secretion experiments	43
5.2.2. Protein biochemical methods	43
5.2.2.1. Expression of recombinant VWF	43
5.2.2.2. Concentration of VWF protein	43
5.2.2.3. Dialysis of VWF samples.....	44
5.2.2.4. Determination of VWF concentration.....	44
5.2.2.5. Functional assays.....	45
5.2.2.5.1. Collagen binding ELISA	45
5.2.2.5.2. GPIIb binding ELISA	45
5.2.2.5.3. GPIIb/IIIa binding ELISA	46
5.2.2.5.4. Multimer analysis	47
5.2.2.5.5. Static ADAMTS13 cleavage.....	47
5.2.2.6. Immunofluorescence	48
5.2.3. Molecular biological methods.....	48
5.2.3.1. Quantity and Quality measurement of nucleic acids.....	48
5.2.3.2. Mutagenesis of VWF coding sequence	48
5.2.3.2.1. PCR with Phusion Site-directed mutagenesis	49
5.2.3.2.2. PCR with the QuikChange Multi site-directed mutagenesis	49
5.2.3.2.3. DpnI digestion	50
5.2.3.2.4. Agarose gel electrophoresis	50
5.2.3.2.5. Sequencing of pIRES neo2 VWF plasmids	50
5.2.3.3. Sequencing of Exon 45 from patient DNA samples	51
5.2.3.3.1. DNA isolation.....	51
5.2.3.3.2. Polymerase Chain reaction.....	51
5.2.3.3.3. PCR purification.....	52
5.2.3.3.4. Sequencing of Exon 45	52

5.2.4. Microbiological methods.....	52
5.2.4.1. Transformation of MACH1T1 competent <i>E. coli</i>	52
5.2.4.2. Plasmid isolation	52
5.2.5. Processing of blood samples.....	53
5.2.5.1. Platelet Isolation from Buffy coat	53
5.2.5.2. Platelet Isolation from whole blood donations.....	53
5.2.5.3. Isolation of erythrocytes from full blood donations	54
5.2.6. Light transmission aggregometry (LTA)	54
5.2.7. Microfluidic methods	54
5.2.8. <i>In vivo</i> animal experiments	55
5.2.8.1. Hydrodynamic injection	55
5.2.8.2. Detection of VWF:Ag in mouse blood samples.....	55
5.2.8.3. Tail-clip assay.....	56
5.2.8.4. Thrombosis model.....	56
5.2.9. Statistics	56
6. Results	57
6.1. Identification of novel VWF GOF variants.....	57
6.1.1. Selection of VWF variants in the C4 domain.....	57
6.1.2. Selection of VWF variants in C domains other than C4	59
6.1.3. Identification of VWF variants in a patient cohort.....	60
6.1.4. Characterization of VWF variants.....	61
6.1.4.1. Secretion of VWF variants from HEK293F cells.....	62
6.1.4.1.1. Intracellular localization of poorly secreted variants.....	66
6.1.4.2. Multimer analysis of VWF variants	67
6.1.4.3. Degradation of VWF variants by ADAMTS13	69
6.1.4.4. Binding capacities of VWF variants under static conditions	72
6.1.4.4.1. Collagen binding of VWF variants	72
6.1.4.4.2. GPIIb α binding of VWF variants	74
6.1.4.4.3. GPIIb/IIIa binding of VWF variants	77
6.1.4.5. Shear-dependent platelet binding of VWF variants.....	78
6.1.4.5.1. Ristocetin-dependent platelet agglutination of VWF variants	79
6.1.4.6. Formation of VWF-platelet collective networks by VWF variants	84
6.1.4.7. Role of GPIIb/IIIa in the activity of gain-of-function variants	92
6.1.5. Structure prediction of VWF GOF variants using Alphafold2-Multimers.....	100
6.2. Disease association of VWF GOF variants.....	104
6.2.1. Correlation of variant p.Phe2561Tyr prevalence and the occurrence of MI ..	104

6.2.1.1. Control group	106
6.2.1.2. CAD group	108
6.2.1.2.1. Classification of CAD.....	110
6.2.2. <i>In vivo</i> mouse studies of VWF variants	111
6.2.2.1. Expression of mVWF variants.....	111
6.2.2.2. Evaluation of hemostasis of mVWF variants.....	112
6.2.2.3. Evaluation of thrombotic potential of mVWF variants	115
6.3. Measures to counteract a VWF GOF effect	118
6.3.1. Dynamics of C4 domain.....	119
6.3.2. Evaluation of inhibitory peptides on the activity of the C4 domain	120
6.3.3. Characterization of variant p.Trp2521Gly.....	122
7. Discussion	127
7.1. Characterization of novel VWF variants.....	127
7.1.1. Set-up for quantification of VWF GOF variants under shear conditions	129
7.1.2. Loss-of-function variants.....	130
7.1.2.1. Variants p.Cys2557Tyr and p.Cys2574Arg in the C4 domain	130
7.1.2.2. Variant p.Cys2671Tyr in the C6 domain.....	131
7.1.2.3. Variants p.Arg2535Gln and p.Trp2521Gly in the C4 domain	132
7.1.2.3.1. Suggested motion of the C4 domain and the role of Trp2521	133
7.1.2.4. Variants in the C1 and C2 domains	134
7.1.3. Gain-of-functions variants.....	134
7.1.3.1. Variant p.Gly2705Arg in the C6 domain.....	134
7.1.3.2. Variants in the C4 domain.....	135
7.1.3.3. Inhibition of VWF GOF variants.....	137
7.2. Disease association	139
7.2.1. Association of VWF GOF variants with myocardial infarction in patients	139
7.2.2. Effect of VWF GOF variants on thrombosis and hemostasis in mice.....	140
7.3. Suggested mode of action for VWF GOF variants.....	141
7.4. Summary	145
7.5. Outlook.....	147
8. References.....	149
9. Supplement	173
9.1. Safety and disposal.....	173
9.2. Hazardous materials.....	173
Danksagung	177
Eidesstattliche Erklärung.....	179

ABBREVIATIONS

aa	amino acid
ACS	acute coronary syndrome
ADAMTS13	a disintegrin and metalloproteinase with a thrombospondin type 1 motif, member 13
APC	activated protein C
AS	aggregate size
AVWS	acquired von Willebrand syndrome
bp	base pair
BSA	bovine serum albumin
CAD	coronary artery disease
CD	circular dichroism
CDS	coding sequence
cGMP	cyclic guanosine monophosphate
CK	cystine knot
CPA	cone and plate aggregometry
CVD	cardiovascular disease
DDAVP	desmopressin
ddH ₂ O	double-distilled dH ₂ O
DMEM	Dulbecco's Modified Eagle's Medium
DMSO	dimethyl sulfoxide
DNA	deoxyribonucleic acid
dNTP	deoxy nucleoside triphosphate
EC	endothelial cells
ECM	extracellular matrix
EDTA	ethylenediaminetetraacetic acid
ELISA	enzyme-linked immunosorbent assay
ER	endoplasmic reticulum
ERK	extracellular signal-regulated
et al.	and others (et alii/et aliae)
FBS	fetal bovine serum

FCS	fluorescence correlation spectroscopy
Fwd-Primer	forward-primer
G418	geneticin
GOF	gain-of-function
GP	glycoprotein
GTH	Gesellschaft für Thrombose- und Hämostaseforschung
HD	healthy donor
HEK293	human embryonic kidney cells 293
HITS	Heidelberg Institute for Theoretical Studies gGmbH
HMWM	high molecular weight multimers
HRP	horseradish peroxidase
hVWF	human von Willebrand Factor
IF	immunofluorescence
IMWM	intermediate molecular weight multimers
ISTH	International Society for Thrombosis and Hemostasis
kb	kilo base pairs
kDa	kilo Dalton
KO	knock-out
LB	Lysogeny broth
LD-RIPA	low-dose ristocetin-induced platelet aggregation
LMWM	low molecular weight multimers
LOF	loss-of-function
LRRD	leucine-rich repeat domain
LTA	light transmission aggregometry
MAP	mitogen-activated protein
MD	molecular dynamics
MEM	modified Eagle Medium
MI	myocardial infarction
mPNP	murine pooled normal plasma
MSD	mechanosensitive domain
MST	microscale thermophoresis

mutGPIb α	mutant GPIb α -Gly233Val/Met239Val
mVWF	murine von Willebrand Factor
MW	molecular weight
NMR	nuclear magnetic resonance
OD	optical densities
OR	odds ratio
PBS	phosphate-buffered saline
PCR	polymerase chain reaction
PDB	protein data bank
PDGF	platelet-derived growth factor
PDI	protein disulfide isomerase
PFA	paraformaldehyde
PI3K	phosphoinositide 3-kinase
PMA	phorbol 12-myristate 13-acetate
PRP	platelet-rich plasma
PT-VWD	platelet-type von Willebrand disease
Rev-Primer	reverse-primer
RIPA	ristocetin induced platelet aggregation
RT	room temperature
SEM	standard error of the mean
SD	subdomain
SNP	single nucleotide polymorphisms
SOCE	store-operated Ca ²⁺ entry
SP	signal peptide
TAE	tris acetate EDTA
TF	tissue factor
TGN	<i>trans</i> -Golgi network
TMB	3,3',5'5'-tetramethylbenzidine
Tris	tris(hydroxymethyl)-aminomethan
TTP	thrombocytopenic purpura
UKE	University Medical Center Hamburg-Eppendorf

ULMWM	ultra-large molecular weight multimers
UMIF	UKE Microscopy Imaging Facility
VSMC	vascular smooth muscle cell
VTE	venous thromboembolism
VWD	von Willebrand disease
VWF	von Willebrand factor
VWF:Ac	von Willebrand factor activity
VWF:Ag	von Willebrand factor antigen
VWF:CB	von Willebrand factor collagen binding
VWF:FVIII	von Willebrand factor factor VIII binding
WPB	Weibel-Palade body
wt	wildtype

1. ZUSAMMENFASSUNG

Der von Willebrand Faktor (VWF) zirkuliert als multimeres Multidomänen-Glykoprotein im Blutkreislauf und initiiert die Hämostase bei Gefäßverletzungen. Durch eine schervermittelte mechanische Aktivierung ermöglicht die strukturell exponierte Bindungsstelle für den Thrombozytenrezeptor GPIb α in der A1-Domäne des VWF die reversible Thrombozytenadhäsion. Diese weist ein scherabhängiges, biphasisches „catch-slip“-Bindungsverhalten auf, welches bei erhöhten Scherkräften zur Signaltransduktion und intrazellulären Kalziummobilisierung führt. Die darauffolgende intermediäre Aktivierung des zuvor inaktiven GPIIb/IIIa-Rezeptors ermöglicht die Interaktion mit Agonisten, wie der VWF C4-Domäne und Fibrin und damit eine Quervernetzung der Thrombozyten. Die vollständige Aktivierung des GPIIb/IIIa-Rezeptors hingegen, und damit die stabile, irreversible Aggregation, erfolgt erst anschließend mit der Aktivierung der Thrombozyten durch eine länger anhaltende, erhöhte Scherexposition über den extrazellulären Kalziumeinstrom.

Kürzlich wurden zwei Einzelnukleotid-Polymorphismen (SNPs) p.Phe2561Tyr und p.Pro2555Arg in der C4-Domäne des VWF *in vitro* als „gain-of-function“ (GOF)-Varianten identifiziert. Während die Variante p.Phe2561Tyr eine höhere Sensitivität gegenüber Scherkräften zeigt, bildet die Variante p.Pro2555Arg größere Thrombozytenaggregate. Die Prävalenz der Variante p.Phe2561Tyr war mit einem signifikant erhöhten Risiko für das Auftreten eines Myokardinfarkts bei jungen Frauen assoziiert worden.

In dieser Studie wurde in einem weiteren Kollektiv bei einem Patienten mit Myokardinfarkt ein SNP identifiziert, welcher, gemeinsam mit 8 weiteren SNPs in der C4- und C6-Domäne des VWF, im Zuge einer *in vitro* Charakterisierung der rekombinanten Proteine mittels Lichttransmissionsaggregometrie und mikrofluidischer Experimente, als GOF-Variante klassifiziert werden konnte. Im Rahmen dieser Untersuchung wurden zusätzlich 9 „loss-of-function“ (LOF)-Varianten in der C2- und der C4-Domäne identifiziert, die bei rekombinanter Expression in HEK293F-Zellen entweder einen Sekretions- oder Multimerisierungsdefekt aufwiesen, oder eine reduzierte Aktivität in den scherabhängigen Assays darlegten. Die identifizierten GOF-Varianten ähnelten phänotypisch den Varianten p.Pro2555Arg oder p.Phe2561Tyr. Während die

Aggregatgröße in mikrofluidischen Experimenten eine starke Abhängigkeit von der GPIIb/IIIa-VWF-Interaktion zeigte, war die erhöhte Schersensitivität GPIIb/IIIa-unabhängig. *In vivo* Studien an Mäusen untermauerten eine prothrombotische Wirkung der Variante p.Pro2555Arg und wiesen auf die Bildung instabiler Aggregate durch die Variante p.Phe2561Tyr, und damit auf ein mögliches erhöhtes Risiko für Thromboembolien, hin.

Unter Einbezug aller in der vorliegenden Studie erhobenen Daten und in Übereinstimmung mit bereits publizierten Ergebnissen, lässt sich nun ein neuer Mechanismus postulieren, der der GOF schersensitiver Varianten zugrunde liegen könnte: Variante p.Phe2561Tyr und ähnliche Varianten scheinen die Stabilität der dimeren Stammregion zu beeinträchtigen, wodurch gestrecktere Multimere ausgebildet werden. Dadurch wird die für die Thrombozytenadhäsion über GPIIb α notwendige Scherkraft reduziert, was die Ausbildung der GPIIb α -VWF-A1 „catch-bond“ beschleunigt, sodass bereits bei niedrigeren Scherraten eine intermediäre Aktivierung von GPIIb/IIIa erreicht wird. Durch die nun voraktivierten GPIIb/IIIa-Rezeptoren bilden sich auch die über GPIIb/IIIa-VWF quervernetzten Thrombozytenaggregate bei geringeren Scherraten aus. Da jedoch die für eine vollständige Aktivierung notwendige Zugkraft bei niedrigen Scherkräften nicht vorliegt, ist die Thrombozytenaktivierung unvollständig und die ausgebildeten Aggregate instabil, was deren Fortreißen ermöglicht und damit das Risiko für Thromboembolien erhöhen und das erhöhte Myokardinfarktrisiko erklären könnte. Varianten wie p.Pro2555Arg hingegen scheinen durch eine erhöhte GPIIb/IIIa-vermittelte Quervernetzung der Aggregate eine Gefäßokklusion zu begünstigen. Die vorliegende Studie hat damit maßgeblich dazu beigetragen, neue, klinisch relevante Erkenntnisse über den GOF-Mechanismus zu generieren, der dem prothrombotischen Effekt der VWF-GOF-Varianten zugrunde liegen könnte.

2. ABSTRACT

The von Willebrand factor (VWF) circulates as a multimeric, multidomain glycoprotein in the bloodstream and initiates hemostasis at sites of vascular injuries. Through shear-mediated mechanical activation, the structurally exposed binding site for the platelet receptor GPIIb/IIIa in the A1 domain of VWF enables reversible platelet adhesion. This interaction exhibits a shear-dependent, biphasic 'catch-slip' binding behavior, which leads to signal transduction and intracellular calcium mobilization at increased shear forces. The subsequent intermediate activation of the previously inactive GPIIb/IIIa receptor enables binding to agonists, such as the VWF C4 domain and fibrin, and cross-linking of platelets. However, full activation of GPIIb/IIIa, and thus stable irreversible aggregation, only occurs after platelet activation via extracellular calcium influx in presence of prolonged increased shear rates.

Recently, two single nucleotide polymorphisms (SNPs) p.Phe2561Tyr and p.Pro2555Arg in the C4 domain of VWF were identified *in vitro* as gain-of-function (GOF) variants. While variant p.Phe2561Tyr shows a higher sensitivity to shear forces, the variant p.Pro2555Arg forms larger platelet aggregates. The prevalence of variant p.Phe2561Tyr was associated with a significantly increased risk of myocardial infarction in young women.

In this study, a SNP was identified in another cohort, in a patient with myocardial infarction. Together with 8 other SNPs in the C4 and C6 domain of VWF this SNP was classified as a GOF variant in the course of an *in vitro* characterization of the recombinant protein using light transmission aggregometry and microfluidic experiments. Additionally, 9 loss-of-function (LOF) variants in C2 and C4 domain were identified which, when recombinantly expressed in HEK293F cells, either showed a secretion or multimerization defect, or exhibited reduced activity in shear-dependent assays. The identified GOF variants were phenotypically similar to variants p.Pro2555Arg or p.Phe2561Tyr. While aggregate size in microfluidic experiments showed a strong dependence on the GPIIb/IIIa interaction, the increased shear sensitivity was demonstrated to be GPIIb/IIIa-independent. *In vivo* studies in mice underlined a prothrombotic effect of variant p.Pro2555Arg and revealed a tendency to unstable

thrombi formation and thus a possible increased risk of thromboembolism for variant p.Phe2561Tyr.

Taking into account all the data collected in the present study and in agreement with previously published results, a new mechanism can be postulated that could be responsible for the GOF of shear-sensitive variants: Variant p.Phe2561Tyr and similar variants appear to impair the stability of the dimeric stem region, resulting in the formation of more elongated multimers. This reduces the shear force required for platelet adhesion via GPIb α , which accelerates the formation of the GPIb α -VWF-A1 'catch-bond', allowing intermediate activation of GPIIb/IIIa to be achieved at lower shear rates. Due to the pre-activated GPIIb/IIIa receptor, the platelet aggregates are cross-linked via GPIIb/IIIa-VWF-C4 interactions at lower shear rates. However, since the required tensile force for complete activation is not present, platelet activation might be incomplete and the formed aggregates may be unstable, allowing it to be torn away. This could therefore increase the risk of thromboembolism, which is in agreement with the increased risk of myocardial infarction described for p.Phe2561Tyr. On the other hand, variants such as p.Pro2555Arg appear to promote vascular occlusion due to increased GPIIb/IIIa-mediated cross-linking of platelets. The present study has thus contributed significantly to generating new, clinically relevant insights into the GOF mechanism that could account for the prothrombotic effect of VWF GOF variants.

3. INTRODUCTION

3.1. Vessel anatomy and function

The vasculature is a closed blood distribution system that supplies the body with nutrients and oxygen. It consists of a branched vessel network that can be divided into three main parts: arteries, veins and capillaries. While arteries and smaller branches, called arterioles, transport the oxygenated blood away from the heart, veins and smaller venules transport the deoxygenated blood back to the heart. Capillaries are the connecting vessels between arteries and veins. Due to their small size and thin walls, nutrients and oxygen can be exchanged between blood and tissue. (Tucker et al., 2023).

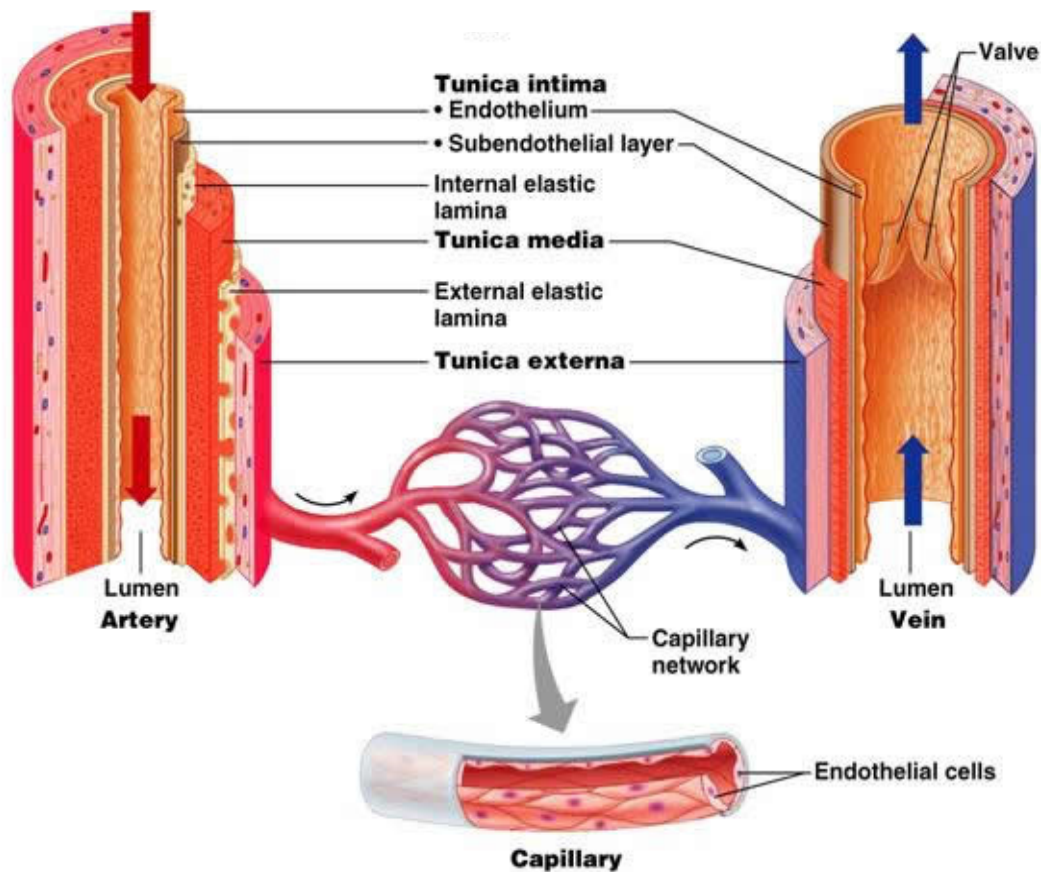


Figure 1: Anatomy of arteries, veins and capillaries. Arteries are shown in red, veins in blue and capillaries in transparent. Arteries and veins consists of three main layers: the tunica intima, tunica media and tunica externa, whereas capillaries are composed only of an inner endothelial cell layer (from Elaine Nicpon Marieb, 2004).

Arteries and veins have a similar anatomy (**Figure 1**). The central space containing the blood is called lumen. It is surrounded by three main layers: the tunica intima, tunica media and tunica externa (Tucker et al., 2023). The first barrier that encloses the lumen is the endothelium composed of a monolayer of endothelial cells (ECs). A subendothelial extracellular matrix (ECM) is localized right underneath the ECs. The ECM is a network of macromolecules that offers stability and elasticity for cells and tissue. It is mainly composed of (glyco)proteins such as collagens, elastin, laminins and tenascins, as well as proteoglycans and glycosaminoglycans (Karamanos et al., 2021). The tunica media is the thickest layer and contains vascular smooth muscle cells (VSMCs). VSMCs tightly regulate the blood flow and pressure by tuning the lumen diameter due to their ability to contract and to relax through processes of vasoconstriction and vasodilation, respectively. The tunica externa is the outermost layer which provides protection and reinforcement for the vessel. It anchors the vessel to surrounding tissues.

Comparing arteries to veins, arteries have a thicker tunica media and additional elastic laminas. This results in a smaller vessel lumen but a higher blood pressure. Arteries are estimated to contain only 10 % to 15 % of the total human blood volume (Tucker et al., 2023). In contrast, veins have a larger lumen and a slower blood flow. Furthermore, veins are equipped with valves, which are protrusions that prevent the backflow of blood in locations where blood has to return to the heart against the force of gravity, such as in the lower limbs.

3.2. Hemostasis

Hemostasis is the physiological process that takes place when a blood vessel is damaged. It is the first stage of wound healing that aims to stop bleeding and prevent further blood loss. This complex mechanism is highly conserved and can be divided into three main steps: vasoconstriction, primary hemostasis, and secondary hemostasis (Rodrigues et al., 2018). Vasoconstriction reduces the blood loss by contraction of VSMCs of the tunica media. The primary hemostasis leads to the adhesion, activation and aggregation of platelets which form a platelet plug, whereas secondary hemostasis involves the coagulation cascade and results in the formation of a stable platelet clot. In order to limit the clotting reaction and to prevent excessive clot formation and occlusion of a blood vessel, antithrombotic countermeasures can take place (**Figure 2**).

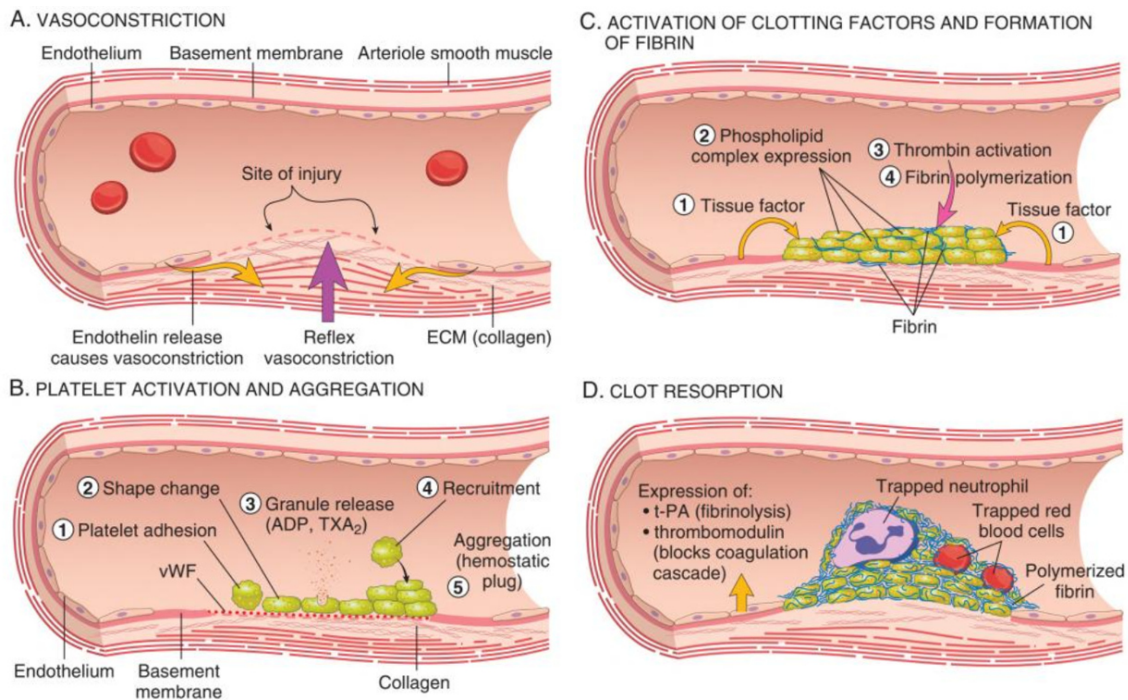


Figure 2: Steps of hemostasis. (A) Vasoconstriction describes the contraction of VSMCs. (B) Platelet activation and aggregation during primary hemostasis is initiated by VWF adhesion to exposed collagen, which then mediates platelet recruitment to the site of injury, followed by platelet shape change, granule release and platelet aggregation. (C) Activation of clotting factors and formation of fibrin, as part of secondary hemostasis, includes the release of tissue factor, phospholipid complex expression, thrombin activation and fibrin polymerization. (D) Clot resorption, as a process of wound healing, is triggered by fibrinolysis and blocking of the coagulation cascade by thrombomodulin (from Kumar et al., 2017).

3.2.1. Vasoconstriction

Damage of the vascular endothelium triggers the release of various molecules from injured cells and surrounding tissue. The first goal is to initiate the contraction of VSMCs, called vasoconstriction. This will reduce the vessel diameter and limit the blood loss. The contraction is initiated by local myogenic spasm, nervous reflexes and molecules secreted from the traumatized tissues, so called vasoconstrictors (Rodrigues et al., 2018). These include endothelin, which is secreted by ECs upon rupture of the endothelial monolayer (Davenport et al., 2016), and adrenergic agonist such as epinephrine and norepinephrine (Rickles et al. 1976; Vischer and Wollheim 1997), which are released after activation of the sympathetic nervous system by pain stimuli. Additionally, hormones such as angiotensin II (Nguyen Dinh Cat and Touyz, 2011) or vasopressin (Mannucci et al., 1977) can also act as vasoconstrictors. During primary

hemostasis, activated platelets maintain the vasoconstriction by the release of thromboxane A₂, serotonin and platelet-derived growth factor (PDGF) (Berk et al., 1986; Teller and White, 2009).

3.2.2. Primary hemostasis

Primary hemostasis describes the platelet plug formation at the site of a vascular injury. When the endothelium is disrupted, the subendothelial extracellular matrix (ECM) is exposed to the bloodstream. Revealed collagen molecules play a crucial role in the formation of a platelet plug by serving as an anchor point. Despite the fact that platelets possess two collagen receptors, the glycoprotein (GP) Ia/IIa (integrin $\alpha_2\beta_1$) and GPVI, they are unable to bind collagen under high shear conditions, which are prevalent at sites of damaged vessels (Nuyttens et al., 2011). To overcome this limitation, they require a connector for immobilization, provided by von Willebrand Factor (VWF), a large glycoprotein that circulates in the bloodstream and recognizes collagen molecules of the ECM even at high shear rates (Fuchs et al., 2010). VWF that is anchored to collagen experiences a higher shear force that stretches its structure and gives access to its platelet binding site in its A1 domain (Fu et al., 2017). Platelets adhere to the activated A1 domain of VWF with their GPIIb α receptor (Ju et al., 2015a), which mediates an outside-in signaling (Zhang et al., 2015), and in subsequent steps an inside-out-signaling that activates platelet receptor GPIIb/IIIa (integrin $\alpha_{IIb}\beta_3$). In resting circulating platelets GPIIb/IIIa has a low-affinity, inactive state (Estevez and Du, 2017), but once activated, integrin-binding proteins, including fibrin (generated during secondary hemostasis) and VWF (Hantgan et al., 1990; Rosado et al., 2001), can bind via their RGD motifs. Full platelet activation is achieved after GPIIb/IIIa interactions at high shear forces (Chen et al., 2019) that induce strong intracellular calcium increase (Varga-Szabo et al., 2009). Activated platelets undergo cytoskeleton reorganization and degranulation, resulting in the release of mediators of vascular tone and platelet activators, such as thromboxane A₂, ADP, serotonin and VWF (Palta et al., 2014). As this process continues, more platelets and more VWF molecules are recruited and activated.

3.2.3. Secondary hemostasis

Secondary hemostasis directly follows primary hemostasis but they also temporally overlap. It results in a stable platelet-fibrin clot that seals the site of injury. To achieve this, fibrin needs to be converted from its inactive form fibrinogen through cleavage by the coagulation factor thrombin, which itself requires activation throughout the course of the coagulation cascade involving a series of coagulation factors (Palta et al., 2014) (**Figure 3**). Coagulation factors are proenzymes which need to be proteolytically activated from their zymogen form in order to continue the downstream signal transmission. The coagulation factor thrombin is the upstream activator of fibrinogen, but it needs to be released from its zymogen prothrombin. Two pathways trigger the generation of thrombin from prothrombin: the intrinsic pathway, which only requires components present in the blood and the extrinsic pathway, which is triggered by the release of tissue factor (TF) from extravascular tissue, including smooth muscle cells and fibroblasts (Mackman et al., 2007).

The intrinsic pathway can be triggered, for example, by a damaged surface which exposes collagen type I (van der Meijden et al., 2009) or activated platelets (Monroe and Hoffman, 2006). It involves the stepwise activation of the plasma-located coagulation factors XII, XI, and IX. Activated factor IX together with activated factor VIII form the intrinsic tenase complex. In contrast, the extrinsic pathway starts with the release of TF from disclosed extravascular tissue. TF activates and binds factor VII to form the extrinsic tenase complex. The extrinsic and intrinsic tenase complex can trigger the common pathway, which activates factor X that forms the prothrombinase complex together with factor V and converts prothrombin to thrombin (Palta et al., 2014). Thrombin additionally amplifies the clotting reaction by activating coagulation factors XI, VIII and V (Licari and Kovacic, 2009). However, its main task is to activate fibrin by cleavage of fibrinogen.

When fibrin is generated from fibrinogen by the extrinsic and intrinsic coagulation cascades, it can polymerize and form covalent crosslinks with the help of activated factor XIII (Ariëns et al., 2002). Polymerized and cross-linked fibrin becomes a sticky and elastic substance providing a mesh for platelets, which can bind fibrin with their

activated GPIIb/IIIa receptor (Rosado et al., 2001). Interconnection between fibrin, platelets and factor XIII supports formation of an insoluble and dense clot.

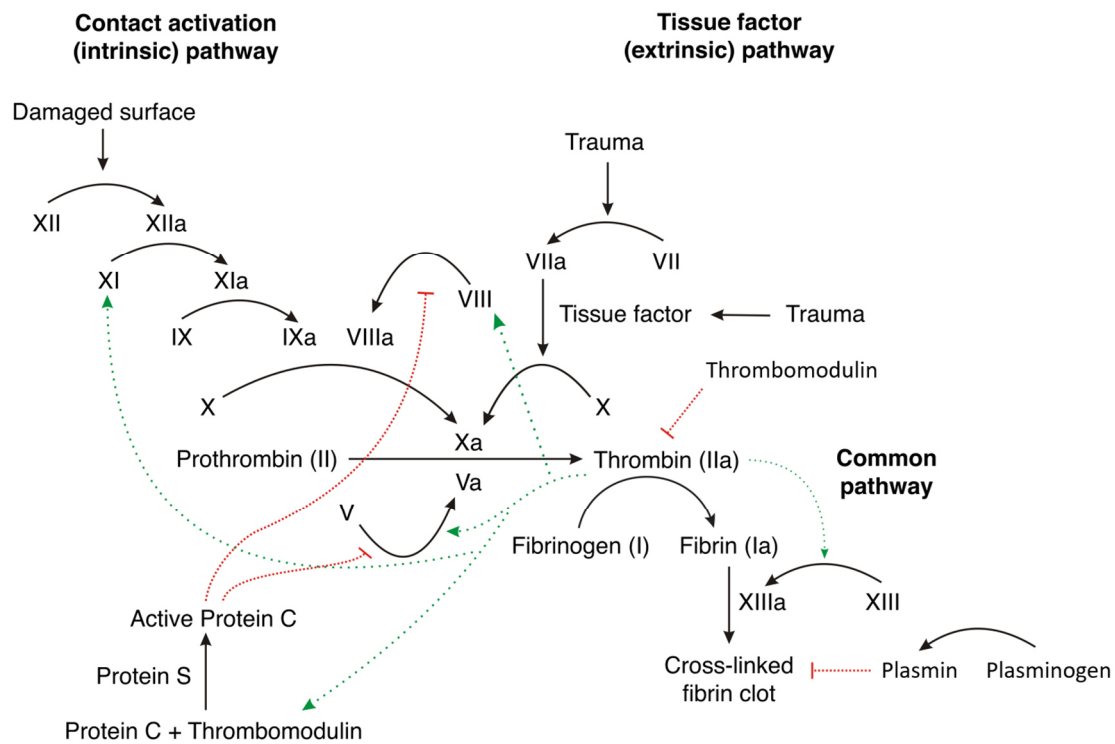


Figure 3: The coagulation cascade of the secondary hemostasis. Coagulation factors are presented with their number in roman numerals. Activation is indicated by black arrows. Activated coagulation factors contain the suffix 'a'. The promotion of a process is indicated by green dotted arrows, while inhibition is represented by red dotted lines (modified from Opoku et al. 2019).

3.2.4. Clot resorption

During wound healing, thrombi are degraded to restrict blood clotting and prevent the onset of pathophysiological thrombi. The process of fibrinolysis, which involves the proteolytic degradation of fibrin by the key enzyme plasmin, released from its zymogen form plasminogen, balances fibrin clot formation (Miles et al., 2021) (**Figure 3**). Moreover, the coagulation cascade can be blocked by thrombomodulin expressed on the surface of ECs. Thrombomodulin binds thrombin from the circulation and reduces its potency to generate fibrin (Watanabe-Kusunoki et al., 2020). Furthermore, activated protein C (APC) is capable of inactivating coagulation factors VIII and V by proteolysis, thereby counteracting secondary hemostasis (Vehar and Davie, 1980; Walker et al., 1979). Also VWF fibers can be cleaved into smaller fragments and liberate adhered

platelets by the cleaving protease ADAMTS13 (a disintegrin and metalloproteinase with a thrombospondin type 1 motif, member 13) (Crawley et al., 2011).

3.3. Thrombosis

Thrombosis is defined as the formation of a thrombus that impedes the blood flow or occludes a blood vessel. In both cases, the tissue is undersupplied, which can cause organ failure. A thrombus can either directly occlude the vessel at the site of its formation or be torn off and occlude a vessel at a distant site, which is called thromboembolism. The associated disease and the severity of the thrombosis depend on its anatomical location. Cardiovascular diseases (CVD), affecting the heart, and stroke, occurring in the brain, are the most common cause of death worldwide. In 2021, 19.91 million and 7.44 million deaths worldwide were attributed to CVD and stroke, respectively (Martin et al., 2024). The global prevalence of myocardial infarction (MI) was calculated in a meta-analysis including 8 million individuals and resulted in an occurrence of 9.5 % in individuals >60 years of age and 3.8 % for individuals <60 years of age (Salari et al., 2023).

3.3.1. Virchow's Triad

The causes that progressively lead to the development of thrombosis were described in the Virchow's Triad (Virchow R, 1856). These three causes are: alterations of the vessel wall, hemodynamic changes, and hypercoagulability.

Alterations of the vessel wall include endothelial damage, which can be caused by laceration, but also by atherosclerosis, hypoxia, toxins or inflammation (Sutton et al., 2014). These circumstances promote EC activation and the release of inflammatory and procoagulant molecules, such as VWF (Pinsky et al., 1996). A physiological, adequate activation of ECs is required to maintain vascular homeostasis. However, an excessive response, termed as endothelial dysfunction, can exacerbate the injury and promote the development of a pathological condition that favors the development of a thrombosis.

Hemodynamic changes refer to the disturbance of laminar flow present at branching vessels and sites of vascular constrictions (Davies, 2009). Constrictions are caused by

stenoses originating from atherosclerotic plaques or blood clots, and can cause turbulences and pulsatile or oscillatory flow (Jain, 2022). The changes of the hemodynamic shear forces promote endothelial dysfunction and particularly accelerated shear flow promotes the activation of VWF, platelets and clot formation (Schneider et al., 2007). A deceleration of the blood flow accompanied by the patients immobility leads to a condition called stasis and is associated with the risk of developing a venous thromboembolism (VTE) (Cushman, 2007).

Hypercoagulability describes alterations in the composition of the blood coagulation system, which have a direct influence on the development of clots and thrombi. Alterations may have genetic causes, but can also result from obesity, cancer, trauma, pregnancy, advanced age, smoking, or hormones (Smalberg et al., 2011).

3.3.2. Venous and arterial thrombi

Based on the mechanism of thrombus formation, a thrombus can further be differentiated into an arterial thrombus (white) and a venous thrombus (red) (Mackman, 2008).

Venous thrombi form slowly at locations of stasis, where the blood flow is deaccelerated. The valves of the veins are a common location where turbulences can occur, which will harm the regular blood flow. The thrombi are rich of fibrin and red blood cells caught in the fibrin network leading to a red appearance (Mackman et al., 2020). The most frequent association with venous thrombi is deep vein thrombosis (Wolberg et al., 2015).

In contrast, arterial thrombi form at locations of high shear stress, where the blood flow is accelerated. Vessels with a decreased vessel diameter due to partial occlusion by stenosis or atherosclerotic lesions are the most common areas of hyper shear reaching wall shear rates of up to $10,000 \text{ s}^{-1}$ (Gogia and Neelamegham, 2015). High shear forces promote a pro-thrombotic microenvironment and the activation of platelets, which lead to a white appearance of the thrombi. Arterial thrombi are causing MI and ischemic stroke when occurring in the heart and brain, respectively. Additionally, atherosclerotic lesions can promote thrombus formation (Borissoff et al., 2010), also after plaque rupture, by two mechanisms: (1) ruptured plaques can travel through the vessels and

cause occlusion at a distant site called embolism; (2) ruptured plaques lead to the exposure of the subendothelial matrix, which initiates hemostasis and may promote local thrombus formation (Owens and Mackman, 2012).

3.4. Von Willebrand Factor

Von Willebrand Factor (VWF) is a multimeric, multidomain glycoprotein that is predominantly found in blood plasma, but also in the endothelium, platelets and subendothelial tissue. It consists of disulfide-linked monomers that can reach a size of up to 20,000 kDa (Sadler, 1998). In the periphery, VWF circulates with a concentration of approx. 10 µg/mL (Borchiellini et al., 1996). It is the key initiator of primary hemostasis by enabling the immobilization of platelets to exposed subendothelial matrix proteins in the event of injury. This process promotes platelet activation, aggregation and the formation of a platelet plug.

3.4.1. Biosynthesis and structure of VWF

Exclusively endothelial cells (ECs) and megakaryocytes, the precursors of platelets, express the VWF protein (Hollestelle et al., 2001; Jaffe et al., 1973; Nachman and Jaffe, 1975; Sporn et al., 1985). It is secreted after a complex cascade of posttranslational modifications that lead to the formation of high molecular weight multimers (HMWM). The VWF gene is encoded in 52 exons on chromosome 12 (12p13.2) and the complete coding sequence (CDS) of VWF includes 8830 base pairs (Ginsburg et al., 1985). The synthesized protein consists of 2813 amino acids (aa) that make up the pre-pro-monomer (Verweij et al., 1986). The first 22 N-terminal aa serve as the signal peptide (SP) that directs VWF to the membrane of the endoplasmic reticulum (ER), where it undergoes SP removal (D. T. Bonthron et al., 1986). The pro-VWF monomer that remains is composed of a 741 aa pro-peptide and a 2050 aa mature VWF monomer (D. Bonthron et al., 1986) that comprises different repetitive domains forming the following domain structure: D1-D2-D'D3-A1-A2-A3-D4-C1-C2-C3-C4-C5-C6-CK (Zhou et al., 2012) (**Figure 4**). Binding sites for platelet receptors GPIIb/IIIa and GPIIb are located in the A1 domain and the C4 domain, respectively (Mohri et al., 1989; Xu et al., 2019). VWF harbors different binding sites for different collagen molecules, including the collagen type I and III binding site in the A3 domain (Romijn et al., 2001) and collagen

type IV and VI in the A1 domain (Flood et al., 2015; Hoylaerts et al., 1997). The ADAMTS13 cleavage site is located in the A2 domain (Crawley et al., 2011).

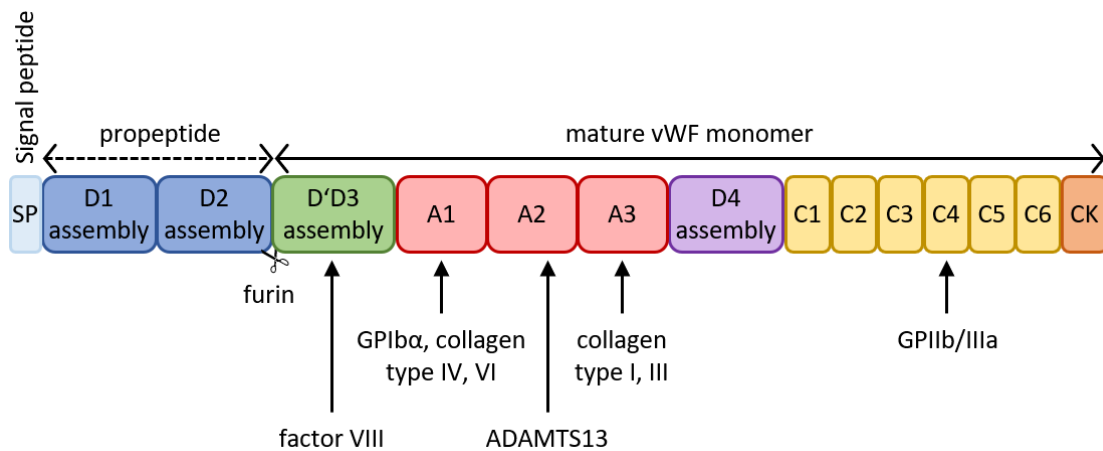


Figure 4: Domain structure of the VWF monomer. The VWF monomer consists of an N-terminal signal peptide (SP) of 22 aa, a pro-peptide of 741 aa, which is cleaved off by furin during maturation, and the mature VWF monomer. The pro-peptide (blue) consists of the D1 and D2 assembly. Mature VWF monomers consist of the D'D3 assembly (green), the A1, A2 and A3 domains (red), the D4 assembly (purple), six C domains (yellow) and a C-terminal cystine knot (CK) domain (orange). Binding sites for the platelet receptor GPIIb/IIIa, and collagens IV and VI are located in A1. The VWF specific protease ADAMTS13 cuts VWF in the A2 domain. Collagen types I and III bind to VWF by its A3 domain. An RGD motif is located in the C4 domain to bind the GPIIb/IIIa receptor on platelets.

In the ER, VWF is dimerized by cysteine bonds between the C-terminal CK domains in a 'tail-to-tail' manner (**Figure 5**). The protein disulfide isomerase (PDI) isoform A1 catalyzes this process by forming two intermolecular bonds between Cys2771 and Cys2773, which are capped by a third covalent bond between Cys2811 of each monomer (Lippok et al., 2016). Dimers arrange in 'bouquet-like' structure by close association of the C-terminal region of VWF forming the 'stem region' (Zhou et al., 2011). Further processing of VWF dimers occurs after translocation to the *trans*-Golgi apparatus. The pro-peptide, consisting of the D1 and D2 assembly, is the essential catalyzer for VWF multimerization (Verweij et al., 1987). In an acidic environment with a low pH of 6.2 and a high Ca^{2+} concentration, the oxidoreductase activity of the pro-peptide is activated (Mayadas and Wagner, 1989) leading to two additional disulfide bonds between two D'D3 domains that connect VWF dimers in a 'head-to-head' manner in the process of multimerization (Purvis and Sadler, 2004). A heterogeneous set of multimers with varying sizes of 2 to 60 dimeric subunits is generated (Lenting et al., 2015). The protease

furin cleaves the pro-peptide from the mature VWF (van de Ven et al., 1990) but the pro-peptide remains non-covalently attached to the VWF multimers. For VWF maturation additional oxidation of thiols are required, which are connected via intradomain disulfide bonds. VWF is extremely cysteine-rich, containing 234 cysteines that make up 8.3 % of all aa; a percentage higher than the average of 2.3 % in human proteins (Miseta and Csutora, 2000). Moreover, VWF is highly glycosylated and contains 16 *N*- and 10 *O*-glycosylation sites (Canis et al., 2010; McKinnon et al., 2010). Further modifications include sialylation and sulfation (Brehm, 2017; Carew et al., 1990; Sodetz et al., 1977)

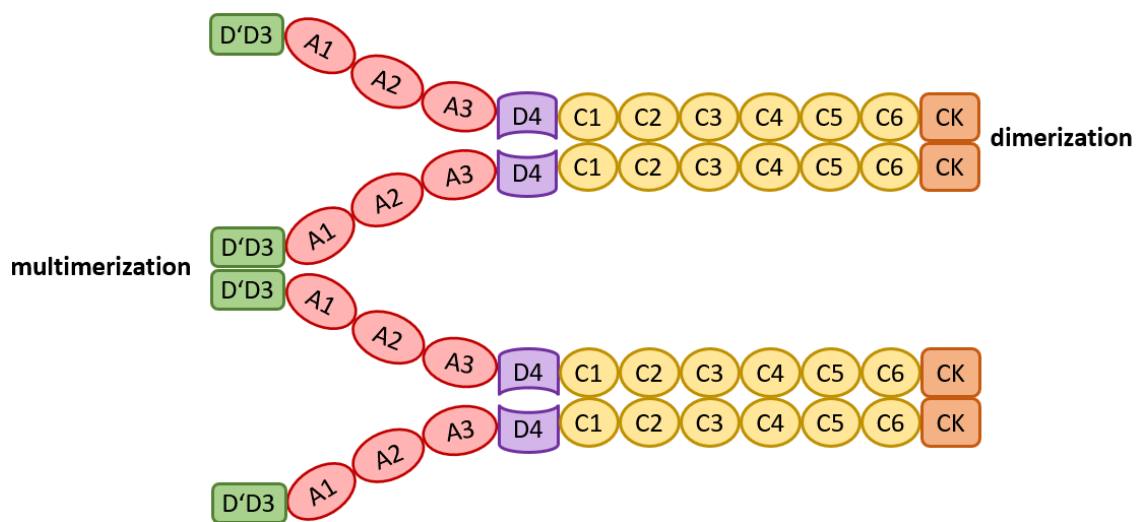


Figure 5: VWF dimerization and multimerization. VWF dimers form in the ER by intermolecular disulfide bonds between the CK domains of single monomers. Subsequently, multimerization takes place in the *trans*-Golgi network (TGN) by covalent disulfide bonds between D'D3 domains of dimers and multimers.

ECs secrete low molecular weight VWF (LMW-VWF) either basolaterally through a constitutive pathway (Da Silva and Cutler, 2016) or store multimers as ultra-large VWF (ULVWF) in tubules within organelles known as Weibel-Palade bodies (WPBs) (Wagner et al., 1982). WPBs are rod-shaped granules with a size of approx. 0.1 μm in width and 4 μm in length (Weibel and Palade, 1964).

Secretion from WPBs occurs predominantly apically via two pathways, the basal secretion and the regulated secretion (Da Silva and Cutler, 2016). Basal secretion involves the continuous release of VWF from WPBs to maintain a constant plasma antigen level of VWF. In contrast, stimulated secretion can be triggered by substances

(Billaud et al., 2014) such as histamine (Hamilton and Sims, 1987), thrombin (Levine et al., 1982), epinephrine (Vischer and Wollheim, 1997) or vasopressin (Kaufmann et al., 2000), resulting in a higher amount of ultra-large VWF being released. This mechanism facilitates the local recruitment of platelets to the vessel wall in cases of injuries. In megakaryocytes and platelets VWF is stored in α -granules (Cramer et al., 1985) and secreted after platelet activation to promote hemostasis (Heijnen et al., 1999).

3.4.2. Function and activity of VWF

VWF fulfills its function in hemostasis via two different mechanisms. On the one hand, it is the main carrier of factor VIII in the blood circulation. Factor VIII is an important player in secondary hemostasis and the coagulation cascade. Under physiological conditions, factor VIII is bound to the D'D3 assembly of VWF, which shields it from degradation in the circulation (Shiltagh et al., 2014). When factor VIII is not bound to VWF it is more prone to be proteolytically inactivated, which shortens its half-life by a 10- to 20-fold (Koedam et al., 1988). On the other hand, VWF is the key initiator of primary hemostasis. It circulates in the blood stream and enables the immobilization of platelets to the vessel wall and induces platelet activation after vessel injury.

3.4.2.1. Shear sensitivity of VWF

VWF is a mechanosensitive protein, which is capable of stretching and shrinking in length depending on the force acting on it. Normally, VWF is circulating in a compact, globular conformation (Zheng et al., 2015), which conceals its binding sites for platelets. However, when subjected to increased shear forces, it undergoes structural changes once a certain threshold is exceeded. The shear forces stretch VWF and lead to unfolding, especially of the A1 domain (Arce et al., 2021). This exposes the binding site for platelet receptor GPIIb α in the A1 domain (Miura et al., 2000). Likewise, the exposure of the ADAMTS13 cleavage site in the A2 domain is regulated by structural unfolding allowing ADAMTS13 to cleave VWF between aa residues Tyr1605 and Met1606 in the A2 domain (Crawley et al., 2011). Thus, activation as well as inactivation of VWF are regulated through shear-dependent mechanisms.

3.4.2.1. Size of VWF determines its activity

Since VWF is a mechanosensitive protein, its activity is highly dependent on its size which is determined by the degree of multimerization (Furlan, 1996). As the degree of multimerization can vary, different VWF sizes range from single dimers, low molecular weight multimers (LMWM), intermediate molecular weight multimers (IMWM), high molecular weight multimers (HMWM) and ultra-large molecular weight multimers (ULMWM) (Stockschlaeder et al., 2014).

In the circulation, VWF exists in a broad range of multimers, with the most prominent form being HMWM. The plasma levels are maintained by constant secretion from ECs (Stockschlaeder et al., 2014). Only after cellular stimulation, e.g. in the context of hemostasis, ECs and platelets can increase VWF plasma levels by secretion of VWF from WPBs and α -granules, respectively (Nichols et al., 2008). In ECs, VWF is stored in WPB as ULMWM, but upon secretion, VWF is subjected to shear forces leading to the formation of VWF strings that are cleaved into HMWM directly at the EC surface by the VWF-specific cleavage protease ADAMTS13 (Dong et al., 2002; Fujikawa et al., 2001). On the one hand, large VWF multimers, such as ULMWM are extensively potent and can promote the rise of thrombosis as observed in thrombotic thrombocytopenic purpura (TTP). On the other hand, small VWF multimers, such as LMW multimers, are not capable of initiating an intact hemostasis, which is the case in von Willebrand disease (VWD) type 2A (Hassenpflug et al., 2006). Therefore, a tight regulation is necessary to maintain a balance of potent but non-thrombotic VWF sizes.

3.4.2.2. Adhesion and activation of platelets

VWF's main function in hemostasis is the initiation of platelet adhesion and activation, which is necessary for stable platelet clot development. Activation of platelets is a multi-step process that is highly dependent on calcium signaling and involves sequential inside-out and outside-in signaling. Initial adhesion of platelets to VWF occurs only after VWF is mechanically activated by elevated shear forces, thereby exposing its binding site for platelet GPIIb α in the A1 domain (Arce et al., 2021). The following GPIIb α -A1 domain interaction is reversible and corresponds to platelet adhesion. It exhibits a biphasic catch-slip bond behavior (Yago et al., 2008). As the shear forces increase, the bond

lifetime rises due to formation of additional supportive catch bonds. However, if shear stress reaches a threshold, transition from catch bonds to slip bonds results in a shortening of bond lifetimes.

The establishment of GPIIb/IIIa domain catch bonds triggers an outside-in signaling by conformational change of the mechanosensitive domain (MSD) (Zhang et al., 2015) and leucine-rich repeat domain (LRRD) within the extracellular region of GPIIb/IIIa (Ju et al., 2015b), which are converted into intracellular signals. This process involves, among others, the intracellular adapter protein 14-3-3 ζ (Dai et al., 2005), the phosphoinositide 3-kinase (PI3K)/Akt signal pathway (Yin et al., 2008), Nitric oxide synthase (Riba et al., 2006) leading to Ca²⁺ mobilization from intracellular stores and further to cyclic guanosine monophosphate (cGMP) generation, mitogen-activated protein (MAP) kinase/extracellular signal-regulated (ERK) pathway activation and inside-out activation of the GPIIb/IIIa receptor (Li et al., 2006, 2001). However, this calcium signaling does not correspond to full platelet activation, but promotes an intermediate state. Likewise, the GPIIb/IIIa receptor switches extracellular domains from an inactive bent conformation to an intermediate active form, which enhances the affinity for agonist binding (Chen et al., 2019) (**Figure 6**). Proteins containing RGD motifs, as for example in VWF C4 domain or fibrin, are then capable of crosslinking platelets. Full activation of GPIIb/IIIa and stable crosslinking is only achieved after binding of agonists to GPIIb/IIIa and enhanced shear force that mediates activation of platelets by calcium influx from the extracellular compartments via store-operated Ca²⁺ entry (SOCE). Blocking of either GPIIb/IIIa interaction or Ca²⁺ influx results in defects in irreversible adhesion and aggregation of platelets (Mazzucato et al., 2002).

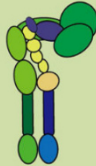

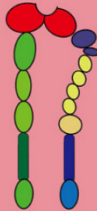
	Inactive	Intermediate	Active
$\alpha_{IIb}\beta_3$ state			
Conformation	BC	EC	EO
Affinity	Low	Intermediate	High
Ligand dissociation	Fast	Intermediate	Slow

Figure 6: Summary of three GPIIb/IIIa ($\alpha_{IIb}\beta_3$) states (inactive, intermediate and active). States are characterized by conformation (BC = bent closed, EC = extended closed and EO = extended open), affinity (low, intermediate, high) and ligand dissociation rate (fast, intermediate, slow). Three colors on the integrin βI and β - propeller domains indicate the three affinity states. (from Chen et al. 2019).

3.4.2.3. Evaluation of VWF function in laboratory testing

Several methods have been established over the past decades to assess VWF activity *in vitro*. Investigation of the multimeric pattern by gel electrophoresis and Western blotting can indicate qualitative defects due to alterations in multimer size, composition and degradation products (Ruggeri and Zimmerman, 1980). Binding to collagen (VWF:CB) and binding to factor VIII (VWF:FVIII) can be measured by ELISA (Roberts and Flood, 2015). However, binding of VWF to platelets requires activation of VWF and platelets, which is physiologically obtained by shear forces (Miura et al., 2000). Alternatively, this activation of VWF can also be achieved chemically by using the molecule ristocetin (Howard and Firkin, 1971). Ristocetin is an antibiotic that was used in patients until it was linked to a concentration-dependent induction of thrombocytopenia (Gangarosa et al., 1960). Studies demonstrate that the cationic charge of ristocetin causes VWF to unfold its tertiary structure, thereby exposing the platelet GPIIb α binding site in the A1 domain. (Higgins and Goodwin, 2019). The ristocetin-induced binding to platelet receptor GPIIb α (VWF:RC α) can be measured by ELISA (Vanhoorelbeke et al., 2000) or in light transmission aggregometry (LTA) by the ristocetin-induced platelet aggregation (RIPA) test. Hereby, ristocetin induces an agglutination of platelets from platelet-rich plasma (PRP), which is recognized by the

determination of the liquids turbidity (Alessi et al., 2020). More recent studies developed a ristocetin-independent measurement which relies on hyperactive GPIb α that binds VWF in absence of force or ristocetin activation. This assay determines the VWF activity (VWF:Ac) and is commercialized as the Siemens INNOVANCE assay (Patzke et al., 2014).

To study VWF activity in a more physiological environment, cone and plate aggregometry (CPA) or microfluidic flow systems can be used. The CPA test is based on shear-induced platelet adhesion and activation induced by spinning a cone on a plate. Staining of aggregates allows the quantification of surface coverage and aggregate size that provide information on platelet adhesion and activation. Microfluidics mimic a blood vessel and recreate the existing shear forces (Lehmann et al., 2018). By fluorescence labeling of platelets the adhesion and aggregation process can be observed in real-time (Brehm et al., 2014).

3.4.3. Pathogenicity of VWF

Since VWF is the major initiator of hemostasis, any alteration in VWF can cause severe pathogenicity. Either the VWF gene can be directly affected, most commonly leading to quantitative or qualitative defects of the VWF protein, resulting in von Willebrand disease (VWD), or HMWM can accumulate in the blood plasma, due to absence of ADAMTS13, causing thrombotic thrombocytopenic purpura (TTP). Below, VWF pathogenicity in hemostasis and thrombosis is presented in more detail.

3.4.3.1. Von Willebrand Disease

Von Willebrand Disease (VWD) is the most common bleeding disorder that affects approximately 0.6 – 1.3 % of the population worldwide. However, about 1 case per 1000 is estimated to have clinical relevance (Seidizadeh et al., 2023). VWD is a hereditary disorder that arises from genetic alterations of the VWF gene. Based on the mutation, VWD can have different pathophysiological consequences and severity of the symptoms. The patients suffer from impaired hemostasis, which manifests in an increased tendency to bleed and develop large hematomas and heavy bleedings, often discovered by severe mucosal bleedings (menorrhagia), frequent nosebleeds, bleeding after surgeries or dental extractions (Nichols et al., 2008). Based on its underlying

etiology, VWD is classified in three main types: it is either caused by a quantitative reduction (type 1), loss of VWF (type 3), or by qualitative defects that compromise its activity (type 2) (Sadler et al., 2006).

Type 1 is the mildest form which accounts for 55-80 % of all cases (Castaman et al., 2003). It is characterized by decreased VWF plasma levels of <30-50 % (Patzke and Schneppenheim, 2010). Thus, type 1 VWD includes a broad range of symptoms ranging from mild to severe. Markedly, only the amount of VWF is affected, but not the activity of single VWF molecules or their multimer distribution (Nichols et al., 2008).

If plasma VWF is barely detectable or undetectable in patients, type 3 VWD is diagnosed. The complete absence of plasmatic VWF protein is often caused by nonsense and frameshift mutations or also large deletions, splice-site mutations and missense mutations (Eikenboom, 2001). Type 3 VWD is rare and only accounts for approx. 3 -10 % of patients with VWD (Sadler et al., 2000).

Functional/qualitative defects of VWF result in VWD type 2 and are responsible for 20-40 % of all VWD cases (Sadler et al., 2000). Several subtypes are known which influence different characteristics of VWF. Subtype 2A is characterized by a loss of HMWV, either by mutations which impair dimerization or multimerization of VWF (Schneppenheim & Budde, 2011) or due to mutations which affect the VWF A2 domain and thus induce increased proteolysis by ADAMTS13 (Nichols et al., 2008). Loss-of-function (LOF) mutations, which cause a defect in platelet or collagen binding (Ciavarella et al., 1985), are classified as subtype 2M. They often map in the A1 and A3 domain where binding sites for platelets and collagens are harbored (Springer, 2014). Subtype 2N decreases the affinity of VWF to factor VIII, which results in enhanced dissociation of factor VIII from VWF (Nishino et al., 1989). Unbound factor VIII is more susceptible to clearance from the circulation (Koedam et al., 1988) resulting in decreased plasma levels and thus dysfunctional secondary hemostasis. Subtype 2B differs from the other subtypes, because it is not caused by LOF mutations, but by GOF mutations. These occur in the A1 domain and increase the affinity of VWF to bind platelet GPIIb/IIIa. However, the resulting VWF-platelet-complexes which form spontaneously are more prone to cleavage by ADAMTS13 and enhanced clearance. This

causes the contradictory effect that VWF and platelets are removed from the circulation, leading to thrombocytopenia and a bleeding phenotype (Ruggeri et al., 1980).

Depending on the subtype, the treatment of VWD varies. Patients can be treated with desmopressin (DDAVP), a synthetic vasopressin analogue which induces the secretion of VWF from ECs (Schneppenheim, 2011). This treatment is not suitable for type 2B patients, as the GOF-VWF-platelet-complexes lead to even faster clearance of remaining VWF and enhanced thrombocytopenia (Lars et al., 1983). Further, the bleeding management can be carried out by plasma-derived or recombinant VWF concentrates or antifibrinolytics, like tranexamic acid (Sharma and Flood, 2017), that inhibits plasmin generation and thus stabilizes clot formation.

A disorder that is similar to VWD is the acquired von Willebrand syndrome (AVWS). It is characterized by increased degradation or clearance of circulating VWF, which can be caused by autoimmune antibodies, cancers, drugs or cardiovascular disorders (Franchini and Mannucci, 2020). For instance, in cardiac valvopathies and left ventricular assist devices, VWF multimers are sheared by increased mechanical forces, leading to enhanced proteolysis by ADAMTS13.

3.4.3.2. Role of VWF in thrombosis

Prothrombotic VWF refers to a pathological increase in the amount of VWF or alterations that enhance its activity, which can elevate the risk of vessel occlusions. ULMWM describe a very high degree of VWF multimerization and are the most potent form of VWF when it comes to binding to platelets or the ECM (Sporn et al., 1987). In the periphery, these ULMWM are immediately stretched due to their large size, which exposes their A2 domains. Under physiological conditions, the protease ADAMTS13 cleaves the ULMWM into smaller multimers, thereby lowering the activity of VWF (Stockschlaeder et al., 2014). The absence of ADAMTS13 leads to the accumulation of ULVWF and to the disorder known as thrombotic thrombocytopenic purpura (TTP) (Moake et al., 1982). Patients suffer from microangiopathic hemolytic anemia and thrombocytopenia as a consequence of thrombotic microangiopathies and ischemic organ dysfunctions (Lämmle et al., 2005). One distinguishes between hereditary TTP (also called Upshaw-Schulman syndrome), caused by genetic mutations of the

ADAMTS13 gene, and acquired TTP, an autoimmune disease triggered by autoantibodies against ADAMTS13 (Alwan et al., 2017).

Consistently, low ADAMTS13 levels were associated with an increased risk of myocardial infarction (Maino et al., 2015) and ischemic stroke (Sonneveld et al., 2015; Zhao et al., 2009). Also high levels of VWF are present in patients with acute coronary syndrome (ACS) (Lip and Blann, 1997). Vice versa, reduced levels of VWF observed in VWD patients reduce the risk of developing cardiovascular diseases (CVD), such as MI (Seaman et al., 2015). Also, mice with low VWF levels are protected from stroke (Kleinschnitz et al., 2009).

Further clinical and epidemical studies indicate that VWF is involved in arterial thrombosis (Spiel et al., 2008) and venous thrombosis (Takahashi et al., 2009). Dysregulation of VWF highly correlates with the incidence of thrombotic diseases (De Meyer et al., 2012) and characterizes VWF as risk factor for coronary artery disease (CAD) (Whincup et al., 2002). Especially at sites of high shear, which are present at sites of lesions, VWF plays a pivotal role in platelet aggregation (Fredrickson et al., 1998).

3.4.3.3. Gain-of-function variants of VWF with mutations in the C4 domain

Recently, variants causing qualitative changes in the VWF protein were identified to increase VWF function. These are distinct from the GOF variants observed in VWD 2B.

In 2019, Schneppenheim et al. discovered, that the frequent single nucleotide polymorphism (SNP) p.Phe2561Tyr (rs35335161) is significantly associated with an increased risk of recurrent MI in younger individuals, particularly in women under 55 years of age. (Schneppenheim et al., 2019). Carriers of p.Tyr2561 also display a significantly earlier onset of MI and a shorter time between the first and second MI. The affected aa is located in the C4 domain of VWF, the same domain that contains the RGD motif for platelet GPIIb/IIIa binding. However, residue 2561 and the RGD sequence are distant from each other in the C4 domain structure (Xu et al., 2019). By ELISA, the study further excluded that the binding affinity of VWF to GPIIb/IIIa is directly affected by the p.Phe2561Tyr mutation. Nevertheless, a GOF was observed for the variant when exposed to shear stress in flow experiments. In cone-and-plate aggregometry (CPA), an increased surface coverage with platelet aggregates was identified in whole blood from

carriers as well as for the recombinant variant in washed blood. In fluidic microchannels, the formation of VWF-induced collective networks occurred at lower shear rates when the recombinant variant was compared to wildtype VWF. In fact, the critical shear rate was decreased to 50 %, indicating a higher shear sensitivity for this variant (**Figure 7**). Structural investigations by circular dichroism (CD) spectroscopy led to the hypothesis that the tertiary structure of the VWF dimer bouquet is disrupted by the p.Phe2561Tyr mutation, which could facilitate the stretching of the VWF multimers by reducing the lower free energy barrier. This would allow for increased exposure of platelet binding sites in A1 and/or C4 domain, or could enhance VWF self-association.

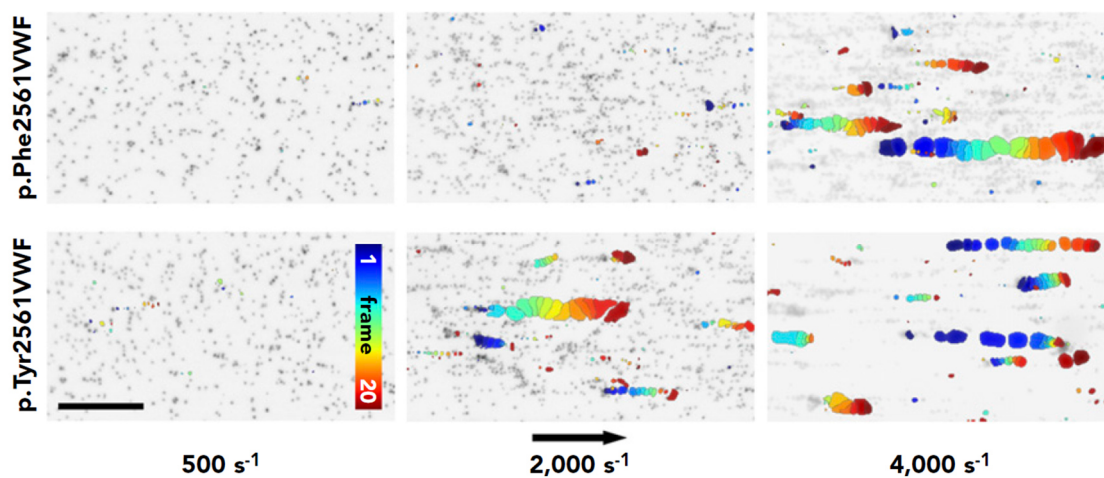


Figure 7: VWF-induced collective network formation of rPhe2561 and rTyr2561 VWF at indicated shear rates. Citrated whole blood was washed and platelets were fluorescently stained (black dots). Washed blood, including 200,000 platelets/ μL , 45 % washed hematocrit and 10 $\mu\text{g}/\text{mL}$ of either recombinant wtVWF (p.Phe2561VWF) or variant p.Tyr2561 was subjected to various shear rates in the range of 500 – 4,000 s^{-1} in air-pressure driven microfluidic channels (Bioflux, San Francisco, California, USA, width: 350 μm , height 70 μm) coated with 50 $\mu\text{g}/\text{mL}$ of the respective variant. Each image represents a composition of 20 sequential frames of a live-cell fluorescence movie taken at a frequency of 8 frames per second. By subtracting identical pixels among frames, a color-coded addition of these differential images from frame 0 (blue) to frame 20 (red) along the color scale, combined with the inverted gray-scaled background image of the start frame, allows precise detection and motion tracking of VWF-induced collective networks. The black arrow indicates the flow direction and the scale bar corresponds to 100 μm (Schneppenheim et al., 2019).

Later, in 2022, Huck et al. identified a second GOF variant, which is also located in the C4 domain, namely p.Pro2555Arg (Huck et al., 2022). Similar to variant p.Phe2561Tyr, this variant is located at a remote position to the RGD motif and does not directly alter

the GPIIb/IIIa binding. However, distinct from variant p.Phe2561Tyr, the variant p.Pro2555Arg does not change the shear sensitivity in microfluidic experiments, but increases the aggregate size (**Figure 8**).

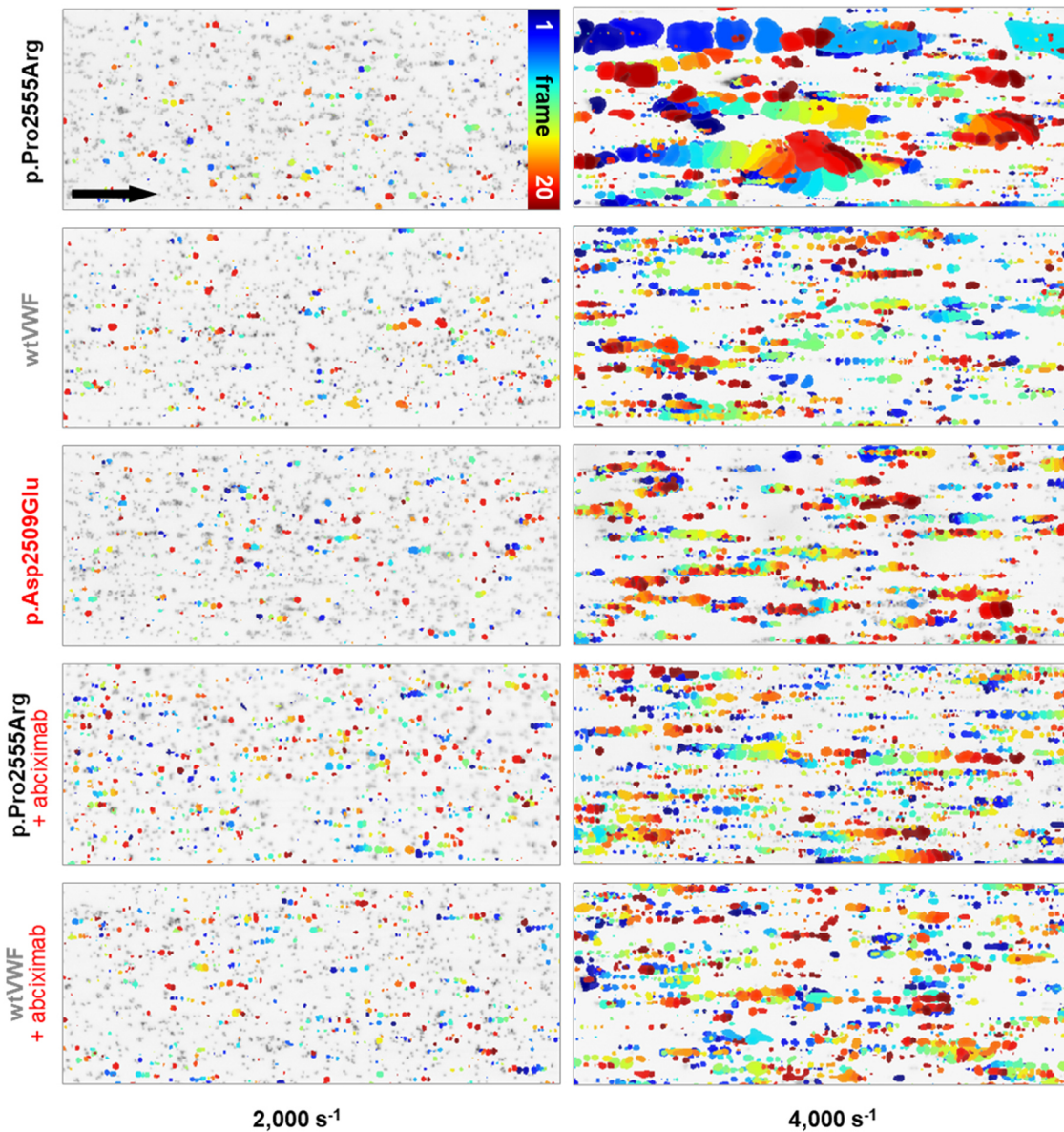


Figure 8: Characteristics of VWF-induced collective network formation of wtVWF and p.Pro2555Arg at indicated shear rates. Citrated whole blood was washed and platelets were fluorescently stained (black dots). Washed blood, including 200,000 platelets/ μL , 45 % washed hematocrit, and 10 $\mu\text{g}/\text{mL}$ of either wtVWF, p.Pro2555Arg (with or without addition of 1.3 $\mu\text{L}/\text{mL}$ abciximab [ReoPro, stock concentration: 2 mg/mL; Centocor, now Janssen Biotech Inc., Horsham, Pennsylvania, US]), or p.Asp2509Glu, was subjected to shear rates in the range of 500-4,000 s^{-1} in air- pressure-driven microfluidic channels (Bioflux, San Francisco, California, United States; width: 350 μm , height: 70 μm) coated with 50 $\mu\text{g}/\text{mL}$ of either recombinant wtVWF, p.Pro2555Arg, or p.Asp2509Glu. Each image represents a composition of 20 sequential

(Figure legend 8 continued from previous page.) frames of a live-cell fluorescence movie taken at a frequency of eight frames/sec. By subtracting identical pixels among frames, a color-coded addition of these differential images from frame 0 (blue) to frame 20 (red) along the color scale, combined with the inverted gray-scaled background image of the start frame, allows precise detection and motion tracking of VWF-induced collective networks. Therefore, only moving networks are displayed in color enabling an exact determination of the critical shear rate. Results for variant p. Pro2555Arg (upper row), wtVWF (second row), GPIIb/IIIa binding-deficient mutant p.Asp2509Glu (third row), variant p.Pro2555Arg in presence of abciximab (fourth row) and wtVWF in presence of abciximab (bottom row) are shown. The black arrow indicates the flow direction and corresponds to 100 μm . One example out of at least four independent experiments is shown (Huck et al. 2022).

Application of the GPIIb/IIIa inhibitor abciximab counteracts the GOF phenotype in microfluidic experiments, concluding a GPIIb/IIIa-dependent GOF. However, the VWF-induced collective network formation, in general, seems to be independent of GPIIb/IIIa, since the GPII/IIIa binding-deficient VWF variant p.Asp2509Glu was capable of producing aggregates at similar shear rates as the wildtype. CD spectroscopy and SAXS experiments, revealed that the variant p.Pro2555Arg is affecting the stem structure within VWF dimers. Further, nuclear magnetic resonance (NMR) spectroscopy and molecular dynamics (MD) simulations revealed extensive local perturbations and a backbone flexibility allowing for conformational switching and increased dynamics in the vicinity of Arg2555. The overall length of subdomain (SD) 2 along its beta sheets is slightly contracted which may explain the stem structure disturbance. Huck et al. hypothesized that this offers an increased 'temporal availability of the RGD domains for GPIIb/IIIa binding, leading to increased VWF-platelet crosslinking' (Huck et al., 2022).

Interestingly, both variants are located just six aa apart from each other but have distinct mechanisms. Further studies are needed to determine, why they have different phenotypes and what exactly is causing the increase in activity.

4. AIM OF THIS THESIS

This study aimed at investigating the prothrombotic effects of VWF variants and their potential as thrombotic risk factors. Previous studies by Schneppenheim et al. and Huck et al. have identified GOF variants p.Phe2561Tyr and p.Pro2555Arg that influence platelet aggregation *in vitro* (Huck et al., 2022; Schneppenheim et al., 2019). Additionally, variant p.Phe2561Tyr was shown to be associated with an increased thrombotic potential *in vivo*. However, the exact mechanisms of these variants' prothrombotic effects remain unclear. Moreover, it is uncertain whether these are the only existing GOF variants with this phenotype. In this study, three different approaches were used to choose variants, which were then recombinantly expressed in HEK293F cells and subsequently characterized *in vitro* under static and flow conditions.

In the first approach, patients who underwent coronary angiography or electrophysiological examination for diagnostic purposes, indicating a cardiovascular or rhythmic conspicuity, were screened for novel variants by sequencing their C4 domain, particularly exon 45, because previously described variants are located in this exon.

In the second approach, previously reported SNPs in the C4 domain listed in the Ensembl database (Hinxton, UK) were selected based on the position in the tertiary structure of the C4 domain and the extent of chemical alterations, caused by the aa exchange.

In the third approach also homologous C domains of VWF were taken into account by choosing homologous positions to Phe2561 and Pro2555 in other C domains. The aim was to investigate whether GOF variants are solely occurring in the C4 domain or if a key feature in all C domains is responsible for this effect. Additionally, variants were included in the study which were previously shown to increase aggregate size in cone and plate aggregometry tests performed in the laboratory of Prof. Dr. Reinhard Schneppenheim (Department of Pediatric Hematology and Oncology, University Medical Center Hamburg-Eppendorf (UKE), Hamburg, Germany).

For those recombinant variants with normal secretion and regular multimer pattern, a characterization of the binding capacity to common interaction partners, such as collagen type III, and platelet receptors GPIIb/IIIa and GPIIb/IIIa was performed under static conditions with specific enzyme-linked immunosorbent assays (ELISA). Moreover,

platelet agglutination was investigated by light transmission aggregometry (LTA), and flow experiments were performed by using microfluidic channels to investigate platelet adhesion and aggregate formation. Furthermore, structure predictions were generated by AlphaFold2-Multimer to gain insight into the impact of GOF variants on the VWF tertiary structure.

To further elucidate the mechanism underlying the prothrombotic effect of variants p.Phe2561Tyr and p.Pro2555Arg, they were analyzed in an *in vivo* mouse model. A tail-clip assay was performed to characterize hemostatic parameters and a thrombosis model was performed to investigate the impact of the variants on vessel occlusion.

The development of inhibitory molecules may offer a risk reduction for thromboembolic events in carriers of VWF GOF variants. To identify such molecules, the C4 domain movement was studied in MD simulations and small interfering peptides were designed *in silico* with the aim of inhibiting the activity of the RGD motif in the C4 domain. The peptides were tested for their potential to decrease VWF activity and counteract the VWF GOF effect.

5. MATERIAL AND METHODS

5.1. Material

Disposables including reaction tubes, pipet tips and cell culture material were acquired from Eppendorf AG (Hamburg, Germany), Sarstedt (Nümbrecht, Germany), Greiner Bio One (Kremsmünster, Austria), VWR (Radnor, US) and Nunc (Roskilde, Denmark). For composition of buffers, solutions and media double-distilled water was used. All deviations are indicated.

5.1.1. Animals

For this study five to eight-week-old C575BL/6 mice or C575BL/6 VWF-knock-out (KO) mice were used. Mice were bred in the INSERM Unit 1176 (Le Kremlin Bicêtre, France) animal facility and housing, and experiments were performed under the French regulations and experimental guidelines of the European Community.

5.1.2. Patient samples

Sodium citrate blood samples of patients from the Medical Clinic for Cardiology, Angiology and Rhythmology at the Jung-Stilling Diakonie Hospital in Siegen, Germany, were kindly provided by Prof. Dr. Dursun Gündüz (Head Physician of Cardiology and Angiology).

5.1.3. Bacteria

For bacterial transformation One Shot™ Mach1™ T1 Phage-Resistant Chemically Competent E. coli (Invitrogen™, Thermo Fisher, Waltham, US) were used.

5.1.4. Cell lines

In this study, 293-F cells (Gibco™, ThermoFisher, Waltham, US) were used, further referred to as HEK293F. This permanent cell line derives from primary embryonal human kidney and is transformed with sheared human adenovirus type 5 DNA. These fast-growing cells are adapted to efficiently grow in serum-free medium and produce a high protein concentrations.

5.1.5. Instruments

Table 1: List of all used instruments and manufacturers.

Instrument	Company (headquarter)
766 Laboratory pH Meter	Knick Elektronische Messgeräte- GmbH & Co. KG (Berlin, Germany)
Axio Observer Microscope	Zeiss (Oberkochen, Germany)
Azure 400 Visible Fluorescent Western System	Biozym (Hessisch Oldendorf, Germany)
Bioflux 200	Fluxion Biosciences (Oakland, US)
Biometra P25 Electrophoresis Power Supply	Analytik Jena GmbH (Jena, Germany)
Biometra TAdvanced PCR Thermal Cyclers	Analytik Jena GmbH (Jena, Germany)
Capillary Blotter	Apelex (Lisses, France)
CELL-DYN Emerald	Abbott (North Chicago, US)
Centrifuge 5810R	Eppendorf (Hamburg, Germany)
Chrono-Log Model 700 Aggregometer	Chrono-Log Corporation (Havertown, USA)
Dual-cooled vertical electrophoresis systems, SE 600 Ruby™	Cytiva Life Sciences (Marlborough, US)
EBA 12 Centrifuge	Hettich (Tuttlingen, Germany)
EBA12R Centrifuge	Hettich (Tuttlingen, Germany)
Fluorescence Microscope BZ-9000	Keyence (Osaka, Japan)
FV3000 Confocal Laser Scanning Microscope	Olympus (Tokyo, Japan)
Heidolph 3001 series magnetic stirring hotplate	Heidolph (Schwabach, Germany)
Heracell™ 150i CO ₂ incubator	Thermo Fisher Scientific (Waltham, US)
Heraeus™ Megafuge 1.0R Centrifuge	Heraeus (Hanau, Germany)
Heraeus™ Multifuge™ X3R	Thermo Fisher Scientific (Waltham, US)
Heraeus™ Thermo B20 incubator	Heraeus (Hanau, Germany)
Herasafe™ HS Biological Safety Cabinet	Thermo Fisher Scientific (Waltham, US)
HT3 Microtiter Plate Reader Model 12 600	Anthos Labtec Instruments (Wals-Siezenheim, Austria)
iCycler PCR Thermal Cyclers	Bio-Rad Laboratories (Hercules, US)
IKA® KMO 2 basic IKAMAG™ stirrer	VWR (Radnor, US)

Instrument	Company (headquarter)
Orbital platform shakers, Innova® 2000	New Brunswick Scientific Co. Inc. (New York, US)
peqLab perfect Spin Mini	VWR (Radnor, US)
Pipetboy acu 2	Integra Biosciences (Princeton, US)
Pipetus	Hirschmann (Eberstadt, Germany)
Precision balance 440-45N	Kern (Balingen, Germany)
Qubit 2.0 Fluorometer	Thermo Fisher Scientific (Waltham, US)
Refrigerated Centrifuge 5910R	Eppendorf (Hamburg, Germany)
Sartorius BP211D Analytical Balance	Sartorius (Göttingen, Germany)
Sartorius Handy H 120 precision balance	Sartorius (Göttingen, Germany)
UNIHOOD Incubation hood	UNIEquip (Munich, Germany)
Vortex Genie 2	Scientific Industries (Bohemia, US)
Water bath	Memmert (Schwabach, Germany)
Water bath	GFL (Burgwedel, Germany)

5.1.6. Consumables

Table 2: List of used consumables and manufacturers.

Consumable	Company
μ-Slide 8 Well	Ibidi (Gräfelfing, Germany)
48-well high shear plate (0-200 dynes/cm ²)	Fluxion Biosciences (Oakland, US)
Amicon® Ultra-15 Centrifugal Filter Unit	MerckMillipore Life Sciences (Darmstadt, Germany)
Immobilon-P Membran, PVDF, 0.45 μm	MerckMillipore Life Sciences (Darmstadt, Germany)
Millex-HV Filter, 0.45 μm	MerckMillipore Life Sciences (Darmstadt, Germany)
Safety-Multifly® needle, 20G x 3/4", yellow	Sarstedt (Nümbrecht, Germany),
S-Monovette® Citrate 9NC 0.106 mol/l 3.2 %, 8.2 ml, cap green	Sarstedt (Nümbrecht, Germany),
Whatman® Gel-Blotting papers GB005	GE Healthcare (Chicago, US)

5.1.7. Chemicals

Table 3: List of all used chemicals and manufacturers.

Chemical	Company
Agarose IEF	GE Healthcare (Chicago, US)
Agarose LE	Biozym (Hessisch Oldendorf, Germany)
Aqua	B. Braun (Melsungen, Germany)
Bovine Serum Albumin (BSA)	Sigma-Aldrich (St. Louis, US)
Bromophenol Blue	Bio-Rad (Hercules, US)
Calcium chloride dihydrate ($\text{CaCl}_2 \cdot 2 \text{H}_2\text{O}$)	Carl Roth (Karlsruhe, Germany)
Carbenicillin disodium salt	Carl Roth (Karlsruhe, Germany)
CellTrace™ Calcein Green	Thermo Fisher Scientific (Waltham, US)
cOmplete™, Mini, EDTA-free Protease Inhibitor Cocktail	Roche (Basel, Switzerland)
D(+)-Glucose	Carl Roth (Karlsruhe, Germany)
D(+)-Glucose-Monohydrate	Merck (Darmstadt, Germany)
Dimethylsulfoxid (DMSO)	TH Geyer (Renningen, Germany)
EDTA disodium salt dihydrate	VWR (Radnor, US)
Ethanol	TH Geyer (Renningen, Germany)
G418 (Geneticin)	InvivoGen (San Diego, US)
GeneRuler DNA Ladder Mix	Thermo Fisher Scientific (Waltham, US)
Gibco™ DMEM (Dulbecco's Modified Eagle's Medium), high glucose, GlutaMAX™ Supplement	Thermo Fisher Scientific (Waltham, US)
Gibco™ Kanamycin Sulfate	Thermo Fisher Scientific (Waltham, US)
Gibco™ Fetal Bovine Serum (FBS)	Thermo Fisher Scientific (Waltham, US)
Gibco™ L-Glutamine (200 mM)	Thermo Fisher Scientific (Waltham, US)
Gibco™ Opti-MEM™ I Reduced Serum Medium, GlutaMAX™ Supplement	Thermo Fisher Scientific (Waltham, US)
Gibco™ Trypsin-EDTA (0.05 %), phenol red	Thermo Fisher Scientific (Waltham, US)
Glycine	Sigma-Aldrich (St. Louis, US)
HEPES	Biowest (Nuaille, France)
Human Collagen Type III Solution	SouthernBiotech (Birmingham, USA)
Hydrochloric acid (HCl)	Carl Roth (Karlsruhe, Germany)

Chemical	Company
Hygromycin B Gold	InvivoGen (San Diego, US)
Invitrogen™ LB Agar (Lennox L Agar)	Thermo Fisher Scientific (Waltham, US)
Invitrogen™ Lipofectamine™ LTX Reagent with PLUS™ Reagent	Thermo Fisher Scientific (Waltham, US)
Invitrogen™ One Shot™ Mach1™ T1 Phage-Resistant Chemically Competent E. coli	Thermo Fisher Scientific (Waltham, US)
Invitrogen™ S.O.C. Medium	Thermo Fisher Scientific (Waltham, US)
Invitrogen™ UltraPure™ Tris-Puffer	Thermo Fisher Scientific (Waltham, US)
Isopropanol (2-Propanol)	Carl Roth (Karlsruhe, Germany)
LB-Medium (Luria/Miller)	Carl Roth (Karlsruhe, Germany)
Magnesium chloride hexahydrate (MgCl ₂ · 6 H ₂ O)	Carl Roth (Karlsruhe, Germany)
Paraformaldehyde 20 %	Electron Microscopy Sciences (Hatfield, US)
Penicillin-Streptomycin (10,000 U/mL)	Thermo Fisher Scientific (Waltham, US)
Potassium chloride (KCl)	Carl Roth (Karlsruhe, Germany)
Propionic acid	Sigma-Aldrich (St. Louis, US)
ROTI®GelStain	Carl Roth (Karlsruhe, Germany)
Seakem® HTG Agarose	Lonza (Basel, Switzerland)
Sodium chlorid (NaCl)	Carl Roth (Karlsruhe, Germany)
Sodium dihydrogen phosphate dehydrate (NaH ₂ PO ₄ · 2 H ₂ O)	Merck (Darmstadt, Germany)
Sodium hydrogen carbonate (NaHCO ₃)	Carl Roth (Karlsruhe, Germany)
Sodium Hydroxide (NaOH)	Merck (Darmstadt, Germany)
Sulfuric acid 0.5 M	TH Geyer (Renningen, Germany)
Triton X-100	Sigma-Aldrich (St. Louis, US)
TriTrack DNA Loading Dye (6X)	Thermo Fisher Scientific (Waltham, US)
Trizma® base	Sigma-Aldrich (St. Louis, US)
Urea	Eurobio Scientific (Dorking, UK)

5.1.8. Buffers and Media

Table 4: Composition of all used buffers and media.

Buffer/Media	Composition
50x TAE buffer, pH 8.0	40 mM Tris base 20 mM Acetic acid 50 mM EDTA pH 8.0
Blocking buffer for ELISA	1 % BSA in PBS
Coating buffer for ELISA	5 mM Na ₂ CO ₃ 5 mM NaHCO ₃ 0.75 mM NaN ₃ pH 9.6
DMEM medium for cell culture	500 mL DMEM + Glutamax™ 10 % FBS 1x Penicillin-Streptomycin
Electrophoresis buffer for multimer gel	500 mM Tris UltraPure 750 mM Glycine pH 8.45
HEPES buffer	140 mM NaCl 5 mM KCl 1 mM MgCl ₂ · 6 H ₂ O 1 mM CaCl ₂ · 2 H ₂ O 5 mM D(+)-Glucose 10 mM HEPES
Resuspension buffer	Tyrode's buffer 5 % BSA pH 7.4
Running gel buffer for multimer gel	200 mM Tris UltraPure 100 mM Glycine 0.4 % SDS pH 9.0
Sample buffer for multimer gel	50 mL stacking gel buffer 54 g Urea 0.1 g Bromophenol Blue 5 mL 20 % SDS Ad 100 mL

Buffer/Media	Composition
Sample buffer for ELISA	5 % BSA in PBS
Serum-free medium for cell culture	1 L OptiPRO™ SFM 4 mM L-Glutamine 50 U/mL Penicillin-Streptomycin
Tyrode's buffer	1.37 mM NaCl 26.83 mM KCl 5.43 mM NaH ₂ PO ₄ · 2 H ₂ O 50 mM HEPES 27.75 mM Glucose · H ₂ O pH 6.5
Washing buffer for ELISA	0.1 % BSA in PBS

5.1.9. Peptides

Peptides were synthesized by Proteogenix (Schiltigheim, France). Amino acid sequences are given in **Table 5**.

Table 5: List of all peptides. Amino acid sequence is given.

Name	Amino acid sequence
Peptide short	GSQWASPEN
Peptide long	GSQWASPENPCLINE

5.1.10. Oligonucleotides

Oligonucleotides were purchased from Eurofins Scientific SE (Luxembourg). Name and sequence are given in **Table 6**.

Table 6: List of all oligonucleotides. Name and sequences are given.

Name	Sequence (5'-3')
hVWF_Exon45_Fwd	ACCACCTTCCTGAGAGAAGAGC
hVWF_Exon45_Rev	AGCCAAAAGTGGAAGAGAGGC
hVWF_p.Arg2535Gln	GCCTCATCAATGAGTGTGTCCAAGTGAAGGAGGAGGTCTTTATAC
hVWF_p.Arg2575Cys	CTCAGCGTGCTGCCCAAGCTGTTGCTGTGAGCGCATGGAGGCCT G
hVWF_p.Arg2575His	CTCAGCGTGCTGCCCAAGCTGTCACTGTGAGCGCATGGAGGCCT G
hVWF_p.Cys2557Tyr	CCCAGCTGGAGGTCCCTGTCTACCCCTCGGGCTTTCAGCTGAG
hVWF_p.Cys2574Arg	GACCTCAGCGTGCTGCCCAAGCCGTCGCTGTGAGCGCATGGAG
hVWF_p.Cys2574Phe	GACCTCAGCGTGCTGCCCAAGCTTTCGCTGTGAGCGCATGGAG
hVWF_p.Glu2525Lys	CGGCTCCCAGTGGCCTCCCCGAAGAACCCTGCCTCATCAATG
hVWF_p.Glu2553Lys	CGTCTCCTGCCCCAGCTGAAGGTCCCTGTCTGCCCTCGGG
hVWF_p.Gly2560Arg	GAGGTCCCTGTCTGCCCTCGCGCTTTCAGCTGAGCTGTAAG
hVWF_p.Gly2560Ser	GAGGTCCCTGTCTGCCCTCGAGCTTTCAGCTGAGCTGTAAG
hVWF_p.Gly2705Arg	GAACACAAGTGTCTGGCTGAGAGAGGTAAAATTATGAAAATTCC
hVWF_p.Phe2481Tyr	GAGGACAGCTGTCGGTCGGGCTACACTTACGTTCTGCATGAAGG C
hVWF_p.Pro2302Arg	GCCCTGCCCCACGGCCAAAGCTCGCACGTGTGGCCTGTGTGAAG TAG
hVWF_p.Pro2302Thr	GCCCTGCCCCACGGCCAAAGCTACCACGTGTGGCCTGTGTGAAGT AG
hVWF_p.Pro2373Arg	GTGCAAAAGAGTGTCCCCACGCTCCTGCCCCCGCACCGTTTG
hVWF_p.Pro2373Ser	GTGCAAAAGAGTGTCCCCATCCTCCTGCCCCCGCACCGTTTG
hVWF_p.Pro2558Ser_fwd	GAGGTCCCTGTCTGCTCCTCGGGCTTTCAG
hVWF_p.Pro2558Ser_rev	CAGCTGGGGCAGGAGACGTTCTTTGTTG
hVWF_p.Ser2559Leu	CTGGAGGTCCCTGTCTGCCCTTGGGCTTTCAGCTGAGCTGTAAG
hVWF_p.Ser2559Trp	CCTGGAAGAGTGTGCGCTCCAGGGGGCCTCCCCGGAACCC TGC
hVWF_p.Ser2564Arg	CTGCCCTCGGGCTTTCAGCTGCGCTGTAAGACCTCAGCGTGCTG
hVWF_p.Ser2573Arg	GACCTCAGCGTGCTGCCCAAGATGTCGCTGTGAGCGCATGG
hVWF_p.Trp2521Gly	CCTGGAAGAGTGTGCGCTCCAGGGGGCCTCCCCGGAACCC TGC

Name	Sequence (5'-3')
hVWF_SEQ01	ATGATTCCTGCCACATTTGCCGG
hVWF_SEQ02	CCCCCTGCCAGGAGGTAAGTGC
hVWF_SEQ03	TTGTTTGTCAATGGTACCGTGACAC
hVWF_SEQ04	CAGACAGATACTTCAACAAGACC
hVWF_SEQ05	ATCTCCTCCCAGCAGCTCATGC
hVWF_SEQ06	GACTTTGTGTGAGTGTGCTGGG
hVWF_SEQ07	AGTGTGTGTCCCTTGCGCCAGG
hVWF_SEQ08	TTGCCAGGACCACTCCTTCTCC
hVWF_SEQ09	TGCGGCCTGTGTGGGAATTAC
hVWF_SEQ10	CAGCTATGCCGCGGCCTGCGC
hVWF_SEQ11	GCTGCCTGACGCTGTCTCAG
hVWF_SEQ12	TGGCTGCAACACTTGTGTCTG
hVWF_SEQ13	GGACCGCCACCTGAGCATC
hVWF_SEQ14	TGGTGGACCCCGAGCCATATCTGG
hVWF_SEQ15	ATGCCCACTGCCCTCCAGGG
hVWF_SEQ16	GCCTTTGTGGTGGACATGATGG
hVWF_SEQ17	CCAGCGAGGTCTTGAAATACAC
hVWF_SEQ18	GGATGTGGCGTTCGTCTGG
hVWF_SEQ19	CAACCTGGTCTACATGGTCACC
hVWF_SEQ20	AGGATTGGCTGGCCCAATGC
hVWF_SEQ21	CAGTATGGAAGCATCACCACC
hVWF_SEQ22	GCCCAGCTACGGATCTTGGA
hVWF_SEQ23	GTAAAGTGAAGAGACCTGT
hVWF_SEQ24	TGGGTGGGAACATGGAAGTC
hVWF_SEQ25	AGTGTCTTGTCCCGACAGC
hVWF_SEQ26	TGGGGACCATCCCTCCGAAGG
hVWF_SEQ27	AGCTGTGACCTGCCCCAGTGC
hVWF_SEQ28	GAAGCACCATCTACCCTGTG
hVWF_SEQ29	TCCGAGTGAAGGAGGAGGTC
hVWF_SEQ30	ATAACACAGGTGAATGTTGTGG
hVWF_SEQ31	GAAGAGGGTCACAGGCTGCC
hVWF_SEQ32	CCCATGCAGGTGGCCCTGCAC
mVWF_p.Phe2561Tyr	CTGTCCCTACCTGTCCACAGGCTACCAACTGAACTGTGAGACCTC
mVWF_p.Pro2555Arg	CTCCTGCCACAGCTGGCTGTCCGTACCTGTCCACAGGCTTCCAA C

Name	Sequence (5'-3')
mVWF_SEQ01	ATGAACCCTTTCAGGTATGAG
mVWF_SEQ02	GACCTTTGGCTTTGCGGCCAG
mVWF_SEQ03	GTCCTGTA CTCTTGAGTATG
mVWF_SEQ04	GCTTCGACAACAGGTACTTC
mVWF_SEQ05B	GTCTATTCTGGGAAGACCTG
mVWF_SEQ06	CCTGCAACCTGACCTGCCGC
mVWF_SEQ07	CTACGACCTGGAGTGTATGAG
mVWF_SEQ08	CAGGAAGCGGGTGACCATCCTG
mVWF_SEQ09	CGATGGTGGACTCAGCCTGC
mVWF_SEQ10	GAACTTCTGCAGACCTGCGTAG
mVWF_SEQ11	GTGGTAGAGTACCATGATGGC
mVWF_SEQ12	GATGAGATAGTCAGCTACCTC
mVWF_SEQ13	CAGTACCTTTCTGAGCACAG
mVWF_SEQ14	CTCCTCTAGCTTGCCAGAGTC
mVWF_SEQ15	GATGAAGCCCAGCTGAGGATC
mVWF_SEQ16	CAAGCTTACTGGTAGCTGCTC
mVWF_SEQ17	GATGGCACGGTCACCACAGAC
mVWF_SEQ18	GATGGGAACACTAGCTTCTG
mVWF_SEQ19	CAGACCCACCTTTACCTGTG
mVWF_SEQ20	GAGTGCTGTGGAAGGTGCCTG
mVWF_SEQ21	GTTGACCTATGCACGACCTG
mVWF_SEQ22	GATGAACACAAGTGTCTGGCTG
mVWF_SEQ23	GATACACAGACAGGCTCATTC
mVWF_SEQ24	GTA CTCTGCACCCTGATGGAAG

5.1.11. Plasmids

For plasmid transfection of HEK293F cells the pIRESneo2 vector, containing the CDS of different human VWF variants, was used (**Table 7**). The vector harbors a resistance gene for carbenicillin for selection of the vector-containing bacteria during cloning and a resistance gene for the antibiotic G418 for selection of transfected HEK293F cells (**Figure 9**).

For hydrodynamic injection in VWF knock-out (KO) mice the pLIVE vector with the incorporated murine VWF gene was used. Kanamycin resistance was used for successful cloning and amplification of the plasmid (**Figure 9**).

Table 7: List of all plasmids. Expressed markers and proteins and the used application are given.

Name	Marker	Expression	Application
pIRES neo2	carbenicillin, G418	hVWF variants, GPIIb	transfection of HEK293F cells
pIRES hygroTO	hygromycin B	GPIIIa	transfection of HEK293F cells
pLIVE	kanamycin	mVWF variants	hydrodynamic injection in mice

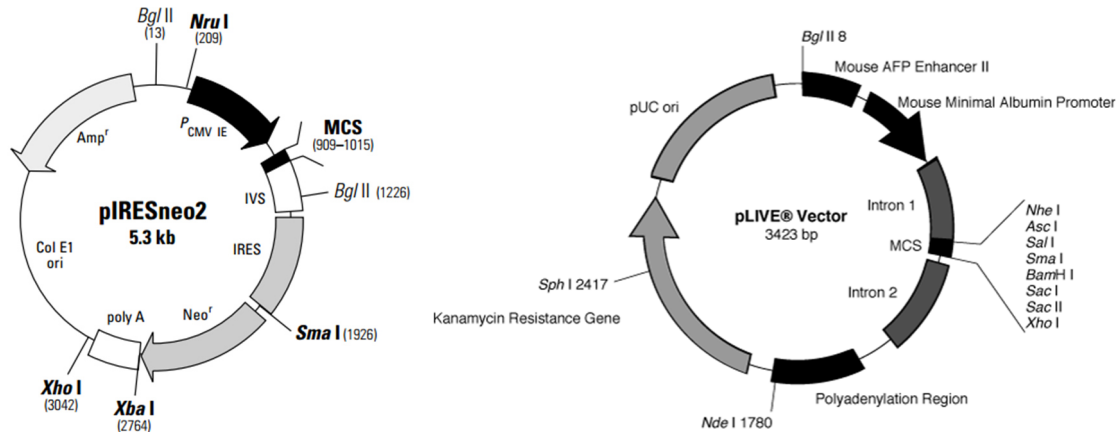


Figure 9: Structure of pIRESneo2 vector (from lifescience-market) and pLIVE vector (from MirusBio).

5.1.12. Kit systems and enzymes

Table 8: List of used kits and enzymes. The reference no., purpose and manufacturers are given.

Kit/Enzyme	Reference no.	Purpose	Company
Apyrase from potatoes	A6535	platelet isolation	Sigma-Aldrich (St. Louis, US)
BD OptEIA™ TMB Substrate Reagent Set	555214	detection of ELISA, substrate for HRP	BD BioSciences (Franklin Lakes, US)
DAB Substrate Kit, Peroxidase (HRP), with Nickel, (3,3'-diaminobenzidine)	SK-4100	multimer analysis	Vector Laboratories (Newark, US)
Invitrogen™ PureLink Quick Plasmid Miniprep Kit	K210011	miniprep	Thermo Fisher Scientifics (Waltham, US)
Invitrogen™ Qubit™ dsDNA BR Assay Kits	Q32853	dsDNA quantitation	Thermo Fisher Scientifics (Waltham, US)
Phusion™ Site-Directed Mutagenesis Kit	F542	mutagenesis	Thermo Fisher Scientifics (Waltham, US)
PrimeSTAR® HS DNA polymerase	R010B	mutagenesis	Takara (Kyoto, Japan)
QIAamp DNA Blood Mini Kit	51104	DNA purification from whole blood	QIAGEN (Hilden, Germany)
QIAGEN EndoFree® Plasmid Maxi Kit	12362	maxiprep	QIAGEN (Hilden, Germany)
QIAGEN Plasmid Midi Kit	12143	midiprep	QIAGEN (Hilden, Germany)
QuikChange Multi Site-Directed Mutagenesis Kit	200514	mutagenesis	Agilent Technologies (Santa Clara, US)

5.1.13. Antibodies

Table 9: List of primary antibodies. Manufacturer, host, application and dilution are given.

Target	Manufacturer	Host species	Application	Dilution
Abciximab	Invitrogen™ (MA5-41766)	chimeric human- murine monoclonal antibody 7E3	microfluidics	2.6 µg/mL
CD41-CD61 complex	Antibodies online (ABIN784612)	mouse	ELISA	1:1000
FLAG-Tag	Sigma-Aldrich (F13165)	mouse	ELISA	1:2000
PDI	abcam (ab2792)	mouse	IF	1:500
VWF	DAKO (A0082)	rabbit	ELISA, IF	1:500 or 1:1000
VWF-HRP	DAKO (P0226)	rabbit	ELISA	1:500

Table 10: List of secondary antibodies. Manufacturer, host, conjugation and dilution are given.

Target	Manufacturer	Host	Conjugation	Dilution
Rabbit IgG	DAKO (P0448)	goat	HRP	1:2000
Mouse IgG	DAKO (P0447)	goat	HRP	1:2000
Rabbit IgG	Invitrogen™ (A11034)	goat	Alexa Fluor™ 488	1:5000
Mouse IgG	Invitrogen™ (A11003)	goat	Alexa Fluor™ 546	1:5000

5.1.14. Software

Image J Software (Wayne Rasband, National Institutes of Health) was used for preparation of immunofluorescence images and for densitometric analysis of multimer gels. ZEN Software (Zeiss, Oberkochen) was used in microfluidic experiments to take images. The PyQtGraph-based custom software Clusterquant developed by Christian Meß (Dermatology and Venereology, UKE) was used for video analysis and quantification of platelet aggregates (Moore et al., 2023). Structures were visualized and investigated by UCSF Chimera, developed by the Resource for Biocomputing, Visualization, and Informatics at the University of California, San Francisco, with support from NIH P41-GM103311 (Pettersen et al., 2004). Predictions of the VWF dimer structure were performed by AlphaFold2 and AlphaFold2-Multimers (Evans et al., 2022; Jumper et al., 2021) on ColabFold (Mirdita et al., 2022). For visualization of data, GraphPad Prism 5 (Boston, US) and Microsoft Excel (Redmond, USA) was used. Mendeley Reference Manager (Elsevier, Amsterdam, NL) was used for citation.

5.2. Methods

5.2.1. Cell biological methods

5.2.1.1. Culturing cell lines

All cells were cultured in DMEM medium for cell culture at 37 °C in presence of 5 % CO₂. Stably transfected cells were additionally treated with either 500 µg/mL G418 (geneticin) or 250 µg/mL hygromycin B. Passage of the cells was performed when the cells reached a confluence of 80-100 %. Hence, the medium was removed, and the cells were washed with sterile PBS (phosphate-buffered saline). To detach the cells from the flask, 1 mL 0.05 % trypsin-EDTA (ethylenediaminetetraacetic acid) was added for 3 min. The reaction was stopped with the same amount of culture media. The suspension was centrifuged at 200 g for 5 min and the supernatant was discarded. The pellet was resuspended in culture medium and split to the desired ratio for further cultivation. The remaining cell suspension could be used for subsequent experiments.

5.2.1.2. Plasmid transfection with Lipofectamine LTX

Plasmid transfection was performed with Lipofectamine™. HEK293F cells were seeded on a cell culture dish in a cell density according to **Table 11**.

Table 11: Compilation of transfection reagents. The used cell culture dish, cell density, amount of DNA, PLUS reagent and LTX in Opti-MEM and cell culture medium is given.

Cell culture dish	Cell density	DNA	PLUS reagent	LTX	Opti-MEM	Medium
8-well	50 000	0.25 µg	0.17 µL	0.5 µL	12.5 µL	250 µL
6-well	500 000	1.6 µg	1 µL	3.2 µL	80 µL	1,2 mL
T25	1 500 000	4 µg	2,66 µL	8 µL	200 µL	5 mL

Attachment of the cells was allowed for 24 h. The transfection solution was prepared in Opti-MEM with addition of plasmid DNA and PLUS reagent and incubated for 5 min at room temperature (RT). Subsequently, LTX was added and incubated for another 35 min. The transfection suspension was added to the cells with fresh culture medium and left for 24 h. Cells were washed with PBS and cultured in DMEM medium. These transiently transfected cells were either used for secretion experiments or stained for

immunofluorescence imaging. For stable transfection, a treatment with the antibiotic G418 (500 µg/mL) or hygromycin B (250 µg/mL) for at least 2 weeks was conducted.

5.2.1.3. VWF secretion experiments

Secretion of VWF variants was investigated in transiently transfected HEK293F cells. 24 h after transfection, cells were washed with PBS and protein secretion was allowed for 24 h in 1.6 mL serum-free medium for cell culture. Protein containing cell supernatant was collected. PMA-induced secretion was investigated subsequently for 2 h in presence of 200 ng/mL PMA in 1.6 mL serum-free medium for cell culture. Collected samples were centrifuged for 5 min at 300 g to remove remaining cells and VWF concentrations were determined by VWF:Ag ELISA.

5.2.2. Protein biochemical methods

5.2.2.1. Expression of recombinant VWF

Recombinant VWF protein was obtained from stably transfected HEK293F cells. These cells are cultivated in DMEM medium for cell culture supplemented with 500 µg/mL G418 to ensure the incorporation of the resistance gene and hence the VWF gene with the variant of interest.

HEK293F cells are seeded on several T-175 flasks and cultured to a confluence of 70-80 %. Medium is discarded, cells are washed with PBS and secretion of VWF into the serum-free medium for cell culture is allowed for 72 h. The supernatant from several flasks with the same HEK293F cells are pooled and centrifuged at 300 g for 5 min to remove residual cells or cell debris from the supernatant. The supernatant is referred to as unconcentrated VWF sample. For stabilization of the protein 1x cOmplete™ Mini, EDTA-free Protease Inhibitor Cocktail was added and samples were stored at -80 °C.

5.2.2.2. Concentration of VWF protein

Unconcentrated VWF samples harvested from cell culture were concentrated via size-based filtration using Amicon® Ultra 15 mL Centrifugal Filters with a molecular weight cut-off of 100 kDa. The filtration was conducted through a series of successive centrifugation steps at 4 °C and 4200 rpm, with the duration gradually increasing from 5 min to 45 min. In this way, unconcentrated VWF samples were concentrated by

approximately a factor of 100. The sample was dissolved from the Amicon® membrane by pipetting up and down and transferred to a fresh tube. Centrifugation for 5 min at 4200 rpm was performed to remove any membrane particles or aggregates. The supernatant was supplemented with 1x cOmplete™ Mini, EDTA-free Protease Inhibitor Cocktail for stabilization of the protein and concentrated VWF samples were stored at -80 °C.

5.2.2.3. Dialysis of VWF samples

To clean the VWF samples from any other smaller proteins and molecules present in the collected cell culture medium, dialysis was performed. A dialysis membrane with a pore size of 300 kDa was prepared by pre-wetting in double distilled H₂O (ddH₂O) and rinsing several times, followed by an incubation for 30 min. Subsequently, 1-2 mL of a VWF sample was loaded into the dialysis tubing and placed into 4.5 L of 5 mM Tris-HCl pH 8 overnight at 4 °C. Samples were stored at -80 °C and concentration was determined by VWF:Ag ELISA.

5.2.2.4. Determination of VWF concentration

To determine the concentration of unconcentrated, concentrated and dialyzed VWF samples a VWF:Ag ELISA was used. For this, 96-well microtiter plates were coated overnight at 4 °C with polyclonal rabbit anti-hVWF antibody diluted 1:1000 in coating buffer. The next day, the wells were washed three times with washing buffer and VWF samples were added at appropriate dilutions of 1:100-1:400 for unconcentrated and 1:3000-1:12000 for concentrated samples in sample buffer. Noteworthy, standard plasma was used as reference at a concentration of 0.2 µg/mL and in a stepwise 1:2 dilution series. Samples were allowed to bind for 1 h at 37 °C, followed by three wash steps. To detect bound VWF, an HRP-conjugated polyclonal rabbit anti-hVWF antibody diluted 1:2000 in sample buffer was added for 1 h at 37 °C. Subsequent addition of TMB (3,3',5,5'-tetramethylbenzidine) substrate led to a blue color development within 2-5 min, which was stopped with 0.5 M sulfuric acid. The resulting color change to yellow was detected with an ELISA plate reader at 450 nm. VWF quantification of the samples was calculated by regression of the standard dilution series. The VWF:Ag ELISA was

repeated three times in triplicate with a maximum deviation of 5 % to ensure the correct VWF concentration.

5.2.2.5. Functional assays

The produced VWF variants were first characterized for their function *in vitro*. Common features of VWF, such as binding to the interaction partners collagen type III or the platelet receptors GPIb α and GPIIb/IIIa, were investigated under static conditions by ELISA. For all ELISA common buffers were used as described in **Table 4**. Each experiment was conducted in triplicate using samples of the same protein batch, with three repetitions per experiment. The conduction of ELISAs for variants p.Pro2302Arg/Thr, p.Pro2373Arg/Ser, p.Phe2481Tyr and p.Tyr2631Phe was supported by bachelor student Niko Remmert (University of Siegen, Germany).

5.2.2.5.1. Collagen binding ELISA

For the measurement of collagen binding, a 96-well plate was coated with 3 $\mu\text{g}/\text{mL}$ Human Collagen Type III in PBS overnight at 4 °C, washed three times with washing buffer and blocked 1 hour with blocking buffer at RT. Subsequently, VWF samples were incubated in a concentration of 0.75 ng/mL for one hour at RT. After washing three times, VWF binding to collagen was detected by incubation with a polyclonal anti-hVWF antibody (1:500) and an HRP-conjugated secondary goat anti-rabbit antibody (1:2000), each diluted in blocking buffer, for 1h at RT. Catalysis of the HRP substrate TMB was allowed for 2-5 min and stopped by addition of 0.5 M sulfuric acid. Quantification of the binding capacity was determined by measuring the optical absorbance at 450 nm in comparison to a wildtype sample.

5.2.2.5.2. GPIb α binding ELISA

Binding of different VWF variants to platelet receptor GPIb α was investigated either with wildtype GPIb α fragment in presence of different ristocetin concentrations or with a GOF GPIb α fragment harboring the mutations p.Gly233Val and p.Met239Val (mutant GPIb α -Gly233Val/Met239Val, hereafter abbreviated as mut-GPIb α) (Patzke et al., 2014). First, a 96-well plate was coated with 100 $\mu\text{L}/\text{well}$ mouse anti-FLAG monoclonal antibody clone M2 diluted 1:2000 in PBS and incubated overnight at 4 °C. The next day, the plate

was washed three times with washing buffer and blocked 1 h with blocking buffer. FLAG-tagged fragments of the GPIIb α protein diluted 1:10 in blocking buffer were allowed to bind for 1 h. Hereby, either GPIIb α or mut-GPIIb α fragment was used. After washing three times, 0.75 μ g/mL VWF samples were added in presence of 0.0 mg/mL, 0.3 mg/mL, 0.6 mg/mL or 1.0 mg/mL ristocetin and incubated for 1 h. For detection, the washed plate was incubated with a primary polyclonal anti-hVWF antibody (1:500) and an HRP-conjugated secondary goat anti-rabbit antibody (1:2000), each diluted in blocking buffer, for 1 h at RT. For detection, HRP substrate TMB was added for 2-5 min and the reaction was stopped by addition of 0.5 M H₂SO₄. Quantification of the binding capacity was determined by measuring the optical absorbance at 450 nm in comparison to a wildtype sample.

5.2.2.5.3. GPIIb/IIIa binding ELISA

The binding of VWF to the platelet receptor GPIIb/IIIa was performed according to König et al. (König et al., 2019). This method relies on HEK293F cells expressing GPIIb/IIIa after stable integration of the genes for integrins α_{IIb} and β_3 . Under physiological conditions, GPIIb/IIIa requires an inside-out signal that results in structural change and activation of the receptor in order to bind to VWF. The constitutively active mutant with the single missense mutation p.Thr588Asn incorporated in the integrin β_3 mimics the active conformation of the receptor (Kashiwagi et al., 1999) and is used to measure binding to VWF without the need of an inside-out signaling.

96-well plates are coated overnight at 4°C with 100 μ L/well polyclonal rabbit anti-hVWF antibody diluted 1:1000 in coating buffer. After three times of washing with washing buffer, 1 μ g/mL VWF samples were incubated for 1h at 37 °C, followed by incubation with $7.5 \cdot 10^5$ cells/mL in serum-free medium for 1 h at 37 °C and 5 % CO₂. Unbound cells were carefully washed away by washing twice with washing buffer and remaining bound cells were fixed with 3 % paraformaldehyde in PBS for 10 min at 37 °C. Unspecific binding sites were blocked with blocking buffer for 1 h at 37 °C. HEK293F cells were detected by incubation with the mouse anti-CD41-61 primary antibody (1:1000) and goat anti-mouse HRP-conjugated secondary antibody (1:2000) in blocking buffer for 1 h each. Addition of HRP substrate TMB allowed colorimetric detection. The reaction was stopped after 2-5 min by addition of 0.5 M H₂SO₄. Quantification of the binding capacity was

determined by measuring the optical absorbance at 450 nm in comparison to a wildtype sample.

5.2.2.5.4. Multimer analysis

For multimer analysis of recombinant hVWF, samples were sent to MEDILYS GmbH, Hamburg, Germany, and were kindly investigated by Dr. Sonja Schneppenheim.

Multimer analysis of murine VWF (mVWF) was performed at the INSERM Unit 1176 (Le Kremlin Bicêtre, France) in the Group of Dr. Cécil Denis. The gel was casted with a running gel, containing 1 % Seakem® HTG Agarose and 1 % Agarose IEF in running gel buffer, and a stacking gel containing 1 % Seakem® HTG Agarose in stacking gel buffer. 2.5 µg/mL murine plasma samples were prepared in sample buffer, heated to 65 °C for 15 min and centrifuged at 10,000 g for 5 min at RT. Electrophoresis was performed at 57 V for 21 h by using an anode buffer consisting of 1x electrophoresis buffer, and a cathode buffer containing 0.1 % SDS in 2x electrophoresis buffer. Size-separated samples were transferred from the gel to a PVDF membrane. The membrane was preactivated by 5 min incubation in methanol, washed with PBS and assembled into a 'sandwich' using Whatman filter papers. Transfer was performed in a capillary blotter overnight. The membrane was washed with 0.1 % Tween20 in PBS and detected by the stepwise incubation with 1:7500 rabbit anti-hVWF and 1:2000 HRP-conjugated goat anti-rabbit antibody in 0.1 % Tween20 in PBS for 2 h at RT on an orbital shaker. The membrane was washed four times with 0.1 % Tween20 in PBS and once with PBS for 15 min before detection. Bands were visualized by incubation with DAB and stopped by rinsing with water. Membranes were dried and scanned for digitization.

5.2.2.5.5. Static ADAMTS13 cleavage

ADAMTS13 is a VWF-specific cleavage protease that degrades VWF multimers into smaller fragments. Efficient degradation depends on VWF structure, especially the accessibility of the A2 domain. Hence, investigations of the rate of degradation by ADAMTS13 can not only reflect the multimer state in plasma, but also give a hint to structural changes in the VWF protein.

Dialyzed VWF samples with a final concentration of 5 µg/mL were incubated with 500 ng/mL ADAMTS13 in 5 mM Tris-HCl pH 8.0 at 37 °C shaking. 50 µL samples were collected after 5 h, 24 h and 48 h and mixed with 450 µL stop buffer (25 mM Tris-HCl, 150 mM NaCl, 1 % BSA, 10 mM EDTA pH 7.4). Multimer analysis was performed by Dr. Sonja Schneppenheim (MEDILYS GmbH, Hamburg, Germany).

5.2.2.6. Immunofluorescence

Immunofluorescence staining was conducted in 8-well ibidi µ-Slides. Cells were washed with PBS, and 3 % PFA in PBS was added to fix the cell membrane and proteins. After washing with PBS, the cell membranes were permeabilized with 0.1 % Triton™ X-100 in PBS. The cells were washed again with PBS and 5 % BSA in PBS was added for 1 h to block unspecific interaction sites. Subsequently, the cells were incubated overnight with different primary antibodies diluted in PBS under their respective incubation conditions (see **Table 9**). After incubation, the cells were washed three times for 5 min with PBS and incubated with secondary antibodies diluted in PBS for 1 h at RT (see **Table 10**). Cells were washed again three times for 5 min with PBS and analyzed with Olympus FV3000 microscope at the UKE Microscopy Imaging Facility (UMIF) (DFG Research Infrastructure; RI_00489).

5.2.3. Molecular biological methods

5.2.3.1. Quantity and Quality measurement of nucleic acids

The DNA concentration was determined by the Qubit® 2.0 fluorometer using the Qubit™ dsDNA BR Assay Kit. The working solution containing 198 µL Qubit™ dsDNA BR Buffer and 1 µL Qubit™ dsDNA BR Reagent (200x) was incubated with 1 µL of DNA sample and measured in a 0.5 mL tube.

5.2.3.2. Mutagenesis of VWF coding sequence

Mutagenesis of the CDS of hVWF in the pIRES neo2 vector was performed with Phusion Site-Directed Mutagenesis. Mutagenesis was only successful for variant p.Pro2558Ser. Forward and reverse primers were designed with a length of approx. 25 bp and the aa exchange located in the middle of the primer.

Remaining desired variants were obtained by mutagenesis with QuikChange Multi Site-Directed Mutagenesis Kit (Agilent Technologies). One gene-specific forward mutagenesis primer was designed to induce a single point mutation. These primers had a length of approx. 40 bp and harbor the mutation in the middle of the primer.

QuikChange Multi Site-Directed Mutagenesis Kit (Agilent Technologies) was similarly used for mutagenesis of mVWF in pLIVE vector.

The mutagenesis includes PCR amplification with mutagenesis primers, a DpnI digestion and the transformation into MACH1T1 competent *E. coli* cells for isolation of individual plasmids.

5.2.3.2.1. PCR with Phusion Site-directed mutagenesis

Each reaction consists of 150 ng template DNA, 200 μ M dNTPs, 0.5 μ M forward and reverse primer, and 0.02 U/mL Phusion Hot Start DNA Polymerase in 1x Phusion HF Buffer. PCR was performed by using initial denaturation at 98 °C for 2 min, followed by 32 cycles of denaturation at 98 °C for 10 sec, annealing at 63 °C for 30 sec, and extension at 72 °C for 10.5 min. Final extension was performed for 10 min at 72 °C (**Table 12**).

Table 12: Cycling parameters for mutagenesis with the Phusion Site-directed mutagenesis Kit.

Phase	Temperature	Time
Initial denaturation	98 °C	2 min
<u>Cycle 32x</u>		
Denaturation	98 °C	10 sec
Annealing	63 °C	30 sec
Extension	72 °C	10.5 min
Final Extension	72 °C	10 min

5.2.3.2.2. PCR with the QuikChange Multi site-directed mutagenesis

Each reaction was set up with 2.5 μ L of 10x QuikChange Multi reaction buffer, 1 μ L dNTP mix, 100 ng of the corresponding mutagenic primer, 100 ng plasmid template, 0-0.75 μ L QuikSolution and 0.5 U QuikChange Multi enzyme blend to a total volume of 25 μ L. Mutagenesis of Trp2521 to glycine was only successful after utilizing 1 U PrimeSTAR® HS DNA polymerase instead of QuikChange Multi enzyme. Amplification was started with

an initial denaturation at 95 °C for 3 min followed by 40 cycles of 95 °C for 30 sec, 55 °C for 1 min and 65 °C for 28 min. (**Table 13**).

Table 13: Cycling parameters for mutagenesis with QuikChange Multi Site-Directed Mutagenesis Kit.

Phase	Temperature	Time
Initial denaturation	95 °C	3 min
<u>Cycle 40x</u>		
Denaturation	95 °C	30 sec
Annealing	55 °C	1 min
Extension	65 °C	28 min

5.2.3.2.3. DpnI digestion

DpnI digestion was performed to disrupt the methylated template DNA that did not contain the desired mutation, leaving the newly synthesized, unmethylated DNA strands intact. According to the manufacturer's instructions, 1 µL DpnI was added to 25 µL PCR product and incubated at 37 °C for 1 h.

5.2.3.2.4. Agarose gel electrophoresis

Agarose gels were cast with 1.5 % agarose and 1x ROTI® GelStain in 1x Tris-acetate-EDTA (TAE) buffer. Samples were mixed with 1xTriTrack DNA Loading Dye. Size distinction was performed by application of GeneRuler DNA Ladder Mix. The gel was run in 1x TAE buffer at 120 V for 30 min. Documentation was done with the Azure 400 Fluorescent Western Blot Imager.

5.2.3.2.5. Sequencing of pIRES neo2 VWF plasmids

For sequencing of the plasmid DNA of human VWF, 32 gene specific primers were designed to amplify the whole cDNA of VWF. The reaction was prepared with 3 µL sequencing buffer, 1.5 µL Big Dye, 1 µL primer and 500 ng DNA in 20 µL Aqua. Amplification was started with an initial denaturation at 95 °C for 3 min and 99 cycles of 95 °C for 30 sec, 52 °C for 30 sec and 60 °C for 4 min (**Table 14**). The amplified product was sequenced by Florian Oyen (Pediatric Hematology and Oncology, UKE Hamburg).

Table 14: Cycling parameters for amplification of products for sequencing.

Phase	Temperature	Time
Initial denaturation	95 °C	3 min
<u>Cycle 99x</u>		
Denaturation	95 °C	30 sec
Annealing	52 °C	30 sec
Extension	60 °C	4 min

5.2.3.3. Sequencing of Exon 45 from patient DNA samples

Blood samples from 522 patients were collected by Prof. Dr. Dursun Gündüz (Head Physician of Medical Clinic for Cardiology, Angiology and Rhythmology at the Jung-Stilling Diakonie Hospital in Siegen, Germany). DNA was isolated and exon 45 of VWF was amplified by PCR. Results were controlled by agarose gel electrophoresis and Sanger sequencing was performed by Eurofins Scientific SE (Luxembourg) using the PlateSeq service.

5.2.3.3.1. DNA isolation

DNA was isolated from leukocytes from whole blood samples of collected citrated blood samples from patients using QIAamp DNA Blood Mini Kit (Qiagen, Hilden) following the manufacturer's protocol. Isolation was kindly performed by Katharina Albrecht, Leah Glowacki and Milena Grützmann (University of Siegen, Germany). Samples were stored at -20 °C.

5.2.3.3.2. Polymerase Chain reaction

PCR was set up to sequence exon 45. The binding sites of the forward and reverse primers are located in the introns at the 5' and 3' ends of exon 45, respectively. Each sequence reaction included 25 µL GoTaq® G2 Master Mix, 1 mM MgCl₂, 100 ng DNA, 10 pmol forward primer, 10 pmol reverse primer ad 50 µL Aqua. PCR was performed by using an initial denaturation at 95 °C for 5 min, followed by 35 cycles of denaturation at 95 °C for 40 sec, annealing at 65 °C for 30 sec and extension at 72 °C for 1 min. Final extension was performed for 5 min at 72 °C.

The correct size of PCR products was confirmed using agarose gel electrophoresis as described in 5.2.3.2.4.

5.2.3.3.3. PCR purification

PCR products were purified by ExoI and FastAP treatment. The reaction included 10 µL PCR product, 3.8 µL Aqua, 0.8 µL FastAP and 0.4 µL ExoI and was incubated at 37 °C for 45 min. Heat inactivation of the enzymes was performed at 85 °C for 15 min.

5.2.3.3.4. Sequencing of Exon 45

Approximately 15-75 ng of purified PCR product and 20 pmol reverse primer were diluted in Aqua to a total volume of 17 µL. Samples were sequenced by Eurofins Scientific SE (Luxembourg) using the PlateSeq service.

5.2.4. Microbiological methods

5.2.4.1. Transformation of MACH1T1 competent *E. coli*

For transformation 50 µL One Shot™ Mach1™ T1 Phage-Resistant Chemically Competent *E. coli* were thawed on ice for 20 min and incubated with 5 µL of the plasmid for 30 min on ice. Heat shock was performed at 42 °C for 30 sec with subsequent incubation for 2 min on ice to allow uptake of the plasmid. The cells were recovered in 250 µL S.O.C. medium at 37 °C for 1 h at 225 rpm, plated on Lysogeny *broth* (LB) agar plates containing 0.1 mg/mL carbenicillin or 0.1 mg/mL kanamycin and incubated overnight for cultivation of single colonies.

5.2.4.2. Plasmid isolation

Colonies were picked from agar plates and cultivated overnight in 2 mL LB medium containing 0.1 mg/mL carbenicillin or 0.1 mg/mL kanamycin for enrichment of the cell mass. The next day, plasmids were isolated with PureLink™ Quick Plasmid MiniPrep-Kit according to the manufacturer's protocol. For higher plasmid yields, *E. coli* were grown in 24 mL LB medium or 200 mL LB medium and plasmids were isolated using QIAGEN Plasmid Plus Midi or Maxi Kit, respectively, according to the manufacturer's protocol. Quality and quantity of plasmid yield was evaluated with the Qubit® 2.0 Fluorometer (see 5.2.3.1).

5.2.5. Processing of blood samples

5.2.5.1. Platelet Isolation from Buffy coat

Buffy coat samples from healthy donors were collected from the Institute of Transfusion Medicine (UKE, Hamburg, Germany). Approximately 50 mL Buffy coat from a 500 mL whole blood donation was obtained. 0.65 U/mL apyrase and Tyrode's buffer ad 100 mL was added and centrifuged at 2700 rpm for 15 min at RT with a decreased deceleration of = 4. The supernatant was discarded without disturbing the platelet-rich layer. The washing procedure was repeated three times by addition of Tyrode's buffer ad 100 mL and apyrase. The apyrase concentration is stepwise halved each wash step to 0.325 U/mL and 0.1625 U/mL. The last wash step contains no apyrase. The washed platelets are resuspended by addition of resuspension buffer ad 50 mL and centrifuged at 2700 rpm for 15 min at RT with a decreased deceleration of = 4. The platelet-rich layer is collected, and platelet concentration is determined using the hematology analyzer Cell-dyne Emerald of the Department of Pediatric Hematology and Oncology (UKE, Hamburg, Germany).

5.2.5.2. Platelet Isolation from whole blood donations

Fresh whole blood is collected from healthy donors in sodium citrate tubes with a 20G gauge needle. After incubation for 30 min at RT the blood is separated into its different components by centrifugation at 120 g for 15 min at RT with a decreased acceleration and deceleration to 1 and 0, respectively. Platelet-rich plasma is collected and added to the same volume of Tyrode's buffer including apyrase in a final concentration of 1 U/mL. The platelet suspension is centrifuged again at 1200 g for 15 min under the same centrifugation conditions. The supernatant is discarded, and the platelets are resuspended in 1 mL Tyrode's buffer. Staining is performed by addition of CellTrace™ Calcein Green, AM. After incubation for 10 min in the dark, 10 mL Tyrode's buffer including 1 U/mL apyrase is added and platelets are pelleted by centrifugation as described above. The supernatant is discarded, and the platelet pellet is resuspended in 500 µL resuspension buffer. The platelet count is determined by the hematology analyzer Cell-dyne Emerald of the Department of Pediatric Hematology and Oncology (UKE, Hamburg, Germany).

5.2.5.3. Isolation of erythrocytes from full blood donations

Blood is collected and separated in its individual components as described in 5.2.5.2. After removal of the platelet-rich plasma, the remaining buffy coat is discarded generously. Remaining erythrocytes are washed with the double volume of HEPES buffer and centrifuged at 800 g for 15 min. The supernatant is discarded, and three additional washing steps with HEPES are performed. The isolated erythrocytes are considered as 100 % hematocrit and used in subsequent microfluidic experiments.

5.2.6. Light transmission aggregometry (LTA)

For determination of the adhesion of platelets to different VWF variants and the platelet agglutination under mechanical shear, light transmission aggregometry (LTA) was used. 300.000/ μ L isolated platelets from buffy coat, 10 μ g/mL VWF and 1 μ M CaCl₂ is solved in resuspension buffer and analyzed in the light transmission aggregometer. Platelet agglutination was induced by addition of 0.3 or 0.6 mg/mL ristocetin, and dissolution of the platelet agglutinates was achieved by addition of 1000 U/mL recombinant ADAMTS13. Agglutination curves were analyzed for spontaneous agglutination, maximum agglutination, and agglutinate stability in presence of ADAMTS13. Each experiment was repeated at least three times including different donor blood samples.

5.2.7. Microfluidic methods

Microfluidic experiments are performed with the BioFlux System. A 48-well plate for 0-200 dyne/cm² is coated with 50 μ g/mL of different VWF variants in HEPES buffer at 37 °C for 3 h. After rinsing with HEPES buffer, samples are pipetted into the inlet of the channel. Samples are composed of 45 % hematocrit, 20 μ g/mL VWF and 250.000/ μ L platelets. A stepwise increase in shear is applied including 10, 20, 40, 60, 80, 100 and 120 dyne/cm². Platelet adhesion and platelet aggregate formation is observed in real time with an Axio Observer Microscope by detecting the fluorescence of calcein-green-labeled platelets at 488 nm in a time series with 8 frames/sec. Detection of aggregates is performed automatically by using the Clusterquant software provided by Christian Meß from the Department of Dermatology and Venereology (UKE, Hamburg, Germany).

5.2.8. *In vivo* animal experiments

Animal experiments were conducted at the INSERM Unit 1176 (Le Kremlin Bicêtre, France) in the group of Dr. Cécile Denis according to national guidelines. Experiments were performed by Dr. Cécile Denis, Dr. Peter Lenting and Eloïse Pascal and myself. I contributed to the handling of the mice, determination of mVWF:Ag and mVWF multimerization, and performance of the tail-clip assay. Experiments were performed for VWF GOF variants p.Phe2561Tyr and p.Pro2555Arg. Both aa positions are conserved in mice. Thus, the same positions were mutated for mVWF as for hVWF. Mutagenesis was performed as described in 5.2.3.2. To investigate the impact of mVWF variants in comparison to wildtype mVWF in an *in vivo* model, five to eight-week-old VWF-KO mice with a C575BL/6 background were used (Denis et al., 1998). Expression of mVWF was achieved by hydrodynamic injection of a mVWF coding pLIVE vector into the mice's tail vein, and confirmed three days after injection by mVWF:Ag ELISA and multimer analysis (5.2.2.5.4). The impact of VWF variants was investigated on day four. Tail-Clip was performed to investigate the impact on bleeding events and hemostasis. Impacts on thrombosis were investigated by induced vessel damage with ferric chloride (FeCl₃).

5.2.8.1. Hydrodynamic injection

A total volume of 10 % of the body weight, which corresponds to approximately 2 ml, with 100 µg pLIVE vector containing the mVWF-CDS was injected into the tail vein of the mice within 5 seconds (Casari et al., 2013). Mice were left under observation for 20 min.

5.2.8.2. Detection of mVWF:Ag in mouse blood samples

Mouse blood samples were collected on day three. Mice were anesthetized with isoflurane and approximately 200 µL of blood were taken retrobulbar. 10 % Sodium citrate was added to the sample as an anticoagulant. Blood samples were centrifuged at 1,500 g for 20 min at RT, and plasma was collected and frozen at -80 °C.

For mVWF:Ag ELISA, 5 µg/mL rabbit anti-hVWF was prepared in a buffer containing 10 mM NaHCO₃ and 50 mM Na₂CO₃ at pH 9.6. 50 µL/well and coated onto ½ well ELISA plates overnight at 4 °C. The plate was washed four times with 100 µL/well wash buffer containing 0.1 % tween 20 in PBS and subsequently blocked with 75 µL/well 3 % BSA in

wash buffer. Samples and murine pooled normal plasma (mPNP) as a standard were thawed at 37 °C and pipetted at stepwise dilutions of 1:25 to 1:6000 and 1:10 to 1:640, respectively. After incubation at 37 °C for 2 h, the plate was washed four times with wash buffer containing 0.1 % tween 20 in PBS und incubated with 50 µL/well HRP-conjugated rabbit anti-hVWF antibody in a dilution 1:6000 in 0.1 % BSA in PBS. Establishment of the signal was allowed for 5 min by addition of freshly prepared BD OptEIA™ TMB Substrate Reagent, according to the manufacturer's protocol. Reaction was stopped by addition of 2 N H₂SO₄ and read in the HT3 Microtiter Plate Reader Model 12 600 at an absorbance of 450 nm.

5.2.8.3. Tail-clip assay

Tail-clip assays were performed to investigate the general bleeding time and blood loss. Mice were anesthetized with intraperitoneal injection of 100 µg/g ketamine and 10 µg/g xylazine. 3 mm of the tail was cut off and the injured tails were placed immediately in 0.9 % sodium citrate. Bleeding time was recorded, and lost blood was collected for 20 min. After the experiment, the mice were sacrificed by cervical dislocation. Collected blood samples were centrifuged at 1,500 g for 20 min and the supernatant was discarded. Erythrocytes were lysed by addition of 10 mL ddH₂O and vortex to a homogeneous solution. The amount of hemoglobin was determined colorimetrically by measuring of the absorption at 416 nm.

5.2.8.4. Thrombosis model

In short, C575BL/6 VWF-deficient mice with a VWF-KO were hydrodynamically injected with the mVWF pLIVE vector (as described in **5.2.8.1**). Thrombosis is induced on the right common carotid artery by ferric chloride. A doppler flow probe connected to a flowmeter is used to measure the flow of the artery as previously described by Tang et al. (Tang et al. 2020). A reduction in flow by 90 % is considered as occlusion.

5.2.9. Statistics

Statistics were performed using the one-sided or unpaired two-tailed t-test. Significant results were obtained with p-values <0.05, marked by one asterisk (*), <0.01, marked by two asterisks (**) or <0.001, marked by three asterisks (***)

6. RESULTS

6.1. Identification of novel VWF GOF variants

Previous studies by Schneppenheim et al. and Huck et al. have identified GOF variants in the C4 domain of VWF that may have a prothrombotic effect, in contrast to the well-known GOF variants in the A1 domain causing VWD type 2B (Huck et al., 2022; Schneppenheim et al., 2019). *In vitro*, these variants, p.Phe2561Tyr and p.Pro2555Arg, promote the early onset of platelet aggregates at low shear rates and increase platelet aggregate size, respectively. The occurrence of myocardial infarction (MI) was previously shown to correlate with the prevalence of variant p.Phe2561Tyr in patients with coronary artery disease (CAD). However, the exact prothrombotic mechanism remains to be unraveled.

To this end, one part of this study aims to identify additional single nucleotide variants of VWF that could help to narrow down the specific region responsible for the GOF effect and provide insight into the mode of action of GOF variants. Three different strategies were pursued to identify novel GOF variants in the VWF stem region composed of repetitive VWC-domains. The following section outlines the strategies employed and the resulting variants characterized in this study.

6.1.1. Selection of VWF variants in the C4 domain

To identify novel GOF variants the first approach focused on known SNPs in the C4 domain of human VWF. Selection was based on the SNP database Ensembl (Hinxton, UK) and represents rare human SNPs with a mean allele frequency of <0.1. Particularly, attention was paid to aa exchanges causing a severe change in size or polarity of the side chain. Since >60 missense mutations are registered for the C4 domain, it was necessary to restrict the selection. The NMR structure of the C4 domain was used, to assess the structural environment of the residues (Xu et al., 2019). Residues in different structural elements of the C4 domain were selected. Two in subdomain (SD) 1 (p.Glu2525Lys, p.Arg2535Gln, positions shown in **Figure 10A**) and twelve in SD2 (p.Pro2558Ser, p.Ser2564Arg, p.Glu2553Lys, p.Cys2557Tyr, p.Ser2559Leu, p.Gly2560Arg, p.Gly2560Ser, p.Ser2573Arg, p.Cys2574Arg, p.Cys2574Phe, p.Arg2575Cys and p.Arg2575His (positions

shown in **Figure 10B**). In total, 14 variants were chosen to be further investigated by this first approach.

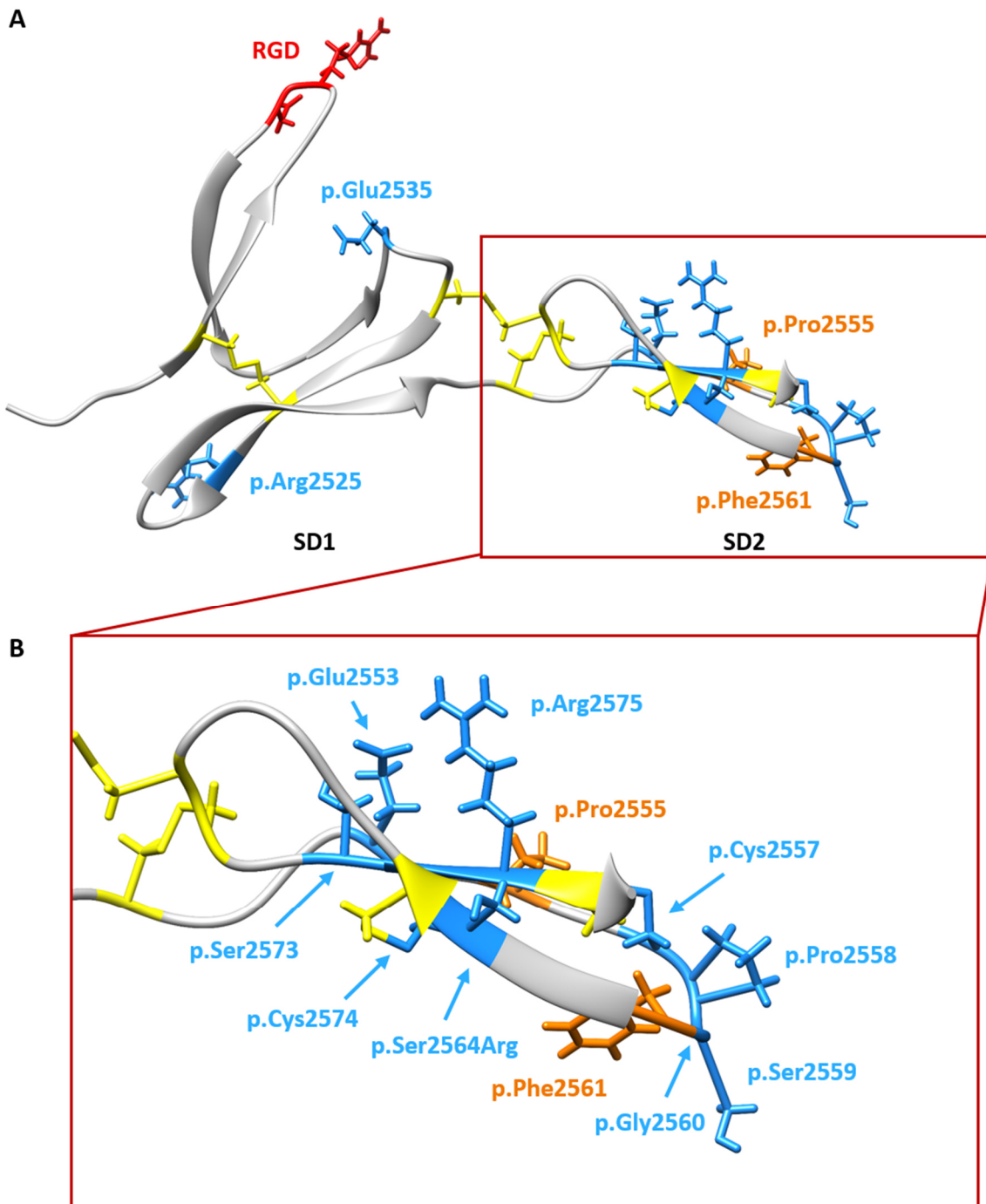


Figure 10: NMR structure of VWF C4 domain (A) with close-up of subdomain (SD) 2 (B) (PDB entry 6FWN). RGD motif (red), published GOF variants (orange), disulfide bonds (yellow) and selected residues (blue).

6.1.2. Selection of VWF variants in C domains other than C4

The second approach involved the investigation of variants in C domains of VWF other than C4. A sequence alignment of all C domains was used to select residues in C1, C2, C3 and C5, which represent equivalent residues to the two reported GOF variants p.Phe2561Tyr and p.Pro2555Arg (**Figure 11**). Based on the sequence alignment the position Pro2302 in C1 and Pro2373 in C2 were mutated to arginine, homogenously to variant p.Pro2555Arg. Additionally, one SNP in each of these positions was already reported in the Ensembl database, but with a different resulting aa. These SNPs p.Pro2302Thr and p.Pro2373Ser were likewise selected for further investigation. For position Phe2561 only one matching position was found in the sequence alignment, which is Phe2481 in the C3 domain. Accordingly, it was mutated to tyrosine. Interestingly, the matched aa in C5 is not a phenylalanine but a tyrosine in position 2631. Since the mutation of Phe2561 to tyrosine caused a GOF in the C4 domain, Tyr2631 was reversely mutated to phenylalanine.

VWFC1 2255	-----TQC - IGEDGVQHQL EAWVPD-----	HQPCQIC - TCLSGR -	2287
VWFC2 2334	-----LPPVPHCERGLQPTLTNPGE-----	CRPNFTCAC - R -	2363
VWFC3 2429	-----KVC --VHRSTIYPVGQFW-----	EEGCDVC - TCTDMED	2458
VWFC4 2497	-----SACEVVTGSP	RGD SQSSWKSVGSQWASPENPCLIN -	ECVRVKE 2538
VWFC5 2578	RM-----EAC --MLNGTVIGPGKTM-----	IDVCTTC - RCMVQVG	2610
VWFC6 2647	-----TACTIQLRGGQIMTLKRDETL-----	QDGC	DTHF - CKVNER 2681
VWFC1 2288	-----KVNCTTQPCPTAKAPT	CGLCEVARLRQNADQCCPEYECVCDPVSCD	2333
VWFC2 2364	-----KEE-----	CKRVSP	SCPPHRLPTLRKT - QCCDEYECACNCVNST 2402
VWFC3 2459	AVMGLRVAQCSQKPCEDS-----	CRS -	GFTYVLHEG - ECCGR - CLP - - - - - 2496
VWFC4 2539	---EV - F IQQRNVSCPQLEVP	VCPS -	GFQLSCKTS - ACCPS - - CRC - - - - - E2577
VWFC5 2611	VISGF - KLECRKTCNP - - - - -	CPL -	GYKEENNTG - ECCGR - - CLP - - - - - 2646
VWFC6 2682	G - - EY - FWEKRVTGCPPFDEHKCLAE	GGKIMKIPG -	TCCDT - - CEEP - - - - - 2722

Figure 11: Sequence alignment of VWF C domains (modified from Zhou et al. 2012). C domains are indicated in the first column of each row. First and last aa numbers are given at the beginning and end of each row. The aa are indicated in one-letter-code. RGD sequence for binding of GPIIb/IIIa is marked in red. Published GOF variants p.Phe2561Tyr and p.Pro2555Arg are marked in orange. Matching aa positions are highlighted in yellow.

Additionally, variants in the C5 and C6 domains, which have previously been pre-analyzed in experiments by our research group, were included for further investigation. In cone and plate aggregometry (CPA) experiments three variants that

caused an increase in platelet aggregate size were identified, namely p.Tyr2631Phe and p.Cys2671Tyr in C5 and p.Gly2705Arg in C6 (**Figure 12**).

Taken together, 8 variants were selected to be investigated by the second approach.

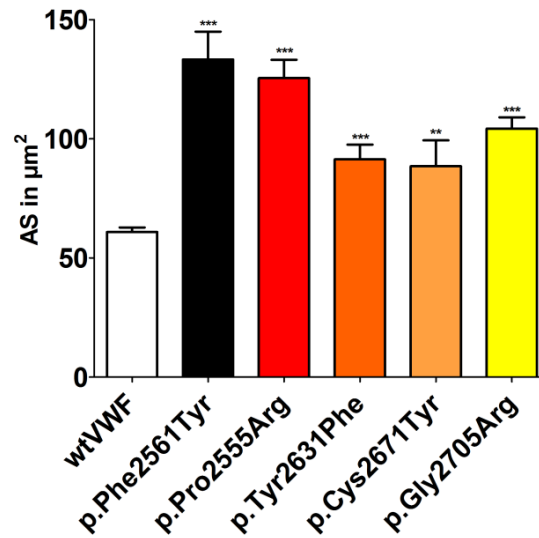


Figure 12: Cone-and-plate aggregometry of VWF variants. Citrated whole blood was washed and plasma was replaced with VWF-deficient plasma donated by an adult patient with Type 3 von Willebrand Disease and supplemented with 25 $\mu\text{g}/\text{ml}$ of the indicated recombinant VWF variants. Platelet aggregate size (AS) was determined by the internal software of the ImpactR CPA device. Mean values \pm SEM (standard error of the mean) are shown. Significance was calculated by one-sided t-test: $p = <0.05$ (*), <0.01 (**), <0.001 (***) (Experiments performed by Dr. Ulrike Klemm, Department of Pediatric Hematology and Oncology, UKE, Hamburg, Germany).

6.1.3. Identification of VWF variants in a patient cohort

In order to identify variants that are directly associated with the risk of developing myocardial infarction (MI), the third approach included a patient cohort of 522 patients with cardiovascular or rhythmic conspicuities, who were hospitalized in the Medical Clinic for Cardiology, Angiology and Rhythmology at the Jung-Stilling Diakonie Hospital in Siegen, Germany. Patients were divided into a control group of 236 patients and a disease group of 286 patients. The disease group is characterized by diagnosis of coronary artery disease (CAD). For each patient and control patient, genetic variations including SNPs, deletions, insertions or silent mutations in the exon 45 of VWF were determined by Sanger sequencing. This allowed to directly correlate genetic variations with the occurrence and severity of CAD and MI.

The common SNP p.Phe2561Tyr was found in 35 patients, which results in a prevalence of 6.7 %. Two out of 35 patients were identified carrying a homozygous p.Phe2561Tyr mutation. Additionally, a new SNP which results in a silent mutation changing the codon for the proline at position 2524 from CCG to CCA was identified in one patient. This patient is male, 42 years old and has neither been diagnosed with CAD nor did he suffer from MI. As the resulting aa remains unaltered, this patient was included into the wildtype group and the SNP was not further investigated. Moreover, a SNP which results in the aa exchange p.Ser2559Trp was found in one patient. The codon is changed from TCG to TGG. The patient is male, 44 years of age, has been diagnosed with two-vessel CAD and has experienced one MI. This SNP is listed in the Ensembl database (Hinxton, UK) with the variant number rs778732929. This SNP was selected to be characterized in detail in this study.

A detailed evaluation of the patient cohort and the correlation of variants with myocardial infarction is displayed in the section disease association (6.2).

6.1.4. Characterization of VWF variants

The selection of variants described above is summarized in **Table 15**. All selected variants were produced by transfection and expression from HEK293F cells and have been fully characterized. Secretion from HEK293F cells was investigated by VWF:Ag ELISA of the supernatant and multimer pattern and ADAMTS13 cleavage by Western blotting. Binding to common interaction partners, such as, collagen type III and the platelet receptors GPIIb/IIIa and GPIIb were quantified by ELISA. Ristocetin-induced platelet agglutination was measured in light transmission aggregometry (LTA) and platelet aggregate formation under shear forces was observed in real time by using immunofluorescence imaging of microfluidic channels. The results for all variants are subdivided by the type of experiment below.

Table 15: Selected variants. Location in domain, Ensembl number, chemistry of the initial and resulting side chain and size difference of the amino acids (aa) are given.

Domain	Variant	Ensembl no.	Chemistry of initial aa	Chemistry of resulting aa	Size difference of aa [g/mol]
C1	p.Pro2302Arg	not listed	hydrophobic	basic	+59
C1	p.Pro2302Thr	rs1478398589	hydrophobic	nucleophilic	+4
C2	p.Pro2373Arg	not listed	hydrophobic	basic	+59
C2	p.Pro2373Ser	rs148908677	hydrophobic	nucleophilic	-10
C3	p.Phe2481Tyr	not listed	aromatic	aromatic	+16
C4	p.Glu2525Lys	rs1249655559	acidic	basic	-1
C4	p.Arg2535Gln	rs137987906	basic	amid	-28
C4	p.Glu2553Lys	rs1211095597	acidic	basic	-1
C4	p.Cys2557Tyr	rs774929265	nucleophilic	aromatic	+60
C4	p.Pro2558Ser	rs373158962	hydrophobic	nucleophilic	-10
C4	p.Ser2559Leu	rs778732929	nucleophilic	hydrophobic	+26
C4	p.Ser2559Trp	rs778732929	nucleophilic	aromatic	+41
C4	p.Gly2560Arg	rs749106300		basic	+99
C4	p.Gly2560Ser	rs749106300		nucleophilic	+30
C4	p.Ser2564Arg	rs767664790	nucleophilic	basic	+69
C4	p.Ser2573Arg	rs192262780	nucleophilic	basic	+69
C4	p.Cys2574Arg	rs1475565311	nucleophilic	basic	+53
C4	p.Cys2574Phe	rs1374402576	nucleophilic	aromatic	+44
C4	p.Arg2575Cys	rs375991463	basic	nucleophilic	-53
C4	p.Arg2575His	rs373321657	basic	basic	-19
C5	p.Tyr2631Phe	not listed	aromatic	aromatic	-16
C5	p.Cys2671Tyr	rs61751303	nucleophilic	aromatic	+60
C6	p.Gly2705Arg	rs7962217		basic	+99

6.1.4.1. Secretion of VWF variants from HEK293F cells

Secretion of the VWF variants was studied *in vitro* by transfection of HEK293F cells with the pIRES neo2 vector harboring the cDNA of the selected VWF variants. The mutations were inserted using QuikChange site-directed mutagenesis. Concentration of secreted variants in the supernatant of transiently transfected HEK293F cells was determined after 24 h by VWF:Ag ELISA (**Figure 13**).

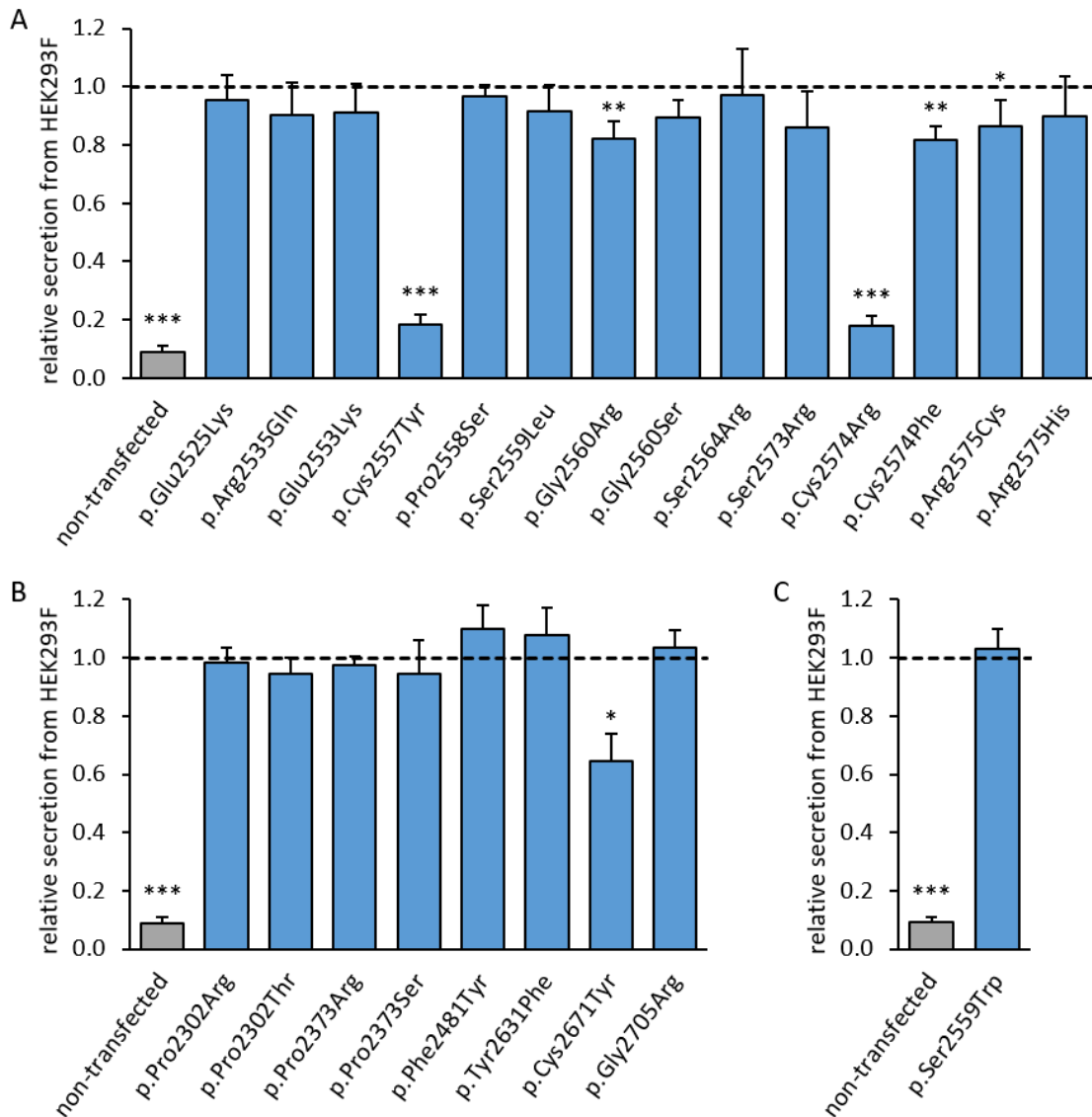


Figure 13: Secretion of VWF variants from HEK293F cells within 24 h. Cells after transient transfection with the expression vector pIRES coding for indicated VWF variants were grown in cell culture plates for 24 h. Supernatant was collected and VWF concentrations were determined by VWF:Ag ELISA. Values are given in relation to the wildtype, which is set to 1 and indicated as a dotted line. Mean values \pm SEM are shown. Significance was calculated by one-sided t-test: $p = <0.05$ (*), <0.01 (**), <0.001 (***). **(A)** Variants from approach 1 located in C4. **(B)** Variants from approach 2 located in C1, C2, C3, C5, C6. **(C)** Variant from approach 3 identified in a patient cohort.

The optical density (OD) at a wavelength of 450 nm is given in relation to the wildtype, which was set to 1. As negative control non-transfected HEK293F cells were used, which do not express the VWF protein. The relative OD of non-transfected HEK293F cells was 9 % and can be regarded as the background signal.

Variants p.Cys2557Tyr and p.Cys2574Arg were barely secreted with a relative expression of 18.3 % and 17.8 %, respectively. The secretion of variant p.Cys2671Tyr was significantly reduced to 65 %, indicating a secretion defect. The majority of the remaining variants displayed secretion that was close to normal. Variants p.Gly2560Arg, p.Cys2574Phe and p.Arg2575Cys showed a slight but significant decrease of secretion.

Secretion of VWF from HEK293F cells can be induced by different stimulators, such as the PKC activator phorbol 12-myristate 13-acetate (PMA) (Michaux et al., 2003). If secretion is not inducible, the expression, post-translational modification, packaging, or storage of VWF may be impaired, preventing the formation or release of VWF from pseudo-WPB. Secretion of VWF was stimulated with 200 $\mu\text{g}/\mu\text{L}$ PMA for 2 h and VWF:Ag levels were determined by ELISA (**Figure 14**). The values are given in relation to the secretion of corresponding VWF variants by unstimulated cells.

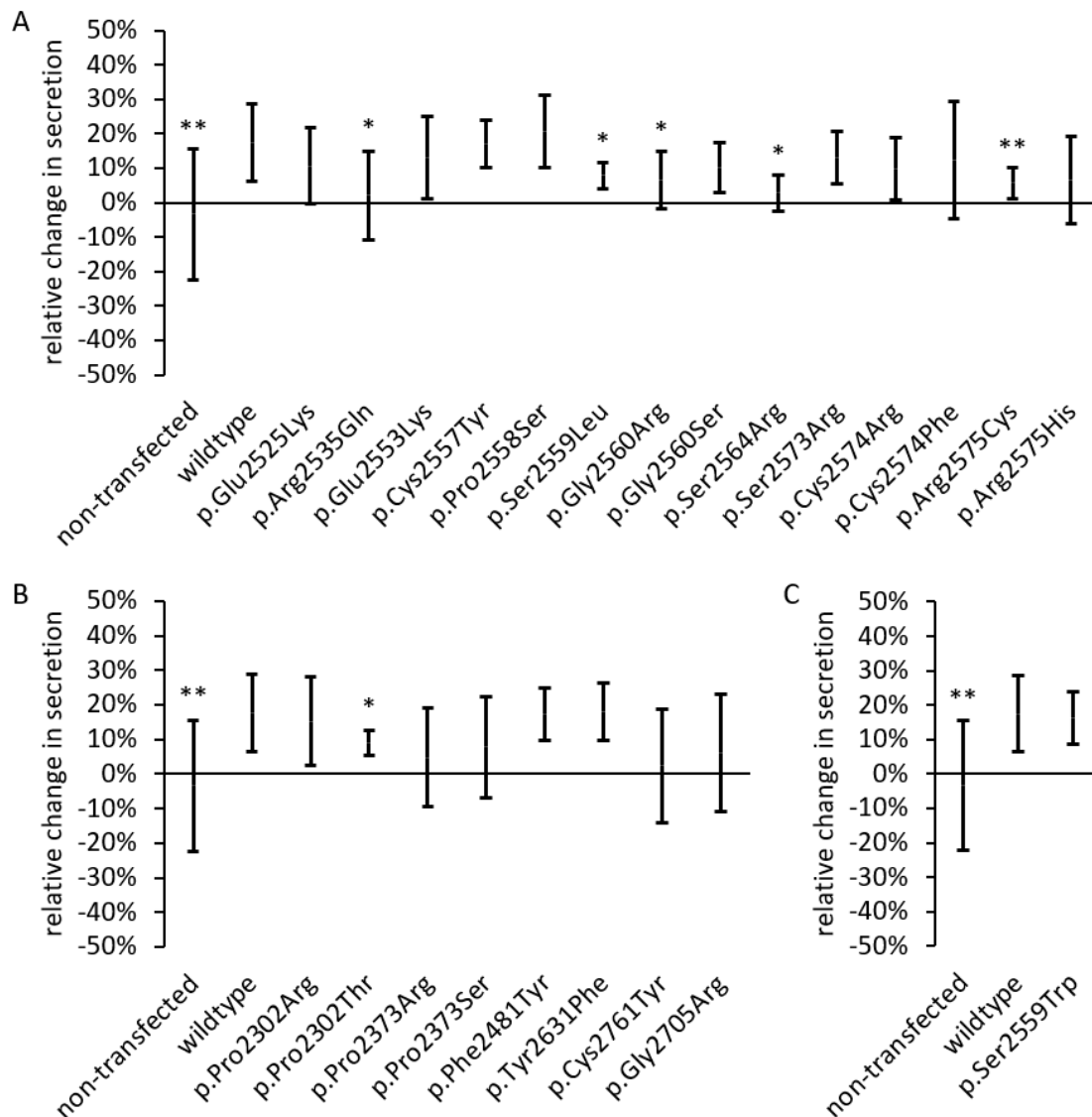


Figure 14: Relative change in secretion after treatment with 200 μ g/mL PMA for 2h. Cells after transient transfection with the expression vector pIRES coding for indicated VWF variants were cultivated for 24 h and stimulated with 200 μ g/mL PMA for 2 h. Supernatant was collected and VWF concentrations were determined by VWF:Ag-ELISA. Values are given in relation to the wildtype. \pm SEM are shown. Significance was calculated by unpaired t-test: $p = <0.05$ (*), <0.01 (**), <0.001 (***) . **(A)** Variants from approach 1 located in C4. **(B)** Variants from approach 2 located in C1, C2, C3, C5, C6. **(C)** Variants from approach 3 identified in a patient cohort.

PMA increased the secretion of wildtype VWF by approximately 20 %. The values for the non-transfected control were not increased or decreased after PMA treatment and thus significantly differed from the wildtype. The majority of variants showed increased secretion by the same factor as the wildtype. However, a significantly reduced inducibility of secretion was identified for variants p.Arg2535Gln, p.Ser2559Leu, p.Gly2560Arg, p.Ser2564Arg, p.Arg2575Cys and p.Pro2302Thr.

6.1.4.1.1. Intracellular localization of poorly secreted variants

Since the above-shown results indicate that variants p.Cys2557Tyr and p.Cys2574Arg are not properly secreted from HEK293F cells, immunofluorescence staining was performed to investigate their intracellular localization (**Figure 15**) and to elucidate whether VWF expression, packaging, or storage is affected. To this end, VWF and protein disulfide isomerase (PDI), an endoplasmic reticulum (ER) marker protein, were stained.

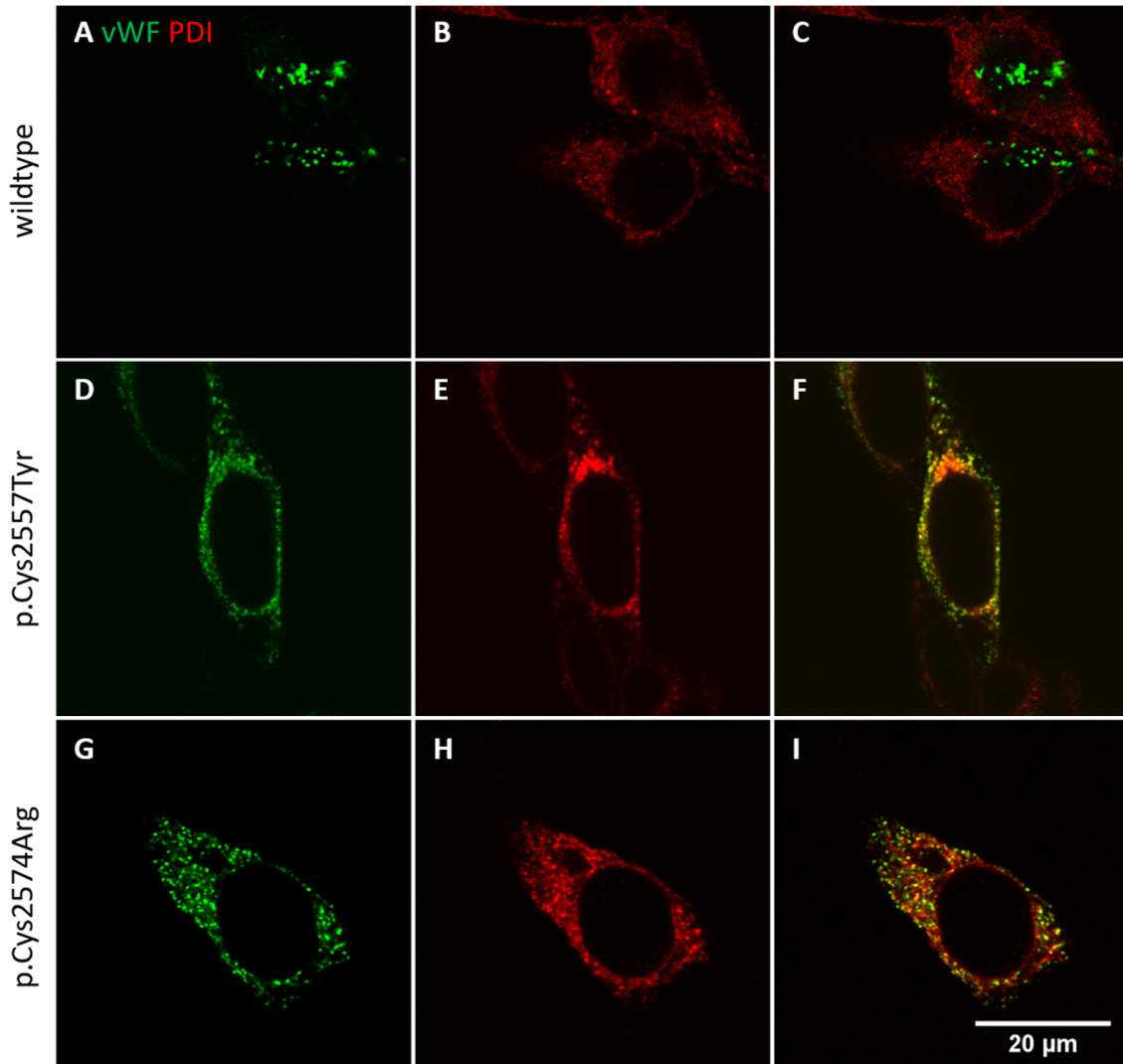


Figure 15: Immunofluorescence of wildtype VWF and variants p.Cys2557Tyr and p.Cys2574Arg transiently expressed in HEK293F cells. In transiently transfected HEK293F cells, VWF variants were stained using rabbit-anti-VWF and goat-anti-rabbit-alexa488 (**A,D,G**). PDI was detected employing mouse-anti-PDI and goat-anti-mouse-alexa546 antibody (**B,E,H**). Z-stacks of approximately 12 μm were imaged with 60x magnification using Olympus FV3000 microscope at UMIF and merged (**C,F,I**). Scale bar of 20 μm . The experiment was repeated three times and representative images were chosen.

Expression of wildtype VWF in HEK293F cells results in the formation of cigar shaped storage organelles often referred to as of pseudo Weibel-Palade Bodies (WPB) (Hannah et al., 2002). These are located close to the plasma membrane for fast secretion upon stimulation. In contrast, PDI is localized in the ER, close to the cell nucleus. There, it catalyzes the cysteine bond formation of various proteins among them VWF. Hence, colocalization of VWF and PDI is expected (Lippok et al., 2016), but excessive signals are rather indicating that VWF is retained in the ER due to defective folding or posttranslational modification (Rawley et al., 2022). Additionally, a packaging defect is underlined, if pseudo-WPB structures are absent.

In HEK293F cells transfected with wildtype VWF, pseudo WPBs can be identified close to the cell surface (**Figure 15**). These signals do not colocalize with the PDI signal indicating regular processing and storage of VWF in pseudo-WPBs. Distinct from that, the two variants p.Cys2557Tyr and p.Cys2574Arg show a granular staining with a strong colocalization with PDI and no pseudo-WPB formation, suggesting a retention and accumulation of these variants in the ER. Since only an inadequate amount of protein could be harvested, variants p.Cys2557Tyr and p.Cys2574Arg had to be excluded from further protein investigations.

6.1.4.2. Multimer analysis of VWF variants

During VWF synthesis, VWF is arranged into dimers and later multimers, resulting in multimers varying in size. Thereby, activity correlates with the degree of multimerization, making HMWM and ULMWM the most potent ones. Hence, the multimer pattern is an important parameter to characterize VWF activity. Loss of large multimers is either attributed to an impaired synthesis and secretion, or a reduced stability and increased susceptibility to protein degradation. However, since HEK293F do not express ADAMTS13, degradation products only result from digestion by other proteases that are expressed and secreted by HEK293F cells.

The VWF multimer distribution of recombinant VWF variants is assessed by size separation using gel electrophoresis, western blotting and immunodetection (**Figure 16**).

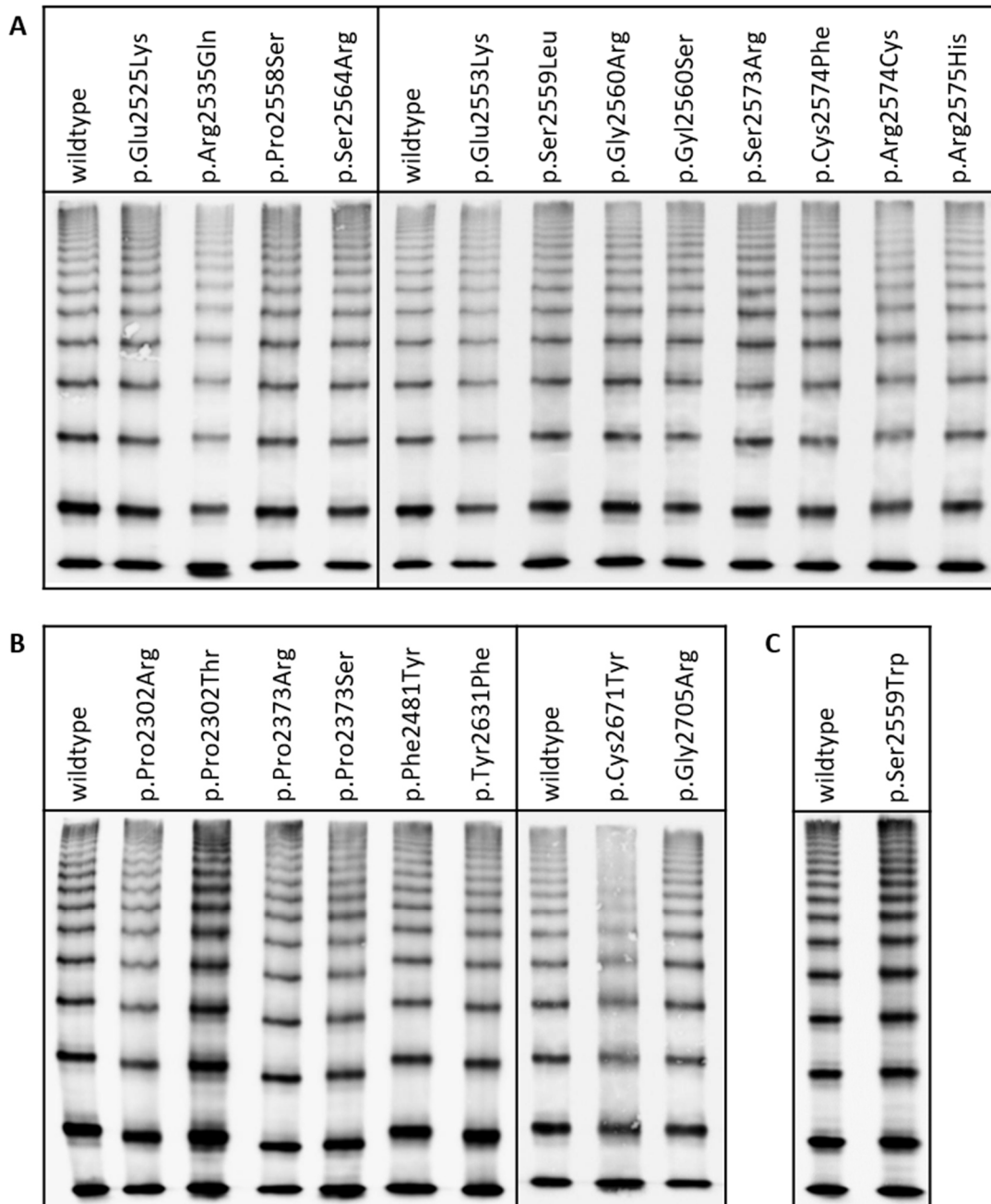


Figure 16: Multimer pattern of VWF variants expressed by HEK293F cells. Secreted VWF variants were collected from the supernatant and investigated by size separation employing gel electrophoresis, western blotting and detection with rabbit-anti-VWF primary (A0082, DAKO) and goat-anti-rabbit-HRP secondary antibody (P0448, DAKO) performed by Dr. Sonja Schneppenheim, MEDILYS GmbH. **(A)** Variants from approach 1 located in C4. **(B)** Variants from approach 2 located in C1, C2, C3, C5, C6. **(C)** Variants from approach 3 identified in a patient cohort.

The majority of the investigated variants display a multimer distribution which is similar to the wildtype without loss or degradation of HMWM. In contrast, variant p.Cys2671Tyr displays a 'smeary' multimer pattern and a loss of HMWM that indicate degradation or

impaired multimerization of VWF. Likewise, but to a lower extent, variant p.Pro2302Thr displays an increased amount of proteolyzed VWF multimers, which is denoted by the blurredness surrounding the multimer bands. However, HMWMs are still intact. It is important to note that increased degradation is not a consequence of ADAMTS13 cleavage, since ADAMTS13 is not expressed by HEK293F cells. Due to the loss of HMWMs and the resulting incomparability of variant p.Cys2671Tyr to the wildtype, no further investigations of this variant were conducted.

Notably, the multimers of variants p.Pro2302Arg, p.Pro2373Arg and p.Pro2373Ser show a faster running behavior compared to the wildtype whereas variants p.Arg2535Gln and p.Phe2481Tyr have a slower running behavior.

6.1.4.3. Degradation of VWF variants by ADAMTS13

In circulation, VWF size is regulated by the VWF-specific cleavage protease ADAMTS13. Increased susceptibility of VWF variants to ADAMTS13 can therefore reduce its size and affect its function. To investigate the proteolysis of VWF variants by ADAMTS13, a static cleavage assay was performed. ADAMTS13 cleaves VWF between aa residues Tyr1605 and Met1606 in the A2 domain (Crawley et al., 2011) resulting in two uneven sized parts. Hence, the nascent digested multimers have either a smaller or a bigger size compared to undigested multimers, with the same degree of multimerization. These bands surround the main multimer band and are called satellite bands. By measuring their intensity, the degree of degradation by ADAMTS13 can be quantified.

VWF samples were incubated with a physiological concentration of ADAMTS13 and multimer patterns are evaluated by multimer analysis. To determine suitable time periods for ADAMTS13 digestion, wildtype VWF samples were collected after 5 h, 24 h and 48 h incubation with ADAMTS13. The HMWMs decrease after 5 h but degradation stagnates after 24 h (**Figure 17**). Therefore, multimer patterns of all variants were investigated after 5 h and 24 h. The intensity of the satellite bands was calculated as ratio to the intensity of the corresponding multimer band. The ratio is increasing over time as ADAMTS13 digestion is increasing the amount of proteolyzed protein. Hence, a ratio of 0 would correspond to no proteolysis, whereas a ratio of 1 states that the satellite band and the multimer band have the same intensity.

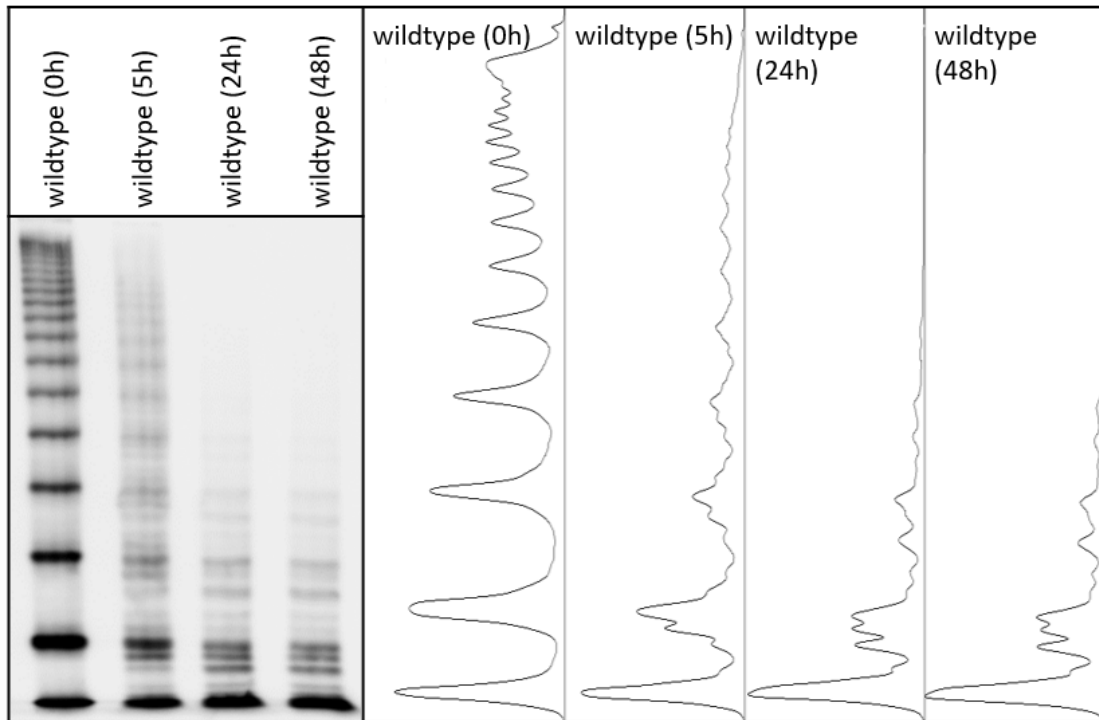


Figure 17: Degradation of wildtype VWF by ADAMTS13. 5 $\mu\text{g}/\mu\text{L}$ recombinant wildtype VWF was incubated with 500 $\text{ng}/\mu\text{L}$ recombinant ADAMTS13 at 37 °C shaking. Samples were collected after 0 h, 5 h, 24 h and 48 h and investigated by size separation by gel electrophoresis, western blotting and detection with rabbit-anti-VWF primary (A0082, DAKO) and goat-anti-rabbit-HRP secondary antibody (P0448, DAKO) performed by Dr. Sonja Schneppenheim, MEDILYS GmbH. Densitometric analysis of lanes was performed with ImageJ.

The calculation for each variant was performed for two oligomer bands and the average is displayed in **Figure 18**. Degradation by ADAMTS13 was comparable to the wildtype for the majority investigated variants. Baseline values at 0 h in absence of ADAMTS13 are already high for variant p.Pro2302Thr, probably due to cleavage by other proteases in the cell culture medium. Moreover, values at 0 h were slightly increased for variants p.Arg2535Gln, p.Gly2560Arg, p.Gly2560Ser and p.Ser2573Arg, indicating slight degradation independent of ADAMTS13. The degradation by ADAMTS13 was slightly decreased for variants p.Arg2535Gln, p.Ser2564Arg p.Pro2373Ser, p.Phe2481Tyr, p.Tyr2631Phe and p.Ser2559Trp, and slightly increased for variants p.Ser2559Leu and p.Pro2302Thr.

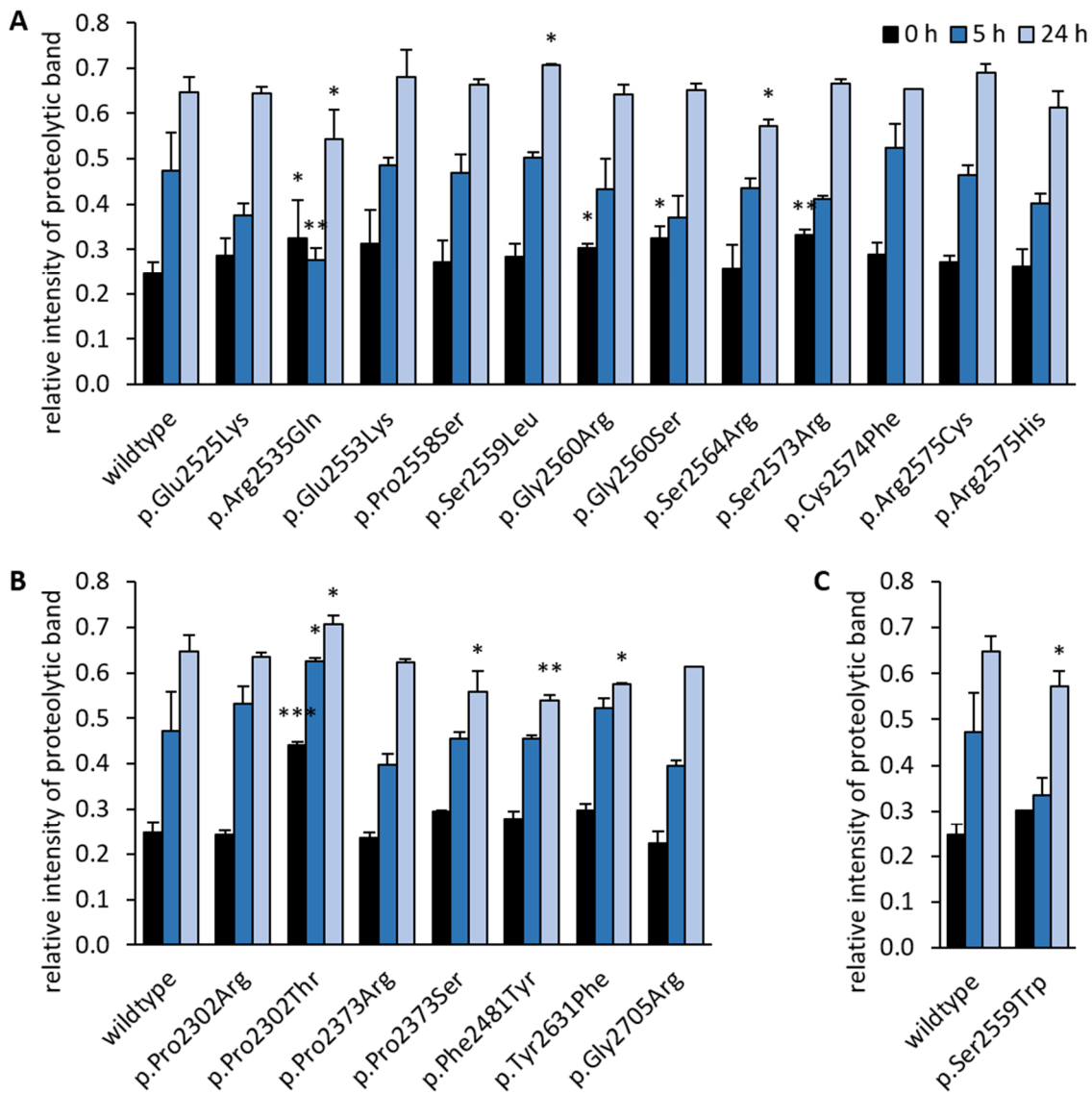


Figure 18: ADAMTS13 digestion of recombinant VWF variants. 5 ng/ μ L VWF variant samples were digested in presence of 500 ng/ μ L ADAMTS13 for 0 h, 5 h or 24 h at 37 °C shaking. Densitometric analysis of bands was performed with ImageJ. The ratio of two proteolytic bands to the corresponding non-proteolyzed band was calculated. Mean values \pm SEM are shown. Significance was calculated by one-sided t-test: $p = <0.05$ (*), <0.01 (**), <0.001 (***) **(A)** Variants from approach 1 located in C4. **(B)** Variants from approach 2 located in C1, C2, C3, C5, C6. **(C)** Variant from approach 3 identified in a patient cohort.

6.1.4.4. Binding capacities of VWF variants under static conditions

Collagens and platelet receptors are the most important interaction partners of VWF. The effective binding is essential for VWF to fulfill its role in hemostasis. Thereby, mutations can affect its activity. From a superficial point of view, the introduced point mutations are not directly located within known binding sites for these interaction partners. However, the binding affinity could still be affected indirectly by, for example, structural alteration of domains and tertiary structures or regulatory mechanisms. Therefore, binding of VWF variants to the most common interaction partners, including collagen type III, and platelet receptors GPIIb/IIIa and GPIIb/IIIa, was investigated by ELISA.

6.1.4.4.1. Collagen binding of VWF variants

Relative collagen type III binding, determined by collagen ELISA, was in a normal range for the majority of investigated variants (**Figure 19**). However, variant p.Arg2535Gln displayed a small decrease in collagen type III binding of 20 %. In contrast, variants p.Pro2302Thr, p.Pro2302Arg and p.Pro2373Ser showed an increased collagen type III binding by approximately 40-50 %.

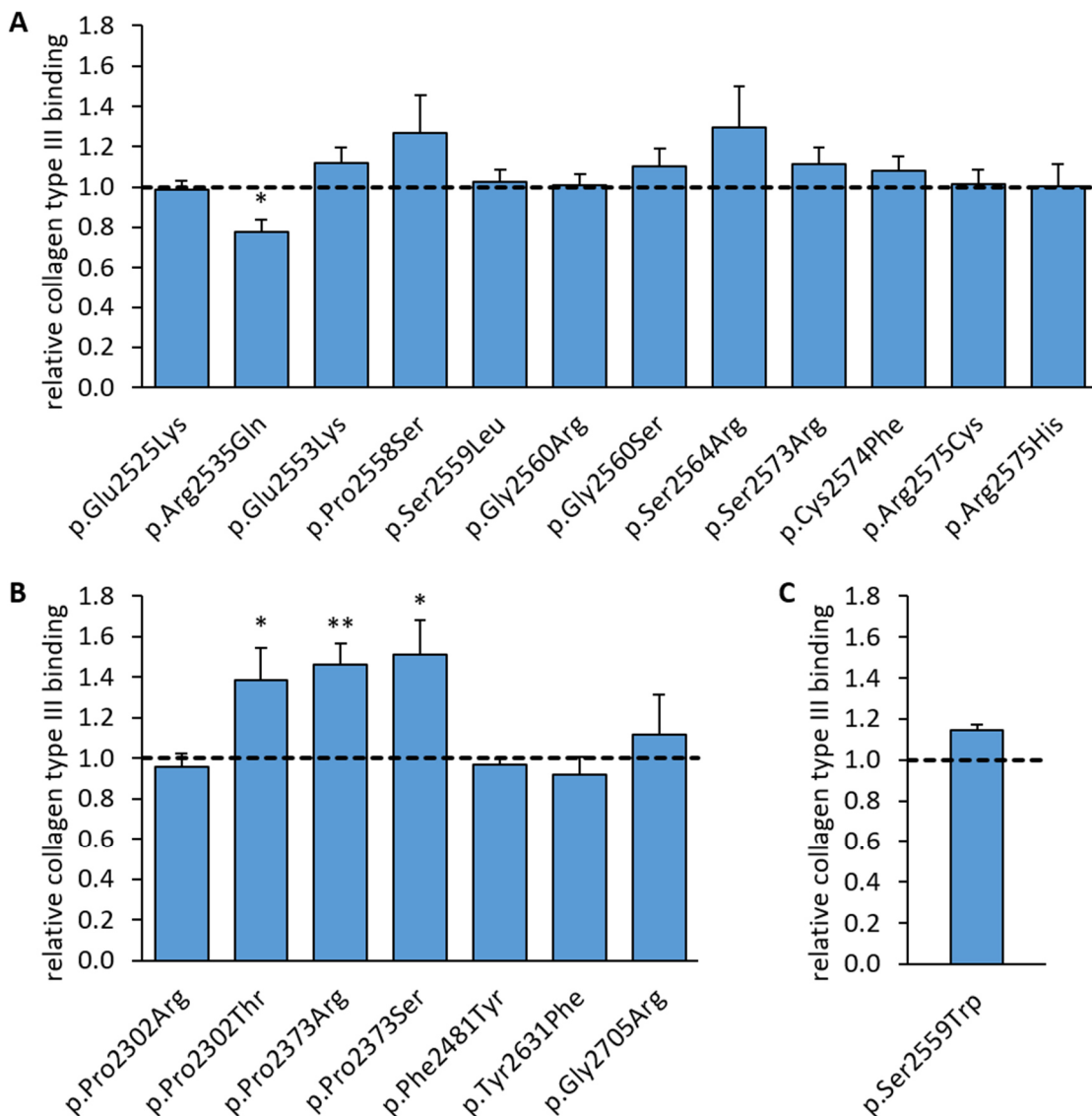


Figure 19: Relative collagen type III binding determined by Collagen-ELISA. Collagen coated ELISA plates were incubated with 0.075 $\mu\text{g}/\mu\text{L}$ VWF sample. Binding of VWF was detected with rabbit-anti-VWF and goat-anti-rabbit-HRP. Values are given in relation to the wildtype, which is set to 1 and indicated as a dotted line. Mean values \pm SEM are shown. Significance was calculated by one-sided t-test: $p = <0.05$ (*), <0.01 (**), <0.001 (***). **(A)** Variants from approach 1 located in C4. **(B)** Variants from approach 2 located in C1, C2, C3, C5, C6. **(C)** Variant from approach 3 identified in a patient cohort.

6.1.4.4.2. GPIIb α binding of VWF variants

For binding of VWF to GPIIb α in a physiological context a structural ‘opening’ of the A1 domain of VWF by force is necessary, which is not feasible in an ELISA format. Thus, the antibiotic ristocetin is used to chemically activate VWF. Ristocetin binds and alters VWF’s structural features, allowing it to bind to platelet receptor GPIIb α (Federici et al., 2004). The antibiotic ristocetin is added in concentrations of 0.0, 0.3, 0.6 and 1.0 mg/mL. The relative binding to a recombinant GPIIb α fragment is calculated as ratio to the maximum activation of wildtype VWF in presence of 1.0 mg/mL ristocetin (**Figure 20**). In this standard method, wildtype VWF does not bind effectively to the GPIIb α fragment in presence of 0.0 – 0.3 mg/mL ristocetin. In presence of 0.6 and 1 mg/mL ristocetin the binding increases almost linearly. The variants behaved similar to the wildtype and did not display an increased binding, as known for VWD type 2B variants like p.Ile1309Val (Schneppenheim et al., 2019). However variants p.Pro2558Ser, p.Ser2573Arg, p.Pro2373Arg, p.P2373Ser and p.Gly2705Arg display a minor significant increase in binding to GPIIb α . In contrast, variants p.Arg2535Gln, p.Phe2481Tyr and p.Tyr2631Phe present a small significant decrease in binding capacity.

A second possibility to investigate VWF binding to GPIIb α is to use a GOF variant of the GPIIb α fragment. This variant harbors two point mutations, p.Gly233Val and p.Met239Val (mutant GPIIb α -Gly233Val/Met239Val, hereafter abbreviated mut-GPIIb α) which allow binding to VWF without the need of ristocetin or force (Patzke et al., 2014). In comparison to the wildtype, variant p.Arg2535Gln exhibits a slightly reduced mut-GPIIb α binding by approximately 30 % (**Figure 21**). Significant increase of the binding was observed for variants p.Pro2558Ser, p.Ser2564Arg, p.Pro2302Arg, p.Pro2302Thr, p.Pro2373Arg and p.Pro2373Ser by approximately 10-30 %.

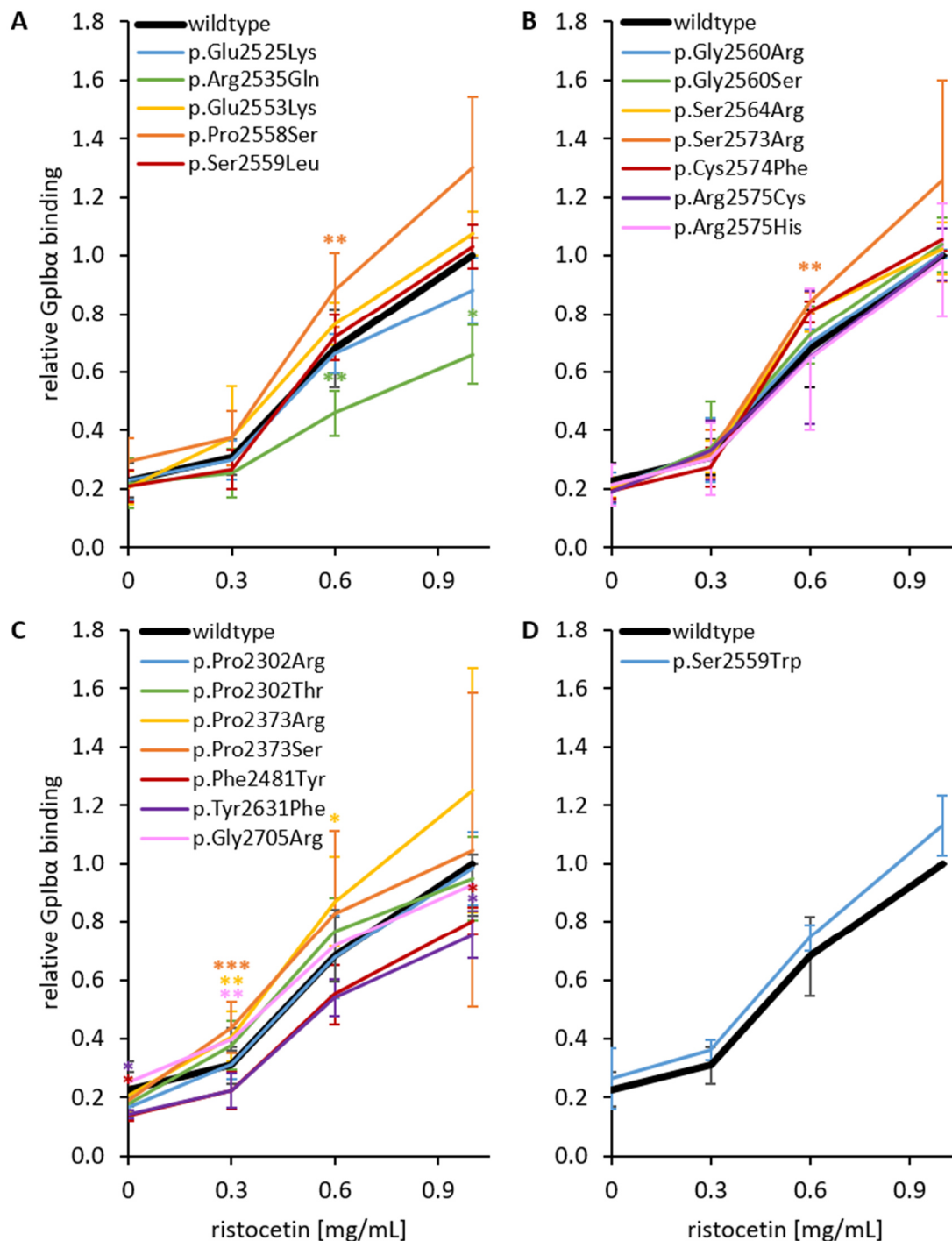


Figure 20: Relative binding to GPIIb/IIIa in presence of ristocetin. Binding of 0.075 $\mu\text{g}/\mu\text{L}$ recombinant VWF variants to recombinant GPIIb/IIIa fragment in presence of 0.0, 0.3, 0.6 or 1.0 mg/mL ristocetin was detected in an ELISA with rabbit-anti-VWF and goat-anti-rabbit-HRP. Values are given in relation to the wildtype at 1 $\mu\text{g}/\mu\text{L}$ ristocetin, which is set to 1. Mean values \pm SEM are shown. Significance was calculated by one-sided t-test and unpaired t-test: $p = <0.05$ (*), <0.01 (**), <0.001 (***). **(A, B)** Variants from approach 1 located in C4. **(C)** Variants from approach 2 located in C1, C2, C3, C5, C6. **(D)** Variant from approach 3 identified in a patient cohort.

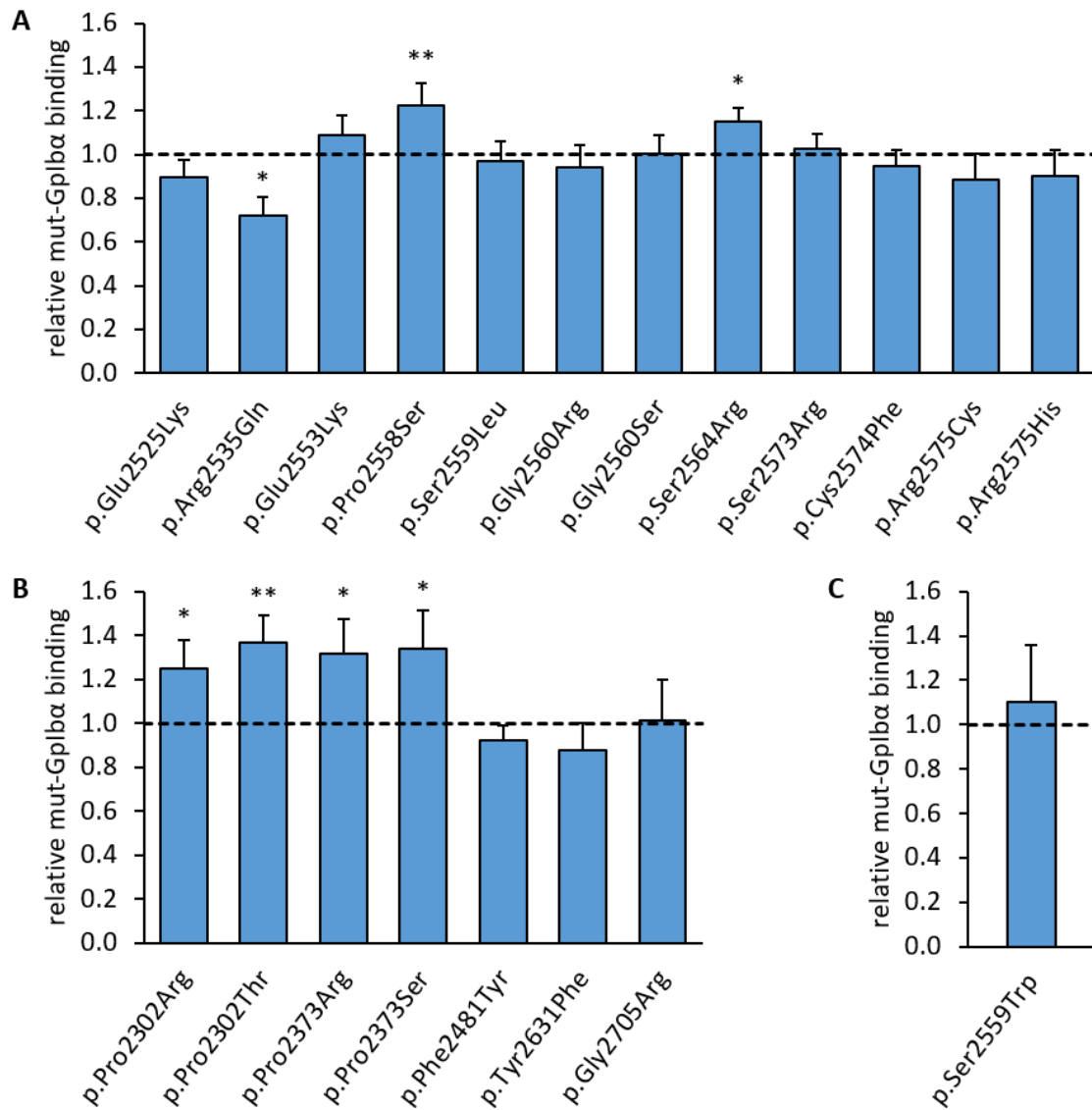


Figure 21: Relative mut-GPIIb α binding. Binding of 0.075 $\mu\text{g}/\mu\text{L}$ recombinant VWF variants to recombinant mut-GPIIb α fragment was detected in ELISA with rabbit-anti-VWF and goat-anti-rabbit-HRP. Values are given in relation to the wildtype, which is set to 1 and indicated as dotted line. Mean values \pm SEM are shown. Significance was calculated by one-sided t-test: $p = <0.05$ (*), <0.01 (**), <0.001 (***) . **(A)** Variants from approach 1 located in C4. **(B)** Variants from approach 2 located in C1, C2, C3, C5, C6. **(C)** Variant from approach 3 identified in patient cohort.

6.1.4.4.3. GPIIb/IIIa binding of VWF variants

Under physiological conditions GPIIb/IIIa is expressed on the surface of platelets and requires activation by inside-out signaling. To circumvent the need for platelets and to assess binding of VWF to activated GPIIb/IIIa in absence of other platelet receptors, such as GPIb α , a cell-based binding assay in an ELISA format was employed as previously described (König et al.). This assay allows quantification of the binding of GPIIb and GPIIIa expressing HEK293F cells to a VWF covered surface. To mimic the activated receptor, missense mutation p.Thr588Asn was inserted into the full-length cDNA of GPIIIa (Kashiwagi et al. 1999, König et al.).

Without immobilized VWF, binding of GPIIb/IIIa-Thr588Asn-HEK293F cells is reduced by 80 %, which corresponds to the background signal (**Figure 22**). Microscopic examination of the ELISA plate did not reveal any adherent HEK293F cells (data not shown). Similar is true, when the experiment is performed with HEK293F cell expressing no GPIIb/IIIa-Thr588Asn or the wildtype GPIIb/IIIa, as previously described (König et al., 2019). In comparison to the wildtype, only variant p.Arg2535Gln showed a significantly decreased binding by approximately 40 %. The remaining variants have a binding capacity similar to the wildtype. Additionally, no binding of GPIIb/IIIa wildtype to the variants was observed (data not shown).

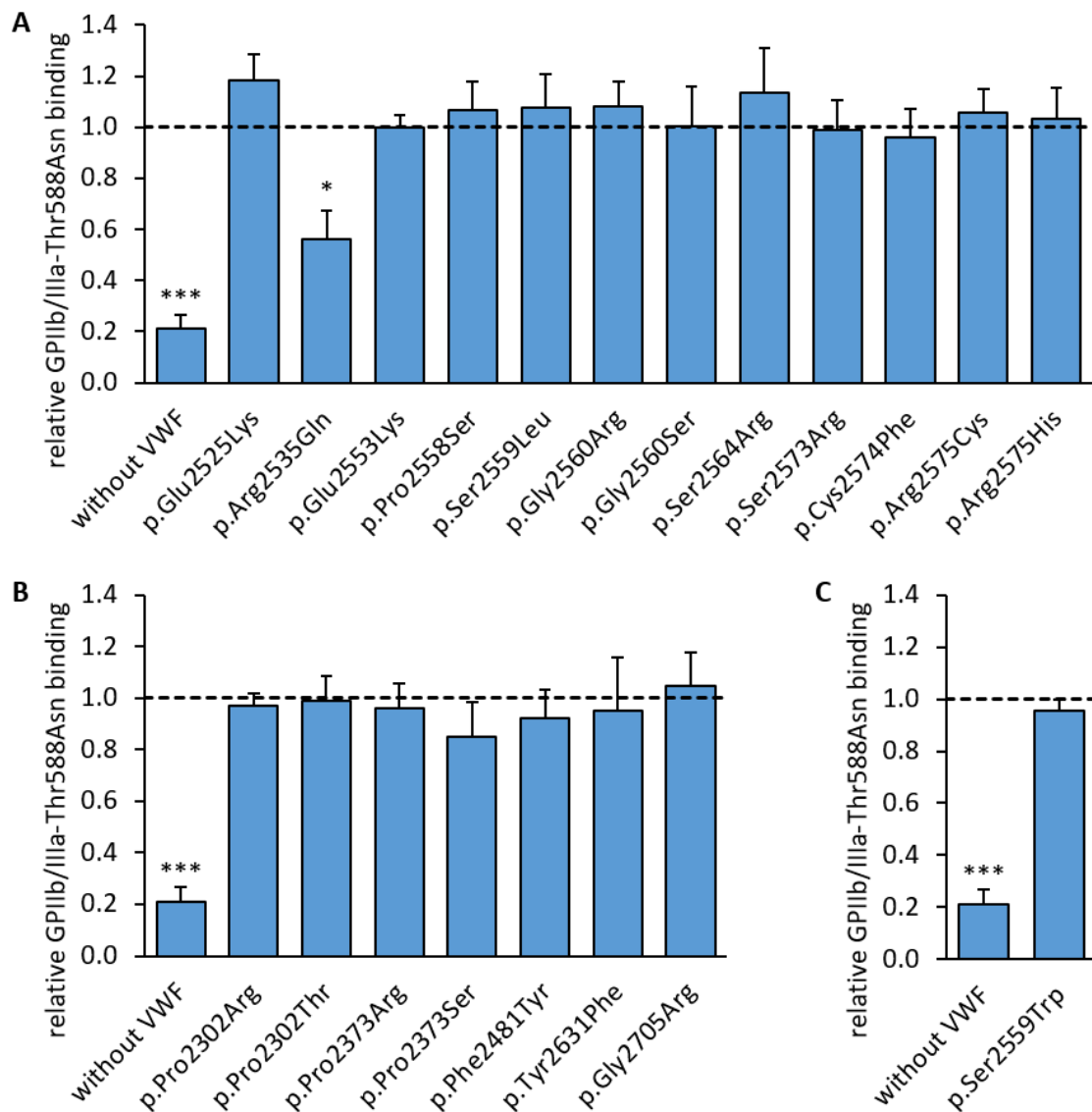


Figure 22: Relative GPIIb/IIIa-Thr588Asn binding. Binding of $7.5 \cdot 10^4$ HEK293F cells expressing GPIIb/IIIa-Thr588Asn to $1 \mu\text{g}/\mu\text{L}$ recombinant VWF variants was detected in ELISA. Binding was quantified by mouse-anti-CD41/CD61 and goat-anti-mouse-HRP antibody. Values are given in relation to the wildtype, which is set to 1 and indicated as dotted line. Mean values \pm SEM are shown. Significance was calculated by one-sided t-test: $p = <0.05$ (*), <0.01 (**), <0.001 (***). **(A)** Variants from approach 1 located in C4. **(B)** Variants from approach 2 located in C1, C2, C3, C5, C6. **(C)** Variant from approach 3 identified in patient cohort.

6.1.4.5. Shear-dependent platelet binding of VWF variants

Since variants p.Phe2651Tyr and p.Pro2555Arg exhibit normal activity under static conditions but show their GOF effect in presence of mechanical shear forces, shear-dependent experiments were performed, including ristocetin-dependent platelet agglutination in Light Transmission Aggregometry (LTA) and platelet aggregation in the microfluidic BioFlux system.

6.1.4.5.1. Ristocetin-dependent platelet agglutination of VWF variants

LTA was used to investigate the activity of VWF variants in presence of shear force. Hereby, washed platelets and recombinant VWF variants are allowed to bind and establish VWF-platelet-complexes, in a stirred solution with a rotation of 1200 rpm. The formation of VWF-platelet-complexes is quantified by measuring the turbidity of the solution. A beam of light is directed onto the sample and the transmitted light is detected by a photocell behind it. While free platelets are evenly distributed in the solution which then appears cloudy, agglutination of platelets leads to the formation of clumps that clear the solution. With increasing agglutination, the absorption of light by the sample decreases and the transmission increases, which is detected by the photocell.

Under normal circumstances VWF-platelet-complexes are not occurring spontaneously but need an agonist, which can be accomplished by addition of ristocetin, as described above. In diagnostics, the VWF:RCo (ristocetin cofactor) of patients plasma is the gold standard to distinguish VWD 2B from other VWD subtypes, since VWD 2B variants show agglutination in low-dose ristocetin-induced platelet aggregation (LD-RIPA) (Roberts and Flood, 2015). In this study, a modified LTA setup was used, which includes washed platelets without plasma components supplemented with recombinant VWF variants. The lack of plasma components leads to the establishment of so called agglutinates composed only of VWF and platelets, which lack the involvement of fibrin and are thus dissolvable by ADAMTS13 (Letzer et al., 2020).

Different concentrations of ristocetin were applied in the modified LTA to assess the potency of VWF variants to induce platelet agglutination. In absence of ristocetin none of the variants induced agglutination of platelets within the first 5 min (**Figure 24**), indicating that the GPIIb α binding activity is not markedly changed. In previous ELISA experiments (described in **6.1.4.4**) a concentration of ≥ 0.6 mg/mL ristocetin was found to induce a strong binding of VWF to GPIIb α . Hence, first, VWF variants were examined at a ristocetin concentration of 0.6 mg/mL. Wildtype VWF induced a maximum agglutination of approximately 86 % after 5 min (**Figure 23**). All tested variants display comparable maximum agglutination with values ranging from 70 to 95 %.

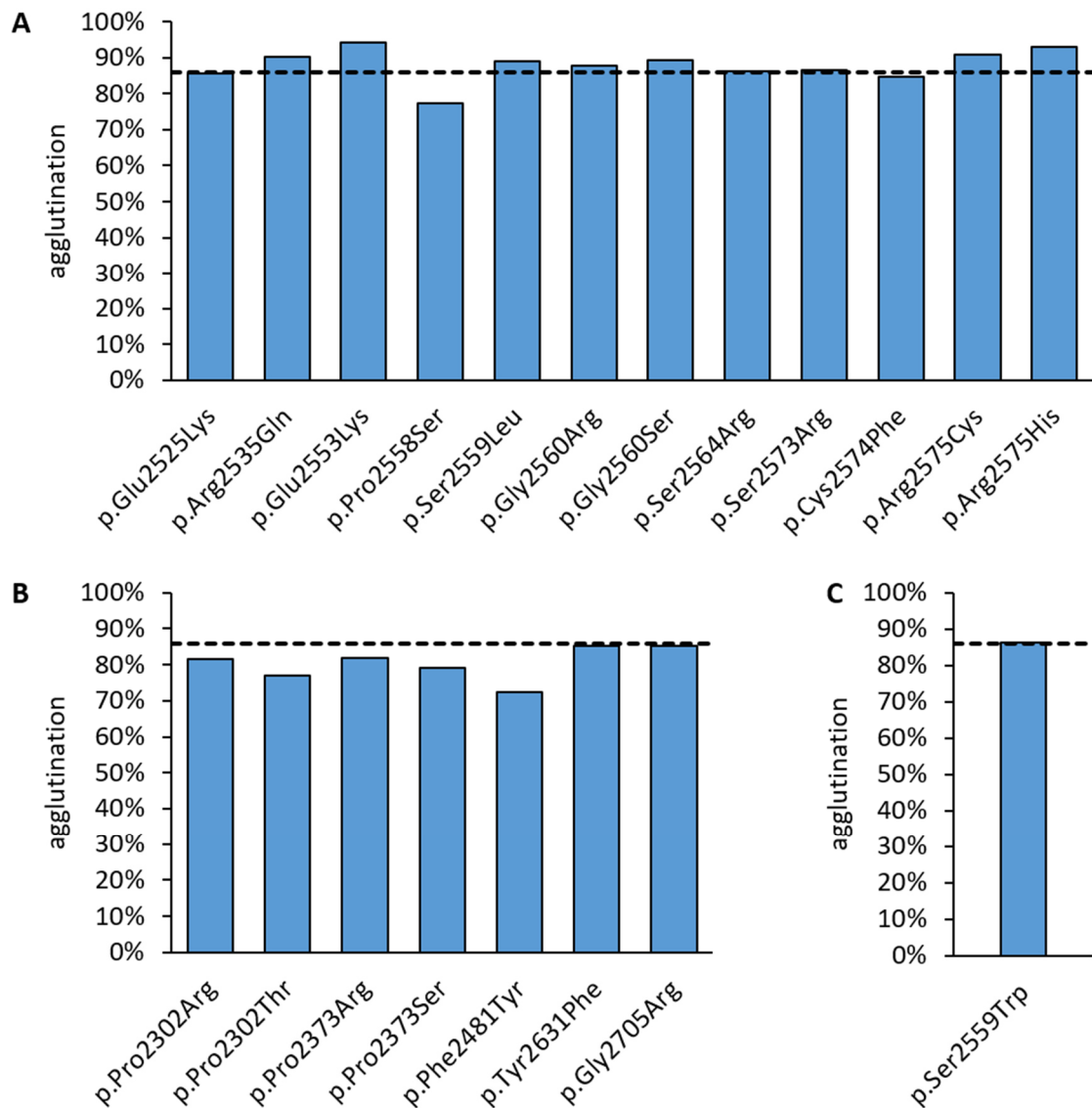


Figure 23: Maximum agglutination of platelets and VWF variants in a modified LTA. 300.000 platelets/ μL were stirred with 10 $\mu\text{g}/\mu\text{L}$ VWF variants at 1200 rpm. Agglutination was stimulated by 0.6 $\mu\text{g}/\mu\text{L}$ ristocetin and quantified after 5 min. Agglutination of wildtype VWF at 86 % is indicated as a dotted line. Mean values \pm SEM are shown. **(A)** Variants from approach 1 located in C4. **(B)** Variants from approach 2 located in C1, C2, C3, C5, C6. **(C)** Variant from approach 3 identified in a patient cohort.

To further reveal if some of the variants exhibit a GOF at a lower ristocetin concentration, the assay was performed in presence of 0.3 mg/mL ristocetin. The experimental setup included 5 min observation in the absence of ristocetin, followed by application of ristocetin and observation of agglutination for 15 min. Subsequently, 1000 ng/ μL ADAMTS13 was added to evaluate, if generated agglutinates are resolvable by proteolytic cleavage (**Figure 24**).

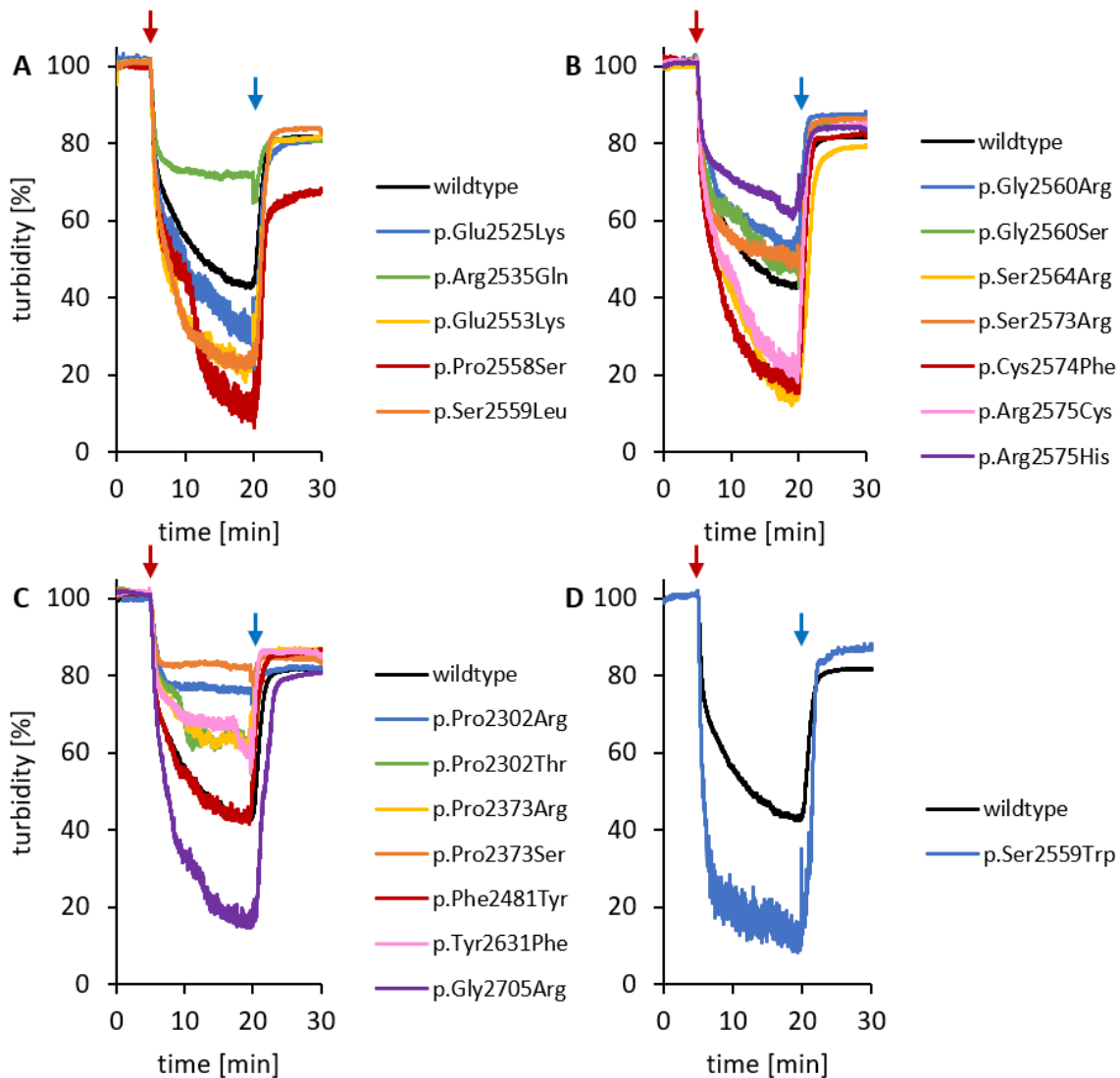


Figure 24: VWF-variant-platelet-complex formation and cleavage by ADAMTS13. 300.000 platelets/ μL were stirred with 10 $\mu\text{g}/\mu\text{L}$ VWF variants at 1200 rpm. After 5 min, 0.3 $\mu\text{g}/\mu\text{L}$ ristocetin (red arrow) was added and agglutination was observed for 15 min. The dissolution of agglutinates was investigated by addition of 1000 $\text{ng}/\mu\text{L}$ ADAMTS13 at minute 20 (blue arrow). Graphs represent the mean values of ≥ 3 replicates. **(A, B)** Variants from approach 1 located in C4. **(C)** Variants from approach 2 located in C1, C2, C3, C5, C6. **(D)** Variant from approach 3 identified in a patient cohort.

No agglutination was observed for all of the VWF variants in the absence of ristocetin within the first 5 min. However, low ristocetin concentration of 0.3 $\mu\text{g}/\mu\text{L}$ induced agglutination in presence of all variants. For wildtype VWF a partial activation and agglutination was observed with a resulting decrease in turbidity of approximately 60 %. Agglutinates were resolvable by addition of ADAMTS13, which restored the turbidity to approximately 80 %. Similar to wildtype VWF, all agglutinates were resolvable by ADAMTS13. All variants induced agglutination of platelets, but to different extend. A

stronger agglutination was observed for variants p.Glu2553Lys, p.Pro2558Ser, p.Ser2559Leu/Trp, p.Ser2564Arg, p.Cys2574Phe, p.Arg2575Cys and p.Gly2705Arg. In contrast, variants p.Arg2535Gln, p.Arg2575His, p.Pro2302Arg/Thr, p.Pro2373Arg/Ser and p.Tyr2631 showed a reduced agglutination. All remaining variants had a similar agglutination as the wildtype VWF.

Average maximum agglutination within 15 min was determined for each variant (**Figure 25**). Wildtype VWF induced a maximum agglutination of approximately 60%. In contrast, significant decrease in agglutination was observed for variants p.Arg2535Gln, p.Pro2302Arg and p.Pro2373Ser and significantly increased average agglutination was observed for variants p.Glu2553Lys, p.Pro2558Ser, p.Ser2559Leu/Trp, p.Ser2564Arg, p.Cys2574Phe, p.Arg2575Cys and p.Gly2705Arg.

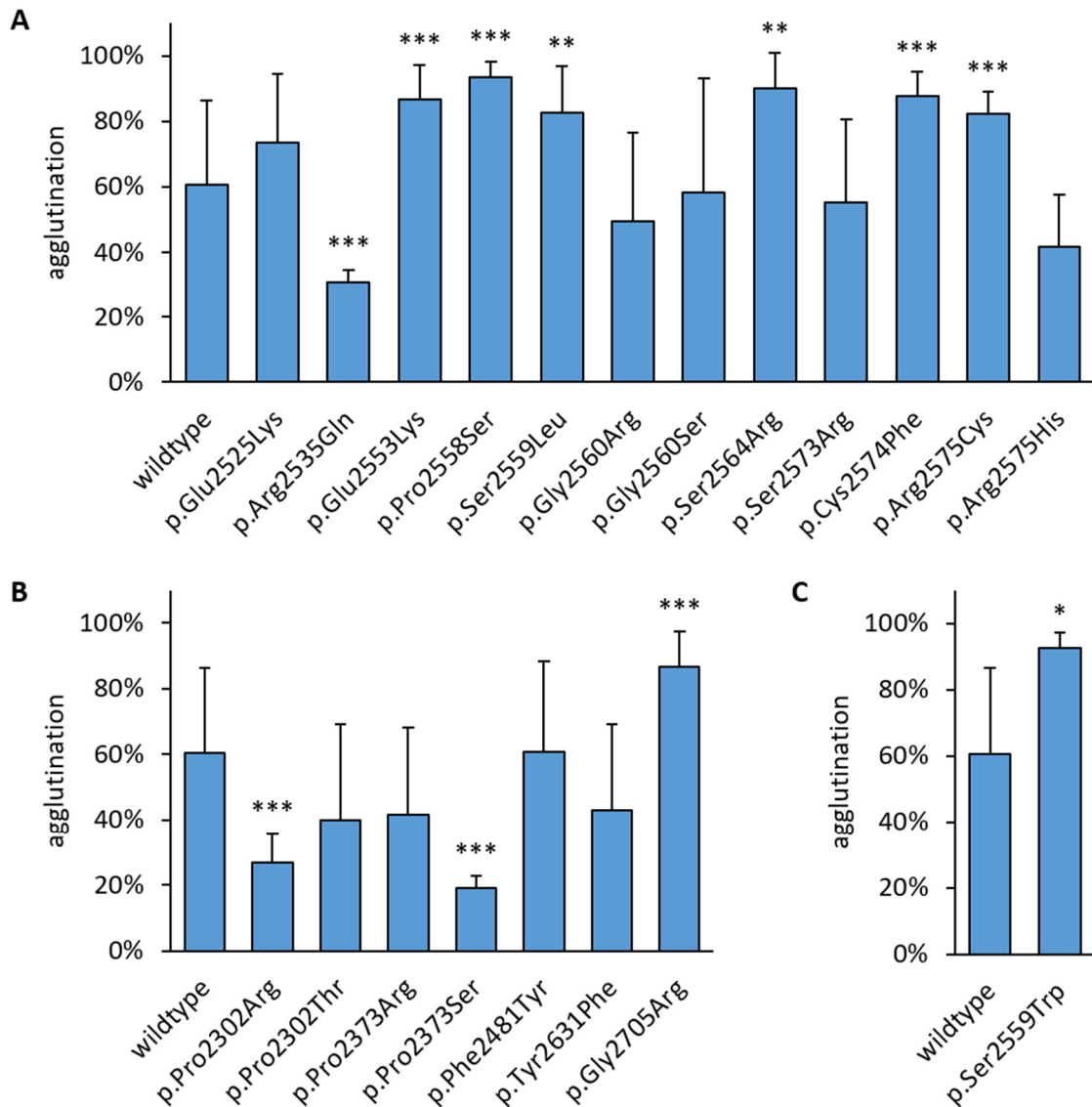


Figure 25: Maximum agglutination of platelets in presence of VWF variants and 0.3 µg/µL ristocetin. Values for maximum agglutination within 15 min were quantified for results of figure 24 in ≥ 3 replicates. Mean values \pm SEM are shown. Significance was calculated by unpaired t-test $p = <0.05$ (*), <0.01 (**), <0.001 (***). **(A)** Variants from approach 1 located in C4. **(B)** Variants from approach 2 located in C1, C2, C3, C5, C6. **(C)** Variant from approach 3 identified in a patient cohort.

Since the average maximum agglutination had a strong deviation for some variants, the proportion of replicates that show an agglutination of $>50\%$ in comparison to agglutination of $<50\%$ was calculated (**Figure 26**). Wildtype VWF induced a strong agglutination of $>50\%$ in approximately 51% of replicates. In contrast, the variants p.Arg2535Gln, p.Pro2302Arg and p.Pro2373Ser only achieved weak agglutination of $<50\%$ in all replicates. Vice versa, variants p.Glu2553Lys, p.Pro2558Ser, p.Ser2564Arg,

p.Cys2574Phe, p.Arg2575Cys, p.Gly2705Arg and p.Ser2559Trp induced a strong agglutination of >50 % in all replicated experiments.

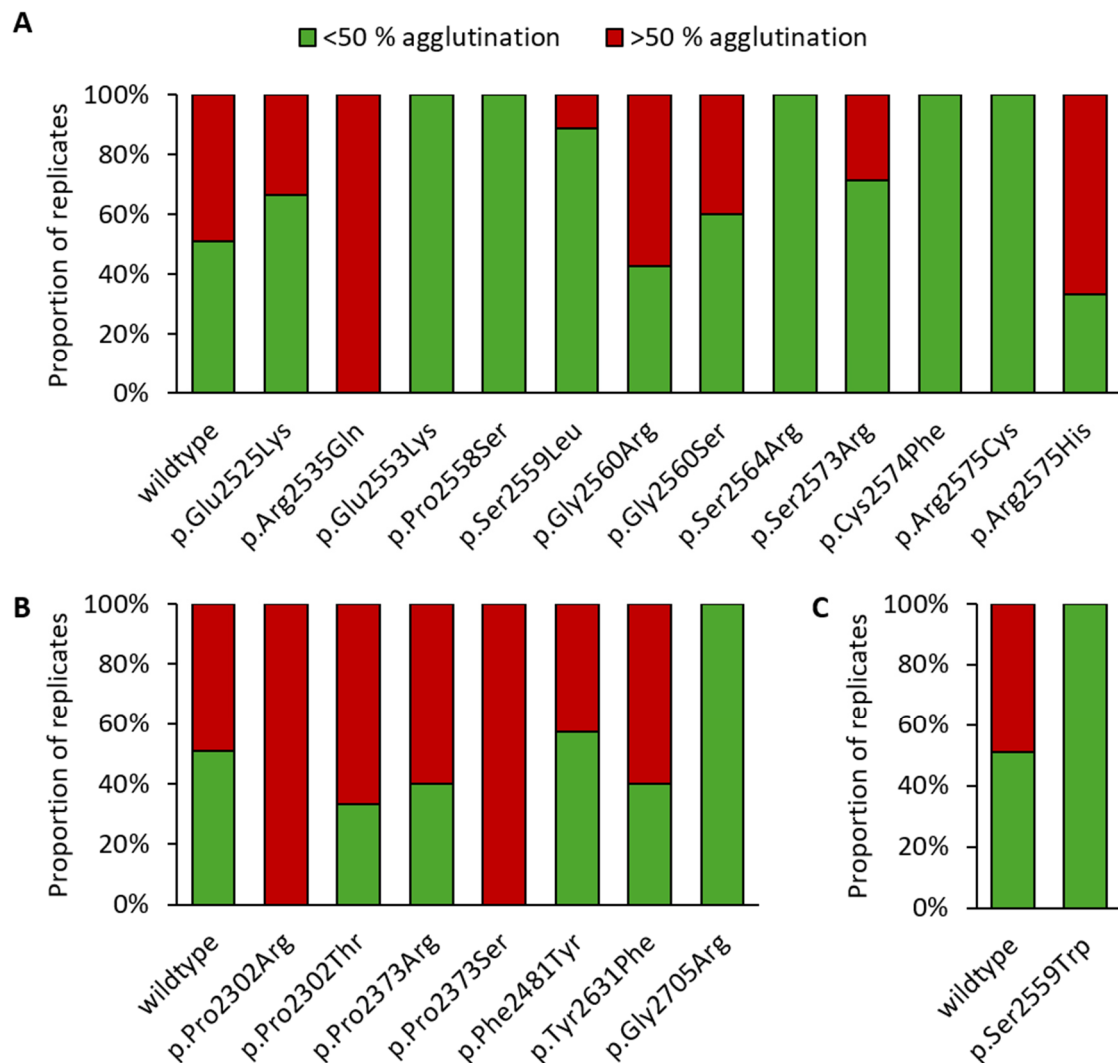


Figure 26: Frequency of weak or strong agglutination in percentage of replicates of the modified LTA in presence of 0.3 $\mu\text{g}/\mu\text{L}$ ristocetin. Values for maximum agglutination within 15 min were quantified from results of figure 24 in ≥ 3 replicates. Percentage of replicates in which strong agglutination of >50 % (green) or weak agglutination of <50 % (red) occurred, is given in percent [%]. **(A)** Variants from approach 1 located in C4. **(B)** Variants from approach 2 located in C1, C2, C3, C5, C6. **(C)** Variant from approach 3 identified in a patient cohort.

6.1.4.6. Formation of VWF-platelet collective networks by VWF variants

Next, variants were tested for their capacity to induce VWF-platelet collective network formation in a microfluidic channel. Washed platelets were stained with calcein-green and mixed with 20 $\mu\text{g}/\mu\text{L}$ recombinant VWF variants and washed erythrocytes to a hematocrit of 45 %. The solution was perfused over a VWF variant coated surface

mimicking a vessel, with injury endothelium and adhered VWF. The pressure was increased from 10 dyne/cm² to 100 dyne/cm² every minute and platelet adhesion and VWF-induced collective network formation was observed by taking consecutive images at 8 frames/second. Each frame has a size of 330,000 μm². The number and size of aggregates for each frame was quantified.

Already in the beginning of the experiment single platelets were immobilized by wildtype VWF and decorated the surface (**Figure 27**). At shear stress of 40 dyne/cm² first platelet-decorated stretched VWF fibers can be identified in presence of wildtype VWF. Subsequently, platelets and VWF form aggregates, which are characterized as collective networks that roll along the surface, so called VWF-induced collective networks or 'rolling aggregates' (Huck et al., 2022; Schneppenheim et al., 2019). Hence, the critical shear rate for aggregate formation was determined as 60 dyne/cm². The number of aggregates increases slightly to 20 aggregates per frame at a shear stress of 80 dyne/cm² and remained stable up to a shear stress of 100 dyne/cm² (**Figure 28**). Aggregate size increased to a maximum of 1400 μm².

Taking a closer look at the variants in the C4 domain, only variant p.Arg2535Gln failed to induce the formation of aggregates (**Figure 27 - Figure 30**, variants sorted by position). Variants p.Glu2525Lys, p.Gly2560Ser, p.Ser2573Arg and p.Arg2575His behaved similar to the wildtype with an onset of rolling aggregate formation at 60-80 dyne/cm². However, variants p.Pro2558Ser, p.Ser2559Leu, p.Gly2560Arg, p.Ser2564Arg, p.Cys2574Phe and p.Arg2575Cys displayed a significantly increased shear sensitivity by initiation of collective network formation already at 20-40 dyne/cm². These variants have a similar phenotype as the published variant p.Phe2561Tyr, since 40 dyne/cm² corresponds to 2000 s⁻¹ (Schneppenheim et al., 2019). However, aggregation of GOF variants decreases slightly at higher shear rates, which is significant for variants p.Gly2560Arg and p.Pro2558Ser. In contrast, variant p.Glu2553Lys needs the same critical shear stress for aggregate formation as the wildtype, but at higher shear stress of 100 dyne/cm² the aggregate size was increased. This phenotype is similar to variant p.Pro2555Arg but to a lesser extent.

Investigated variants located in C1 and C2 lost their activity and either failed to induce platelet aggregation, as observed for variants p.Pro2302Thr and p.Pro2373Ser, or less

aggregates were formed only at higher shear stress (**Figure 31 - Figure 32**). Variants in C3 and C5, namely p.Phe2481Tyr and p.Tyr2631Phe showed a similar aggregate formation as the wildtype. In contrast, variant p.Gly2705Arg, located in the C6 domain, showed a higher shear sensitivity with onset of aggregation at 40 dyne/cm² and an increased average aggregate size of 1800 μm² compared to the wildtype with 1400 μm². Variant p.Ser2559Trp, which was identified in the patient cohort, also displays GOF characteristics. The critical shear stress necessary for platelet aggregation is decreased to 40 dyne/cm² (**Figure 33**) whereas aggregate size is comparable to wildtype VWF.

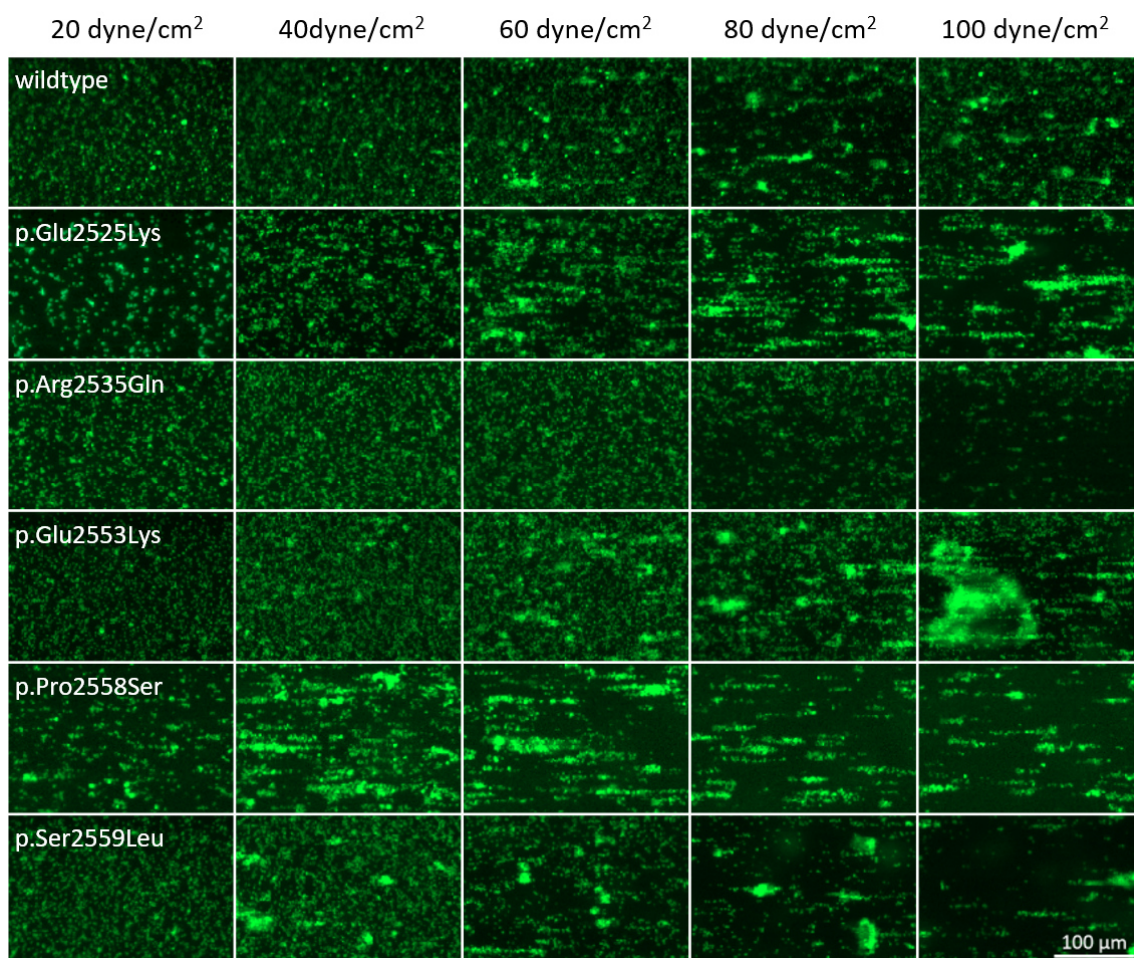


Figure 27: Representative immunofluorescence images of the formation of VWF-platelet collective networks by wildtype VWF and variants p.Glu2525Lys, p.Arg2535Gln, p.Glu2553Lys, p.Pro2558Ser and p.Ser2559Leu at indicated shear stress. A HEPES buffered solution of 250,000 washed and calcein-green stained platelets/μL and 20 μg/mL VWF variants with a hematocrit of 45 % was perfused over a VWF variant coated surface. Shear stress was increased stepwise from 10-100 dyne/cm² and platelet adhesion and aggregate formation were observed for 1 min each. Scale bar of 100 μm.

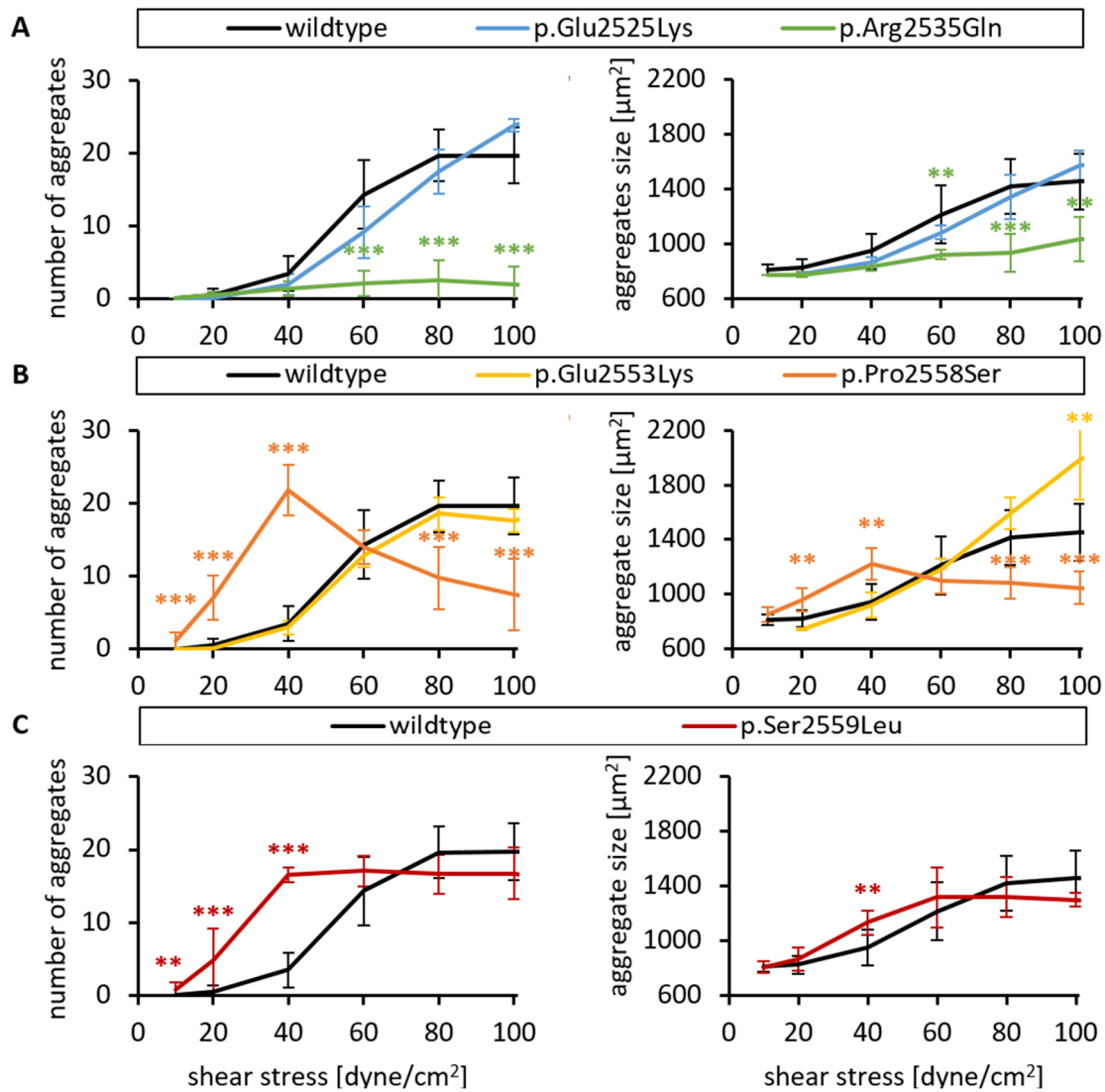


Figure 28: Quantification of the formation of VWF-platelet collective networks by wildtype VWF and variants at indicated shear stress. Average aggregate number per 330,000 μm^2 and average aggregate size for aggregates $>700 \mu\text{m}^2$ from all replicates of the experiments exemplified in figure 27 were calculated for 10, 20, 40, 60, 80 and 100 dyne/cm^2 . Mean values \pm SEM are shown. Significance was calculated by unpaired t-test $p < 0.05$ (*), < 0.01 (**), < 0.001 (***) .

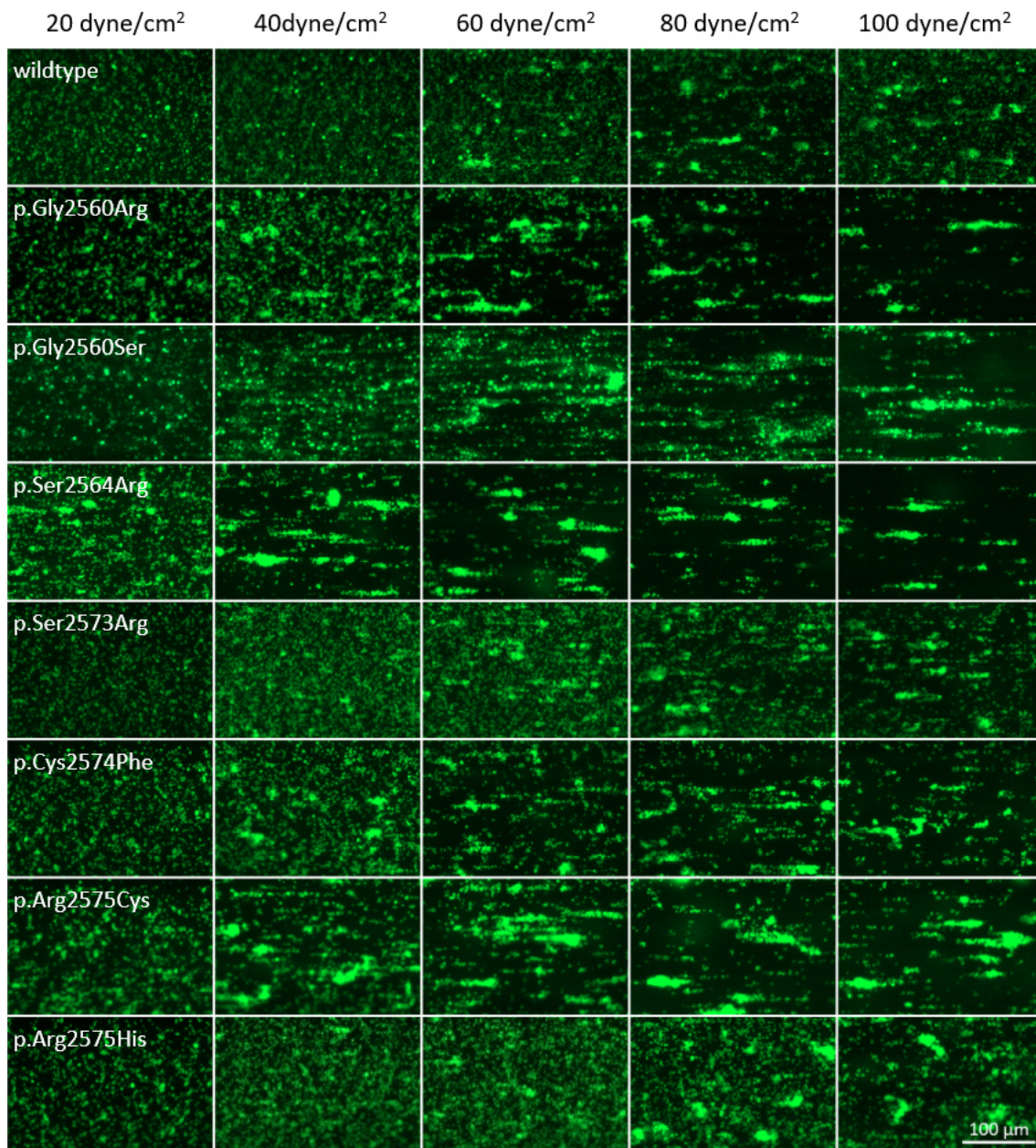


Figure 29: Representative immunofluorescence images of the formation of VWF-platelet collective network by wildtype VWF and variants p.Gly2560Arg/Ser, p.Ser2564Arg, p.Ser2573Arg, p.Cys2574Phe and p.Arg2575Cys/His at indicated shear stress. A HEPES buffered solution of 250,000 washed and calcein-green stained platelets/ μ L and 20 μ g/mL VWF variants with a hematocrit of 45 % was perfused over a VWF variant coated surface. Shear stress was increased stepwise from 10-100 dyne/cm² and platelet adhesion and aggregate formation were observed for 1 min each. Scale bar of 100 μ m.

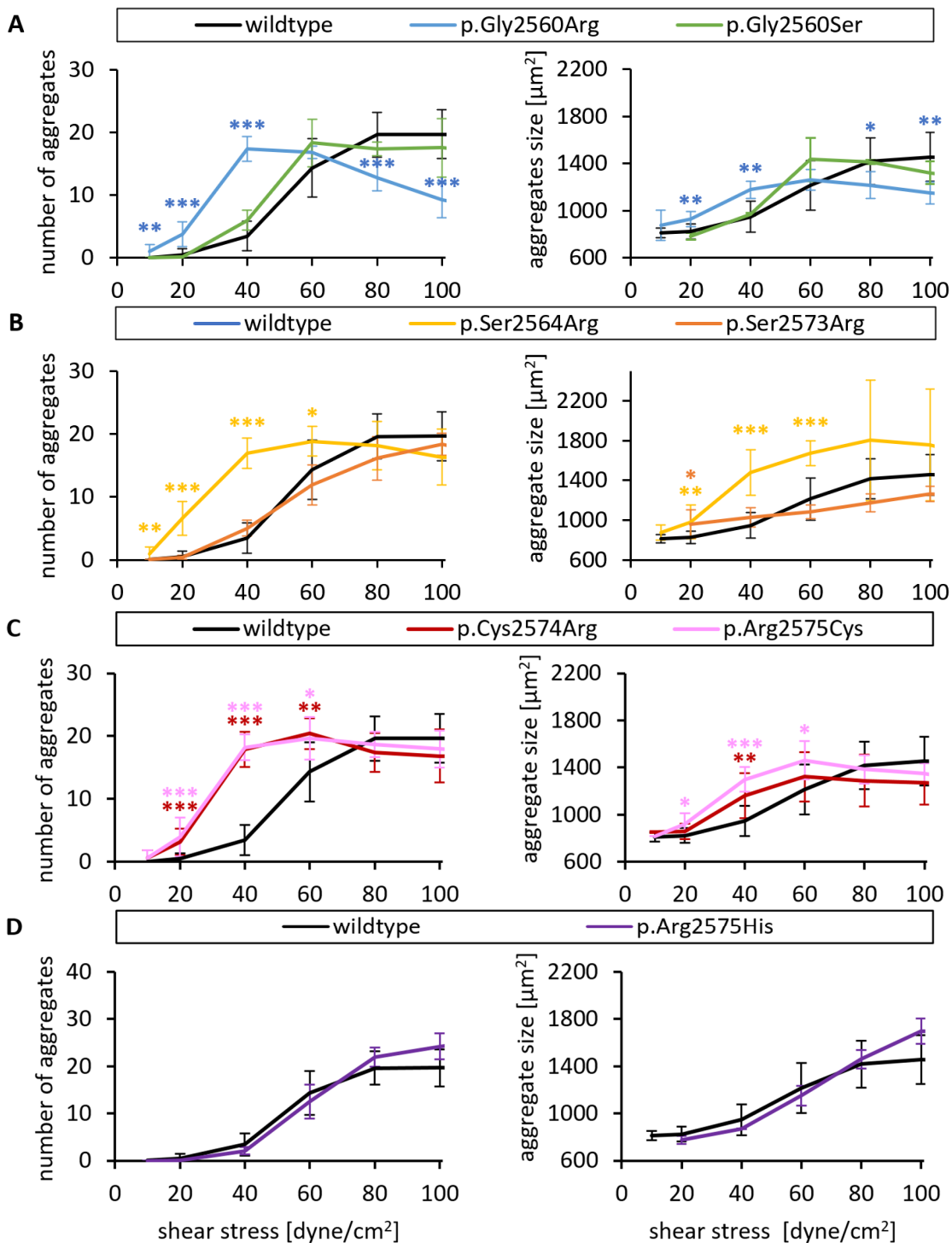


Figure 30: Quantification of the formation of VWF-platelet collective networks by wildtype VWF and variants at indicated shear stress. Average aggregate number per $330,000 \mu\text{m}^2$ and average aggregate size for aggregates $>700 \mu\text{m}^2$ from all replicates of the experiments exemplified in figure 29 were calculated for 10, 20, 40, 60, 80 and 100 dyne/cm^2 . Mean values \pm SEM are shown. Significance was calculated by unpaired t-test $p = <0.05$ (*), <0.01 (**), <0.001 (***)

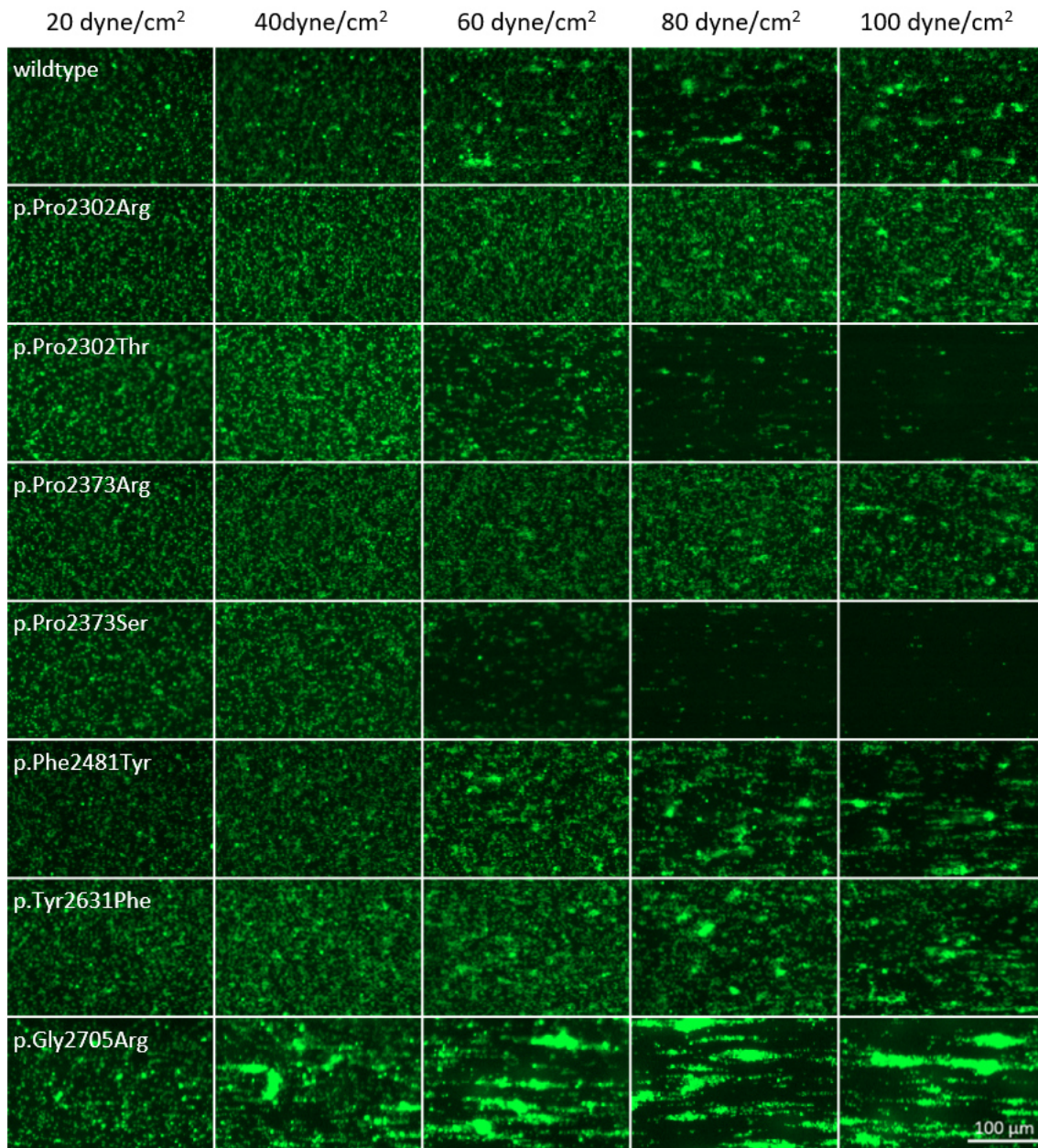


Figure 31: Representative immunofluorescence images of the formation of VWF-platelet collective network by wildtype VWF and variants p.Pro2302Arg/Thr, p.Pro2373Arg/Ser, p.Phe2481Tyr, p.Tyr2631Phe and p.Gly2705Arg at indicated shear stress. A HEPES buffered solution of 250,000 washed and calcein-green stained platelets/ μ L and 20 μ g/mL VWF variants with a hematocrit of 45 % was perfused over a VWF variant coated surface. Shear stress was increased stepwise from 10-100 dyne/cm² and platelet adhesion and aggregate formation were observed for 1 min each. Scale bar of 100 μ m.

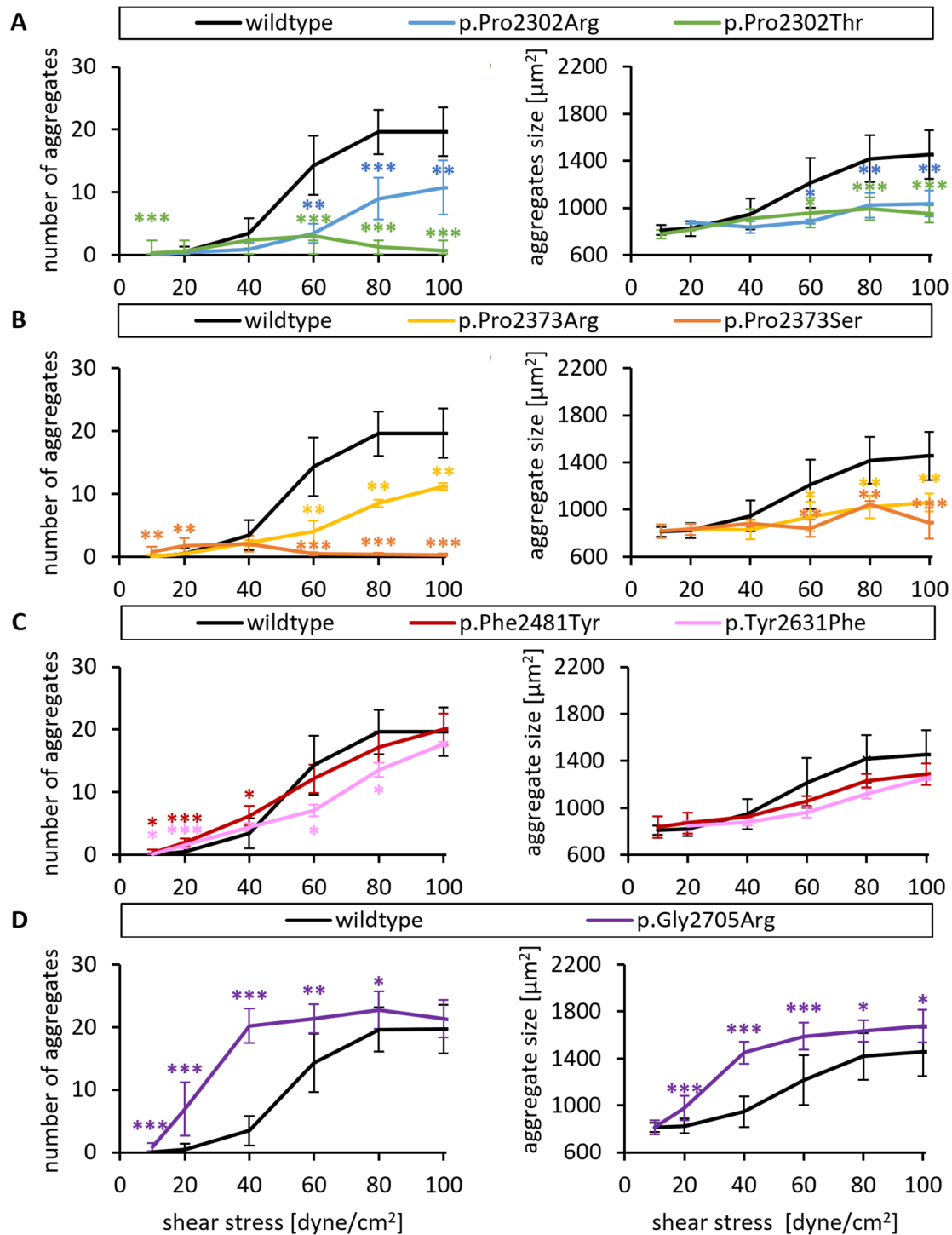


Figure 32: Quantification of the formation of VWF-platelet collective networks by wildtype VWF and variants at indicated shear stress. Average aggregate number per $330,000 \mu\text{m}^2$ and average aggregate size for aggregates $>700 \mu\text{m}^2$ from all replicates of the experiments exemplified in figure 31 were calculated for 10, 20, 40, 60, 80 and 100 dyne/cm^2 . Mean values \pm SEM are shown. Significance was calculated by unpaired t-test $p = <0.05$ (*), <0.01 (**), <0.001 (***)

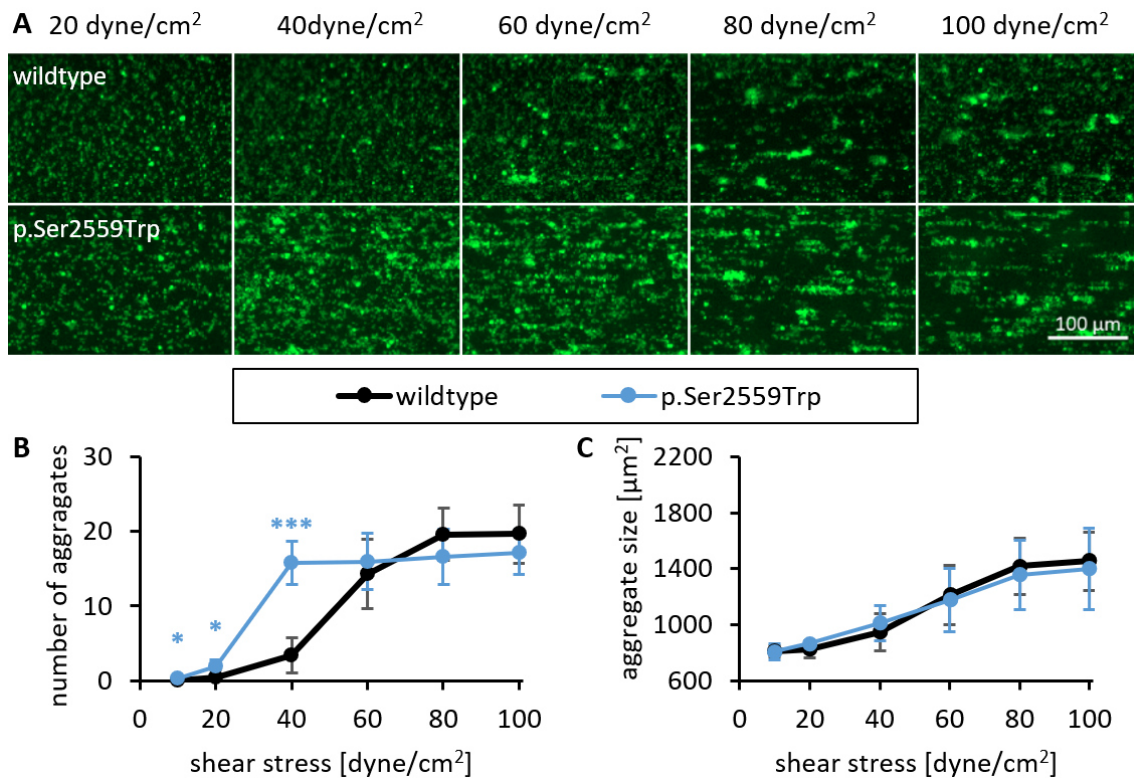


Figure 33: Formation of VWF-platelet collective network by wildtype VWF and variant p.Ser2559Trp at indicated shear stress. (A) A HEPES buffered solution of 250,000 washed and calcein-green stained platelets/ μL and 20 $\mu\text{g}/\text{mL}$ VWF variants with a hematocrit of 45 % was perfused over a VWF variant coated surface. Shear stress was increased stepwise from 10-100 dyne/cm² and platelet adhesion and aggregate formation were observed for 1 min each. Scale bar of 100 μm . **(B)** Average aggregate number per 330,000 μm^2 and average aggregate size for aggregates $>700 \mu\text{m}^2$ were calculated for 10, 20, 40, 60, 80 and 100 dyne/cm². Mean values \pm SEM are shown. Significance was calculated by unpaired t-test $p = <0.05$ (*), <0.01 (**), <0.001 (***)).

6.1.4.7. Role of GPIIb/IIIa in the activity of gain-of-function variants

For those variants that displayed an increased shear sensitivity in the microfluidic setup, further experiments were performed to investigate the role of GPIIb/IIIa in the GOF effect. The GPIIb/IIIa inhibitor abciximab was added in a concentration of 2.6 $\mu\text{g}/\text{mL}$ to washed and stained platelets, washed erythrocytes, and 20 $\mu\text{g}/\mu\text{L}$ recombinant VWF variants in the same microfluidic assay described above. In presence of wildtype VWF, abciximab resulted in a slightly increased platelet aggregation at lower shear stress of 40 dyne/cm² and decreased platelet aggregation at higher shear stress of 80-100 dyne/cm² compared to the control without abciximab (Figure 34). For the GOF variants, a similar effect was observed, but to a higher extend (Figure 34 - Figure 38,

variants sorted by position, quantification in **Table 16 - Table 17**). All variants did not lose their ability to induce aggregation at low shear stress, but the number of aggregates was decreased or even completely abolished at high shear stress of 80-100 dyne/cm². Also, aggregate size was reduced in presence of abciximab.

Table 16: Average aggregate number per 330,000 μm^2 for aggregates $>700 \mu\text{m}^2$ induced by VWF variants at 10, 20, 40, 60, 80 and 100 dyne/cm². Mean values are shown.

VWF variant	shear stress [dyne/cm ²]					
	10	20	40	60	80	100
wildtype	0.02	0.49	3.45	14.3	19.61	19.67
+ abciximab	0.26	2.91	8.89	13.84	15.70	14.33
p.Pro2558Ser	1.10	7.04	21.81	14.01	9.74	7.5
+ abciximab	3.74	7.91	6.59	1.67	0.39	0.07
p.Ser2559Leu	0.78	4.80	16.57	17.08	16.61	16.73
+ abciximab	3.87	9.26	12.44	11.27	5.73	2.72
p.Ser2559Trp	0.27	1.88	15.81	15.98	16.66	17.18
+ abciximab	2.51	7.27	8.54	7.89	5.00	3.28
p.Gly2560Arg	1.02	3.77	17.32	16.81	12.70	9.19
+ abciximab	1.47	6.32	13.01	6.33	2.02	0.83
p.Ser2564Arg	0.90	6.59	16.95	18.84	18.11	16.34
+ abciximab	3.77	10.03	8.63	5.38	3.35	1.69
p.Cys2574Phe	0.57	3.14	17.91	20.43	17.41	16.85
+ abciximab	2.04	5.30	11.62	8.34	5.86	2.75
p.Arg2575Cys	0.60	3.96	18.20	19.69	18.67	17.94
+ abciximab	2.86	10.89	14.84	10.45	4.59	2.07
p.Gly2705Arg	0.82	6.94	20.22	21.37	22.72	21.38
+ abciximab	1.21	11.44	18.96	12.56	8.09	4.21

Table 17 Average aggregate size [μm^2] per 330,000 μm^2 for aggregates $>700 \mu\text{m}^2$ induced by VWF variants at 10, 20, 40, 60, 80 and 100 dyne/cm². Mean values are shown.

VWF variant	shear stress [dyne/cm ²]					
	10	20	40	60	80	100
wildtype	792	826	946	1219	1452	1505
+ abciximab	858	998	1129	1119	1213	1217
p.Pro2558Ser	851	958	1167	1115	1148	1116
+ abciximab	900	896	902	866	820	805
p.Ser2559Leu	804	862	1132	1318	1322	1300
+ abciximab	850	923	970	957	929	909
p.Ser2559Trp	807	864	1011	1175	1359	1399
+ abciximab		886	938	971	953	959
p.Gly2560Arg	876	926	1176	1261	1214	1149
+ abciximab	835	886	985	924	883	870
p.Ser2564Arg	872	995	1456	1614	1503	1362
+ abciximab	894	972	1011	1140	1040	943
p.Cys2574Phe	851	858	1162	1322	1287	1271
+ abciximab	887	890	964	959	922	878
p.Arg2575Cys	835	936	1267	1407	1344	1307
+ abciximab	795	946	1004	955	907	857
p.Gly2705Arg	814	995	1473	1592	1642	1681
+ abciximab	863	945	1284	1151	1058	992

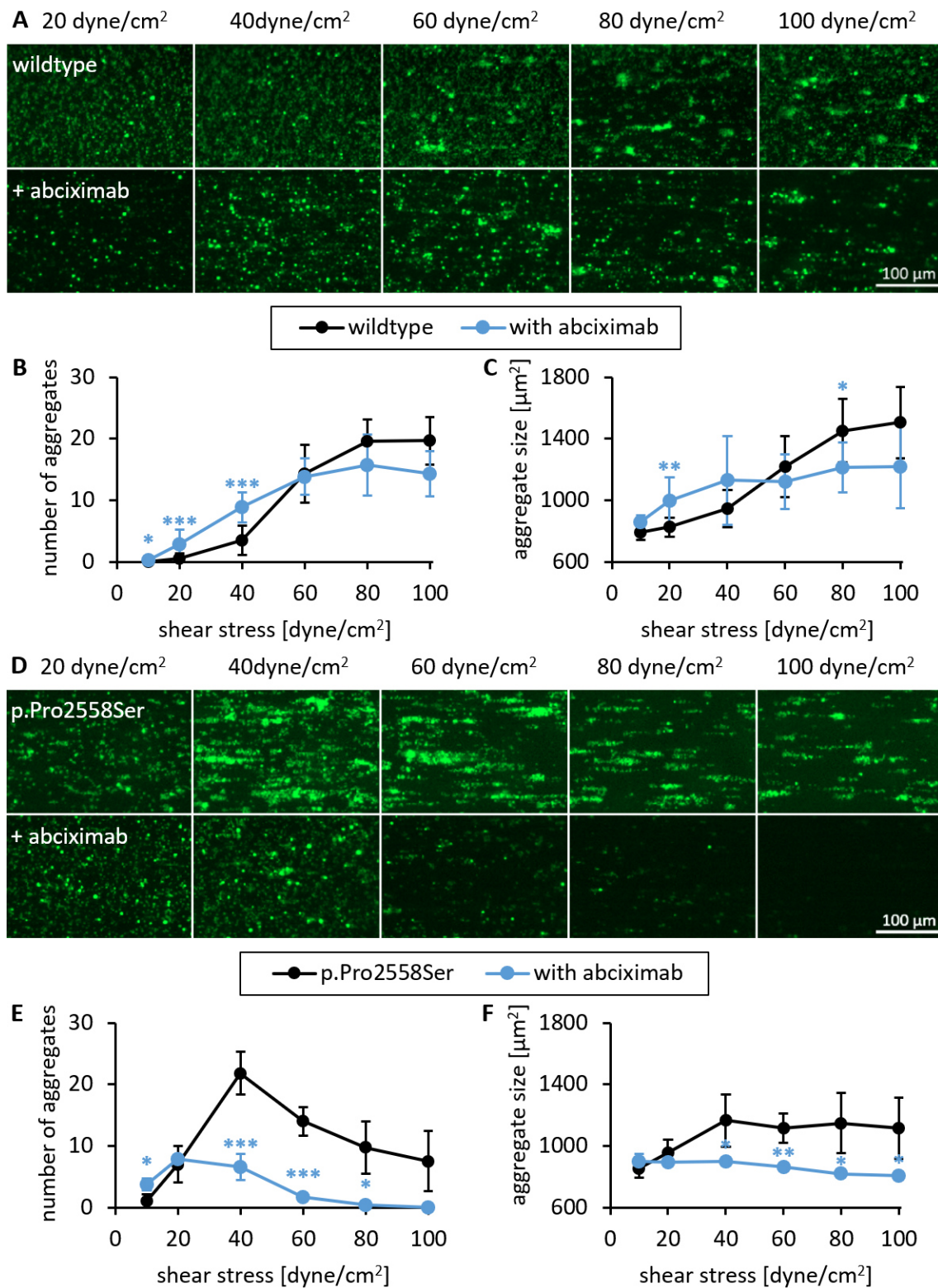


Figure 34: Formation of VWF-platelet collective network by wildtype VWF and variant p.Pro2558Ser in absence and presence of 2.6 µg/mL abciximab at indicated shear stress. (A,D) Representative immunofluorescence images of platelet adhesion and aggregation. Scale bar of 100 µm. (B,C; E,F) Quantification of average aggregate number per 330,000 µm² and average aggregate size for aggregates >700 µm². Mean values ± SEM are shown. Significance was calculated by unpaired t-test p = <0.05 (*), <0.01 (), <0.001 (***)**

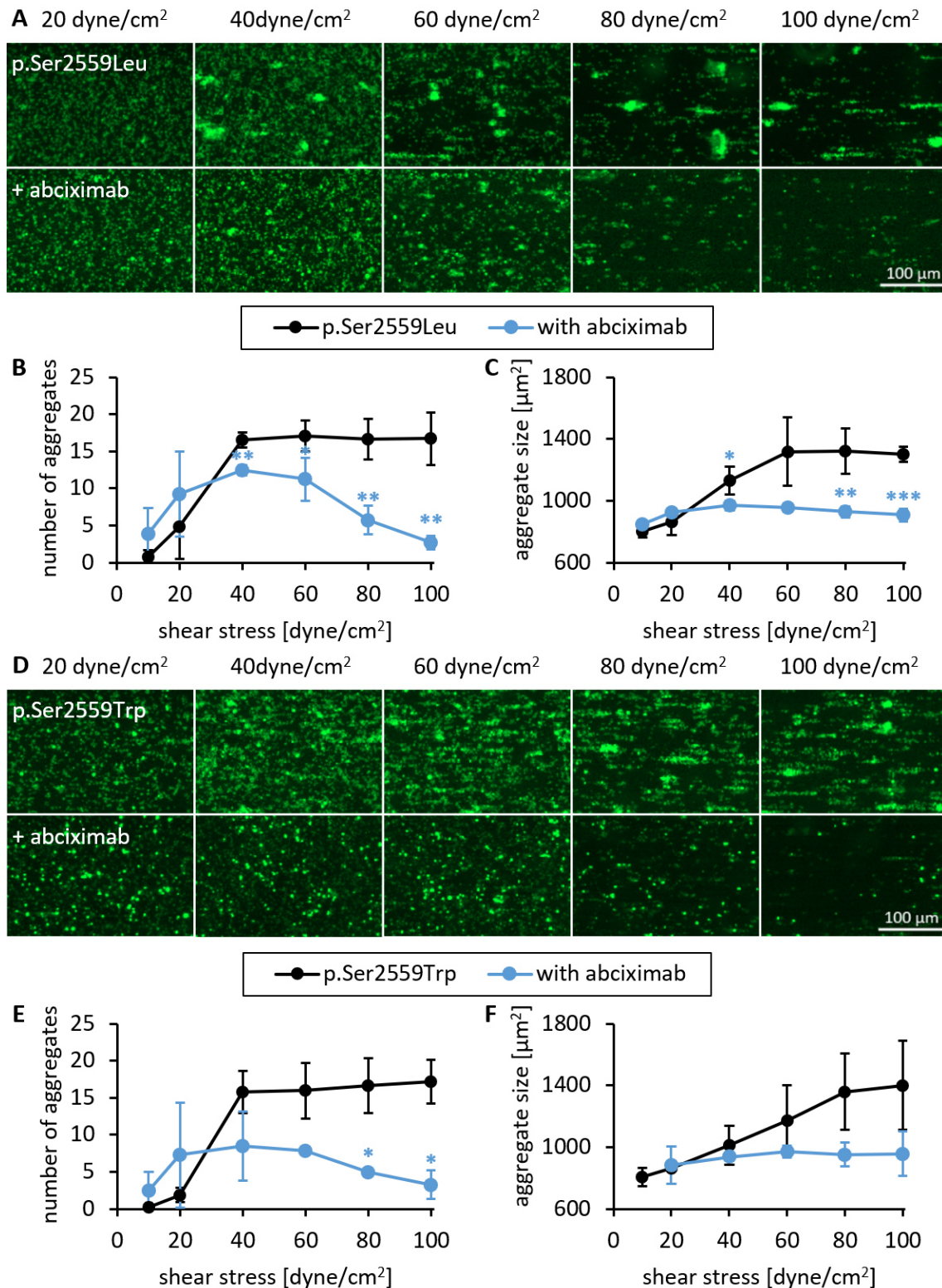


Figure 35: Formation of VWF-platelet collective networks by VWF variants p.Ser2559Leu and p.Ser2559Trp in absence and presence of 2.6 μg/mL abciximab at indicated shear stress. (A,C) Representative immunofluorescence images of platelet adhesion and aggregation. Scale bar of 100 μm. (B,C; E,F) Quantification of average aggregate number per 330,000 μm² and average aggregate size for aggregates >700 μm². Mean values ± SEM are shown. Significance was calculated by unpaired t-test $p = <0.05$ (*), <0.01 (), <0.001 (***)**.

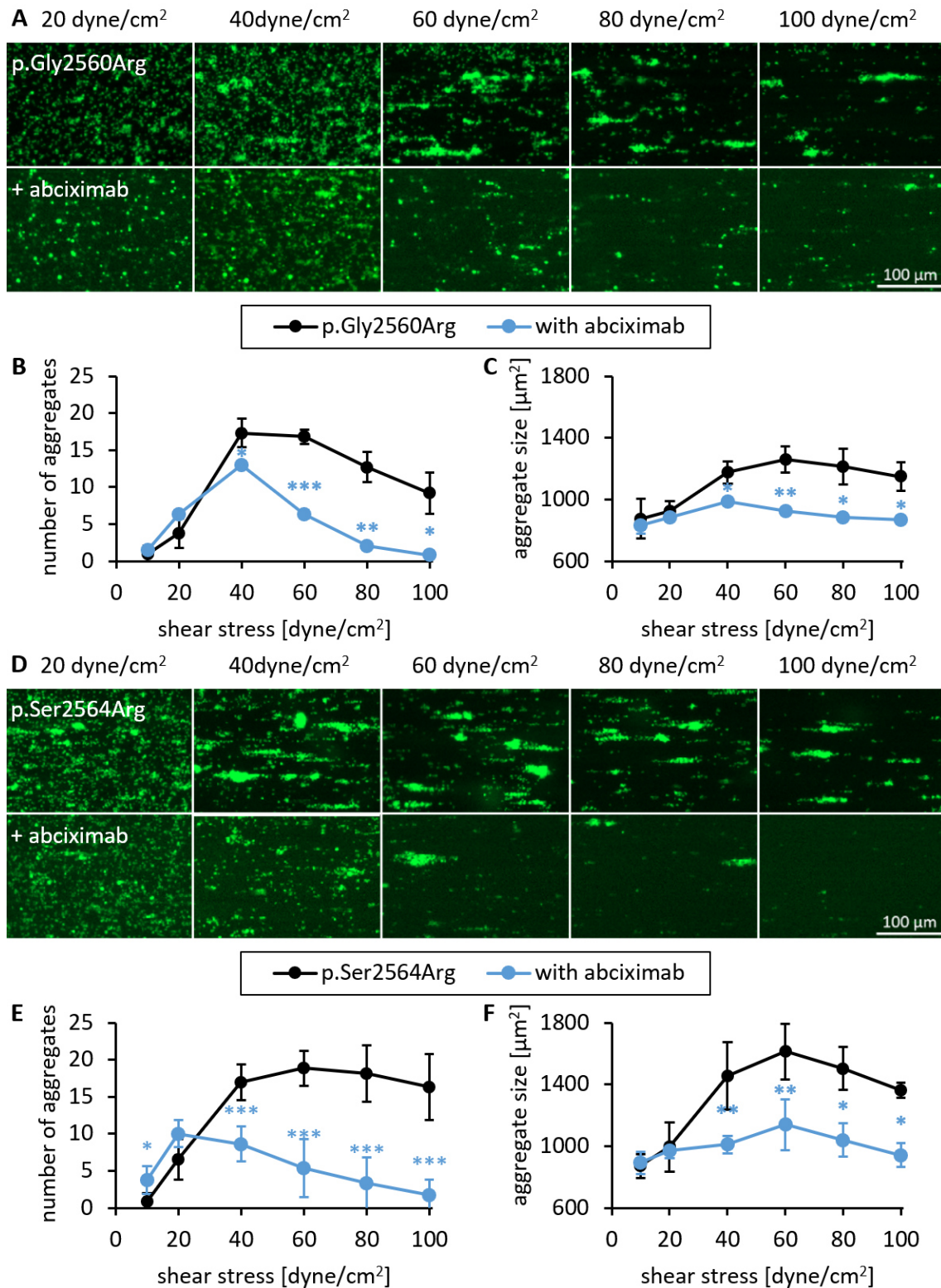


Figure 36: Formation of VWF-platelet collective network by VWF variants p.Gly2560Arg and p.Ser2564Arg in absence and presence of 2.6 µg/mL abciximab at indicated shear stress. (A,C) Representative immunofluorescence images of platelet adhesion and aggregation. Scale bar of 100 µm. (B,C; E,F) Quantification of average aggregate number per 330,000 µm² and average aggregate size for aggregates >700 µm². Mean values ± SEM are shown. Significance was calculated by unpaired t-test p < 0.05 (*), < 0.01 (), < 0.001 (***)**

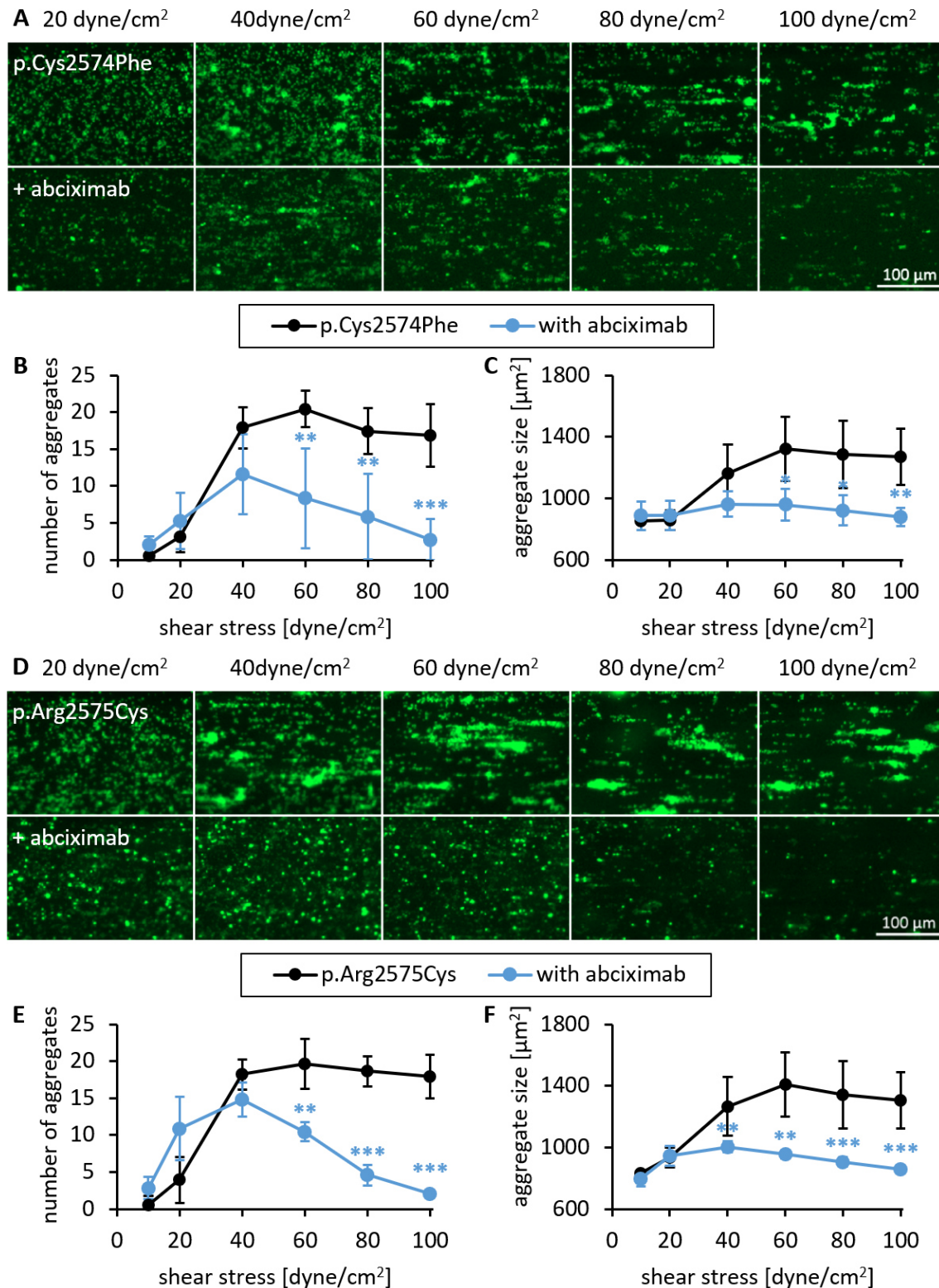


Figure 37: Formation of VWF-platelet collective network by VWF variants p.Cys2574Phe and p.Arg2575Cys in absence and presence of 2.6 µg/mL abciximab at indicated shear stress. (A,C) Representative immunofluorescence images of platelet adhesion and aggregation. Scale bar of 100 µm. (B,C; E,F) Quantification of average aggregate number per 330,000 µm² and average aggregate size for aggregates >700 µm². Mean values ± SEM are shown. Significance was calculated by unpaired t-test $p = <0.05$ (*), <0.01 (), <0.001 (***)**.

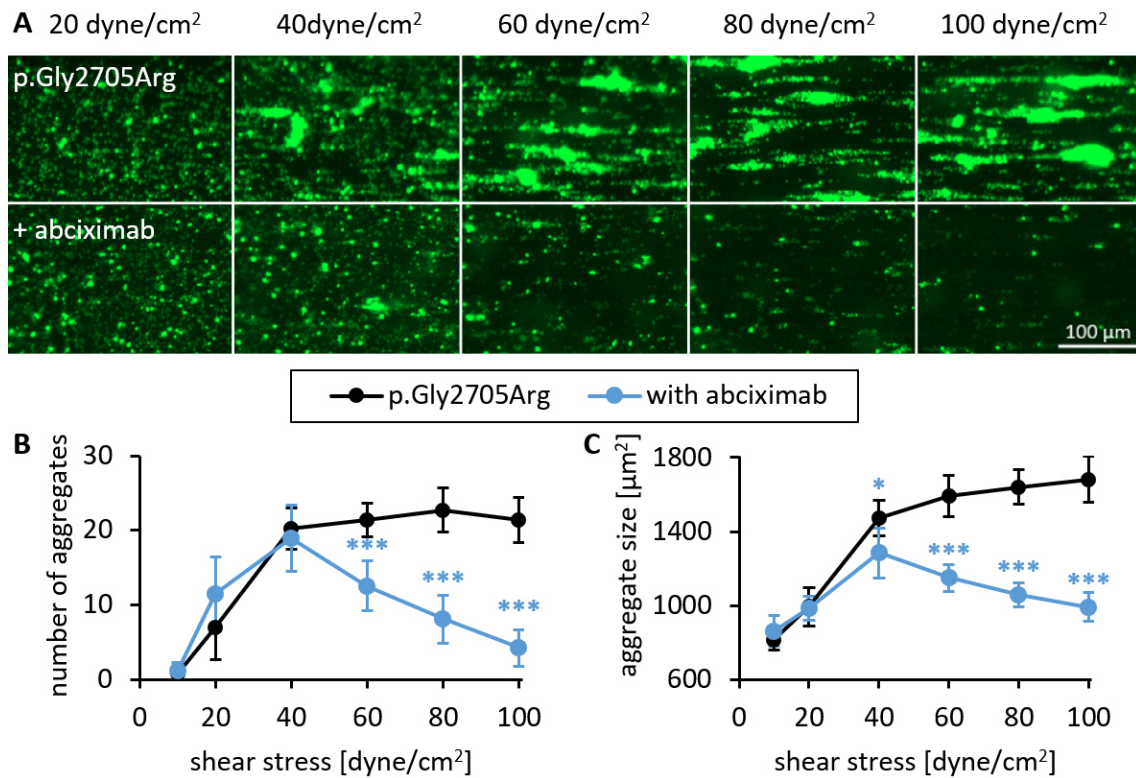


Figure 38: Formation of VWF-platelet collective network by VWF variant p.Gly2705Arg in absence and presence of 2.6 µg/mL abciximab at indicated shear stress. (A) Representative immunofluorescence images of platelet adhesion and aggregation. Scale bar of 100 µm. **(B, C)** Quantification of average aggregate number per 330,000 µm² and average aggregate size for aggregates >700 µm². Mean values ± SEM are shown. Significance was calculated by unpaired t-test p = <0.05 (*), <0.01 (**), <0.001 (***)

6.1.5. Structure prediction of VWF GOF variants using Alphafold2-Multimers

To complete the characterization of VWF GOF variants, structure predictions were performed to investigate the impact of the GOF mutation on the VWF structure. Already Schneppenheim et al. and Huck et al. suggested a GOF mechanism for the variants, which impacts the structure and conformation of the VWF dimeric stem (Huck et al., 2022; Schneppenheim et al., 2019). However, it is not possible to determine the precise structure of proteins as large as VWF by NMR spectroscopy or crystallography. Recently a computational method, called Alphafold2, which predicts protein structures with atomic accuracy, was developed (Jumper et al., 2021). Moreover, a protein complex structure and the multimeric interfaces can be predicted by AlphaFold-Multimer (Evans et al., 2022). With this tool, the dimeric stem of wildtype VWF and all identified GOF variants were predicted. However, due to computational limitations of Alphafold2-Multimer the total size of the VWF monomeric subunit exceeds the size restriction. Therefore, only the C domains including C1 to CK were used as input for structure predictions.

Alphafold2-Multimer predicts the two monomers to associate to a dimer stem conformation with a slightly spiral-shaped twisting (**Figure 39**). Thereby, each domain of the first dimer interacts with the corresponding domain in the second dimer, similar to electron microscopy images of the dimeric stem (Zhou et al., 2011). Solely the C1 and C2 domains form an exception, as they are not predicted to have a common interface, which may also be an artifact due to missing N-terminal domains that further stabilize the closed dimeric stem. The C-terminal CK domains were predicted to be arranged in a knot, similar to the published structure. (Zhou and Springer 2014). Also the C4 and C6 domains were predicted to have a similar structure as published (Chen et al., 2022; Xu et al., 2019).

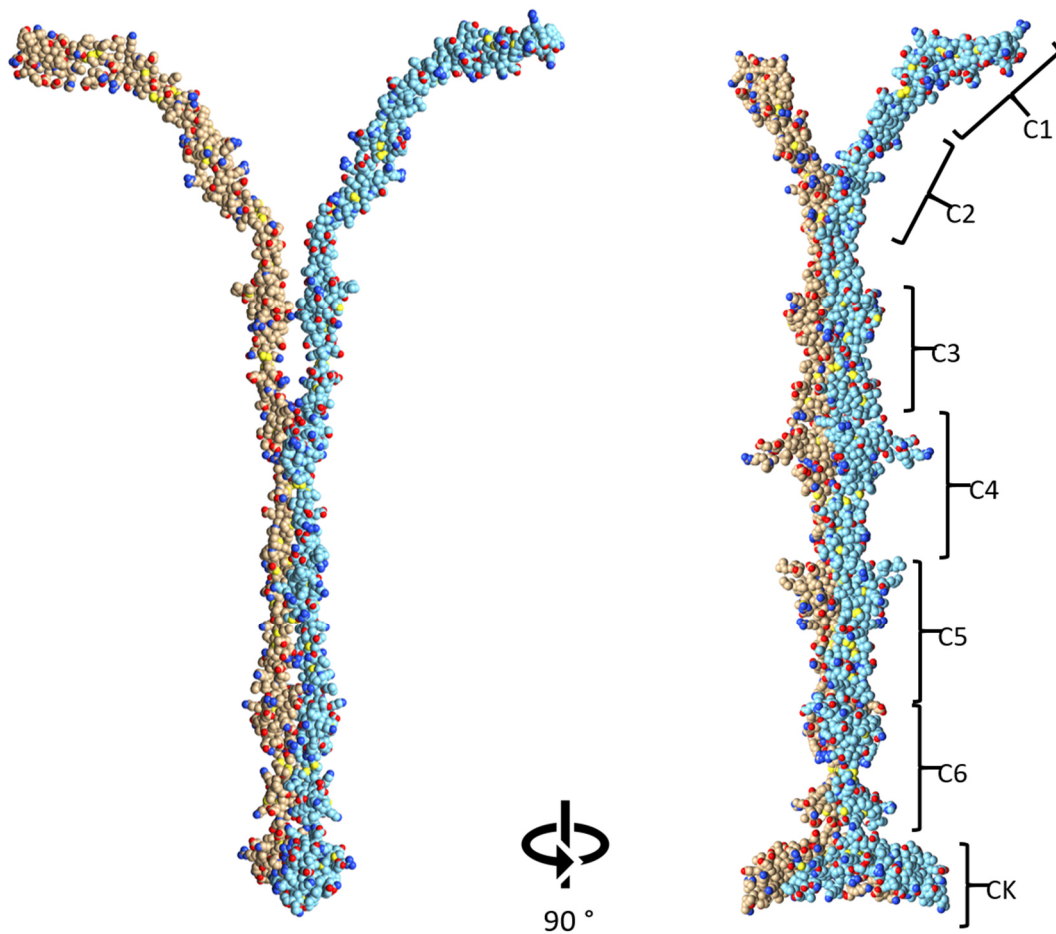


Figure 39: Prediction of the dimeric structure of wildtype VWF, including domains C1-CK, by Alphafold2-Multimer. One monomer is colored in blue, the other in brown. Heteroatoms are colored in red (oxygen, O), blue (nitrogen, N) and yellow (sulfur, S). Structure is turned by 90°. Domains are labeled with C1-CK.

The dimeric stem of novel GOF variants in the C4 domain (p.Pro2558Ser, p.Ser2559Leu/Trp, p.Gly2560Arg, p.Ser2564Arg, p.Cys2574Phe and p.Arg2575Cys) and already published GOF variants (p.Pro2555Arg, p.Phe2561Tyr) is predicted to have a similar structure without disruption of the stem association (**Figure 40A**). Except for Phe2574, all GOF residues are predicted to be surface exposed and not involved in the dimeric interface. (**Figure 40B**). Interestingly, GOF residues Ser2558, Leu/Trp2559, Arg2560 and Tyr2561 are pointing towards the C5 domain.

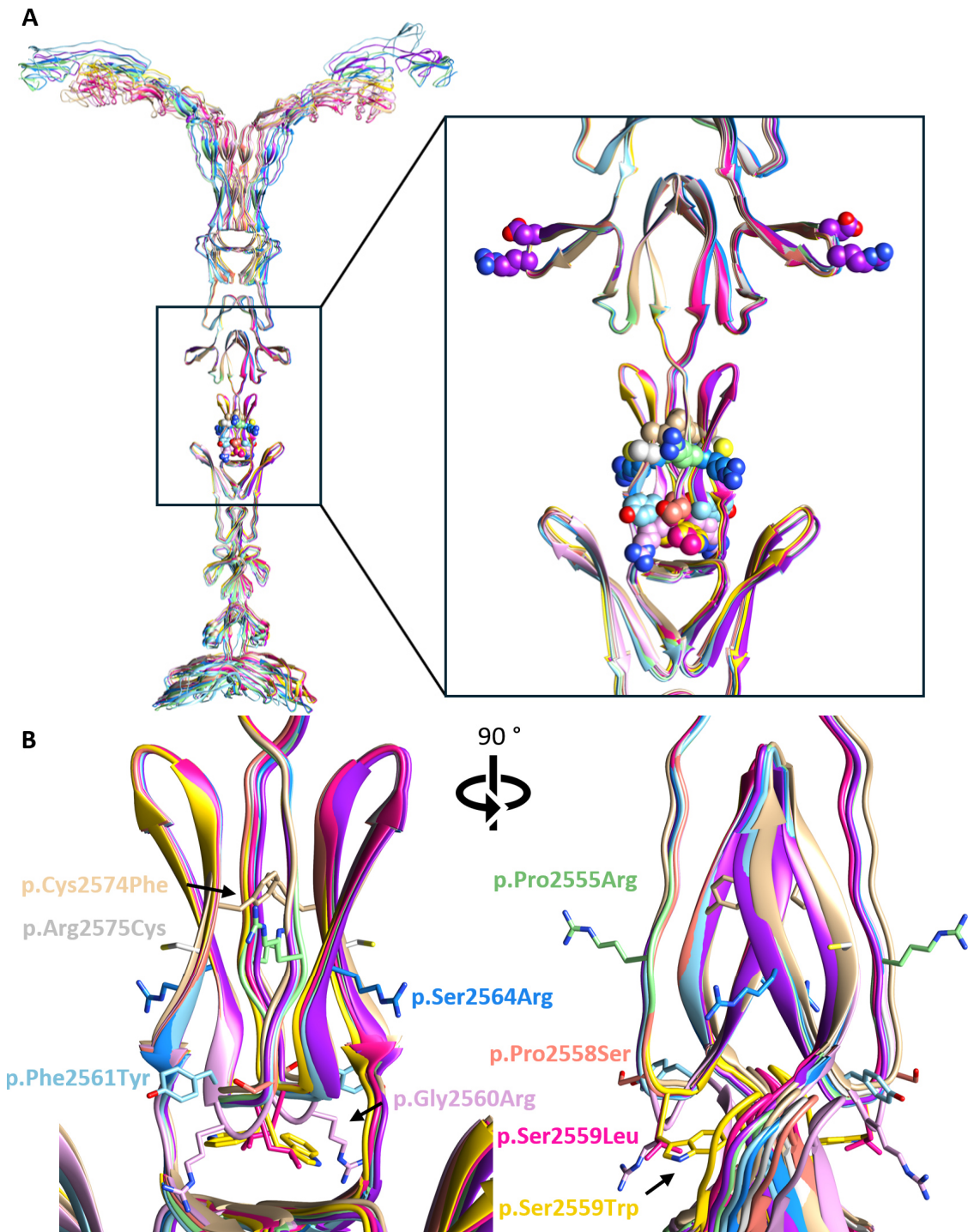


Figure 40: Prediction of the dimeric structure of VWF C1-CK domain of wildtype and GOF variants in the C4 domain by Alphafold2-Multimer. (A) Overlay of the C4 domain of all predicted structures by MatchMaker, Chimera with close-up of the predicted C4 domain association in the dimeric stem region. Each structure is colored differently. GOF residues are displayed as spheres and colored by heteroatom. Heteroatoms are colored in red (oxygen, O), blue (nitrogen, N) and yellow (sulfur, S). (B) Close-up of the SD2 of the C4 domain with representation of GOF residues as sticks.

Variant p.Gly2705Arg was the only GOF variant identified in the C6 domain of VWF and published as collaborative work (Chen et al., 2022). Alphafold2-Multimer predicts a similar dimeric stem interface as the wildtype (**Figure 41**). However, presence of arginine at position 2705 introduced a novel ionic bond with Asp2726 in the CK domain and a reorganization of beta sheets and hydrogen bonds in the CK domain.

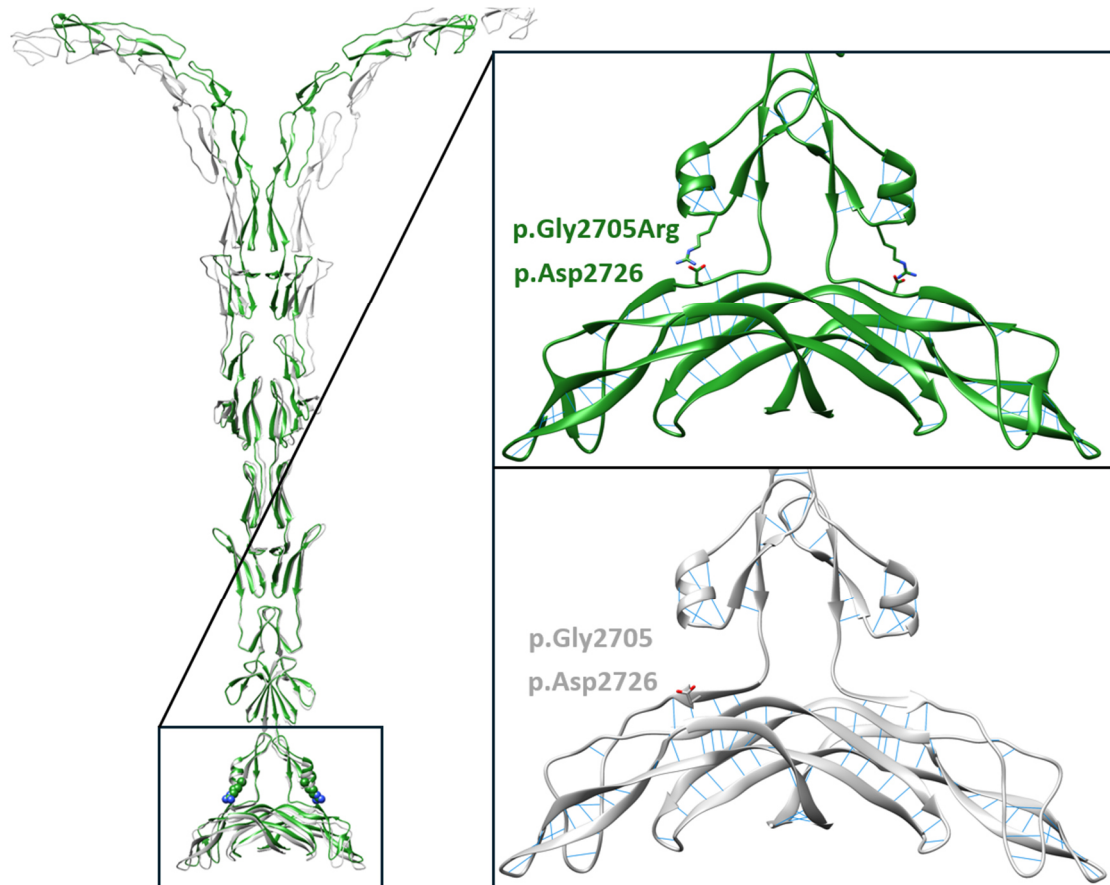


Figure 41: Prediction of the dimeric structure of VWF C1-CK domain of wildtype (grey) and GOF variant p.Gly2705Arg (green) in the C6 domain by Alphafold2-Multimer. Overlay of the C6 domain of both structures by MatchMaker, Chimera with close-up of the predicted C6 and CK domain association in the dimeric stem region. GOF residues are displayed as spheres or sticks and colored by heteroatom. Heteroatoms are colored in red (oxygen, O), blue (nitrogen, N) and yellow (sulfur, S). Hydrogen bonds are indicated as blue lines.

6.2. Disease association of VWF GOF variants

Previous studies of Schneppenheim et al. and Huck et al. characterize the variants p.Phe2561Tyr and p.Pro2555Arg as GOF variants (Huck et al., 2022; Schneppenheim et al., 2019). In the LURIC study, a correlation between the prevalence of the VWF variant p.Phe2561Tyr and the recurrence of MI was found, which reached significance in the subgroup of female patients with an age <55 years (Schneppenheim et al., 2019; Winkelmann et al., 2001). In this thesis, a second patient cohort study was performed including 522 patients. Accordingly, the prevalence and correlations of the GOF variant p.Phe2561Tyr and the onset of MI were calculated for this cohort. Moreover, to assess whether the GOF variants are causal for thrombotic events, *in vivo* studies were performed with mice expressing VWF variants and hemostasis and thrombosis were investigated.

6.2.1. Correlation of variant p.Phe2561Tyr prevalence and the occurrence of MI

The patient cohort of 522 patients was divided into a control group with 236 patients and a CAD group with 286 patients diagnosed with CAD. In total 306 males and 216 females were included with an average age of 67.3 years (**Table 18**).

Table 18: Patients cohort divided in control group and CAD group. Sex, genotype, average age and numbers of patients with myocardial infarction (MI) are given.

	control group	CAD group	total
total	236 (100 %)	286 (100 %)	522 (100 %)
sex			
female	130 (55.1 %)	86 (30.1 %)	216 (41.4 %)
male	106 (44.9 %)	200 (69.9 %)	306 (58.6 %)
average age [years]	64.8	69.4	67.3
genotype			
wildtype	218 (92.4 %)	268 (93.7 %)	486 (93.1 %)
p.Phe2561Tyr	18 (7.6 %)	17 (5.9 %)	35 (6.7 %)
p.Ser2559Trp	0 (0 %)	1 (0.3 %)	1 (0.2%)
patients with MI	5 (2.1 %)	107 (37.4 %)	112 (20.3 %)
thereof wildtype	4 (80 %)	103 (96.3 %)	107 (95.5 %)
thereof p.Phe2561Tyr	1 (20 %)	3 (2.8 %)	4 (3.6 %)
thereof p.Ser2559Trp	0 (0%)	1 (0.9 %)	1 (0.9 %)

Across both groups, 35 out of 522 patients harbor the p.Phe2561Tyr genotype, accounting for 6.7 % of patients. One patient with genotype p.Ser2559Trp was found. Out of 236 control patients, 5 experienced 1 MI (= 2.1 %) whereas in the CAD group 107 patients suffered from ≥ 1 MIs (= 37.4 %), resulting in a total of 112 patients. However, only 4 out of 112 patients (= 3.3 %), who developed ≥ 1 MI, are p.Phe2561Tyr carriers. The odds ratio (OR) for the development of an MI in p.Phe2561Tyr carriers across groups is 0.46 (95 % confidence interval: 0.16 – 1.32), which results in a reduced risk by a 0.52-fold (95 % confidence interval: 0.18 – 1.44), contrary to expectations.

The average age at the first MI for all patients is 63.7 years (± 12.8 years). Two patients had to be excluded from the calculations because the date of the MI was unknown. When considering only p.Phe2561Tyr carriers, the average age to develop a first MI was found to be lower than that of wildtype carriers, with an average age of 53.8 years (± 17.5 years) compared to 64.1 years (± 12.4 years). This results in a decreased event-free survival, with the event defined as the first MI (**Figure 42**).

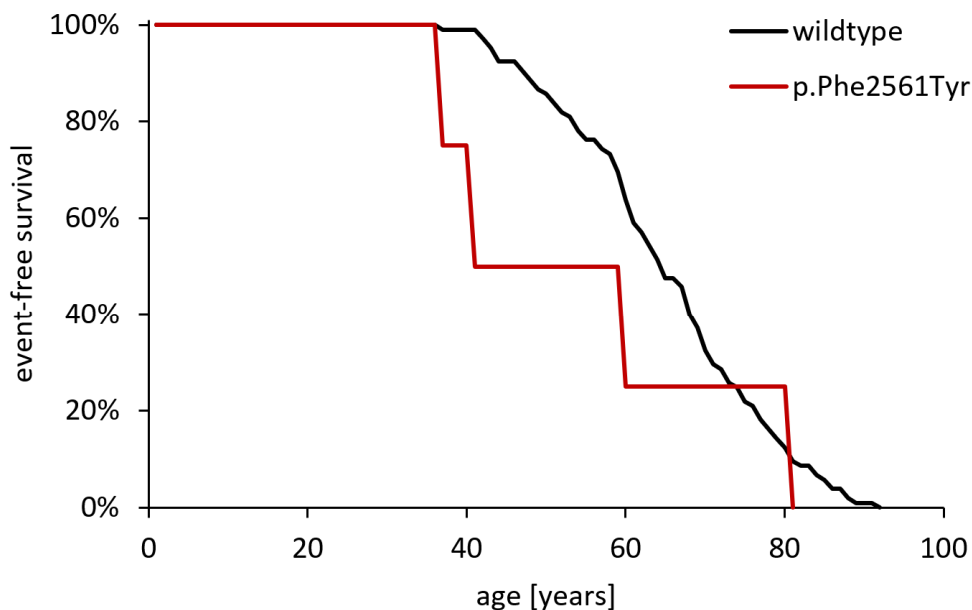


Figure 42: Event-free survival in patients with ≥ 1 MI and p.Phe2561Tyr or wildtype phenotype.

The proportion of patients without MI over time is given on the y-axis as event-free survival. The event is defined as first MI. The age at onset of the first MI is presented on the x-axis.

Further calculations for each groups are made in the following sections.

6.2.1.1. Control group

The control group consists of 236 patients, from which 55.1 % are females and 44.9 % are males (**Table 19**). 18 patients harbor the variant p.Phe2561Tyr, which results in a prevalence of 7.6 %. The prevalence for p.Phe2561Tyr varies between sexes with a prevalence of 10 % for females and 4.7 % for males.

Table 19: Number of patients with 0, 1 or >1 MI in the control group, characterized by patients, who were not diagnosed with CAD. Further differentiation by sex and age are given in each row.

control group	myocardial Infarctions [no]			total
	0	1	>1	
all	231	5	0	236
wildtype	214	4	0	218
p.Phe2561Tyr	17	1	0	18
female (all)	127	3	0	130
wildtype	115	2	0	117
p.Phe2561Tyr	12	1	0	13
female (<55)	18	0	0	18
wildtype	17	0	0	17
p.Phe2561Tyr	1	0	0	1
female (≥55)	109	3	0	112
wildtype	98	2	0	100
p.Phe2561Tyr	11	1	0	12
male (all)	104	2	0	106
wildtype	99	2	0	101
p.Phe2561Tyr	5	0	0	5
male (<55)	30	1	0	31
wildtype	28	1	0	29
p.Phe2561Tyr	2	0	0	2
male (≥55)	74	1	0	75
wildtype	71	1	0	72
p.Phe2561Tyr	3	0	0	3

One p.Phe2561Tyr carrier in the control group experienced one MI, which results in a proportion of 5.6 % for the total of 18 p.Phe2561Tyr carriers (**Figure 43**). This carrier is female and 59 years of age. In contrast, 4 out of 218 patients with wildtype genotype developed an MI, resulting in a proportion of 1.8 %. The sex and age distribution of these 4 patients is relatively uniform, as 2 out of 4 patients are male, and 3 out of 4 are ≥ 55 years of age.

Taken together, from all 5 patients in the control group, who suffered from MI, 1 patient is carrying the variant p.Phe2561Tyr, resulting in a proportion of 20 %. The odds ratio (OR) for the development of an MI in p.Phe2561Tyr carriers of the control group is 3.15 (95 % confidence interval: 0.33 – 29.75), which results in an elevated risk by a 3.03-fold (95 % confidence interval: 0.52 – 17.56).

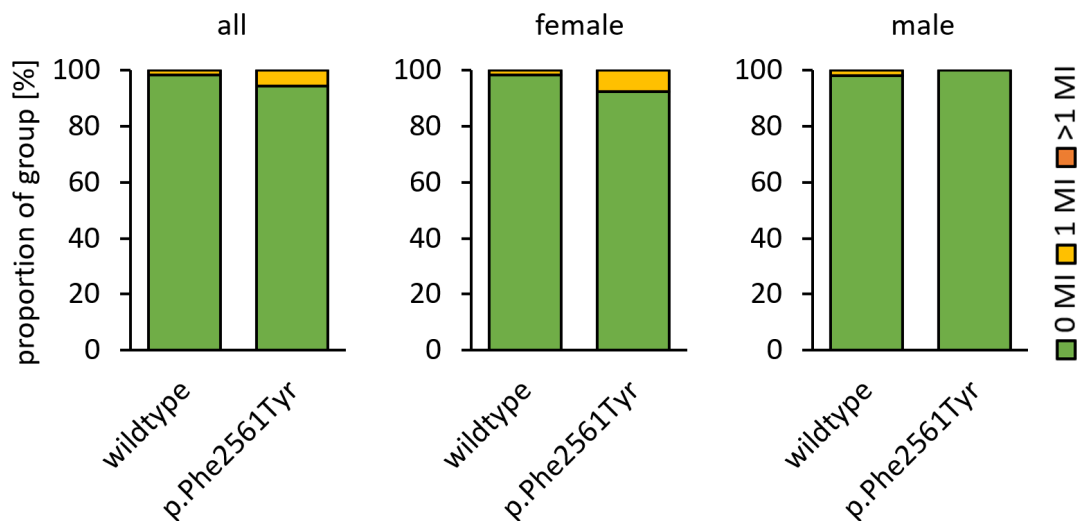


Figure 43: Proportion of patients with 0 MI (green), 1 MI (yellow), and >1 MI (orange) for the control group and female or male subgroup.

6.2.1.2. CAD group

The CAD group consists 286 patients, from which 30.1 % are female and 69.9 % male (**Table 20**). The majority of males and females are ≥ 55 years old, namely 95.3 % of females and 92 % of males. 17 patients out of 286 have a p.Phe2561Tyr genotype, which results in a proportion of 5.9 %. There is a slight difference in the prevalence of the p.Phe2561Tyr genotype between the sexes, with a prevalence of 4.7 % in females and 6.5 % in males.

Table 20: Number of patients with 0, 1 or >1 MI in the CAD group, characterized by patients, who were diagnosed with CAD. Further differentiation by sex and age are given in each row.

CAD group	myocardial Infarctions [no]			total
	0	1	>1	
all	179	91*	16	286*
wildtype	165	87	16	268
p.Phe2561Tyr	14	3	0	17
female (all)	52	30	4	86
wildtype	48	30	4	82
p.Phe2561Tyr	4	0	0	4
female (<55)	2	2	0	4
wildtype	2	2	0	4
p.Phe2561Tyr	0	0	0	0
female (≥ 55)	50	28	4	82
wildtype	46	28	4	78
p.Phe2561Tyr	4	0	0	4
male (all)	127	61*	12	200*
wildtype	117	57	12	186
p.Phe2561Tyr	10	3	0	13
male (<55)	6	9*	1	16
wildtype	6	7	1	14
p.Phe2561Tyr	0	1	0	1
male (≥ 55)	121	52	11	184
wildtype	111	50	11	172
p.Phe2561Tyr	10	2	0	12

* = includes one patient with p.Ser2559Trp

3 out of 17 p.Phe2561Tyr carriers developed one MI, which results in a proportion of 17.6 % (**Figure 44**). No female p.Phe2561Tyr carrier who experienced an MI was identified. Instead, 3 male p.Phe2561Tyr carriers suffered from one MI, accounting for 23.1 % of all male p.Phe2561Tyr carriers. Two of these patients were ≥ 55 years of age.

In contrast, 87 out of 269 wildtype carriers in the CAD group developed one MI and 16 patients developed >1 MI, accounting for 32.3 % and 5.9 %, respectively. In total 103 patients developed at least 1 MI, of which 69 are male (= 67 %). This proportion is similar to the total amount of males in the CAD group. From 69 male patients, 57 developed one MI and 12 males developed >1 MI, corresponding to 30.6 % and 6.5 %, of all male wildtype carriers, respectively. Only 8 out of 69 male patients are <55 years of age. Of all females in the wildtype group, 30 (36,6 %) developed one MI and 4 (4.9 %) developed >1 MI. Only 2 out of these 34 females are <55 years of age.

Of all patients in the CAD group who developed MI, p.Phe2561Tyr carriers account for 2.8 % (3 out of 107). The odds ratio (OR) for the development of an MI in p.Phe2561Tyr carriers of the CAD group is 0.34 (95 % confidence interval: 0.1 – 1.22), which results in a reduced risk by 0.46-fold (95 % confidence interval: 0.13 – 1.56).

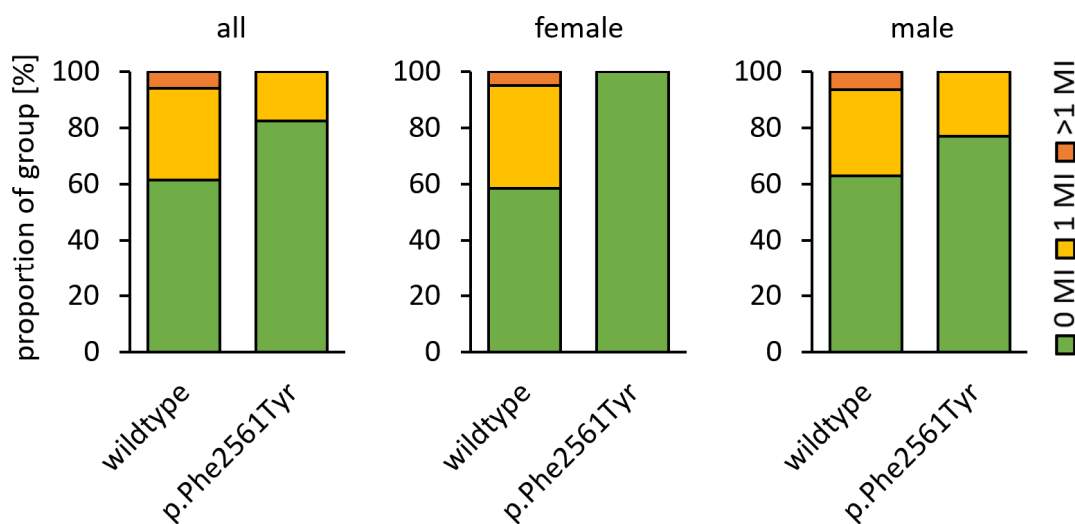


Figure 44: Proportion of patients with 0 MI (green), 1 MI (yellow), and >1 MI (orange) for the CAD group and the female or male subgroup.

Two p.Phe2561Tyr carriers were genotyped to be homozygous. These patients are both male, 77 and 73 years of age, respectively, and did not suffer from MI. However, the 77-year-old patient was diagnosed with one-vessel CAD and has experienced a pulmonary arterial embolism and an infarct pneumonia with deep vein thrombosis in the vena femoralis and vena poplitea, whereas the 73-year-old patients was diagnosed with two-vessel CAD and suffered from cerebral ischemia in the arteria cerebri media.

6.2.1.2.1. Classification of CAD

The patient cohort of CAD can be further subdivided into one-vessel, two-vessel, three-vessel CAD and CAD with atherosclerosis but without significant stenosis, depending on how many coronary arteries are affected. Two patients had to be excluded from the subdivision because the CAD was not further classified. In total, 39.4 % of all patients had three-vessel CAD, 28.5 % had two-vessel CAD, 24.6 % had one-vessel CAD and 7.4 % had sclerosis but no significant stenosis (**Table 21**). The distribution is similar for patients with the genotype p.Phe2561Tyr.

Table 21: Classification of coronary artery disease (CAD) and their distribution. Numbers and percentages of patients with one-vessel (1), two-vessel (2) or three-vessel (3) CAD and CAD with atherosclerosis but without significant stenosis (sclerosis) are shown for all CAD patients and separately for the wildtype and p.Phe2561Tyr carriers.

	sclerosis	1	2	3	Total
Total	21 (7.4 %)	70 (24.6 %)	81 (28.5 %)*	112 (39.4 %)	284 (100 %)*
wildtype	20 (7.5 %)	66 (24.8 %)	75 (28.1 %)	106 (39.7 %)	267 (100 %)
p.Phe2561Tyr	1 (6.25 %)	4 (25 %)	5 (31.3 %)	6 (37.5 %)	16 (100 %)

* = includes one patient with p.Ser2559Trp

6.2.2. *In vivo* mouse studies of VWF variants

To investigate whether GOF variants might be causal for an increased risk of thrombosis *in vivo*, mouse studies were performed. For the experimental setup C575BL/6 mice with a VWF knock-out (KO) were used. These mice have an impaired hemostasis and present extensive bleeding (Denis et al., 1998). To introduce the VWF protein, mice were hydrodynamically injected with the pLIVE vector, which harbors the murine VWF CDS. Hydrodynamically injected pLIVE vector is primarily taken up by the liver, which subsequently produces and secretes VWF (Casari et al., 2013). The vector either contained the wildtype VWF sequence or the VWF variant with the desired mutation. As control an empty pLIVE vector was injected.

To reduce the need of animal experiments to a minimum, not all identified variants were investigated. Since, all GOF variants identified in this study have a similar phenotype as variants p.Phe2561Tyr or p.Pro2555Arg, the study focused on the evaluation of these two GOF variants. Human VWF and murine VWF share a high sequence identity of 83.19 % (The UniProt Consortium, 2023). Both variants p.Phe2561 and p.Pro2555 are conserved in mice. Accordingly, these positions were mutated in the pLIVE vector and introduced into mice. The secretion of VWF was quantified and the degree of multimerization was determined. Subsequently, the mice were evaluated for hemostatic potency in a tail-clip assay or for the genesis of thrombosis in a ferric chloride-induced model.

6.2.2.1. Expression of mVWF variants

To ascertain the efficacy of the hydrodynamic injection and the presence of murine VWF (mVWF), plasma samples of mice were collected three days post-injection, expression of mVWF was verified by ELISA and the multimer pattern was studied by immunoblotting. The mVWF:Ag in mice after hydrodynamic injection was approximately 12-14 times higher than in standard murine pooled normal plasma (mPNP) collected from parental mice (**Figure 45A**), which is consistent with the anticipated outcome for this method (Casari et al., 2013). Multimer analysis revealed that mVWF produced from hydrodynamically injected mice are correctly multimerized and display only a slight reduction of HMWM, when compared to the murine standard (**Figure 45B**).

The mVWF variants p.Phe2561Tyr and p.Pro2555Arg exhibit no significant difference in expression or multimerization when compared to the wildtype control, indicating that the point mutations themselves have no effect on the expression or secretion of mVWF in mice.

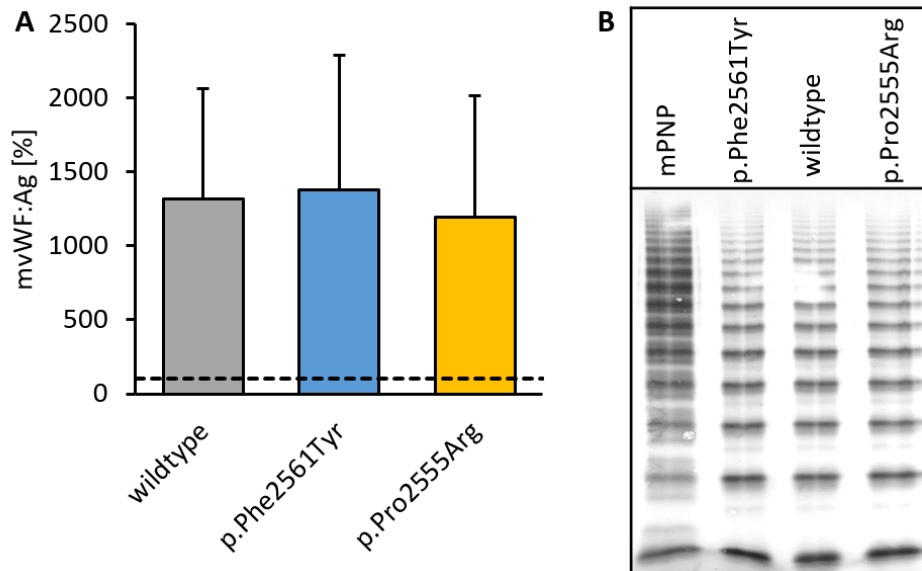


Figure 45: mVWF from platelet-poor plasma collected from C57BL/6 VWF-KO mice three days after hydrodynamic injection of the VWF variant expression vector pLIVE. (A) Plasma mVWF:Ag levels of mice expressing wildtype VWF or VWF variants p.Phe2561Tyr or p.Pro2555Arg were determined by ELISA using rabbit-anti-VWF primary and goat-anti-rabbit-HRP secondary antibody. The dotted line corresponds to mVWF:Ag levels of murine pooled normal plasma (mPNP) of 100 %. **(B)** Multimer analysis of mVWF from mPNP, as well as wildtype and variant mVWF from mice injected with the pLIVE vector. Samples were investigated by size separation with gel electrophoresis, western blotting and detection with rabbit-anti-VWF primary and goat-anti-rabbit-HRP secondary antibody.

6.2.2.2. Evaluation of hemostasis of mVWF variants

The evaluation of hemostasis was conducted on VWF-KO mice four days post-hydrodynamic injection. The tail-clip assay was performed on anesthetized mice by cutting 3 mm of the tail tip and observing the bleeding behavior. Lost blood was collected in 0.9 % saline buffer and quantified by colorimetric analysis. Five mice were injected with empty vector control, 11 mice with wildtype VWF, and 8 mice with each VWF variant. By noting the bleeding times, mice were classified as ‘no stop’, ‘stop with rebleeds’ or ‘stop without rebleeds’ (**Figure 46A**).

As expected, mice lacking mVWF exhibit a disturbed hemostasis. All individuals did not stop bleeding, whereas mice expressing wildtype VWF after hydrodynamic injection stopped bleeding in 90.9 % of cases (10 out of 11). However, 63.6 % still had rebleeds, indicating that hydrodynamic injection can only partially restore the function of VWF. Variant p.Phe2561Tyr displayed a defect in hemostasis as bleedings did not stop in 50 % of the cases (4 out of 8). Also, variant p.Pro2555Arg showed a mild defect as 25 % of mice did not stop bleeding (2 out of 8). The amount of mice which stopped bleeding without rebleeding was decreased to 0 % in the p.Phe2561Tyr group and increased to 37.5 % (3 out of 8) in the p.Pro2555Arg group, compared to approx. 27.3 % (3 out of 11) in the wildtype group.

The first arrest of bleeding was determined for all mice that achieved a bleeding stop. Mice expressing wildtype VWF mainly stopped bleeding after 175.5 seconds, whereas variants p.Phe2561Tyr and p.Pro2555Arg led to an average bleeding time of approximately 214 and 191 seconds, respectively (**Figure 46B**).

Mice expressing wildtype mVWF lost an averaged blood volume of 121.3 μL (**Figure 46C**). In contrast, the empty vector control had a significantly increased value of 617.6 μL . Mice in the p.Phe2561Tyr and p.Pro2555Arg groups lost an average blood volume of 329.5 μL and 276 μL , respectively. Although higher, no significant difference is calculated by unpaired t-test.

Noteworthy, a high number of mice expressing wildtype VWF after hydrodynamic injection suffered from rebleeds. However, the blood flow observed after rebleeding was weak and usually stopped after a very short time. Consequently, blood loss was low in mice with wildtype VWF. In contrast, mice with variants p.Phe2561Tyr or p.Pro2555Arg suffered from stronger rebleeds, which was also reflected in the increased blood loss. The observation of bleeding behavior led to the assumption that the sealing blood clot may be unstable and torn away, resulting in a recurrent severe bleeding. Similarly, mice that failed to stop bleeding over the course of 20 min displayed periods where blood flow decreased over time, but unexpectedly increased again at one point, indicating impaired hemostasis. This phenomenon differs from mice injected with the empty vector, in which bleeding did not stop and blood flow is steady from start to finish.

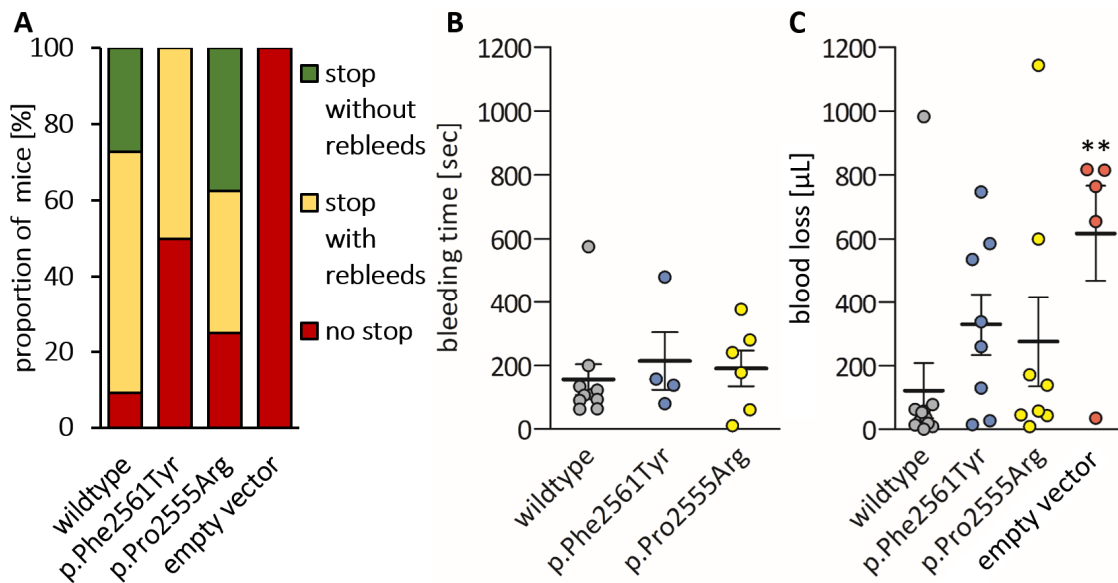


Figure 46: Bleeding behavior of C57BL/6 VWF-KO mice with hydrodynamic injection of empty pLIVE vector control, wildtype mVWF plasmid or plasmids containing the variant p.Phe2561Tyr or p.Pro2555Arg in tail-clip assay. 3 mm of the tail was cut and incubated in 37 °C saline buffer. Bleeding time was noted. Collected blood was quantified by colorimetric analysis. **(A)** Proportion of mice per group that stopped and did not rebleed (green), stopped but rebled (yellow) or did not stop bleeding (red). **(B)** Average time for the first bleeding arrest in all mice with rebleeds per group. **(C)** Average blood loss in μL per group. Single mice are indicated as dots. Mean values \pm SEM are shown. Significance was calculated by unpaired t-test: = <0.05 (*), <0.01 (**), <0.001 (***)

To exclude that the observed effect of the mVWF variants is an artefact that is caused by different mVWF:Ag levels, the blood loss was plotted against the mVWF:Ag levels (**Figure 47**). A coefficient of determination (R^2) of 0.0112 states no correlation. Hence, hemostasis is independent from the varying mVWF:Ag levels, and the observed effect is caused by the mVWF variants.

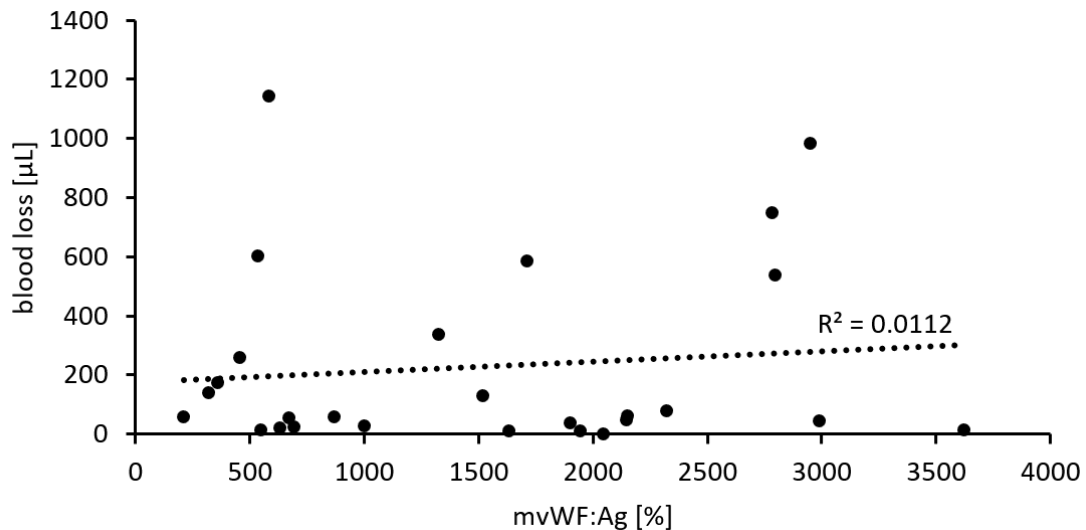


Figure 47: Correlation of mVWF expression and blood loss in tail-clip assay from C575BL/6 VWF-KO mice expressing wildtype VWF or variants after hydrodynamic injection. The amount of blood loss [μL] and the mvWF:Ag levels [%] were plotted for each mouse. A coefficient of determination (R^2) of 0.0112 was calculated.

6.2.2.3. Evaluation of thrombotic potential of mVWF variants

To investigate a putative prothrombotic effect by the GOF variants *in vivo*, a thrombosis model was employed. A doppler flow probe connected to a flowmeter was used to measure the flow of the artery and thrombosis formation was induced by vessel injury using ferric chloride. Experiments were performed for parental mice, VWF-KO mice, and VWF-KO mice injected with wildtype VWF or VWF variant coding pLIVE vector (**Figure 48**).

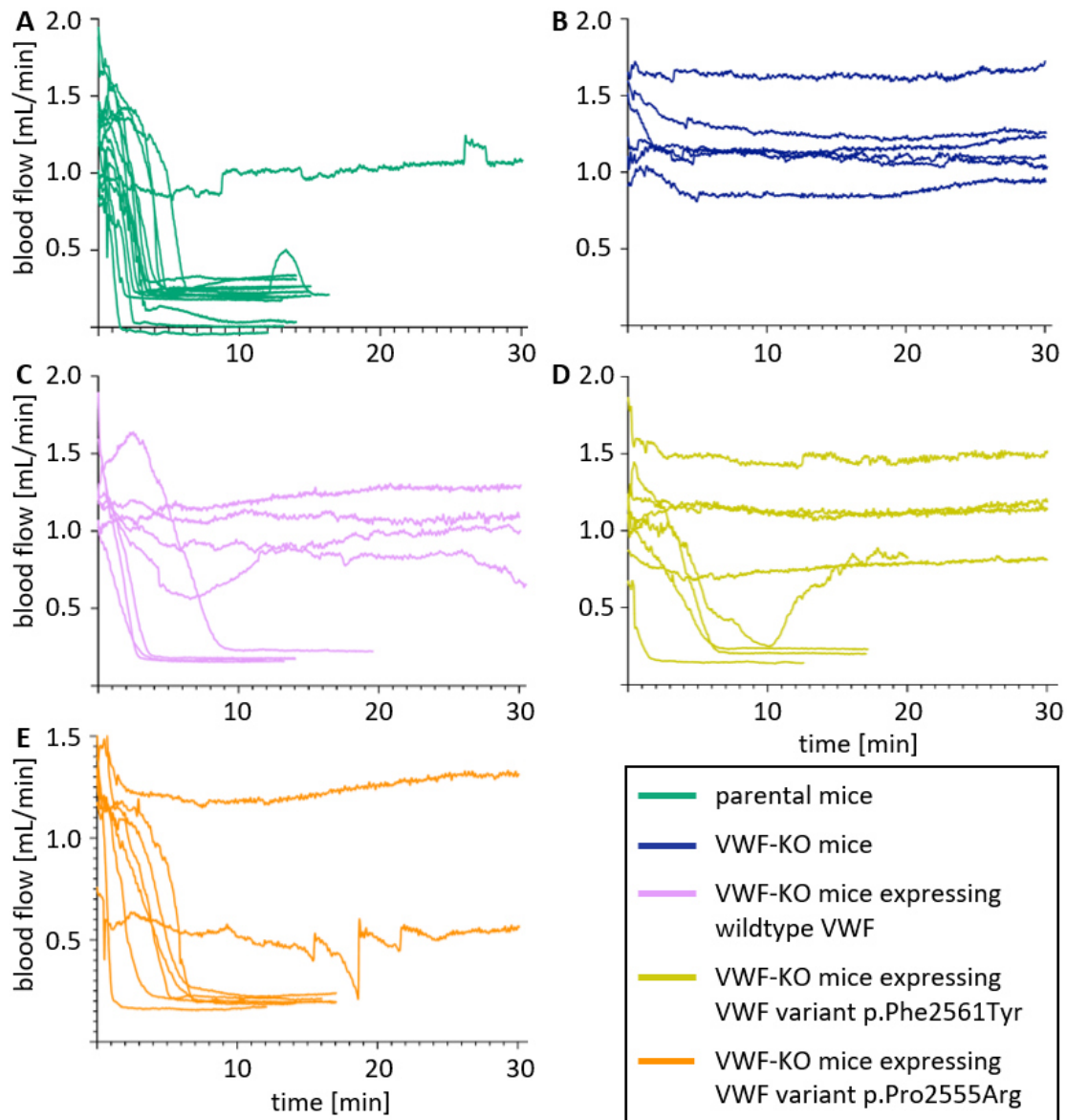


Figure 48: Blood flow of the right common carotid artery of C575BL/6 parental mice, VWF-KO mice or VWF-KO mice with hydrodynamic injection of wildtype mVWF plasmid or plasmids containing the variant p.Phe2561Tyr or p.Pro2555Arg in a thrombosis assay over time. Thrombosis was induced by FeCl_3 treatment of the right common carotid artery. Experiments were performed by the group of Dr. Cécile Denis, INSERM unit 1176, Le Kremlin-Bicêtre. Parental mice **(A)**, VWF-KO mice **(B)**, VWF-KO mice expressing wildtype VWF **(C)**, variant p.Phe2561Tyr **(D)** or variant p.Pro2555Arg **(E)** after hydrodynamic injection are given. Each line represents one mouse.

In control parental mice, the artery was occluded in 13 of 14 cases (= 92.9 %) (**Figure 49A**). In contrast, in VWF-KO mice no occlusion was observed in 6 cases (= 0 %), indicating that VWF is essential for thrombus formation. The phenotype could be partially restored when wildtype VWF was present after hydrodynamic injection. The

artery of 4 out of 8 mice occluded (= 50 %). Similar results were obtained for the mice expressing VWF variant p.Phe2561Tyr. Here, also 4 out of 8 mice (= 50 %) developed an occlusion. However, the vessel of one mouse was reperfused after occlusion, indicating that the thrombus might be unstable. In mice expressing VWF variant p.Pro2555Arg, the proportion of mice which developed an occlusion was increased to 7 out of 8 mice (= 87.5 %).

In the majority of cases, the occlusion developed within the first 600 sec. The average time for an occlusion to occur in parental mice is 534 seconds (**Figure 49B**). An increased average occlusion time of 1159 sec was measured in VWF-KO mice injected with wildtype VWF. For the variant p.Phe2561Tyr, occlusion time was not significantly prolonged with an average occlusion time of 1219 sec and for the variant p.Pro2555Arg, the occlusion time was not significantly shortened to 828 sec.

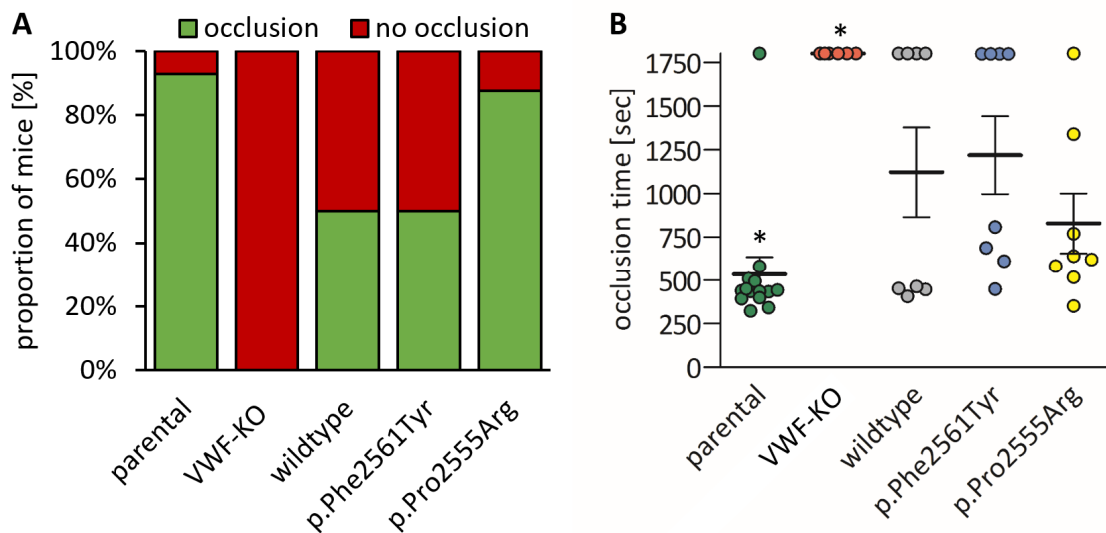


Figure 49: Vessel occlusion in C575BL/6 parental mice, VWF-KO mice or VWF-KO mice with hydrodynamic injection of wildtype mVWF plasmid or plasmids containing the variant p.Phe2561Tyr or p.Pro2555Arg in a thrombosis assay. Thrombosis was induced by FeCl₃ treatment of the right common carotid artery. Experiments were performed by the group of Dr. Cécile Denis, INSERM unit 1176, Le Kremlin-Bicêtre. **(A)** Percentage of mice per group that developed a vessel occlusion (red) versus mice whose artery was not occluded (green). **(B)** Average vessel occlusion time [sec] per group. Single mice are indicated as dots. Values of 1800 sec indicate that occlusion did not occur. Mean values ± SEM are shown. Significance was calculated by unpaired t-test: p = <0.05 (*), <0.01 (**), <0.001 (***)

Similar to the tail-clip assay, an impact of the mVWF:Ag on the occlusion time was excluded. By plotting the occlusion time against the mVWF:Ag levels an R^2 of 0.1054 was calculated, indicating that the observed phenotypes are caused by the VWF variants themselves (**Figure 50**).

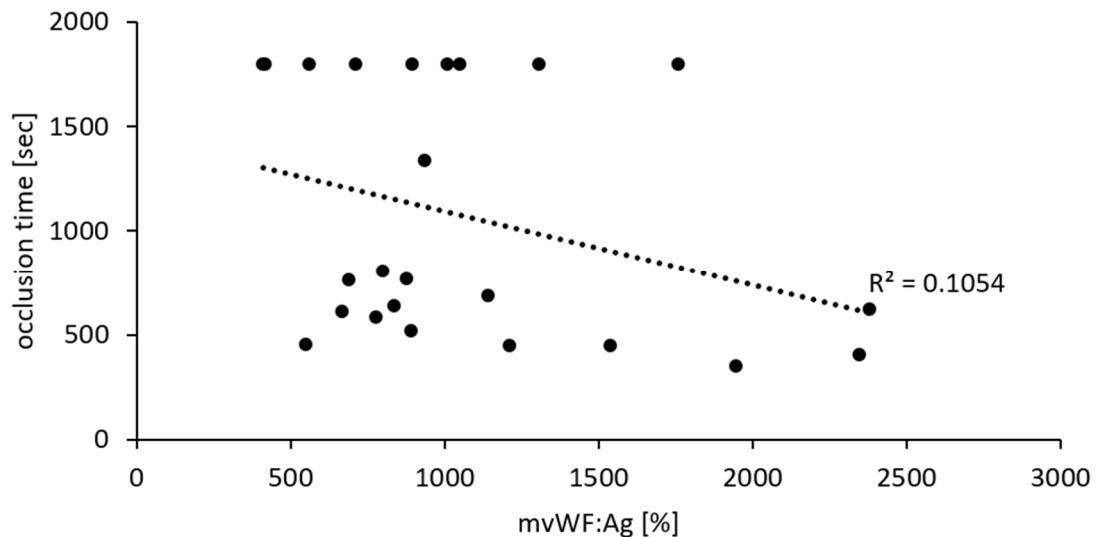


Figure 50: Correlation of mVWF expression and occlusion time in thrombosis assay from C575BL/6 VWF-KO mice expressing wildtype VWF or variants after hydrodynamic injection. The occlusion time [sec] and the mVWF:Ag levels [%] were plotted for each mouse. A coefficients of determination (R^2) of 0.1054 was calculated.

6.3. Measures to counteract a VWF GOF effect

VWF promotes the stable aggregation of platelets via cross-linking of its C4 domain with activated platelet receptor GPIIb/IIIa. This interaction was shown to participate in the GOF effect of variant p.Pro2555Arg, as inhibition by the GPIIb/IIIa inhibitor abciximab abolished the GOF effect (Huck et al., 2022). Since abciximab is no longer approved for use in patients, alternative countermeasures are desirable to reverse the GOF effect. The goal of the study was to identify inhibitory peptides which might be applicable to restore normal VWF function. For the design of such peptides a deeper understanding of C domain dynamics is necessary. Thus, molecular dynamics simulations were performed by our collaboration partners at the Heidelberg Institute for Theoretical Studies gGmbH (HITS), Germany.

6.3.1. Dynamics of C4 domain

The binding site for GPIIb/IIIa is an RGD motif located the SD1 of the C4 domain. However, the exact structure of the interaction between the RGD motif and GPIIb/IIIa is still unknown. Under physiological conditions VWF binds GPIIb/IIIa in presence of high shear. Therefore, Molecular dynamics (MD) simulations were performed by our cooperation partner Dr. Camilo Aponte-Santamaría (HITS) to predict, how the structure of VWF changes upon a pulling force (**Figure 51**). To allow more flexibility a reducing environment was applied. As initial structure, the published NMR structure of VWF C4 domain was used (Xu et al., 2019). The obtained pulled structures predict a flattening of SD2 and a reorientation of the two beta hairpins in SD1, particularly residues Ser2497-Ser2516 and Gly2518-Cys2528 (**Figure 51A**). In an equilibrium, this beta hairpins do not interact but rather form a gap. However, upon application of pulling force, a direct interface is established that is closing this gap.

To further investigate the flexibility and movements of the C4 domain an all atom trajectory in an equilibrium was run through TRAPP by our cooperation partner Dr. Nicholas Michelarakis (HITS, Germany). This resulted in the conformation shown in **Figure 51B** (left panel). With this conformation as starting point, a Coarse Grained (MARTINI) version of mixed solvent MD was run. This revealed the closed structure where the two beta hairpins of the SD1 closely interact, similar to the MD simulations discussed above. The simulations predict that tryptophan residue at position 2521 is located in between the two beta hairpins, but upon pulling force, the residue turns and moves to the back, to allow the association of the two beta hairpins.

The predictions identified a movement of the C4 domain that involves the beta hairpin containing the RGD motif necessary for binding to the platelet receptor GPIIb/IIIa. This suggests that the movement of the C4 domain may affect the RGD binding site and thus impact its activity. In order to determine whether the interaction of the two beta hairpins of SD1, can be inhibited and whether inhibition is affecting GPIIb/IIIa binding, short interfering peptides were designed and investigated for their inhibitory capacity. Additionally, the impact of residue Trp2521 as a regulator of C4 domain activity, was evaluated by mutagenesis of tryptophan to glycine and characterization of the variant's structure and activity.

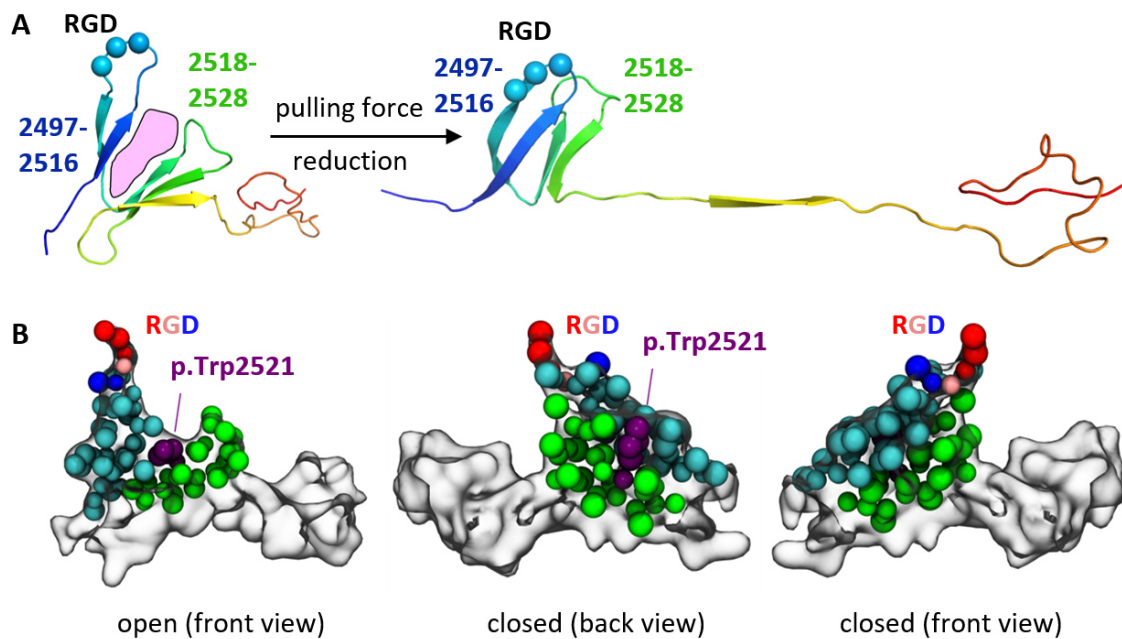


Figure 51: Structure simulations of the C4 domain. (A) MD simulations of the C4 domain under pulling force and reduced conditions. Backbone is colored from N- to C-terminus in blue to red. RGD sequence marked by three blue dots. The two beta hairpins of SD1 are colored in blue and green, respectively. The gap between the hairpins is indicated in pink. **(B)** CG simulation of a TRAPP predicted structure of the C4 domain revealing an open conformation (left), that changes its structure to a closed conformation (right), shown in front and back view. The two beta hairpins of SD1 are colored in cyan and green, respectively. RGD motif is colored in red (R), nude (G) and blue (D). Residue Trp2521 is colored in purple.

6.3.2. Evaluation of inhibitory peptides on the activity of the C4 domain

We explored the possibility to design a short peptide which would interfere with the interaction between the two beta hairpins described in 6.3.1. This way, we wanted to target the structural movement, which occurs *in silico* upon force application and to inhibit the interaction of the C4 domain with platelet receptor GPIIb/IIIa. Current inhibitors of the GPIIb/IIIa-VWF C4 domain interaction target GPIIb/IIIa on the platelet surface, such as abciximab. However, abciximab is not only specific for the GPIIb/IIIa receptor, but also for other integrins, e.g. $\alpha_v\beta_3$ integrin or leukocyte integrins, which can cause undesirable side effects when used in patients (Huang et al., 2019). Furthermore, the blockade of the GPIIb/IIIa receptor also inhibits platelet binding to all interaction partners with an RGD sequence, such as fibrinogen, in a non-selective manner, rather than solely affecting VWF binding. A direct target on the C4 domain of the VWF would offer the application in patients with a minimized side effects. Additionally, it could reduce the risk of thrombotic events in carriers of GPIIb/IIIa-dependent GOF variants.

As template, the aa sequence of the second beta hairpin was used, resulting in two peptides: a shorter version corresponding to the first 9 aa (GSQWASPEN) and a longer peptide including the entire beta hairpin consisting of 15 aa (GSQWASPENPCLINE).

The peptides were commercially synthesized and interference of the GPIIb/IIIa-VWF C4 domain interaction was evaluated in the GPIIb/IIIa-Thr588Asn ELISA. A high peptide concentration of 1 µg/mL was applied during the incubation time of GPIIb/IIIa-Thr588Asn-HEK293F cells to immobilized VWF. Representatively, the wildtype and variants p.Phe2561Tyr and p.Pro2555Arg were investigated (**Figure 52**). The binding was not significantly changed in comparison to the control condition lacking inhibitory peptides, indicating that the peptides do not directly interfere with the binding of VWF to GPIIb/IIIa.

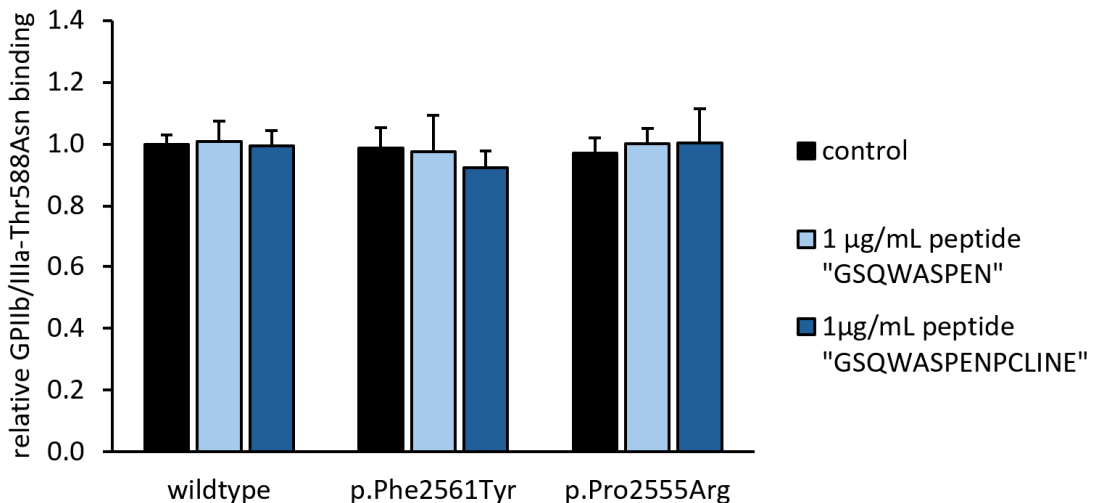


Figure 52: Relative binding of wildtype VWF and variants to GPIIb/IIIa-Thr588Asn in presence of 1 µg/mL short peptide 'GSQWASPEN' or 1 µg/mL long peptide 'GSQWASPENPCLINE'. Binding of $7.5 \cdot 10^4$ HEK293F cells expressing GPIIb/IIIa-Thr588Asn to 1 µg/mL recombinant VWF variants was detected in ELISA. Binding was quantified by mouse-anti-CD41/CD61 and goat-anti-mouse-HRP antibody. Values are given in relation to the wildtype, which is set to 1. Mean values \pm SEM are shown. Significance was calculated by one-sided t-test: $p < 0.05$ (*), < 0.01 (**), < 0.001 (***)).

6.3.3. Characterization of variant p.Trp2521Gly

MD simulations suggested that the conformational change described in **6.3.1** is necessary for effective binding of VWF to platelet receptor GPIIb/IIIa. To test this hypothesis, the side chain of tryptophan was removed by mutagenesis of Trp2521 to glycine. The resulting variant p.Trp2521Gly was reported as rare human SNP by the Ensembl database (rs1282400728), but was not further investigated. Hence, variant p.Trp2521Gly was recombinantly expressed and characterized *in vitro* similarly to the variants described in **5.2**.

Recombinant expression of VWF variant p.Trp2521Gly in HEK293F cells revealed a partial defect in secretion, which is reduced to approximately 47 % (**Figure 53A**). However, stimulation of VWF secretion by PMA is effective, indicating that VWF expression and storage is not completely impaired (**Figure 53B**). Immunofluorescence images of variant p.Trp2521Gly in transiently transfected HEK293F cells revealed a defect of the formation of pseudo-WPB (**Figure 53C**). In some cells, only small round shaped dots indicate the assembly of VWF in storage organelles. However, other cells have an increased number and size of pseudo-WPB, suggesting a storage defect. Likewise, a strong colocalization with the ER marker PDI was observed, which indicates a retention of VWF in the ER.

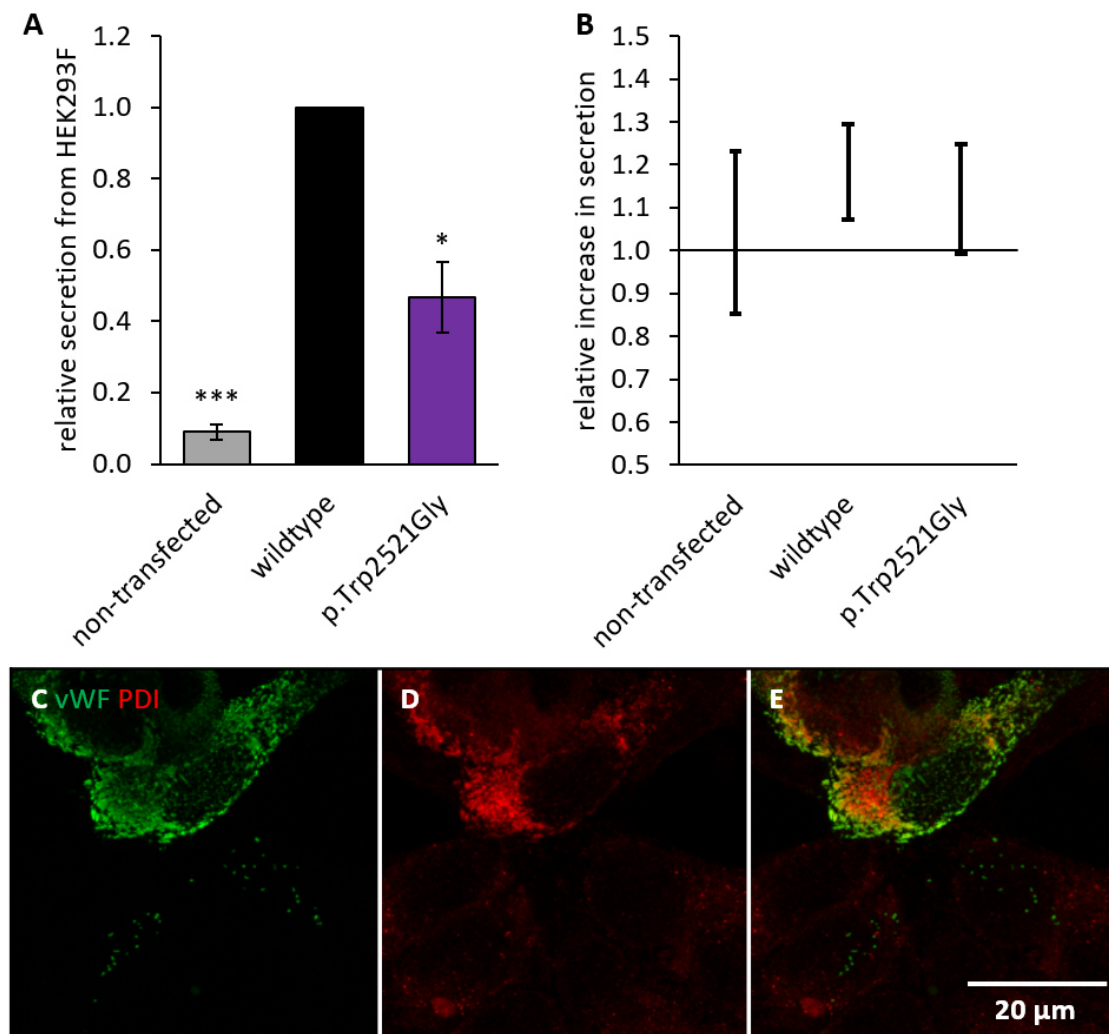


Figure 53: VWF variant p.Trp2521Gly secretion and intracellular localization. (A) Secretion of VWF variants from HEK293F cells within 24h as described in figure 13 (B) Relative increase in secretion after treatment with 200 μ g/mL PMA for 2h as described in figure 14. (A+B) Values are given in relation to the wildtype. (Mean value) \pm SEM are shown. Significance was calculated by unpaired t-test: $p = <0.05$ (*), <0.01 (**), <0.001 (***). (C, D, E) Immunofluorescence of HEK293F cells transfected with VWF variant p.Trp2521Gly as described in figure 15. Scale bar of 20 μ m.

The secreted VWF variant p.Trp2521Gly has a multimer distribution similar to the wildtype (Figure 54A). However, an elevated amount of proteolytically degraded protein is observed, already in the absence of ADAMTS13, indicating a decreased stability (Figure 54B). Functional characterization of the binding capacity of the recombinant VWF variant p.Trp2521Gly to interaction partners in ELISAs revealed a collagen type III, mut-GPIb α and GPIIb/IIIa-Thr588Asn binding similar to the wildtype (Figure 54C, E, F). However, ristocetin-dependent binding to GPIb α was significantly decreased (Figure 54D).

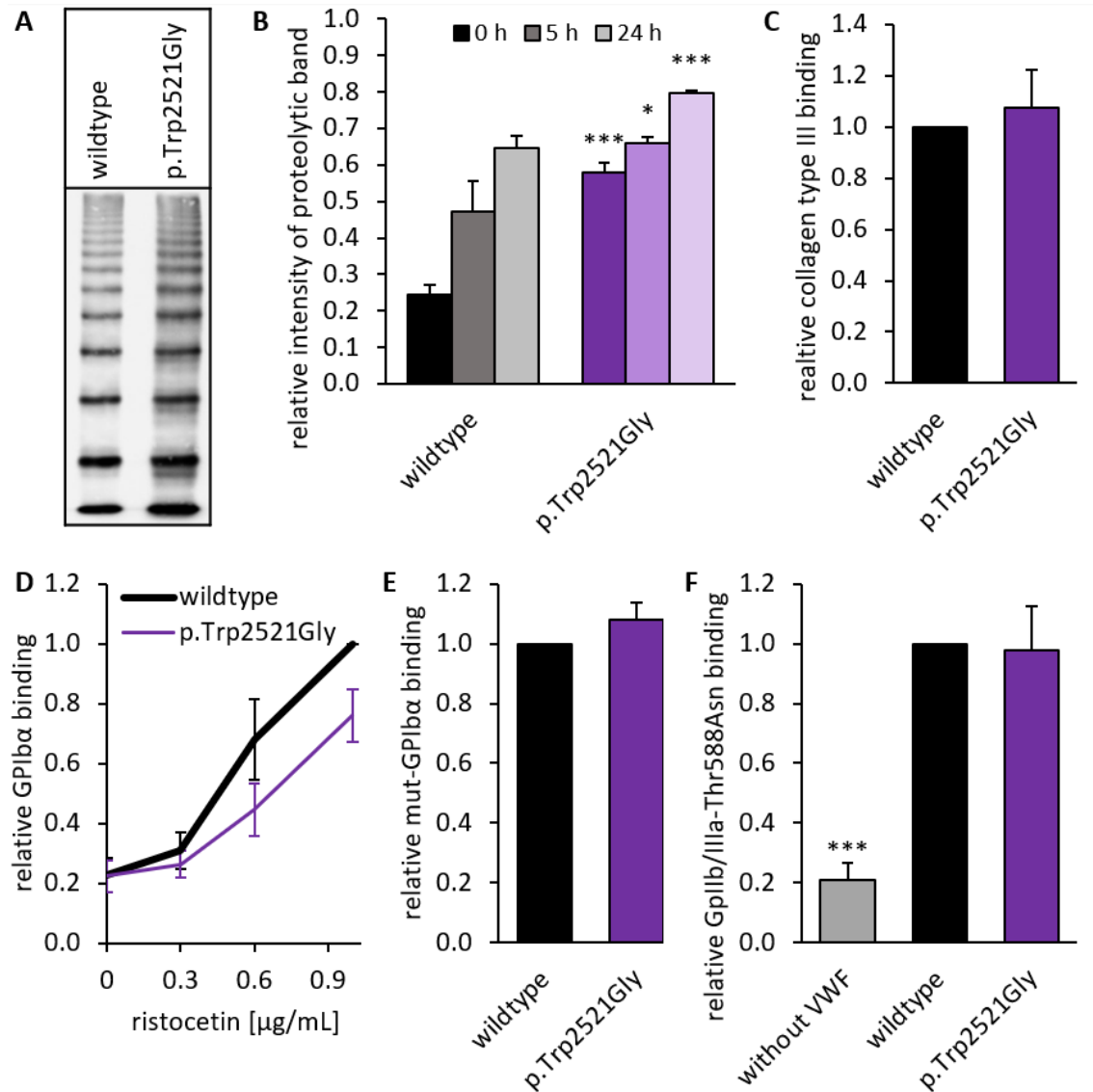


Figure 54: Functional quantification of VWF variant p.Trp2521Gly activity. (A) Multimer pattern of recombinant variant p.Trp2521Gly expressed by HEK293F cells as described in figure 16. Multimer analysis performed by Dr. Sonja Scheppenheim, MEDILYS GmbH. **(B)** ADAMTS13 digestion of recombinant p.Trp2521Gly variant as described in figure 18. **(C,D,E,F)** Relative binding to collagen type III, GPIIb/IIIa in presence of ristocetin, mut-GPIIb/IIIa and GPIIb/IIIa-Thr588Asn in ELISA as described in figure 19-22. Mean values \pm SEM are shown. Significance was calculated by one-sided t-test and unpaired t-test: $p = <0.05$ (*), <0.01 (**), <0.001 (***)).

Modified LTA was applied to investigate the potency to variant p.Trp2521Gly to form agglutinates. Likewise to ristocetin-dependent experiments in ELISA, variant p.Trp2521Gly displayed a decreased responsiveness. Maximum agglutination in presence of 0.6 mg/mL ristocetin was slightly reduced to 69 % in contrast to wildtype

with 86 % (**Figure 55A**). In presence of a ristocetin concentration of 0.3 mg/mL a milder agglutination is observed (**Figure 55B**). The maximum agglutination is decreased to an average of 26 % (**Figure 55C**). Likewise, variant p.Trp2521Gly failed to induce strong agglutination of >50 % in all replicated experiments (**Figure 55D**).

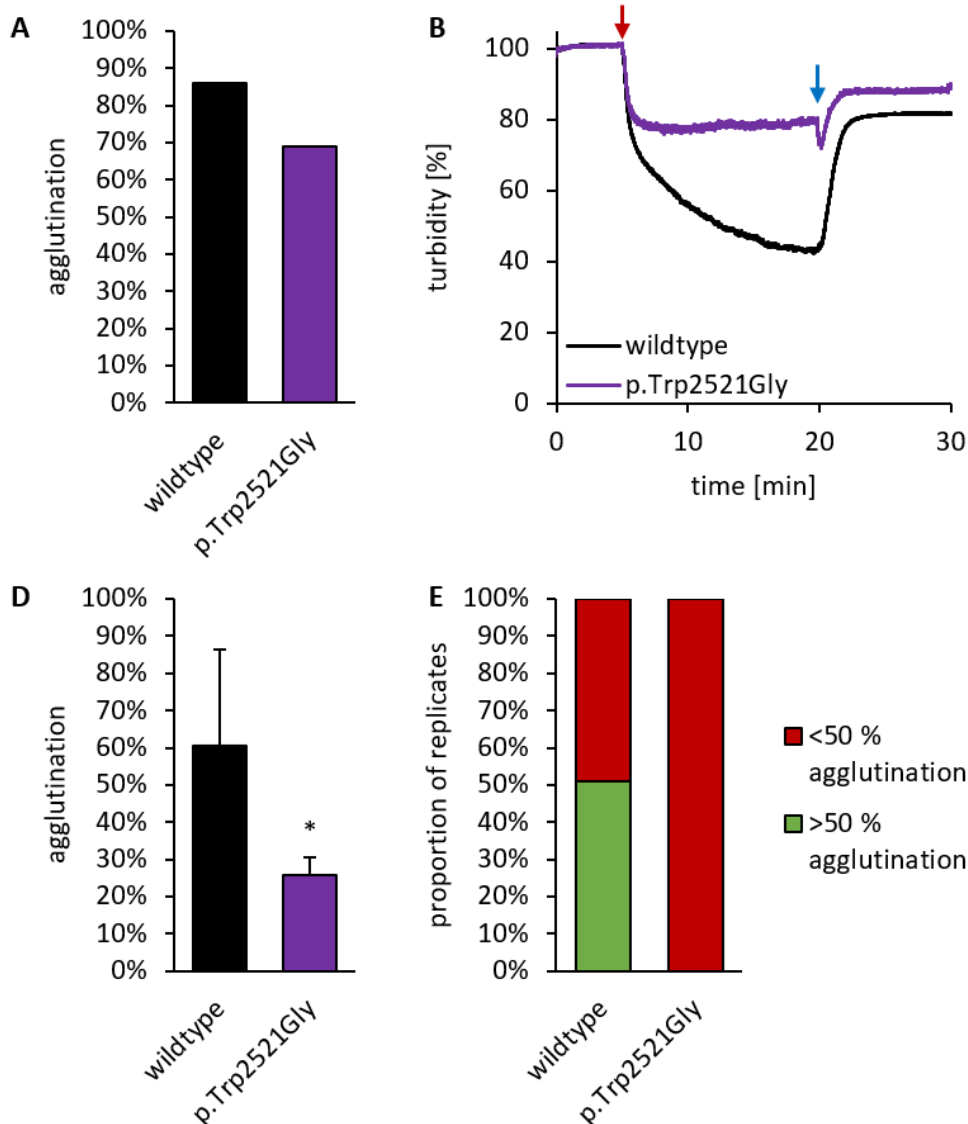


Figure 55: Platelet agglutination and cleavage by ADAMTS13 in LTA. (A) Maximum agglutination 5 min after stimulation with 0.6 mg/mL ristocetin as described in figure 23 **(B)** Setup as described in figure 24: after 5 min, 0.3 $\mu\text{g}/\mu\text{L}$ ristocetin (red arrow) was added and agglutination was observed for 15 min. The dissolution of agglutinates was investigated by addition of 1000 ng/ μL ADAMTS13 at minute 20 (blue arrow). Graphs represent the mean values of ≥ 3 replicates. **(C)** Maximum agglutination of results from B. Mean values \pm SEM are shown. Significance was calculated by unpaired t-test: $p = <0.05$ (*), <0.01 (**), <0.001 (***). **(D)** Frequency of weak (<50 %, red) and strong agglutination (>50 %, green) of results from B.

Evaluation of the capability of variant p.Trp2521Gly to form platelet aggregates was performed with microfluidic experiments. Adhesion and aggregation of platelets to a VWF-variant coated surface was quantified at shear stress of 10-100 dyne/cm². Platelet adhesion at low shear stress of 20-40 dyne/cm² was not impaired by the variant. However, at higher shear stress, platelets failed to stay attached at the VWF coated surface. Likewise, almost no platelet-VWF collective networks are formed and the size of aggregates is decreased in comparison to wildtype VWF.

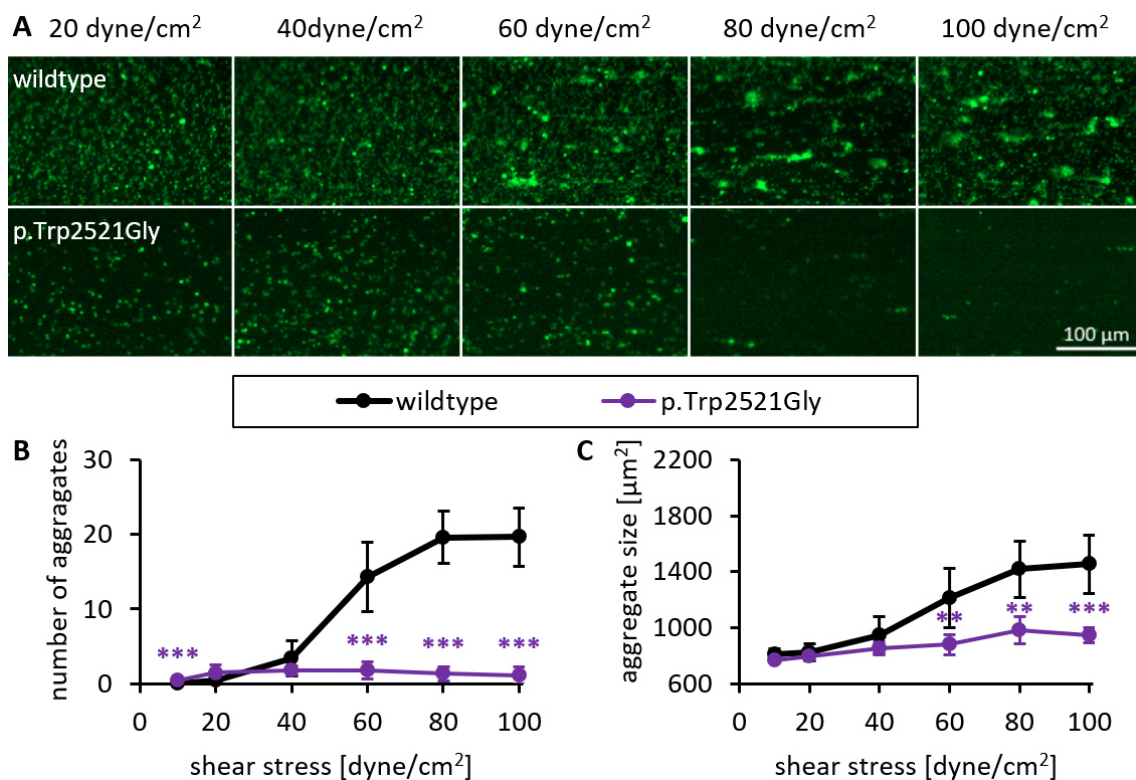


Figure 56: Formation of VWF-platelet collective network by wildtype VWF and variant p.Trp2521Gly at indicated shear stress. (A) Representative immunofluorescence images of platelet adhesion and aggregation as described in figure 27. Scale bar of 100 μm. (B, C) Quantification of average aggregate number per 330,000 μm² and average aggregate size for aggregates >700 μm². Mean values ± SEM are shown. Significance was calculated by unpaired t-test p = <0.05 (*), <0.01 (**), <0.001 (***)).

7. DISCUSSION

For decades, VWF has been known to be an essential regulator of hemostasis. The absence or malfunction of VWF has been linked to wound healing disorders and bleeding tendencies (Sadler et al., 2006). However, elevated levels of VWF have been associated with an increased risk of thrombosis and MI (Lip and Blann, 1997). The first VWF variant that affects thrombogenesis due to qualitative changes in VWF was published in 2019 (Schneppenheim et al., 2019). Soon thereafter, a second variant with a GOF effect was reported (Huck et al., 2022). Both variants are SNPs localized in the C4 domain of VWF that have no direct influence on the binding site of VWF to its interaction partners, but appear to increase its activity via structural changes. While the first variant, p.Phe2561Tyr, has been demonstrated to enhance the shear sensitivity of VWF, the second variant, p.Pro2555Arg, has been shown to cause the formation of oversized aggregates. The objective of this study was to gain deeper insights into the mechanism by which these variants increase the activity of VWF. To this end, another 24 variants in the C domains of VWF were characterized. A patient cohort, comprising 286 patients with CAD and 236 controls, was screened for SNPs and a risk correlation was calculated. Furthermore, *in vivo* experiments were conducted to assess the effects of GOF variants on an organism. Additionally, an attempt was made to inhibit the VWF GOF by application of short interfering peptides.

7.1. Characterization of novel VWF variants

By selecting and characterizing 24 different VWF SNPs in VWF's C domains, this study identified 9 novel GOF variants (p.Glu2553Lys, p.Pro2558Ser, p.Ser2559Leu/Trp, p.Gly2560Arg, p.Ser2564Arg, p.Cys2574Phe, p.Arg2575Cys, p.Gly2705Arg) and 9 LOF variants (p.Pro2302Arg/Thr, p.Pro2373Arg/Ser, p.Arg2535Gln, p.Cys2557Tyr, p.Cys2574Arg, p.Cys2671Tyr, p.Trp2521Gly). Variants p.Cys2557Tyr and p.Cys2574Arg were observed to exhibit a secretion defect, while variant p.Cys2671Tyr was found to reduce the amount of HMWM. Thus, these three LOF variants were excluded from further characterization. Variants p.Pro2302Arg/Thr and p.Pro2373Arg/Ser located in C1 and C2 display ambiguous results. Six variants were observed to not significantly alter the activity of VWF in the performed experiments (p.Phe2481Tyr, p.Glu2525Lys,

p.Gly2560Ser, p.Ser2573Arg, p.Arg2575His, p.Tyr2631Phe). The results of the performed assays are summarized in **Table 22**.

Table 22: Summary of variant characteristics. Relative secretion and stimulated secretion from HEK293F cells by 200 ng/ μ L PMA, formation of pseudo-WPB in HEK293F cells, multimerization, static cleavage by ADAMTS13, binding to collagen type III, ristocetin-induced binding to GPIIb/IIIa-Thr588Asn in ELISA, platelet agglutination in LTA and platelet network formation in microfluidic experiments. Red downwards arrows (\downarrow) indicate a reduced activity, green upwards arrows (\uparrow) indicate an increased activity, blue lines ($-$) indicate an activity similar to wildtype, yellow dots (\bullet) indicate a difference in VWF oligomer running behavior. Domain localization is given in the first column.

		secretion	stimulation by PMA	multimerization	ADAMTS13 cleavage	collagen type III binding	GPIIb binding	mut-GPIIb binding	GPII/IIIa-Thr588Asn binding	platelet agglutination (LTA)	platelet network formation (microfluidics)
C1	p.Pro2302Arg	-	-	\bullet	-	-	-	\uparrow	-	\downarrow	\downarrow
	p.Pro2302Thr	-	\downarrow	\downarrow	\uparrow	\uparrow	-	\uparrow	-	-	\downarrow
C2	p.Pro2373Arg	-	-	\bullet	-	\uparrow	\uparrow	\uparrow	-	-	\downarrow
	p.Pro2373Ser	-	-	\bullet	\downarrow	\uparrow	\uparrow	\uparrow	-	\downarrow	\downarrow
C3	p.Phe2481Tyr	-	-	\bullet	\downarrow	-	\downarrow	-	-	-	-
C4	p.Trp2521Gly	\downarrow	-	\downarrow	\uparrow	-	\downarrow	-	-	\downarrow	\downarrow
	p.Glu2525Lys	-	-	-	-	-	-	-	-	-	-
	p.Arg2535Gln	-	\downarrow	\bullet	\downarrow	\downarrow	\downarrow	\downarrow	\downarrow	\downarrow	\downarrow
	p.Glu2553Lys	-	-	-	-	-	-	-	-	\uparrow	\uparrow
	p.Pro2558Ser	-	-	-	-	-	\uparrow	\uparrow	-	\uparrow	\uparrow
	p.Ser2559Leu	-	\downarrow	-	\uparrow	-	-	-	-	\uparrow	\uparrow
	p.Ser2559Trp	-	-	-	\downarrow	-	-	-	-	\uparrow	\uparrow
	p.Gly2560Arg	\downarrow	\downarrow	-	-	-	-	-	-	-	\uparrow
	p.Gly2560Ser	-	-	-	-	-	-	-	-	-	-
	p.Ser2564Arg	-	\downarrow	-	\downarrow	-	-	\uparrow	-	\uparrow	\uparrow
	p.Ser2573Arg	-	-	-	-	-	-	-	-	-	-
	p.Cys2574Phe	\downarrow	-	-	-	-	-	-	-	\uparrow	\uparrow
p.Arg2575Cys	\downarrow	\downarrow	-	-	-	-	-	-	\uparrow	\uparrow	
p.Arg2575His	-	-	-	-	-	-	-	-	-	-	
C5	p.Tyr2631Phe	-	-	-	\downarrow	-	\downarrow	-	-	-	-
C6	p.Gly2705Arg	-	-	-	-	-	\uparrow	-	-	\uparrow	\uparrow

7.1.1. Set-up for quantification of VWF GOF variants under shear conditions

Since most of the investigated VWF variants are rare SNPs with a minor allele frequency (MAF) of <0.1 , no patient samples were available for analysis. Consequently, only recombinant VWF was examined. In LTA and microfluidics the blood donor's VWF needed to be washed away carefully, to prevent its influence on the experiment. By that, plasmatic compounds, including VWF but also coagulation factors, ADAMTS13 and fibrinogen are removed. The resulting set-up is not completely physiological, however it allows to focus specifically on the initial steps of VWF-platelet clot formation. Moreover, presence of ADAMTS13 would directly counteract the development of clots, and presence of coagulation factors and fibrinogen, could bypass or overshadow the effect of VWF, as fibrinogen has been demonstrated to substitute for VWF (Wu et al., 2000). This would impede the identification of VWF GOF variants and the characterization of its mode of action. One cannot exclude, that platelets secrete VWF and fibrin upon activation. However, this would equally interfere with all experiments.

GOF variants were primarily recognized by assays under shear forces, such as LTA and microfluidics. In LTA, the GOF effect was observed at low ristocetin concentrations of $0.3 \mu\text{g/mL}$, which is below the recommended low dose of ristocetin of $0.6 \mu\text{g/mL}$ (Hayward et al., 2010). This low dose appears to mark a threshold concentration for the activation of VWF, since the wildtype did not initiate full platelet agglutination in approximately 50 % of cases, thereby demonstrating a high variability in the intensity of platelet agglutination. Deviations in LTA are not uncommon (Alessi et al., 2020), which highlights the importance of replicates. However, GOF variants clearly stood out as they induced strong agglutination in every replicate. For those variants that achieved a stronger or more frequent agglutination, a higher susceptibility to ristocetin can be concluded, which suggests an alteration in structure and the potency for an accelerated VWF activation. All agglutinates in LTA could be resolved by the addition of ADAMTS13. This suggests that the VWF-platelet agglutinates are not strongly cross-linked, and binding sites are still accessible for ADAMTS13. However, the initial turbidity of 100 % could not be restored, because the recombinant ADAMTS13 solution, which is added in a high volume, is optically clear. This results in a direct decrease in turbidity after its addition, making it impossible to reach a 100 % of the initial turbidity.

7.1.2. Loss-of-function variants

7.1.2.1. Variants p.Cys2557Tyr and p.Cys2574Arg in C4 domain

The most severe LOF variants investigated in this study are variants p.Cys2557Tyr and p.Cys2574Arg. Both variants were not secreted from HEK293F cells and immunofluorescence imaging revealed a defect in the formation of pseudo-WPBs. VWF seems to be retained in the ER, indicating a defect in VWF structure and packaging. Based on the published NMR structure of the C4 domain (Xu et al., 2019), the two mutated cysteine residues are normally paired in intradomain disulfide bonds, namely Cys2557 is paired with Cys2576 and Cys2574 is paired with Cys2565. By mutation of these aa, disulfide bonds are lost, which might have a destabilizing effect on the C4 domain itself or the whole VWF conformation. MD simulations of the C4 domain with reduced cysteine bonds reveal a disturbance of the SD2 structure of the C4 domain, when either the disulfide bond Cys2557-Cys2576 or Cys2574-Cys2565 is reduced (Kutzki et al., 2023). Similarly to these variants, a number of other cysteines in the C domains have been reported to be important for secretion, since mutagenesis to alanine leads to a severe secretion defect and retention of VWF in the ER of HEK293 cells (Shapiro et al., 2014). This indicates that loss of cysteines, and consequently disulfide bridges, can completely abolish the VWF secretion. That mutation of Cys2557 or Cys2574 may disturb the stem association is underlined by the fact, that both cysteines are not predicted to be surface exposed in the dimeric stem structure by AlphaFold2-Multimers. The investigated aa exchanges included the introduction of either tyrosine or arginine. Both exchanges lead to an increase of the side chain by 60 or 53 kDa, respectively, which might sterically hinder the packaging of VWF into 'bouquet'-like structure. Moreover, arginine contains a positively charged side chain that may also chemically interfere with association of the dimeric stem by repulsion or distortion of the backbone structure.

It is likely that these variants will cause VWD type II or III in patients due to a strong secretion defect. However, no patient was identified to date, which may be attributed to the rare frequency of these SNPs. Nevertheless, it remains to be evaluated whether heterozygous expression of these variants rescues the phenotype or partially restores VWF secretion and function.

7.1.2.2. Variant p.Cys2671Tyr in the C6 domain

Although recent results of variant p.Cys2671Tyr in CPA suggested a GOF (**Figure 12**) this variant was classified as LOF in *in vitro* experiments. Substitution of Cys2671 with a tyrosine resulted in a 35 % reduction in VWF secretion from HEK293F cells. Likewise, Wang et al. observed a retention of variant p.Cys2671Tyr in the ER and a reduction in VWF storage in pseudo-WPBs of HEK293 cells (Wang et al., 2012). Similar results have been reported for other cysteine variants that remove intrachain disulfide bonds in VWF's C domains, such as the variant p.Cys2693Tyr in the C6 domain (Wang et al., 2013).

The multimer pattern of secreted variant p.Cys2671Tyr appears 'smeary', indicating reduced stability and increased proteolytic degradation even in the absence of ADAMTS13. Since samples are supplemented with protease inhibitor after harvest, degradation may be caused by proteases which are secreted by HEK293F cells during VWF synthesis in cell culture. Similar multimer patterns were observed for other cysteine variants like variant p.Cys2304Tyr in C1, variant p.Cys2362Phe in C2 or variant p.Cys2477Tyr/Ser in C3, which all are classified as VWD type 2M (Budde et al., 2008). Moreover, variant p.Cys2671Tyr displays a loss of HMWM caused by either degradation or impaired secretion. Since loss of HMWM is associated with a decrease of VWF activity in presence of force, further characterization of variant p.Cys2671Tyr was refrained due to incomparability to the wildtype.

Variant p.Cys2671Tyr was identified as a compound heterozygous mutation in a patient with VWD type 3 (Castaman et al., 2000). However, VWD type 3 was only observed to manifest in combination with a null allele. The parents of this patient, both of whom carry one of the defective alleles, exhibit a reduction of VWF:Ag levels to approximately 50 % and a bleeding time close to normal. Most likely, a wildtype allele is capable of compensating for the deleterious effect of p.Cys2671Tyr. In case of the VWD type 3 patient, a markedly diminished VWF:Ag level and an elevated proportion of small VWF fragments was identified, prompting the authors to suggest a defect in dimerization. However, dimerization was found to be intact in this study. Likewise, Van Schooten et al. ascertained a normal dimerization and multimerization, and characterized variant p.Cys2671Tyr to be more prone to proteolytic degradation in plasma (Van Schooten et al., 2005). Additionally, Wang et al. characterized HEK293 cells expressing variant

p.Cys2671Tyr and identified an increased amount of pro-VWF, which indicates a defect in processing (Wang et al., 2012).

Recently, the structure of the VWF C6 domain was resolved by NMR spectroscopy (Chen et al., 2022). The C6 domain contains two beta sheet subdomains 1 and 2 which are connected by a flexible hinge enabling the domain to move between an extended and bent conformation. The structure illustrates that Cys2671 is paired with Cys2715 in a disulfide bond that is part of the intradomain hinge region. Thus, Cys2671 may serve a stabilizing and regulating function for the C6 domain, such that a loss of this residue could result in domain instability.

7.1.2.3. Variants p.Arg2535Gln and p.Trp2521Gly in the C4 domain

Two variants located in SD1 of the C4 domain were identified to be LOF variants (p.Arg2535Gln and p.Trp2521Gly). Variant p.Arg2535Gln was observed to be expressed normally and exhibited intact multimerization. Notably, oligomers showed a slightly slower running behavior and thus an increase in size or structure. Variant p.Arg2535Gln exhibited diminished activity across all conducted assays. Binding to collagen type III was reduced by 20 %, binding to GPIIb α in presence of 1 mg/mL ristocetin was decreased by 34 %, binding to mut-GPIIb α by 30 % and binding to GPIIb/IIIa-Thr588Asn by 40 %. Likewise, a similar variant, p.Arg2535Pro, identified in a patient with VWD type I, displayed a mild reduction in binding to collagen type III and GPIIb α , while exhibiting a markedly decreased binding to GPIIb/IIIa (Legendre et al., 2015). In flow experiments, agglutination of platelets by variant p.Arg2535Gln was decreased and formation of VWF-platelet networks under flow conditions was completely abolished in comparison to the wildtype control.

Likewise, variant p.Trp2521Gly was identified as LOF in this study, since it failed to induce strong platelet agglutination and platelet network formation under flow conditions. Instead, almost no platelets were immobilized on a VWF covered surface at high shear stress of 80-100 dyne/cm². Additionally, variant p.Trp2521Gly was observed to be retained in the ER of HEK293F cells, resulting in a defective storage in pseudo-WPB and impaired secretion. Although multimerization of variant p.Trp2521Gly is not impaired, stability seems to be decreased due to the presence of degraded VWF

oligomer bands, even in the absence of ADAMTS13, as suggested for variant p.Cys2671Tyr (**7.1.2.2**).

Both presented variants are located in SD1 on the C4 domain, similar to the already published LOF variant p.Gln2520Pro causing VWF type 1 (Budde et al., 2008; Eikenboom et al., 2009). However, the variant p.Glu2525Lys, which is also located in SD1, does not exhibit a LOF phenotype. Regarding the structure of the C4 domain, Glu2525 is located in a loop region that is more flexible in contrast to Trp2521 and Arg2535, which are part of a beta sheet. Furthermore, the SD1 was predicted to be closely associated with the C-terminal end of the C3 domain in Alphafold2-Multimer predictions. Hence, structural alterations may disturb the interdomain structure. Moreover, due to the close proximity of the RGD sequence, these variants may also directly interfere with GPIIb/IIIa binding. This could particularly be assumed for variant p.Arg2535Gln, since a reduced binding to GPIIb/IIIa-Thr588Asn is detected in ELISA.

7.1.2.3.1. Suggested motion of the C4 domain and the role of Trp2521

The results of the MD simulations of the C4 domain led to the hypothesis that it is activated by shear, in a manner similar to that observed for the A1 domain. The simulations indicate that stretching leads to the interaction of two beta hairpins in SD1, and that this interaction is reliant on the rotation of Trp2521 away from its predicted regular position. Hence, variant p.Trp2521Gly was suggested to constitutively activate the C4 domain by introducing more flexibility and allowing for the beta hairpin interaction. However, the complete loss of Trp2521 by mutation to glycine does not increase the activity of VWF under shear forces. Instead, the variant displays a markedly diminished capacity to immobilize platelets and form platelet networks. It is possible that the increased degree of flexibility, which is introduced by the loss of tryptophan, may disrupt the secondary and tertiary structure of the C4 domain and potentially the interdomain association. Structural inconsistencies are emphasized by the observation that secretion and stability of variant p.Trp2521Gly were impaired in HEK293F cells. However, further investigations are required to elucidate whether the motion in the C4 domain observed *in silico* occurs *in vitro* and *in vivo*, and to determine the tryptophan's precise function.

7.1.2.4. Variants in the C1 and C2 domains

In contrast to the other variants, the investigated variants in the C1 and C2 domain of VWF (p.Pro2302Arg/Thr, p.Pro2373Arg/Ser) were challenging to classify. Expression of the variants was normal, however the oligomers had a faster running behavior compared to the wildtype, indicating a decrease in size or structural alteration. It is possible that glycosylation is impaired. The *O*-glycosylation site at Thr2298 is located in close proximity to Pro2302 in C1 (Titani et al., 1986). Likewise, the *N*-glycosylation Asn2400 is predicted to be structurally close to variant Pro2373 in C2 (Zhou et al., 2012). Almost all investigated C1 and C2 variants displayed increased binding to collagen type III and GPIIb α in ELISA. However, under flow conditions, these variants were less efficient or failed completely to induce platelet agglutination of platelets network formation. Since investigations under shear stress represent a more physiological condition of VWF environment, these variants are considered LOF variants. Given that for all these VWF variants proline is replaced, the structure of the C1 and C2 might be compromised. In general, prolines are structural margins of secondary structures and are unable to act as a hydrogen bond donor. The substitution with arginine, threonine or serine allows for additionally hydrogen bonding, which might rearrange the secondary and tertiary structure. Alterations in VWF structure may lead to a better accessibility of binding sites for collagen type III or GPIIb α , which affects the binding capacity in ELISA. However, severe alterations can disturb VWF function under flow conditions.

7.1.3. Gain-of-functions variants

7.1.3.1. Variant p.Gly2705Arg in the C6 domain

In the C6 domain of VWF one GOF variant (p.Gly2705Arg) could be identified. This variant increases platelet agglutination in presence of low ristocetin concentrations of 0.3 $\mu\text{g/mL}$ in LTA and the aggregation in CPA. Moreover, the shear sensitivity of this variant is increased by approx. 50 %, similar to variant p.Phe2561Tyr (Schneppenheim et al., 2019). Additionally, the size of aggregates was slightly increased to an average size of 1800 μm^2 compared to 1400 μm^2 for wildtype VWF. However, the size did not

increase to the same extent observed for the variant p.Pro2555Arg, which resulted in an average aggregate size of approx. 5000 μm^2 (Huck et al., 2022).

The structure of the C6 domain was recently resolved by NMR spectroscopy in a collaborative study (Chen et al., 2022) as discussed in **7.1.2.2**. The study revealed changes the dynamics of the C6 domain by variant p.Gly2705Arg in MD simulations. We hypothesized, that the insertion of a large, charged side chain could disrupt the native arrangement of the C6 region and potentially also the interaction with neighboring domains. Indeed, prediction of the VWF dimeric stem by AlphaFold2-Multimer revealed an alteration in the C6-CK domain interface. Due to incorporation of arginine at position 2705, a novel ionic interaction between Arg2705 of C6 and Asp2726 of the CK domain is predicted to be introduced, indicating that variant p.Gly2705Arg may stabilize the connection to the CK domain. However, this interaction was found to reorganize hydrogen bonds between beta sheets of the CK domain, which may potentially impact the CK domain or its interdomain structure.

With regard to disease association, to date only one patient with VWD type 1 and reduced VWF:Ag levels has been reported to carry the p.Gly2705Arg variation (Sztukowska et al., 2008). However, the findings of studies by Huffmann and Tang which demonstrate normal VWF:Ag levels in a population of p.Gly2705Arg carriers (Huffman et al., 2015; Tang et al., 2015) raise questions about the causal role of variant p.Gly2705Arg in VWD in this patient. It is possible that other mutations outside of the VWF gene impact its plasma concentration in this one patient. Given the high allele frequency of 5.3 % in the global population for p.Gly2705Arg, it is unlikely that only one VWD patient was identified and that this variant is therefore causal for VWD type I.

7.1.3.2. Variants in the C4 domain

In the C4 domain of VWF, 8 novel GOF variants were identified: p.Glu2553Lys, p.Pro2558Ser, p.Ser2559Leu/Trp, p.Gly2560Arg, p.Ser2564Arg, p.Cys2574Phe and p.Arg2575Cys. All variants, except for p.Glu2553Lys, exhibited a comparable phenotype to that observed for the GOF variant p.Phe2561Tyr. This includes an increase in shear sensitivity and a decrease in the critical shear stress necessary for activation by approximately 50 % (Schneppenheim et al., 2019). Moreover, a significant reduction in

aggregate number at higher shear stress of 80-100 dyne/cm² is observed for variants p.Pro2558Ser and p.Gly2560Arg, but a tendency for lower aggregate numbers at higher shear rates is observed in all GOF variants. The size of aggregates was not affected for the majority of variants. Similar to variant p.Phe2561Tyr, static parameter, as binding capacities in ELISA were not affected by these variants. Only, a slight increase in GPIIb α binding was observed for variants p.Pro2558Ser and p.Ser2564Arg. In addition to the results from microfluidic investigations, all GOF variants, except for variant p.Gly2560Arg, showed significantly stronger agglutination in LTA.

All GOF variants in the C4 domain that reduce the critical shear stress required for VWF platelet aggregation are located in the SD2. Alphafold2-Multimer predicted all variant residues to be located close to the C5 domain. Of particular note, the mutation of Gly2560 to arginine introduces a large charged aa that protrudes into the C5 domain. This might impact interdomain stability, thereby facilitating the stem opening.

Notably, variant p.Cys2574Phe was identified as GOF variant whereas variant p.Cys2574Arg displayed a LOF. Hence, the loss of the disulfide bond itself seems to have no deleterious effect on VWF. The study of Ganderton et al. identified Cys2574 to be partially unpaired (Ganderton et al., 2011) which provides evidence that the disulfide bond itself may not be crucial in the overall structure. Moreover, the equivalent disulfide bond in the C6 domain is absent but does not alter the five-strand topology (Chen et al., 2022), which suggests that cysteine bond Cys2574-Cys2565 may have a lower importance for structure stability. In contrast to the non-polar and hydrophobic phenylalanine, arginine is a large charged aa. Since Cys2574 is predicted to point towards the dimeric interface, the substitution to arginine might have a deleterious impact leading to the LOF.

In contrast to the above mentioned GOF variants, variant p.Glu2553Lys exhibit no increased shear sensitivity, but a slightly enhanced aggregate size to an average of approximately 2200 μm^2 at a shear stress of 100 dyne/cm² in microfluidic experiments. However, this effect is less pronounced than that of the GOF variant p.Pro2555Arg, which increased aggregates to an average of 5000 μm^2 at shear rates of 4000 s⁻¹ (Huck et al., 2022), corresponding to 80 dyne/cm².

7.1.3.3. Inhibition of GOF variants

Abciximab was applied in microfluidic experiments to investigate if the GOF of the newly identified variants is triggered by a GPIIb/IIIa-dependent effect, as observed for GOF variant p.Pro2555Arg (Huck et al., 2022). Abciximab is a chimeric antibody fragment that sterically inhibits GPIIb/IIIa binding to its interaction partners. It was applied in a concentration of 2.6 $\mu\text{g}/\text{mL}$, which is comparable with the dosage of abciximab of 0.25 mg/kg used in patients (Dziewierz et al., 2014). Moreover, an approximately 1:1 ratio between abciximab molecules and GPIIb/IIIa receptors is used, to allow for effective inhibition.

Presence of abciximab leads to the formation of small aggregates at shear stress of 20-40 dyne/cm² for wildtype and GOF variants alike, confirming that initial binding of platelets to VWF is not primarily achieved by GPIIb/IIIa binding, but facilitated through GPIb α . Studies show that the GPIb α -VWF interaction alone is capable of platelet aggregation independent of integrin binding and platelets activation (Ruggeri et al., 2006). Hence, single small aggregate can be formed also in the presence of a GPIIb/IIIa inhibitor. However, stable attachment to surface-bound VWF relies on binding through GPIIb/IIIa. The GPIIb/IIIa receptor is present in an inactive conformation in the first place, but is activated to a transient state after inside-out signaling induced by adhesion of platelets to VWF via GPIb α , mainly occurring at higher shear stress (Chen et al., 2015; Takagi et al., 2002). Consequently, abciximab has the largest effect at higher shear stress, where it may promote the detachment of single aggregates. This would explain, why almost no platelets are found to be immobilized at high shear stress. Likewise, the study of Huck et al. demonstrated that abciximab only influenced aggregation at shear rates of $>4000 \text{ s}^{-1}$ (equivalent to 80 dyne/cm²) which aligns with the results of the present study. The presence of abciximab mainly decreased the size of formed aggregates. Since the GPIIb/IIIa interaction strongly participates in crosslinking of platelets (Furlan, 1996), it is conceivable that inhibition reduces aggregate growth.

Moreover, the surplus of abciximab may lead to a coverage of platelets by this 48 kDa protein, which can fundamentally affect platelet size and the accessibility to other receptors. For all variants and the wildtype a small increase in shear sensitivity was observed in presence of abciximab. It is plausible that platelet size is increased due to

decoration of abciximab molecules. Once platelets bind via GPIIb/IIIa to VWF, the increased platelet size may enhance the tensile force acting of VWF and accelerate the stretching of VWF and the adhesion of further platelets. This effect would reduce the critical shear stress, necessary for VWF activation, and affect all VWF variants in an equal manner.

Although abciximab is efficiently reducing the platelet aggregate size, treatment in patients was stopped due to an accompanied increased risk for thrombocytopenia, caused by its strong binding and long lasting inhibitory effect (Hashemzadeh et al., 2008). Since abciximab is also not specific for binding to GPIIb/IIIa, but also binds to $\alpha_v\beta_3$ integrins or Mac-1 receptor on monocytes and neutrophils, it may also inhibit cell and monocyte adhesion and lead to side effects when applied in patients.

An attempt to inhibit the VWF activity by a different mechanism was made by using short interfering peptides, which were designed based on MD simulations. The peptides are suggested to stabilize an inactive conformation of the RGD motif by blocking the motion of two beta hairpins. However, no effect was observed on the binding capacity of VWF to GPIIb/IIIa-Thr588Asn in ELISA. If binding of the RGD motif to GPIIb/IIIa would be hindered by the peptide, either by steric interference with the binding site or due to stabilization of a conformation that is not able to bind GPIIb/IIIa, reduced binding in GPIIb/IIIa-Thr588Asn ELISA would have been detected, as it was shown for the GPIIb/IIIa binding-deficient mutants p.Asp2509Glu/Gly or application of abciximab (König et al., 2019). Therefore, it is likely that the peptides do not influence VWF binding to active GPIIb/IIIa. However, it remains unclear if the peptides do not affect the binding capacity of the GPIIb/IIIa domain or if they are not able to efficiently bind to VWF at its desired location. Given that the size of the peptides is small, it is difficult to determine, if they are binding to the C4 domain. Since peptide tags, such as His-Tags, may impact the total peptide structure and chemistry, less sterically obstructive methods should be used for determination. For instance, microscale thermophoresis (MST) and fluorescence correlation spectroscopy (FCS) are biophysical methods that can assess molecule sizes by measuring the motion speed or the diffusion time, respectively. If peptides efficiently bind to VWF, its motion would be decrease due to an increase in protein size. Similar experiments were performed to investigate the interaction of two proteins (Lippok et al., 2016). Further, *in silico* attempts may be used to mimic the peptide binding to the

C4 domain and also improve or adjust its binding by testing different peptides with single nucleotide exchanges.

7.2. Disease association

7.2.1. Association of VWF GOF variants with myocardial infarction in patients

Schneppenheim et al. published a study with 2197 individuals including 417 controls and 1780 patients with CAD (Schneppenheim et al., 2019). Although smaller, this study presents another patient cohort of 522 patients, of whom 236 are controls and 286 are patients with CAD. The prevalence of p.Phe2561Tyr in this study was lower than in Schneppenheim's study with 6.7 %, compared to 9.9 %. Likewise, the occurrence of MI was lower with 37.4 % of all CAD patients compared to 51.4 % in Schneppenheim's study. This circumstances led to the identification of only 35 patients with p.Phe2651Tyr in total, compared to 217, and only 4 patients with MI, compared to 86 in Schneppenheim's study.

In this study, a total of 5 patients in the control group suffered from MI. This results in a proportion of 3.4 %, which is higher than in Schneppenheim's study. The risk of developing an MI was increased in the control group, but not the CAD group. This may indicate that CAD is not a requirement for increased risk of MI in p.Phe2561Tyr carriers.

In Schneppenheim's study, significant risk was only observed for p.Phe2561Tyr carriers with <55 years of age, specifically for females. Moreover, the risk for the time between first and second MI was shorter in p.Phe2561Tyr carriers. Unfortunately, in this cohort no p.Phe2561Tyr carrier with CAD was identified with >1 MI, and no female with an MI in the CAD group. Therefore, no time between MIs can be determined. However, the average age of the first MI was decreased in p.Phe2561Tyr carriers in this cohort to 53.8 years in comparison to 64.1 years for patients with wildtype alleles.

Altogether, the group size of this cohort is small, with only 1 out of 18 p.Phe2561Tyr carriers with MI in the control group and 3 out of 17 with MI in the CAD group. Since MI is a multifactorial disease that is be predisposed by various risk factors such as obesity, nicotine abuse, arterial hypertrophy or other genetic factors (Zhan et al., 2019), other cardiovascular risk factors may bias the calculation of the risk profile of p.Phe2561Tyr carriers, especially in small cohorts. Moreover, Schneppenheim's study calculated an

increased risk just for the subgroup of young patient <55 years of age and especially for woman. Hence, patient number needs to be increased, especially in the subgroup of young females, in order to draw further conclusions.

7.2.2. Effect of VWF GOF variants on thrombosis and hemostasis in mice

The mouse studies on VWF-KO mice allowed to determine the effect of GOF variants on hemostasis and thrombogenesis. Focus was set on variants p.Phe2561Tyr and p.Pro2555Arg, since all novel GOF variants identified in this study display a similar or weaker phenotype *in vitro*. Both positions are conserved in murine VWF and were mutated accordingly to the human SNPs.

The VWF-KO mice received a hydrodynamic injection of the pLIVE vector, which carries the CDS of VWF (Casari et al., 2013). This method allows the expression of different VWF variants without the need for time-consuming genetic modifications of the mice themselves. The majority of transfected cells are reported to be hepatocytes, which reach a high expression of VWF after 2-4 days that remains stable for up to 14 days after injection (Casari et al., 2013). Although the expression of VWF is mainly performed by hepatocytes and not by endothelial cells, the composition of the VWF multimers and the oligomer sizes are comparable to the VWF of parental mice. Likewise, VWF variants p.Phe2561Tyr and p.Pro2555Arg were expressed and multimerized successfully indicating that the SNPs do not interfere with biosynthesis or multimerization of VWF. Although VWF:Ag levels varied among mice, no correlation with blood loss in tail clip or occlusion time in thrombosis assay was detected.

VWF-KO mice that expressed VWF as a result of hydrodynamic injection demonstrated a reduced capacity for hemostasis and thrombosis compared to the parental mice. This indicates that hydrodynamic injection of the VWF CDS in VWF-KO mice can only partially rescue the bleeding phenotype. However, blood loss was low and rebleeds were weak. Given that VWF is primarily expressed by hepatocytes and not by ECs in this model, it is conceivable that ECs may not be able to efficiently respond to injuries.

In the tail-clip assay VWF-KO mice expressing variants p.Phe2561Tyr and p.Phe2555Arg showed a decreased hemostatic potential compared to mice expressing wildtype VWF. It is unlikely that this defect is caused by impaired GPIIb/IIIa or collagen binding, because

studies show, that mice expressing VWF with a GPIIb/IIIa or collagen binding defect, do not increase the bleeding in tail-clip (Marx et al., 2008). Quantification of the blood loss and bleeding time, as well as observations of the blood flow suggest that mice expressing VWF variants p.Phe2561Tyr and p.P2555Arg exhibit deficiencies in stable clot formation. Since these mice suffered from strong and sudden rebleeds, blood loss and bleeding time was high. It appears that arising platelet clots are torn away, which hinders wound healing. This effect was more pronounced for variant p.Phe2561Tyr. Likewise, thrombogenesis of variant p.Phe2561Tyr was slightly reduced, since the occlusion in one mouse was unstable and disappeared quickly after its generation. This supports the hypothesis of unstable clot formation. In contrast, thrombogenesis was increased for variant p.Pro2555Arg. It is possible that aggregates formed by variant p.Pro2555Arg are bigger in size, similar to observations *in vitro*, leading to a higher risk of developing a vessel occlusion.

7.3. Suggested mode of action for VWF GOF variants

Schneppenheim et al. and Huck et al. have suggested that the published GOF variants alter the stem stability of VWF, thereby facilitating the stem opening and, thus, the accessibility to the RGD motif in the C4 domain (Huck et al., 2022; Schneppenheim et al., 2019). However, predictions of the dimeric interface by AlphaFold2-Multimer suggest that the RGD motif is already surface exposed. Nevertheless, it is unknown how the GPIIb/IIIa receptor binds to the RGD domain and which conformation is necessary to enable this interaction. On the one hand, it is conceivable that, despite the RGD motif being already surface exposed, the binding site relies on force. Stretching by shear force might be required to open the dimeric stem or specifically the C4 domain. Similar mechanisms were observed for the GPIIb α binding site in A1 and the ADAMTS13 cleavage site in the A2 domain of VWF, which highly rely on shear force for their activation (Arce et al., 2021; Crawley et al., 2011). On the other hand, activation of GPIIb/IIIa on platelets is already tightly regulated by GPIIb α binding, platelet signal transduction and force. Hence, additional regulatory mechanisms involving the C4 domain structure may not be necessary to prevent spontaneous binding of VWF to GPIIb/IIIa.

This study identified novel variants that cause enlargement of aggregates, namely p.Glu2553Lys and p.Gly2705Arg. Nevertheless, the variant p.Pro2555Arg was observed to generate by far the largest platelet aggregates of all GOF variants (Huck et al., 2022). The aggregate size was found to be strongly dependent on GPIIb/IIIa. Hence, it can be postulated that these GOF variants may enhance the crosslinking of platelets by facilitating the establishment of the GPIIb/IIIa-VWF C4 domain bond. All variants introduce a positively charged aa, like arginine or lysine, which may interact by electrostatic complementation with the negatively charged platelet surface and support the encounter of VWF-platelet binding sites, as described for the encounter trajectory of GPIIb with A1 (Fu et al., 2017). The accelerated tracking of GPIIb/IIIa by the RGD motif may allow for increased GPIIb/IIIa interactions.

The critical shear rate for wildtype activation was determined to be 60-80 dyne/cm² corresponding to 3000-4000 s⁻¹, which is in accordance to previous studies (Huck et al., 2022; Schneppenheim et al., 2019). The effect of GOF variants p.Pro2558Ser, p.Ser2559Leu/Trp, p.Gly2560Arg, p.Ser2564Arg, p.Cys2574Phe, p.Arg2575Cys and p.Gly2705Arg decreased the critical shear rate to 20-40 dyne/cm². This effect was shown to be independent of GPIIb/IIIa, since aggregates formed at lower shear stress even in the presence of the GPIIb/IIIa inhibitor abciximab. Therefore, an additional mechanism needs to be taken into consideration: Adhesion of platelets to VWF is dependent on GPIIb binding to VWF and only takes place if the binding site in the VWF A1 domain is accessible for platelets. Data obtained from AFM imaging suggest that GOF variants consist of an increased proportion of VWF dimers in an open stem conformation (J. Derksen, Department of Digital Health Sciences and Biomedicine, School of Life Sciences, University of Siegen, unpublished data). A partially opened VWF structure would increase the mechanosensitivity of VWF to shear and the susceptibility to structural stretching, as less force is required to break interdomain interactions. Consequently, stretching and opening of the VWF A1 domain may promote initial platelet binding. With rising numbers of adhered platelets tensile force acting on VWF would increase, thereby intensifying the force activation and allowing for more platelets to bind. The presence of a more stretched VWF would furthermore explain, why the critical dose of ristocetin for induction of platelet agglutination in LTA is decreased for

GOF variants. In summary, accessibility of the A1 domain and binding of platelets via GPIIb/IIIa would be more pronounced for GOF variants at lower shear stress. Subsequently, the interaction of the GPIIb/IIIa receptor with the VWF A1 domain would be reinforced due to accelerated conversion into a catch-bond (Ju et al., 2015b; Yago et al., 2008). GPIIb/IIIa is then capable of transmitting an outside-in signal that consequently activates GPIIb/IIIa resulting in an intermediate active state with increased binding affinity to integrin binding sites, such as the RGD motif in the VWF C4 domain (Chen et al., 2019). For GOF variants, the intermediate activation of GPIIb/IIIa would already occur at low shear rates, resulting in cross-linked platelet aggregates that grow in size. However, these aggregates require full activation of GPIIb/IIIa, which is only achieved at high shear forces, to reach stability and solid adhesion. Since aggregates induced by GOF variants already form at low shear rates, the aggregates remain unstable and are therefore more susceptible to being torn away. Fast detachment of VWF platelet aggregates could contribute to deficient hemostasis in mice expressing VWF GOF variants, which suffer from frequent and strong rebleeds. Aggregates that are torn away may pose a risk for the onset of emboli downstream of their generation, which may explain the increased risk for MI in p.Phe2561Tyr carriers.

Enhanced initial adhesion of platelets that subsequently accelerate the process of aggregate formation may also be promoted by VWF self-association (Dayananda et al., 2010; Savage et al., 2001). Self-association describes the direct cross-linking of VWF molecules, which results in increase VWF size and its potency to bind collect platelets. This interaction was shown to be induced by shear and to be mediated by intermolecular disulfide bonds (Li et al., 2008) Free thiols were identified to be crucial for the VWF self-association, including positions that are believed to be paired in a intradomain disulfide bond (Choi et al., 2007). This suggests that disulfide bonds may be susceptible to reduction and converted into free thiols in the circulation. In particular, two cysteines (Cys2431 and Cys2453) in the C2 domain were characterized to be involved in VWF lateral self-association (Ganderton et al., 2011), indicating that cysteines in C domains may serve not only structural but also functional roles in VWF activity. Likewise, free thiols were found to be required for proper collagen binding and platelet adhesion under flow conditions (O'Brien et al., 2021; Solecka et al., 2016). Two identified GOF

variants (p.Cys2574Phe and p.Arg2575Cys) directly impact the disulfide bridges in the C4 domain by removing or adding a cysteines, which increases the number of free thiols. Due to mutation of Cys2574 to phenylalanine, Cys2565 is predicted to be unpaired by AlphaFold2-Multimer, making it available for disulfide interactions. Interestingly, Cys2574 has also been found be partially unpaired in recombinant wildtype VWF (Ganderton et al., 2011), indicating that Cys2565 might also be present in an unpaired state in wildtype VWF and affect its function.

7.4. Summary

The present study identified 9 VWF LOF variants. Variants p.Cys2577Tyr and p.Cys2574Arg exhibit a pronounced secretion defect in HEK293F cells, while variant p.Cys2671Tyr displays a reduction in HMWM multimers. Furthermore, variants p.Pro2302Arg/Thr, p.Pro2373Arg/Ser, p.Trp2521Gly and p.Arg2535Gln demonstrate a diminished capacity to form platelet agglutinates and platelet aggregates in LTA and/or a microfluidic system, respectively.

In consideration of the study by Schneppenheim et al., which identified the VWF GOF variant p.Phe2561Tyr in the C4 domain and described it to increase VWF's shear sensitivity and to elevate the risk of MI in younger women (Schneppenheim et al., 2019), the present study focused on elucidating the underlying mechanism of the GOF effect. In a cohort of 522 patients, comprising 268 individuals with CAD, the average age at first MI was decreased in carriers of the p.Phe2561Tyr allele, from 64.1 to 53.8 years. However, lack of a significant association with MI was attributed to the relatively small cohort size. The SNP p.Ser2559Trp was identified in a single patient who had experienced an MI. The characterization of this and other SNPs in VWF C domains identified 9 novel VWF GOF variants, 8 of which are located in the C4 domain in close proximity to the previously reported GOF variants p.Pro2555Arg and p.Phe2561Tyr (Huck et al., 2022; Schneppenheim et al., 2019). One VWF GOF variant is located in the C6 and published as cooperation study (Chen et al., 2022). Variant p.Gly2705Arg was observed to increase shear sensitivity and aggregate size in microfluidic investigations. Based on structure predictions by Chen et al., introduction of an arginine leads to favoring of a bent C6 domain conformation, which may disturb the dimeric interface (Chen et al., 2022). Likewise, AlphaFold2-Multimer predictions identify an alteration in the structure of the adjacent CK domain.

The remaining GOF variants in C4 domain exhibit comparable increases in shear sensitivity to that observed for variant p.Phe2561Tyr (p.Pro2558Ser, p.Ser2559Leu/Trp, p.Gly2560Arg, p.Ser2564Arg, p.Cys2574Phe, p.Arg2575Cys), or increases in aggregate size (p.Glu2553Lys), albeit to a lesser extent than that seen for variant p.Pro2555Arg. Presence of abciximab in microfluidic experiments revealed that aggregate size, but not VWF shear sensitivity relies on platelet crosslinking via GPIIb/IIIa. Next, *in vivo* studies

disclose that thrombogenesis is augmented for variant p.Pro2555Arg. Given that the GOF effect of variant p.Pro2555Arg is dependent on GPIIb/IIIa, it is reasonable to conclude that enhanced crosslinking of platelets and VWF results in enlarged aggregates. Consequently, it can be postulated that stronger aggregate formation may increase thrombogenesis in mice.

In contrast, variant p.Phe2561Tyr decreased the hemostatic and thrombogenic potential of VWF, and led to the hypothesis that the GOF effect of variant p.Phe2561Tyr and similar variants may cause the formation of unstable clots. The mode of action would depend on accelerated formation of GPII α catch-bonds at lower shear rates due to partially open conformation of VWF dimer stems, as discovered by CD spectroscopy, SAXS (Schneppenheim et al., 2019) and AFM (J. Derksen, Department of Digital Health Sciences and Biomedicine, School of Life Sciences, University of Siegen, unpublished data). Subsequently, intermediate activation but not full activation of GPIIb/IIIa, due to insufficient shear force, promotes the development of unstable platelet clots. Such clots may detach from the surface due to absence of fully activated and thus strongly cross-linked GPIIb/IIIa molecules. Likewise, displacement of generated platelet aggregates at lower shear rates may elevate the risk of thromboembolic events by transport of aggregates to remote sites. This provides a potential explanation for why the risk for MI is increased in GOF variant carriers.

7.5. Outlook

The postulated mechanism of the GOF variants described above is based on the collected data in this study and is consistent with previously published data. Further investigations are needed to support this hypothesis. AFM studies by J. Derksen (Department of Digital Health Sciences and Biomedicine, School of Life Sciences, University of Siegen) display an increased occurrence of VWF dimers with an open stem conformation (unpublished data). Although all GOF variants with increased shear sensitivity behave similarly, the feature of decreased stem stability needs to be confirmed for each variant. Decreased stem stability may also be investigated for novel GOF variants by CD spectroscopy, small-angle X-ray scattering (SAXS), NMR or MD simulations as performed for GOF variants p.Phe2561Tyr and p.Pro2555Arg. In addition, AFM force measurements could determine the critical force required for opening of the stem or individual domains of GOF variants, similar as previously performed for the wildtype (Müller et al., 2016).

Given the hypothesis that platelet aggregation is unstable in presence of GOF variants with increased shear sensitivity, a characterization of platelets after interaction with GOFs at different shear rates, may enhance the understanding of the underlying mechanism. For instance, the conformation and activity of GPIIb/IIIa can be evaluated through the use of a combination of antibodies that detect distinct conformation of the GPIIb and GPIIIa integrins (Chen et al., 2019). Furthermore, the degree of platelet activation can be quantified by measuring the intracellular Ca^{2+} -concentration. Additionally, microfluidic experiments can be conducted in absence of Ca^{2+} to prevent platelet activation. According to the hypothesis GOF variants should not be dependent on extracellular Ca^{2+} . Therefore, the GOF effect should still be visible.

Further, to investigate the impact of VWF self-association by disulfide exchange on the activity of VWF GOF variants, VWF can be pretreated with N-ethylmaleimide (Solecka et al., 2016). This process will block its free thiols, thereby preventing the establishment of new disulfide bonds. The application of NEM-treated VWF in microfluidic experiments would allow determination of the dependence of the GOF effect on free thiols.

Since the risk of myocardial infarctions in patients is hypothesized to be caused by circulating platelet aggregates, an additional assessment of the occurrence of thromboembolic events in GOF carriers may reveal novel correlations. Furthermore, expanding the patient cohort to include all GOF variant carriers, without restriction to CAD, may facilitate the identification of significant correlations. Moreover, the novel hypothesized mode of action precludes the possibility of targeting GPIIb/IIIa binding to inhibit the underlying shear sensitivity associated with GOF variants. Although inhibition of GPIIb/IIIa would decrease aggregate size, platelet adhesion to VWF via GPIb α would still occur. Targeting shear sensitivity by molecules that stabilize a closed stem conformation or that inhibit GPIb α -mediated intermediate activation of GPIIb/IIIa may offer new therapeutic targets.

This study offers fundamental insights into the pathophysiology of shear-sensitive GOF variants and GPIIb/IIIa-dependent GOF variants of VWF, and improves the understanding of the effect of force on VWF activity in health and disease. Furthermore, new insights might help to develop novel approaches to counteract the GOF effect, and thus, reduce the risk of thrombotic events in respective carriers.

8. REFERENCES

- Alessi, M.-C., Sié, P., Payrastre, B., 2020. Strengths and Weaknesses of Light Transmission Aggregometry in Diagnosing Hereditary Platelet Function Disorders. *J. Clin. Med.* 9(3), 763.
- Alwan, F., Vendramin, C., Vanhoorelbeke, K., Langley, K., McDonald, V., Austin, S., Clark, A., Lester, W., Gooding, R., Biss, T., Dutt, T., Cooper, N., Chapman, O., Cranfield, T., Douglas, K., Watson, H.G., van Veen, J.J., Sibson, K., Thomas, W., Manson, L., Hill, Q.A., Benjamin, S., Ellis, D., Westwood, J.-P., Thomas, M., Scully, M., 2017. Presenting ADAMTS13 antibody and antigen levels predict prognosis in immune-mediated thrombotic thrombocytopenic purpura. *Blood* 130(4), 466–471.
- Arce, N.A., Cao, W., Brown, A.K., Legan, E.R., Wilson, M.S., Xu, E.-R., Berndt, M.C., Emsley, J., Zhang, X.F., Li, R., 2021. Activation of von Willebrand factor via mechanical unfolding of its discontinuous autoinhibitory module. *Nat. Commun.* 12(1), 2360.
- Ariëns, R.A.S., Lai, T.-S., Weisel, J.W., Greenberg, C.S., Grant, P.J., 2002. Role of factor XIII in fibrin clot formation and effects of genetic polymorphisms. *Blood* 100(3), 743–754.
- Berk, B.C., Alexander, R.W., Brock, T.A., Gimbrone, M.A., Webb, R.C., 1986. Vasoconstriction: A New Activity for Platelet-Derived Growth Factor. *Science* (80-). 232(4746), 87–90.
- Billaud, M., Lohman, A.W., Johnstone, S.R., Biber, L.A., Mutchler, S., Isakson, B.E., 2014. Regulation of cellular communication by signaling microdomains in the blood vessel wall. *Pharmacol. Rev.* 66(2), 513–569.
- Bonthron, D., Orr, E.C., Mitsock, L.M., Ginsburg, D., Handin, R.I., Orkin, S.H., 1986. Nucleotide sequence of pre-pro-von Willebrand factor cDNA. *Nucleic Acids Res.* 14(17), 7125–7127.

- Bonthron, D.T., Handin, R.I., Kaufman, R.J., Wasley, L.C., Orr, E.C., Mitscock, L.M., Ewenstein, B., Loscalzo, J., Ginsburg, D., Orkin, S.H., 1986. Structure of pre-pro-von Willebrand factor and its expression in heterologous cells. *Nature* 324(6094), 270–273.
- Borchiellini, A., Fijnvandraat, K., ten Cate, J.W., Pajkrt, D., van Deventer, S.J.H., Pasterkamp, G., Meijer-Huizinga, F., Zwart-Huinink, L., Voorberg, J., van Mourik, J.A., 1996. Quantitative Analysis of von Willebrand Factor Propeptide Release In Vivo: Effect of Experimental Endotoxemia and Administration of 1-Deamino-8-D-Arginine Vasopressin in Humans. *Blood* 88(8), 2951–2958.
- Borissoff, J.I., Heeneman, S., Kiliç, E., Kassák, P., Van Oerle, R., Winckers, K., Govers-Riemslog, J.W.P., Hamulyák, K., Hackeng, T.M., Daemen, M.J.A.P., ten Cate, H., Spronk, H.M.H., 2010. Early atherosclerosis exhibits an enhanced procoagulant state. *Circulation* 122(8), 821–830.
- Brehm, M.A., 2017. Von Willebrand factor processing. *Hamostaseologie* 37(1), 59–72.
- Brehm, M.A., Huck, V., Aponte-Santamaría, C., Obser, T., Grässle, S., Oyen, F., Budde, U., Schneppenheim, S., Baldauf, C., Gräter, F., Schneider, S.W., Schneppenheim, R., 2014. von Willebrand disease type 2A phenotypes IIC, IID and IIE: A day in the life of shear-stressed mutant von Willebrand factor. *Thromb. Haemost.* 112(1), 96–108.
- Budde, U., Schneppenheim, R., Eikenboom, J., Goodeve, A., Will, K., Drewke, E., Castaman, G., Rodeghiero, F., Federici, A.B., Batlle, J., Pérez, A., Meyer, D., Mazurier, C., Goudemand, J., Ingerslev, J., Habart, D., Vorlova, Z., Holmberg, L., Lethagen, S., Pasi, J., Hill, F., Peake, I., 2008. Detailed von Willebrand factor multimer analysis in patients with von Willebrand disease in the European study, molecular and clinical markers for the diagnosis and management of type 1 von Willebrand disease (MCMDM-1VWD). *J. Thromb. Haemost.* 6(5), 762–771.
- Canis, K., McKinnon, T.A.J., Nowak, A., Panico, M., Morris, H.R., Laffan, M., Dell, A., 2010. The plasma von Willebrand factor O-glycome comprises a surprising variety of structures including ABH antigens and disialosyl motifs. *J. Thromb. Haemost.* 8(1), 137–145.

- Carew, J.A., Browning, P.J., Lynch, D.C., 1990. Sulfation of von Willebrand factor. *Blood* 76(12), 2530–2539.
- Casari, C., Lenting, P.J., Christophe, O.D., Denis, C. V, 2013. Von Willebrand Factor Abnormalities Studied in the Mouse Model: What We Learned about VWF Functions. *Mediterr. J. Hematol. Infect. Dis.* 5(1), e2013047.
- Castaman, G., Eikenboom, J.C., Lattuada, A., Rodeghiero, F., 2000. Grossly abnormal proteolysis of von Willebrand factor (VWF) in a patient heterozygous for a gene deletion and mutation in the dimerization area of VWF. *Thromb. Haemost.*
- Castaman, G., Federici, A.B., Rodeghiero, F., Mannucci, P.M., 2003. Von Willebrand's disease in the year 2003: towards the complete identification of gene defects for correct diagnosis and treatment. *Haematologica* 88(1), 94–108.
- Chen, P. chia, Kutzki, F., Mojzisch, A., Simon, B., Xu, E.R., Aponte-Santamaría, C., Horny, K., Jeffries, C., Schneppenheim, R., Wilmanns, M., Brehm, M.A., Gräter, F., Hennig, J., 2022. Structure and dynamics of the von Willebrand Factor C6 domain. *J. Struct. Biol.* 214(4), 107923.
- Chen, Y., Ju, L.A., Zhou, F., Liao, J., Xue, L., Su, Q.P., Jin, D., Yuan, Y., Lu, H., Jackson, S.P., Zhu, C., 2019. An integrin $\alpha\text{IIb}\beta\text{3}$ intermediate affinity state mediates biomechanical platelet aggregation. *Nat. Mater.* 18(7), 760–769.
- Chen, Z., Mondal, N.K., Ding, J., Koenig, S.C., Slaughter, M.S., Griffith, B.P., Wu, Z.J., 2015. Activation and shedding of platelet glycoprotein IIb/IIIa under non-physiological shear stress. *Mol. Cell. Biochem.* 409, 93–101.
- Choi, H., Aboulfatova, K., Pownall, H.J., Cook, R., Dong, J., 2007. Shear-induced Disulfide Bond Formation Regulates Adhesion Activity of von Willebrand Factor *. *J. Biol. Chem.* 282(49), 35604–35611.
- Ciavarella, G., Ciavarella, N., Antoncicchi, S., De Mattia, D., Ranieri, P., Dent, J., Zimmerman, T.S., Ruggeri, Z.M., 1985. High-Resolution Analysis of von Willebrand Factor Multimere Composition Defines a New Variant of Type I von Willebrand Disease With Aberrant Structure but Presence of All Size Multimers (Type IC). *Blood* 66(6), 1423–1429.

- Cramer, E.M., Vainchenker, W., Vinci, G., Guichard, J., Breton-Gorius, J., 1985. Gray platelet syndrome: immunoelectron microscopic localization of fibrinogen and von Willebrand factor in platelets and megakaryocytes. *Blood* 66(6), 1309–1316.
- Crawley, J.T.B., De Groot, R., Xiang, Y., Luken, B.M., Lane, D.A., 2011. Unraveling the scissile bond: How ADAMTS13 recognizes and cleaves von Willebrand factor. *Blood* 118(12), 3212–3221.
- Cushman, M., 2007. Epidemiology and risk factors for venous thrombosis. *Semin. Hematol.* 44(2), 62–69.
- Da Silva, M.L., Cutler, D.F., 2016. Von Willebrand factor multimerization and the polarity of secretory pathways in endothelial cells. *Blood* 128(2), 277–285.
- Dai, K., Bodnar, R., Berndt, M.C., Du, X., 2005. A critical role for 14-3-3 ζ protein in regulating the VWF binding function of platelet glycoprotein Ib-IX and its therapeutic implications. *Blood* 106(6), 1975–1981.
- Davenport, A.P., Hyndman, K.A., Dhaun, N., Southan, C., Kohan, D.E., Pollock, J.S., Pollock, D.M., Webb, D.J., Maguire, J.J., 2016. Endothelin. *Pharmacol. Rev.* 68(2), 357 LP – 418.
- Davies, P.F., 2009. Hemodynamic shear stress and the endothelium in cardiovascular pathophysiology. *Nat. Clin. Pract. Cardiovasc. Med.* 6(1), 16–26.
- Dayananda, K.M., Singh, I., Mondal, N., Neelamegham, S., 2010. von Willebrand factor self-association on platelet GpIb α under hydrodynamic shear: effect on shear-induced platelet activation. *Blood* 116(19), 3990–3998.
- De Meyer, S.F., Stoll, G., Wagner, D.D., Kleinschnitz, C., 2012. von Willebrand factor: an emerging target in stroke therapy. *Stroke* 43(2), 599–606.
- Denis, C., Methia, N., Frenette, P.S., Rayburn, H., Ullman-Culleré, M., Hynes, R.O., Wagner, D.D., 1998. A mouse model of severe von Willebrand disease: defects in hemostasis and thrombosis. *Proc. Natl. Acad. Sci. U. S. A.* 95(16), 9524–9529.

- Dong, J., Moake, J.L., Nolasco, L., Bernardo, A., Arceneaux, W., Shrimpton, C.N., Schade, A.J., McIntire, L.V., Fujikawa, K., López, J.A., 2002. ADAMTS-13 rapidly cleaves newly secreted ultralarge von Willebrand factor multimers on the endothelial surface under flowing conditions. *Blood* 100(12), 4033–4039.
- Dziewierz, A., Rakowski, T., Dudek, D., 2014. Abciximab in the management of acute myocardial infarction with ST-segment elevation: evidence-based treatment, current clinical use, and future perspectives. *Ther. Clin. Risk Manag.* 10, 567–576.
- Eikenboom, J., Hilbert, L., Ribba, A.S., Hommais, A., Habart, D., Messenger, S., Al-Buhairan, A., Guilliatt, A., Lester, W., Mazurier, C., Meyer, D., Fressinaud, E., Budde, U., Will, K., Schneppenheim, R., Obser, T., Marggraf, O., Eckert, E., Castaman, G., Rodeghiero, F., Federici, A.B., Batlle, J., Goudemand, J., Ingerslev, J., Lethagen, S., Hill, F., Peake, I., Goodeve, A., 2009. Expression of 14 von Willebrand factor mutations identified in patients with type 1 von Willebrand disease from the MCMDM-1VWD study. *J. Thromb. Haemost.* 7(8), 1304–1312.
- Eikenboom, J.C.J., 2001. Congenital von Willebrand disease type 3: clinical manifestations, pathophysiology and molecular biology. *Best Pract. Res. Clin. Haematol.* 14(2), 365–379.
- Elaine Nicpon Marieb, 2004. Human anatomy & physiology, 6th ed. Pearson Benjamin Cummings, San Francisco, Calif.
- Estevez, B., Du, X., 2017. New concepts and mechanisms of platelet activation signaling. *Physiology* 32(2), 162–177.
- Evans, R., O'Neill, M., Pritzel, A., Antropova, N., Senior, A., Green, T., Žídek, A., Bates, R., Blackwell, S., Yim, J., Ronneberger, O., Bodenstein, S., Zielinski, M., Bridgland, A., Potapenko, A., Cowie, A., Tunyasuvunakool, K., Jain, R., Clancy, E., Kohli, P., Jumper, J., Hassabis, D., 2022. Protein complex prediction with AlphaFold-Multimer. *bioRxiv* 2021.10.04.463034.

- Federici, A.B., Canciani, M.T., Forza, I., Mannucci, P.M., Marchese, P., Ware, J., Ruggeri, Z.M., 2004. A sensitive ristocetin co-factor activity assay with recombinant glycoprotein Ibalpha for the diagnosis of patients with low von Willebrand factor levels. *Haematologica* 89(1), 77–85.
- Flood, V.H., Schlauderaff, A.C., Haberichter, S.L., Slobodianuk, T.L., Jacobi, P.M., Bellissimo, D.B., Christopherson, P.A., Friedman, K.D., Gill, J.C., Hoffmann, R.G., Montgomery, R.R., 2015. Crucial role for the VWF A1 domain in binding to type IV collagen. *Blood* 125(14), 2297–2304.
- Franchini, M., Mannucci, P.M., 2020. Acquired von Willebrand syndrome: focused for hematologists. *Haematologica* 105(8), 2032–2037.
- Fredrickson, B.J., Dong, J.F., McIntire, L. V, López, J.A., 1998. Shear-dependent rolling on von Willebrand factor of mammalian cells expressing the platelet glycoprotein Ib-IX-V complex. *Blood* 92(10), 3684–3693.
- Fu, H., Jiang, Y., Yang, D., Scheiflinger, F., Wong, W.P., Springer, T.A., 2017. Flow-induced elongation of von Willebrand factor precedes tension-dependent activation. *Nat. Commun.* 8(1), 324.
- Fuchs, B., Budde, U., Schulz, A., Kessler, C.M., Fisseau, C., Kannicht, C., 2010. Flow-based measurements of von Willebrand factor (VWF) function: binding to collagen and platelet adhesion under physiological shear rate. *Thromb. Res.* 125(3), 239–245.
- Fujikawa, K., Suzuki, H., McMullen, B., Chung, D., 2001. Purification of human von Willebrand factor–cleaving protease and its identification as a new member of the metalloproteinase family. *Blood* 98(6), 1662–1666.
- Furlan, M., 1996. Von Willebrand factor: molecular size and functional activity. *Ann. Hematol.* 72(6), 341–348.
- Ganderton, T., Wong, J.W.H., Schroeder, C., Hogg, P.J., 2011. Lateral self-association of VWF involves the Cys2431-Cys2453 disulfide/dithiol in the C2 domain. *Blood* 118(19), 5312–5318.

- Gangarosa, E.J., Johnson, T.R., Ramos, H.S., 1960. Ristocetin-Induced Thrombocytopenia: Site and Mechanism of Action. *AMA. Arch. Intern. Med.* 105(1), 83–89.
- Ginsburg, D., Handin, R.I., Bonthron, D.T., Donlon, T.A., Bruns, G.A.P., Latt, S.A., Orkin, S.H., 1985. Human von Willebrand Factor (vWF): Isolation of Complementary DNA (cDNA) Clones and Chromosomal Localization. *Science (80-)*. 228(4706), 1401–1406.
- Gogia, S., Neelamegham, S., 2015. Role of fluid shear stress in regulating VWF structure, function and related blood disorders. *Biorheology* 52, 319–335.
- Hamilton, K.K., Sims, P.J., 1987. Changes in cytosolic Ca²⁺ associated with von Willebrand factor release in human endothelial cells exposed to histamine. Study of microcarrier cell monolayers using the fluorescent probe indo-1. *J. Clin. Invest.* 79(2), 600–608.
- Hannah, M.J., Williams, R., Kaur, J., Hewlett, L.J., Cutler, D.F., 2002. Biogenesis of Weibel–Palade bodies. *Semin. Cell Dev. Biol.* 13(4), 313–324.
- Hantgan, R.R., Hindriks, G., Taylor, R.G., Sixma, J.J., De Groot, P.G., 1990. Glycoprotein Ib, von Willebrand factor, and glycoprotein IIb:IIIa are all involved in platelet adhesion to fibrin in flowing whole blood. *Blood* 76(2), 345–353.
- Hashemzadeh, M., Furukawa, M., Goldsberry, S., Movahed, M.R., 2008. Chemical structures and mode of action of intravenous glycoprotein IIb/IIIa receptor blockers: A review. *Exp. Clin. Cardiol.* 13(4), 192–197.
- Hassenpflug, W.A., Budde, U., Obser, T., Angerhaus, D., Drewke, E., Schneppenheim, S., Schneppenheim, R., 2006. Impact of mutations in the von Willebrand factor A2 domain on ADAMTS13-dependent proteolysis. *Blood* 107(6), 2339–2345.
- Hayward, C.P.M., Moffat, K.A., Raby, A., Israels, S., Plumhoff, E., Flynn, G., Zehnder, J.L., 2010. Development of North American Consensus Guidelines for Medical Laboratories That Perform and Interpret Platelet Function Testing Using Light Transmission Aggregometry. *Am. J. Clin. Pathol.* 134(6), 955–963.

- Heijnen, H.F., Schiel, A.E., Fijnheer, R., Geuze, H.J., Sixma, J.J., 1999. Activated platelets release two types of membrane vesicles: microvesicles by surface shedding and exosomes derived from exocytosis of multivesicular bodies and alpha-granules. *Blood* 94(11), 3791–3799.
- Higgins, R.A., Goodwin, A.J., 2019. Automated assays for von Willebrand factor activity. *Am. J. Hematol.* 94(4), 496–503.
- Hollestelle, M.J., Thinnis, T., Crain, K., Stiko, A., Kruijt, J.K., van Berkel, T.J., Loskutoff, D.J., van Mourik, J.A., 2001. Tissue distribution of factor VIII gene expression in vivo—a closer look. *Thromb. Haemost.* 86(3), 855–861.
- Howard, M.A., Firkin, B.G., 1971. Ristocetin—a new tool in the investigation of platelet aggregation. *Thromb. Diath. Haemorrh.* 26(2), 362–369.
- Hoylaerts, M.F., Yamamoto, H., Nuyts, K., Vreys, I., Deckmyn, H., Vermylen, J., 1997. von Willebrand factor binds to native collagen VI primarily via its A1 domain. *Biochem. J.* 324(1), 185–191.
- Huang, J., Li, X., Shi, X., Zhu, M., Wang, J., Huang, S., Huang, X., Wang, H., Li, L., Deng, H., Zhou, Y., Mao, J., Long, Z., Ma, Z., Ye, W., Pan, J., Xi, X., Jin, J., 2019. Platelet integrin $\alpha\text{IIb}\beta\text{3}$: signal transduction, regulation, and its therapeutic targeting. *J. Hematol. Oncol.* 12(1), 26.
- Huck, V., Chen, P.C., Xu, E.R., Tischer, A., Klemm, U., Aponte-Santamaría, C., Mess, C., Obser, T., Kutzki, F., König, G., Denis, C. V., Gräter, F., Wilmanns, M., Auton, M., Schneider, S.W., Schneppenheim, R., Hennig, J., Brehm, M.A., 2022. Gain-of-Function Variant pPro2555Arg of von Willebrand Factor Increases Aggregate Size through Altering Stem Dynamics. *Thromb. Haemost.* 122(2), 226–239.

- Huffman, J.E., de Vries, P.S., Morrison, A.C., Sabater-Lleal, M., Kacprowski, T., Auer, P.L., Brody, J.A., Chasman, D.I., Chen, M.-H., Guo, X., Lin, L.-A., Marioni, R.E., Müller-Nurasyid, M., Yanek, L.R., Pankratz, N., Grove, M.L., de Maat, M.P.M., Cushman, M., Wiggins, K.L., Qi, L., Sennblad, B., Harris, S.E., Polasek, O., Riess, H., Rivadeneira, F., Rose, L.M., Goel, A., Taylor, K.D., Teumer, A., Uitterlinden, A.G., Vaidya, D., Yao, J., Tang, W., Levy, D., Waldenberger, M., Becker, D.M., Folsom, A.R., Giulianini, F., Greinacher, A., Hofman, A., Huang, C.-C., Kooperberg, C., Silveira, A., Starr, J.M., Strauch, K., Strawbridge, R.J., Wright, A.F., McKnight, B., Franco, O.H., Zakai, N., Mathias, R.A., Psaty, B.M., Ridker, P.M., Tofler, G.H., Völker, U., Watkins, H., Fornage, M., Hamsten, A., Deary, I.J., Boerwinkle, E., Koenig, W., Rotter, J.I., Hayward, C., Dehghan, A., Reiner, A.P., O'Donnell, C.J., Smith, N.L., 2015. Rare and low-frequency variants and their association with plasma levels of fibrinogen, FVII, FVIII, and vWF. *Blood* 126(11), e19–e29.
- Jaffe, E.A., Hoyer, L.W., Nachman, R.L., 1973. Synthesis of antihemophilic factor antigen by cultured human endothelial cells. *J. Clin. Invest.* 52(11), 2757–2764.
- Jain, K., 2022. The effect of varying degrees of stenosis on transition to turbulence in oscillatory flows. *Biomech. Model. Mechanobiol.* 21(3), 1029–1041.
- Ju, L., Chen, Y., Zhou, F., Lu, H., Cruz, M.A., Zhu, C., 2015a. Von Willebrand factor-A1 domain binds platelet glycoprotein Iba in multiple states with distinctive force-dependent dissociation kinetics. *Thromb. Res.* 136(3), 606–612.
- Ju, L., Lou, J., Chen, Y., Li, Z., Zhu, C., 2015b. Force-Induced Unfolding of Leucine-Rich Repeats of Glycoprotein Iba Strengthens Ligand Interaction. *Biophys. J.* 109(9), 1781–1784.
- Jumper, J., Evans, R., Pritzel, A., Green, T., Figurnov, M., Ronneberger, O., Tunyasuvunakool, K., Bates, R., Žídek, A., Potapenko, A., Bridgland, A., Meyer, C., Kohl, S.A.A., Ballard, A.J., Cowie, A., Romera-Paredes, B., Nikolov, S., Jain, R., Adler, J., Back, T., Petersen, S., Reiman, D., Clancy, E., Zielinski, M., Steinegger, M., Pacholska, M., Berghammer, T., Bodenstein, S., Silver, D., Vinyals, O., Senior, A.W., Kavukcuoglu, K., Kohli, P., Hassabis, D., 2021. Highly accurate protein structure prediction with AlphaFold. *Nature* 596(7873), 583–589.

- Karamanos, N.K., Theocharis, A.D., Piperigkou, Z., Manou, D., Passi, A., Skandalis, S.S., Vynios, D.H., Orian-Rousseau, V., Ricard-Blum, S., Schmelzer, C.E.H., Duca, L., Durbeej, M., Afratis, N.A., Troeberg, L., Franchi, M., Masola, V., Onisto, M., 2021. A guide to the composition and functions of the extracellular matrix. *FEBS J.* 288(24), 6850–6912.
- Kashiwagi, H., Tomiyama, Y., Tadokoro, S., Honda, S., Shiraga, M., Mizutani, H., Handa, M., Kurata, Y., Matsuzawa, Y., Shattil, S.J., 1999. A mutation in the extracellular cysteine-rich repeat region of the beta3 subunit activates integrins alphaIIb beta3 and alphaV beta3. *Blood* 93(8), 2559–2568.
- Kaufmann, J.E., Oksche, A., Wollheim, C.B., Günther, G., Rosenthal, W., Vischer, U.M., 2000. Vasopressin-induced von Willebrand factor secretion from endothelial cells involves V2 receptors and cAMP. *J. Clin. Invest.* 106(1), 107–116.
- Kleinschnitz, C., De Meyer, S.F., Schwarz, T., Austinat, M., Vanhoorelbeke, K., Nieswandt, B., Deckmyn, H., Stoll, G., 2009. Deficiency of von Willebrand factor protects mice from ischemic stroke. *Blood* 113(15), 3600–3603.
- Koedam, J.A., Meijers, J.C., Sixma, J.J., Bouma, B.N., 1988. Inactivation of human factor VIII by activated protein C. Cofactor activity of protein S and protective effect of von Willebrand factor. *J. Clin. Invest.* 82(4), 1236–1243.
- König, G., Obser, T., Marggraf, O., Schneppenheim, S., Budde, U., Schneppenheim, R., Brehm, M.A., 2019. Alteration in GPIIb/IIIa Binding of VWD-Associated von Willebrand Factor Variants with C-Terminal Missense Mutations. *Thromb. Haemost.* 119(7), 1102–1111.
- Kumar, V., Abbas, A.K., Aster, J.C., 2017. Robbins Basic Pathology, Robbins Pathology. Elsevier Health Sciences.
- Kutzki, F., Butera, D., Lay, A.J., Maag, D., Chiu, J., Woon, H.-G., Kubař, T., Elstner, M., Aponte-Santamaría, C., Hogg, P.J., Gräter, F., 2023. Disulfide bond reduction and exchange in C4 domain of von Willebrand factor undermines platelet binding. *J. Thromb. Haemost.* 21(8), 2089–2100.

- Lämmle, B., Kremer Hovinga, J.A., Alberio, L., 2005. Thrombotic thrombocytopenic purpura. *J. Thromb. Haemost.* 3(8), 1663–1675.
- Lars, H., Marie, N.I., Lise, B., Margot, G., Elsy, S., 1983. Platelet Aggregation Induced by l-Desamino-8-D-Arginine Vasopressin (dDAVP) in Type IIb von Willebrand's Disease. *N. Engl. J. Med.* 309(14), 816–821.
- Legendre, P., Delrue, M., Boisseau, P., Ternisien, C., Fressinaude, E., Veyradier, A., Denis, C., Lenting, P., Christophe, O., 2015. Abstracts of the XXV Congress of the International Society on Thrombosis and Haemostasis, June 20-25, 2015. PO664-TUE Functional study of two new mutations in the C4 domain of von Willebrand factor. *J. Thromb. Haemost.* 13 Suppl 2(Suppl 2), 1–997.
- Lehmann, M., Ashworth, K., Manco - Johnson, M., Di Paola, J., Neeves, K.B., Ng, C.J., 2018. Evaluation of a microfluidic flow assay to screen for von Willebrand disease and low von Willebrand factor levels. *J. Thromb. Haemost.* 16(1), 104–115.
- Lenting, P.J., Christophe, O.D., Denis, C. V, 2015. von Willebrand factor biosynthesis, secretion, and clearance: connecting the far ends. *Blood* 125(13), 2019–2028.
- Letzer, A., Lehmann, K., Mess, C., König, G., Obser, T., Peine, S., Schneppenheim, S., Budde, U., Schneider, S.W., Schneppenheim, R., Brehm, M.A., 2020. Upshaw-Schulman syndrome-associated ADAMTS13 variants possess proteolytic activity at the surface of endothelial cells and in simulated circulation. *PLoS One* 15(5), e0232637.
- Levine, J., Harlan, J., Harker, L., Joseph, M., Counts, R., 1982. Thrombin-mediated release of factor VIII antigen from human umbilical vein endothelial cells in culture. *Blood* 60(2), 531–534.
- Li, Y., Choi, H., Zhou, Z., Nolasco, L., Pownall, H.J., Voorberg, J., Moake, J.L., Dong, J.-F., 2008. Covalent regulation of ULVWF string formation and elongation on endothelial cells under flow conditions. *J. Thromb. Haemost.* 6(7), 1135–1143.

- Li, Z., Xi, X., Du, X., 2001. A Mitogen-activated Protein Kinase-dependent Signaling Pathway in the Activation of Platelet Integrin α IIb β 3. *J. Biol. Chem.* 276(45), 42226–42232.
- Li, Z., Zhang, G., Feil, R., Han, J., Du, X., 2006. Sequential activation of p38 and ERK pathways by cGMP-dependent protein kinase leading to activation of the platelet integrin α IIb β 3. *Blood* 107(3), 965–972.
- Licari, L.G., Kovacic, J.P., 2009. Thrombin physiology and pathophysiology. *J. Vet. Emerg. Crit. Care* 19(1), 11–22.
- Lip, G.Y., Blann, A., 1997. von Willebrand factor: a marker of endothelial dysfunction in vascular disorders? *Cardiovasc. Res.* 34(2), 255–265.
- Lippok, S., Kolsek, K., Löf, A., Eggert, D., Vanderlinden, W., Müller, J.P., König, G., Obser, T., Röhrs, K., Schneppenheim, S., Budde, U., Baldauf, C., Aponte-Santamaría, C., Gräter, F., Schneppenheim, R., Rädler, J.O., Brehm, M.A., 2016. Von Willebrand factor is dimerized by protein disulfide isomerase. *Blood* 127(9), 1183–1191.
- Mackman, N., 2008. Triggers, targets and treatments for thrombosis. *Nature* 451(7181), 914–918.
- Mackman, N., Bergmeier, W., Stouffer, G.A., Weitz, J.I., 2020. Therapeutic strategies for thrombosis: new targets and approaches. *Nat. Rev. Drug Discov.* 19(5), 333–352.
- Mackman, N., Tilley, R.E., Key, N.S., 2007. Role of the extrinsic pathway of blood coagulation in hemostasis and thrombosis. *Arterioscler. Thromb. Vasc. Biol.* 27(8), 1687–1693.
- Maino, A., Siegerink, B., Lotta, L.A., Crawley, J.T.B., le Cessie, S., Leebeek, F.W.G., Lane, D.A., Lowe, G.D.O., Peyvandi, F., Rosendaal, F.R., 2015. Plasma ADAMTS-13 levels and the risk of myocardial infarction: an individual patient data meta-analysis. *J. Thromb. Haemost.* 13(8), 1396–1404.
- Mannucci, P.M., Ruggeri, Z.M., Pareti, F.I., Capitanio, A., 1977. 1-Deamino-8-d-arginine vasopressin: a new pharmacological approach to the management of haemophilia and von Willebrands' diseases. *Lancet (London, England)* 1(8017), 869–872.

- Martin, S.S., Aday, A.W., Almarzooq, Z.I., Anderson, C.A.M., Arora, P., Avery, C.L., Baker-Smith, C.M., Barone Gibbs, B., Beaton, A.Z., Boehme, A.K., Commodore-Mensah, Y., Currie, M.E., Elkind, M.S. V, Evenson, K.R., Generoso, G., Heard, D.G., Hiremath, S., Johansen, M.C., Kalani, R., Kazi, D.S., Ko, D., Liu, J., Magnani, J.W., Michos, E.D., Mussolino, M.E., Navaneethan, S.D., Parikh, N.I., Perman, S.M., Poudel, R., Rezk-Hanna, M., Roth, G.A., Shah, N.S., St-Onge, M.-P., Thacker, E.L., Tsao, C.W., Urbut, S.M., Van Spall, H.G.C., Voeks, J.H., Wang, N.-Y., Wong, N.D., Wong, S.S., Yaffe, K., Palaniappan, L.P., 2024. 2024 Heart Disease and Stroke Statistics: A Report of US and Global Data From the American Heart Association. *Circulation* 149(8), e347–e913.
- Marx, I., Christophe, O.D., Lenting, P.J., Rupin, A., Vallez, M.-O., Verbeuren, T.J., Denis, C. V, 2008. Altered thrombus formation in von Willebrand factor-deficient mice expressing von Willebrand factor variants with defective binding to collagen or GPIIb/IIIa. *Blood* 112(3), 603–609.
- Mayadas, T.N., Wagner, D.D., 1989. In vitro multimerization of von Willebrand factor is triggered by low pH. Importance of the propolypeptide and free sulfhydryls. *J. Biol. Chem.* 264(23), 13497–13503.
- Mazzucato, M., Pradella, P., Cozzi, M.R., De Marco, L., Ruggeri, Z.M., 2002. Sequential cytoplasmic calcium signals in a 2-stage platelet activation process induced by the glycoprotein Iba mechanoreceptor. *Blood* 100(8), 2793–2800.
- McKinnon, T.A.J., Goode, E.C., Birdsey, G.M., Nowak, A.A., Chan, A.C.K., Lane, D.A., Laffan, M.A., 2010. Specific N-linked glycosylation sites modulate synthesis and secretion of von Willebrand factor. *Blood* 116(4), 640–648.
- Michaux, G., Hewlett, L.J., Messenger, S.L., Goodeve, A.C., Peake, I.R., Daly, M.E., Cutler, D.F., 2003. Analysis of intracellular storage and regulated secretion of 3 von Willebrand disease-causing variants of von Willebrand factor. *Blood* 102(7), 2452–2458.
- Miles, L.A., Ny, L., Wilczynska, M., Shen, Y., Ny, T., Parmer, R.J., 2021. Plasminogen Receptors and Fibrinolysis. *Int. J. Mol. Sci.* 22(4).

- Mirdita, M., Schütze, K., Moriwaki, Y., Heo, L., Ovchinnikov, S., Steinegger, M., 2022. ColabFold: making protein folding accessible to all. *Nat. Methods* 19(6), 679–682.
- Miseta, A., Csutora, P., 2000. Relationship between the occurrence of cysteine in proteins and the complexity of organisms. *Mol. Biol. Evol.* 17(8), 1232–1239.
- Miura, S., Li, C.Q., Cao, Z., Wang, H., Wardell, M.R., Sadler, J.E., 2000. Interaction of von Willebrand factor domain A1 with platelet glycoprotein Ibalpha-(1-289). Slow intrinsic binding kinetics mediate rapid platelet adhesion. *J. Biol. Chem.* 275(11), 7539–7546.
- Moake, J.L., Rudy, C.K., Troll, J.H., Weinstein, M.J., Colannino, N.M., Azocar, J., Seder, R.H., Hong, S.L., Deykin, D., 1982. Unusually large plasma factor VIII: von Willebrand factor multimers in chronic relapsing thrombotic thrombocytopenic purpura. *N. Engl. J. Med.* 307(23), 1432–1435.
- Mohri, H., Yoshioka, A., Zimmerman, T.S., Ruggeri, Z.M., 1989. Isolation of the von Willebrand factor domain interacting with platelet glycoprotein Ib, heparin, and collagen and characterization of its three distinct functional sites. *J. Biol. Chem.* 264(29), 17361–17367.
- Monroe, D.M., Hoffman, M., 2006. What Does It Take to Make the Perfect Clot? *Arterioscler. Thromb. Vasc. Biol.* 26(1), 41–48.
- Moore, O., Jessurun, N., Chase, M., Nemitz, N., Campagnola, L., 2023. PyQtGraph - High Performance Visualization for All Platforms. *Proc. 22nd Python Sci. Conf. (Scipy)*, 106–113.
- Müller, J.P., Löf, A., Mielke, S., Obser, T., Bruetzel, L.K., Vanderlinden, W., Lipfert, J., Schneppenheim, R., Benoit, M., 2016. pH-Dependent Interactions in Dimers Govern the Mechanics and Structure of von Willebrand Factor. *Biophys. J.* 111(2), 312–322.
- Nachman, R.L., Jaffe, E.A., 1975. Subcellular platelet factor VIII antigen and von Willebrand factor. *J. Exp. Med.* 141(5), 1101–1113.
- Nguyen Dinh Cat, A., Touyz, R.M., 2011. Cell signaling of angiotensin II on vascular tone: novel mechanisms. *Curr. Hypertens. Rep.* 13(2), 122–128.

- Nichols, W.L., Hultin, M.B., James, A.H., Manco-Johnson, M.J., Montgomery, R.R., Ortel, T.L., Rick, M.E., Sadler, J.E., Weinstein, M., Yawn, B.P., 2008. Von Willebrand disease (VWD): evidence-based diagnosis and management guidelines, the National Heart, Lung, and Blood Institute (NHLBI) Expert Panel report (USA)1. *Haemophilia* 14(2), 171–232.
- Nishino, M., Girma, J., Rothschild, C., Fressinaud, E., Meyer, D., 1989. New Variant of von Willebrand Disease With Defective Binding to Factor VIII. *Blood* 74(5), 1591–1599.
- Nuyttens, B.P., Thijs, T., Deckmyn, H., Broos, K., 2011. Platelet adhesion to collagen. *Thromb. Res.* 127, S26–S29.
- O'Brien, H.E.R., Zhang, X.F., Sanz-Hernandez, M., Chion, A., Shapiro, S., Mobayen, G., Xu, Y., De Simone, A., Laffan, M.A., McKinnon, T.A.J., 2021. Blocking von Willebrand factor free thiols inhibits binding to collagen under high and pathological shear stress. *J. Thromb. Haemost.* 19(2), 358–369.
- Opoku, A., Iwuji, K., Clough, B., Le, J., Moore, M., Simmons, C., Hyde, B., 2019. Discordance between aPTT and anti-factor Xa levels and implications in patients receiving intravenous unfractionated heparin therapy. *Southwest Respir. Crit. Care Chronicles* 7, 12.
- Owens, A.P. 3rd, Mackman, N., 2012. Role of tissue factor in atherothrombosis. *Curr. Atheroscler. Rep.* 14(5), 394–401.
- Palta, S., Saroa, R., Palta, A., 2014. Overview of the coagulation system. *Indian J. Anaesth.* 58(5), 515–523.
- Patzke, J., Budde, U., Huber, A., Méndez, A., Muth, H., Obser, T., Peerschke, E., Wilkens, M., Schneppenheim, R., 2014. Performance evaluation and multicentre study of a von Willebrand factor activity assay based on GPIb binding in the absence of ristocetin. *Blood Coagul. Fibrinolysis* 25(8).
- Patzke, J., Schneppenheim, R., 2010. Laboratory diagnosis of von Willebrand disease. *Hamostaseologie* 30(4), 203–206.

- Pettersen, E.F., Goddard, T.D., Huang, C.C., Couch, G.S., Greenblatt, D.M., Meng, E.C., Ferrin, T.E., 2004. UCSF Chimera--a visualization system for exploratory research and analysis. *J. Comput. Chem.* 25(13), 1605–1612.
- Pinsky, D.J., Naka, Y., Liao, H., Oz, M.C., Wagner, D.D., Mayadas, T.N., Johnson, R.C., Hynes, R.O., Heath, M., Lawson, C.A., Stern, D.M., 1996. Hypoxia-induced exocytosis of endothelial cell Weibel-Palade bodies. A mechanism for rapid neutrophil recruitment after cardiac preservation. *J. Clin. Invest.* 97(2), 493–500.
- Purvis, A.R., Sadler, J.E., 2004. A covalent oxidoreductase intermediate in propeptide-dependent von Willebrand factor multimerization. *J. Biol. Chem.* 279(48), 49982–49988.
- Rawley, O., Swystun, L.L., Brown, C., Nesbitt, K., Rand, M., Hossain, T., Klaassen, R., James, P.D., Carcao, M.D., Lillicrap, D., 2022. Novel cysteine substitution p.(Cys1084Tyr) causes variable expressivity of qualitative and quantitative VWF defects. *Blood Adv.* 6(9), 2908–2919.
- Riba, R., Oberprieler, N.G., Roberts, W., Naseem, K.M., 2006. von Willebrand factor activates endothelial nitric oxide synthase in blood platelets by a glycoprotein Ib-dependent mechanism. *J. Thromb. Haemost.* 4(12), 2636–2644.
- Rickles, F.R., Hoyer, L.W., Rick, M.E., Ahr, D.J., 1976. The effects of epinephrine infusion in patients with von Willebrand's disease. *J. Clin. Invest.* 57(6), 1618–1625.
- Roberts, J.C., Flood, V.H., 2015. Laboratory diagnosis of von Willebrand disease. *Int. J. Lab. Hematol.* 37 Suppl 1(Suppl 1), 11–17.
- Rodrigues, M., Kosaric, N., Bonham, C.A., Gurtner, G.C., 2018. Wound Healing: A Cellular Perspective. *Physiol. Rev.* 99(1), 665–706.
- Romijn, R.A., Bouma, B., Wuyster, W., Gros, P., Kroon, J., Sixma, J.J., Huizinga, E.G., 2001. Identification of the collagen-binding site of the von Willebrand factor A3-domain. *J. Biol. Chem.* 276(13), 9985–9991.

- Rosado, J.A., Meijer, E.M.Y., Hamulyak, K., Novakova, I., Heemskerk, J.W.M., Sage, S.O., 2001. Fibrinogen binding to the integrin α IIb β 3 modulates store-mediated calcium entry in human platelets. *Blood* 97(9), 2648–2656.
- Ruggeri, Z.M., Orje, J.N., Habermann, R., Federici, A.B., Reininger, A.J., 2006. Activation-independent platelet adhesion and aggregation under elevated shear stress. *Blood* 108(6), 1903–1910.
- Ruggeri, Z.M., Pareti, F.I., Mannucci, P.M., Ciavarella, N., Zimmerman, T.S., 1980. Heightened Interaction between Platelets and Factor VIII/von Willebrand Factor in a New Subtype of von Willebrand's Disease. *N. Engl. J. Med.* 302(19), 1047–1051.
- Ruggeri, Z.M., Zimmerman, T.S., 1980. Variant von Willebrand's Disease: Characterization of two subtypes by analysis of multimeric composition of Factor VIII/Von Willebrand Factor in plasma and platelets. *J. Clin. Invest.* 65(6), 1318–1325.
- Sadler, J.E., 1998. Biochemistry and genetics of von Willebrand factor. *Annu. Rev. Biochem.* 67, 395–424.
- Sadler, J.E., Budde, U., Eikenboom, J.C.J., Favaloro, E.J., Hill, F.G.H., Holmberg, L., Ingerslev, J., Lee, C.A., Lillicrap, D., Mannucci, P.M., Mazurier, C., Meyer, D., Nichols, W.L., Nishino, M., Peake, I.R., Rodeghiero, F., Schneppenheim, R., Ruggeri, Z.M., Srivastava, A., Montgomery, R.R., Federici, A.B., 2006. Update on the pathophysiology and classification of von Willebrand disease: A report of the Subcommittee on von Willebrand factor. *J. Thromb. Haemost.* 4(10), 2103–2114.
- Sadler, J.E., Mannucci, P.M., Berntorp, E., Bochkov, N., Boulyjenkov, V., Ginsburg, D., Meyer, D., Peake, I., Rodeghiero, F., Srivastava, A., 2000. Impact, diagnosis and treatment of von Willebrand disease. *Thromb. Haemost.* 84(2), 160–174.
- Salari, N., Morddarvanjoghi, F., Abdolmaleki, A., Rasoulpoor, S., Khaleghi, A.A., Hezarkhani, L.A., Shohaimi, S., Mohammadi, M., 2023. The global prevalence of myocardial infarction: a systematic review and meta-analysis. *BMC Cardiovasc. Disord.* 23(1), 206.

- Savage, B., Sixma, J.J., Ruggeri, Z.M., 2001. Functional self-association of von Willebrand factor during platelet adhesion under flow. *Proc. Natl. Acad. Sci. U. S. A.* 99, 425–430.
- Schneider, S.W., Nuschele, S., Wixforth, A., Gorzelanny, C., Alexander-Katz, A., Netz, R.R., Schneider, M.F., 2007. Shear-induced unfolding triggers adhesion of von Willebrand factor fibers. *Proc. Natl. Acad. Sci. U. S. A.* 104(19), 7899–7903.
- Schneppenheim, R., 2011. The pathophysiology of von Willebrand disease: Therapeutic implications. *Thromb. Res.* 128(SUPPL. 1), S3.
- Schneppenheim, R., Budde, U., 2011. von Willebrand factor: the complex molecular genetics of a multidomain and multifunctional protein. *J. Thromb. Haemost.* 9, 209–215.
- Schneppenheim, R., Hellermann, N., Brehm, M.A., Klemm, U., Obser, T., Huck, V., Schneider, S.W., Denis, C. V., Tischer, A., Auton, M., März, W., Xu, E.R., Wilmanns, M., Zotz, R.B., 2019. The von Willebrand factor Tyr2561 allele is a gain-of-function variant and a risk factor for early myocardial infarction. *Blood* 133(4), 356–365.
- Seaman, C.D., Yabes, J., Comer, D.M., Ragni, M. V, 2015. Does deficiency of von Willebrand factor protect against cardiovascular disease? Analysis of a national discharge register. *J. Thromb. Haemost.* 13(11), 1999–2003.
- Seidizadeh, O., Cairo, A., Baronciani, L., Valenti, L., Peyvandi, F., 2023. Population-based prevalence and mutational landscape of von Willebrand disease using large-scale genetic databases. *NPJ genomic Med.* 8(1), 31.
- Shapiro, S.E., Nowak, A.A., Wooding, C., Birdsey, G., Laffan, M.A., McKinnon, T.A.J., 2014. The von Willebrand factor predicted unpaired cysteines are essential for secretion. *J. Thromb. Haemost.* 12(2), 246–254.
- Sharma, R., Flood, V.H., 2017. Advances in the diagnosis and treatment of Von Willebrand disease. *Blood* 130(22), 2386–2391.

- Shiltagh, N., Kirkpatrick, J., Cabrita, L.D., McKinnon, T.A.J., Thalassinou, K., Tuddenham, E.G.D., Hansen, D.F., 2014. Solution structure of the major factor VIII binding region on von Willebrand factor. *Blood* 123(26), 4143–4151.
- Smalberg, J.H., Kruijff, M.J.H.A., Janssen, H.L.A., Rijken, D.C., Leebeek, F.W.G., de Maat, M.P.M., 2011. Hypercoagulability and Hypofibrinolysis and Risk of Deep Vein Thrombosis and Splanchnic Vein Thrombosis. *Arterioscler. Thromb. Vasc. Biol.* 31(3), 485–493.
- Sodetz, J.M., Pizzo, S. V, McKee, P.A., 1977. Relationship of sialic acid to function and in vivo survival of human factor VIII/von Willebrand factor protein. *J. Biol. Chem.* 252(15), 5538–5546.
- Solecka, B.A., Weise, C., Fuchs, B., Kannicht, C., 2016. Free thiol groups in von Willebrand factor (VWF) are required for its full function under physiological flow conditions. *Thromb. Res.* 137, 202–210.
- Sonneveld, M.A.H., de Maat, M.P.M., Portegies, M.L.P., Kavousi, M., Hofman, A., Turecek, P.L., Rottensteiner, H., Scheiflinger, F., Koudstaal, P.J., Ikram, M.A., Leebeek, F.W.G., 2015. Low ADAMTS13 activity is associated with an increased risk of ischemic stroke. *Blood* 126(25), 2739–2746.
- Spiel, A.O., Gilbert, J.C., Jilka, B., 2008. Von Willebrand factor in cardiovascular disease: Focus on acute coronary syndromes. *Circulation* 117(11), 1449–1459.
- Sporn, L.A., Chavin, S.I., Marder, V.J., Wagner, D.D., 1985. Biosynthesis of von Willebrand protein by human megakaryocytes. *J. Clin. Invest.* 76(3), 1102–1106.
- Sporn, L.A., Marder, V.J., Wagner, D.D., 1987. von Willebrand factor released from Weibel-Palade bodies binds more avidly to extracellular matrix than that secreted constitutively. *Blood* 69(5), 1531–1534.
- Springer, T.A., 2014. Von Willebrand factor, Jedi knight of the bloodstream. *Blood* 124(9), 1412–1425.

- Stockschlaeder, M., Schneppenheim, R., Budde, U., 2014. Update on von Willebrand factor multimers: focus on high-molecular-weight multimers and their role in hemostasis. *Blood Coagul. Fibrinolysis* 25(3), 206–216.
- Sutton, N.R., Baek, A., Pinsky, D.J., 2014. Endothelial Cells and Inflammation BT - Encyclopedia of Medical Immunology: Autoimmune Diseases, in: Mackay, I.R., Rose, N.R., Diamond, B., Davidson, A. (Eds.), . Springer New York, New York, NY, pp. 367–381.
- Sztukowska, M., Gallinaro, L., Cattini, M.G., Pontara, E., Sartorello, F., Daidone, V., Padrini, R., Pagnan, A., Casonato, A., 2008. Von Willebrand factor propeptide makes it easy to identify the shorter Von Willebrand factor survival in patients with type 1 and type Vicenza von Willebrand disease. *Br. J. Haematol.* 143(1), 107–114.
- Takagi, J., Petre, B.M., Walz, T., Springer, T.A., 2002. Global Conformational Rearrangements in Integrin Extracellular Domains in Outside-In and Inside-Out Signaling. *Cell* 110(5), 599–611.
- Takahashi, M., Yamashita, A., Moriguchi-Goto, S., Marutsuka, K., Sato, Y., Yamamoto, H., Koshimoto, C., Asada, Y., 2009. Critical role of von Willebrand factor and platelet interaction in venous thromboembolism. *Histol. Histopathol.* 24(11), 1391–1398.
- Tang, W., Cushman, M., Green, D., Rich, S.S., Lange, L.A., Yang, Q., Tracy, R.P., Tofler, G.H., Basu, S., Wilson, J.G., Keating, B.J., Weng, L.-C., Taylor, H.A., Jacobs Jr., D.R., Delaney, J.A., Palmer, C.D., Young, T., Pankow, J.S., O'Donnell, C.J., Smith, N.L., Reiner, A.P., Folsom, A.R., 2015. Gene-centric approach identifies new and known loci for FVIII activity and VWF antigen levels in European Americans and African Americans. *Am. J. Hematol.* 90(6), 534–540.
- Tang, Z., Kattula, S., Holle, L.A., Cooley, B.C., Lin, F.C., Wolberg, A.S., 2020. Factor XIII deficiency does not prevent FeCl₃-induced carotid artery thrombus formation in mice. *Res. Pract. Thromb. Haemost.* 4(1), 111–116.
- Teller, P., White, T.K., 2009. The Physiology of Wound Healing: Injury Through Maturation. *Surg. Clin. North Am.* 89(3), 599–610.

- The UniProt Consortium, 2023. UniProt: the Universal Protein Knowledgebase in 2023. *Nucleic Acids Res.* 51(D1), D523–D531.
- Titani, K., Kumar, S., Takio, K., Ericsson, L.H., Wade, R.D., Ashida, K., Walsh, K.A., Chopek, M.W., Sadler, J.E., Fujikawa, K., 1986. Amino acid sequence of human von Willebrand factor. *Biochemistry* 25(11), 3171–3184.
- Tucker, W.D., Arora, Y., Mahajan, K., 2023. Anatomy, Blood Vessels. StatPearls Publishing, Treasure Island (FL).
- van de Ven, W.J., Voorberg, J., Fontijn, R., Pannekoek, H., van den Ouweland, A.M., van Duijnhoven, H.L., Roebroek, A.J., Siezen, R.J., 1990. Furin is a subtilisin-like proprotein processing enzyme in higher eukaryotes. *Mol. Biol. Rep.* 14(4), 265–275.
- van der Meijden, P.E.J., Munnix, I.C.A., Auger, J.M., Govers-Riemslog, J.W.P., Cosemans, J.M.E.M., Kuijpers, M.J.E., Spronk, H.M., Watson, S.P., Renné, T., Heemskerk, J.W.M., 2009. Dual role of collagen in factor XII-dependent thrombus formation. *Blood* 114(4), 881–890.
- Van Schooten, C.J., Tjernberg, P., Westein, E., Terraube, V., Castaman, G., Van Mourik, J.A., Hollestelle, M.J., Vos, H.L., Bertina, R.M., Van Den Berg, H.M., Eikenboom, J.C.J., Denis, C. V., Lenting, P.J., 2005. Cysteine-mutations in von willebrand factor associated with increased clearance. *J. Thromb. Haemost.* 3(10), 2228–2237.
- Vanhoorelbeke, K., Cauwenberghs, N., Vauterin, S., Schlamadinger, A., Mazurier, C., Deckmyn, H., 2000. A reliable and reproducible ELISA method to measure ristocetin cofactor activity of von Willebrand factor. *Thromb. Haemost.* 83(1), 107–113.
- Varga-Szabo, D., Braun, A., Nieswandt, B., 2009. Calcium signaling in platelets. *J. Thromb. Haemost.* 7(7), 1057–1066.
- Vehar, G.A., Davie, E.W., 1980. Preparation and properties of bovine factor VIII (antihemophilic factor). *Biochemistry* 19(3), 401–410.
- Verweij, C.L., Diergaarde, P.J., Hart, M., Pannekoek, H., 1986. Full-length von Willebrand factor (vWF) cDNA encodes a highly repetitive protein considerably larger than the mature vWF subunit. *EMBO J.* 5(8), 1839–1847.

- Verweij, C.L., Hart, M., Pannekoek, H., 1987. Expression of variant von Willebrand factor (vWF) cDNA in heterologous cells: requirement of the pro-polypeptide in vWF multimer formation. *EMBO J.* 6(10), 2885–2890.
- Virchow R, 1856. *Gesammelte Abhandlungen zur Wissenschaftlichen Medizin*. Frankfurt A. M. : Meidinger Sohn & Comp.
- Vischer, U., Wollheim, C., 1997. Epinephrine induces von Willebrand factor release from cultured endothelial cells: involvement of cyclic AMP-dependent signalling in exocytosis. *Thromb. Haemost.* 77(6), 1182–8.
- Wagner, D.D., Olmsted, J.B., Marder, V.J., 1982. Immunolocalization of von willebrand protein in weibel-palade bodies of human endothelial cells. *J. Cell Biol.* 95(1), 355–360.
- Walker, F.J., Sexton, P.W., Esmon, C.T., 1979. The inhibition of blood coagulation by activated protein C through the selective inactivation of activated factor V. *Biochim. Biophys. Acta - Enzymol.* 571(2), 333–342.
- Wang, J.-W., Bouwens, E.A.M., Pintao, M.C., Voorberg, J., Safdar, H., Valentijn, K.M., De Boer, H.C., Mertens, K., Reitsma, P.H., Eikenboom, J., 2013. Analysis of the storage and secretion of von willebrand factor in blood outgrowth endothelial cells derived from patients with von Willebrand disease. *Blood* 121(14), 2762–2772.
- Wang, J.-W., Groeneveld, D.J., Cosemans, G., Dirven, R.J., Valentijn, K.M., Voorberg, J., Reitsma, P.H., Eikenboom, J., 2012. Biogenesis of Weibel-Palade bodies in von Willebrand's disease variants with impaired von Willebrand factor intrachain or interchain disulfide bond formation. *Haematologica* 97(6), 859–866.
- Watanabe-Kusunoki, K., Nakazawa, D., Ishizu, A., Atsumi, T., 2020. Thrombomodulin as a Physiological Modulator of Intravascular Injury. *Front. Immunol.* 11, 575890.
- Weibel, R., Palade, G., 1964. New cytoplasmic components in arterial endothelia. *J. Cell Biol.* 23(1), 101–112.

- Whincup, P.H., Danesh, J., Walker, M., Lennon, L., Thomson, A., Appleby, P., Rumley, A., Lowe, G.D.O., 2002. von Willebrand factor and coronary heart disease: prospective study and meta-analysis. *Eur. Heart J.* 23(22), 1764–1770.
- Winkelmann, B.R., März, W., Boehm, B.O., Zotz, R., Hager, J., Hellstern, P., Senges, J., 2001. Rationale and design of the LURIC study--a resource for functional genomics, pharmacogenomics and long-term prognosis of cardiovascular disease. *Pharmacogenomics* 2(1 Suppl 1), S1-73.
- Wolberg, A.S., Rosendaal, F.R., Weitz, J.I., Jaffer, I.H., Agnelli, G., Baglin, T., Mackman, N., 2015. Venous thrombosis. *Nat. Rev. Dis. Prim.* 1(1), 15006.
- Wu, Y.P., Vink, T., Schiphorst, M., van Zanten, G.H., IJsseldijk, M.J., de Groot, P.G., Sixma, J.J., 2000. Platelet thrombus formation on collagen at high shear rates is mediated by von Willebrand factor-glycoprotein Ib interaction and inhibited by von Willebrand factor-glycoprotein IIb/IIIa interaction. *Arterioscler. Thromb. Vasc. Biol.* 20(6), 1661–1667.
- Xu, E.-R., von Bülow, S., Chen, P.-C., Lenting, P.J., Kolšek, K., Aponte-Santamaría, C., Simon, B., Foot, J., Obser, T., Schneppenheim, R., Gräter, F., Denis, C. V, Wilmanns, M., Hennig, J., 2019. Structure and dynamics of the platelet integrin-binding C4 domain of von Willebrand factor. *Blood* 133(4), 366–376.
- Yago, T., Lou, J., Wu, T., Yang, J., Miner, J.J., Coburn, L., López, J.A., Cruz, M.A., Dong, J.-F., McIntire, L. V, McEver, R.P., Zhu, C., 2008. Platelet glycoprotein Iba forms catch bonds with human WT vWF but not with type 2B von Willebrand disease vWF. *J. Clin. Invest.* 118(9), 3195–3207.
- Yin, H., Stojanovic, A., Hay, N., Du, X., 2008. The role of Akt in the signaling pathway of the glycoprotein Ib-IX-induced platelet activation. *Blood* 111(2), 658–665.
- Zhan, C., Shi, M., Wu, R., He, H., Liu, X., Shen, B., 2019. MIRKB: a myocardial infarction risk knowledge base. *Database* 2019, baz125.
- Zhang, W., Deng, W., Zhou, L., Xu, Y., Yang, W., Liang, X., Wang, Y., Kulman, J.D., Zhang, X.F., Li, R., 2015. Identification of a juxtamembrane mechanosensitive domain in the platelet mechanosensor glycoprotein Ib-IX complex. *Blood* 125(3), 562–569.

- Zhao, B.-Q., Chauhan, A.K., Canault, M., Patten, I.S., Yang, J.J., Dockal, M., Scheiflinger, F., Wagner, D.D., 2009. von Willebrand factor–cleaving protease ADAMTS13 reduces ischemic brain injury in experimental stroke. *Blood* 114(15), 3329–3334.
- Zheng, Y., Chen, J., López, J.A., 2015. Flow-driven assembly of VWF fibres and webs in vitro microvessels. *Nat. Commun.* 6, 7858.
- Zhou, Y.-F., Eng, E.T., Nishida, N., Lu, C., Walz, T., Springer, T.A., 2011. A pH-regulated dimeric bouquet in the structure of von Willebrand factor. *EMBO J.* 30(19), 4098–4111.
- Zhou, Y.-F., Eng, E.T., Zhu, J., Lu, C., Walz, T., Springer, T.A., 2012. Sequence and structure relationships within von Willebrand factor. *Blood* 120(2), 449–458.
- Zhou, Y.-F., Springer, T.A., 2014. Highly reinforced structure of a C-terminal dimerization domain in von Willebrand factor. *Blood* 123(12), 1785–1793.











9. SUPPLEMENT

9.1. Safety and disposal

Material contaminated with cells or bacteria was collected and autoclaved before disposal. Alcohols, dyes, formaldehyde solutions each were collected separately and discarded. Other chemicals were disposed according to the manufacturer's instructions. If not indicated buffers and solutions were discarded in the sink.

9.2. Hazardous materials

Table 23: List of hazardous materials. Chemical, GHS pictogram and H and P statements are given.

Chemicals	pictogram	H statement	P statement
Calcium chloride dihydrate	 GHS07	H319	P280, P305 + P351 + P338
Carbenicillin disodium salt	 GHS08	H317, H334	P272, P280, P302 + P352, P333 + P313, P342 + P311
cComplete™, Mini, EDTA-free Protease Inhibitor Cocktail	 GSH07	H315, H319	P264, P280, P302 + P352, P332 + P313, P337 + P313, P362 + P364
EDTA disodium salt dihydrate	  GHS07 GHS08	H332, H373	P260, P271, P304 + P340 + P312, P314, P501
Ethanol	  GHS02 GHS07	H225, H319	P210, P240, P241, P260, P280, P303 + P361 + P353, P305 + P351 + P338, P501
G418 (Geneticin)	 GHS08	H317, H334	P261, P280, P302 + P352, P304 + P341, P342 + P311, P501
Hydrochloric acid	  GHS05 GHS07	H290, H314, H335	P280, P303 + P361 + P353, P304 + P340, P305 + P351 + P338, P310























Chemicals	pictogram	H statement	P statement
Hygromycin B Gold	   GHS05 GHS06 GHS08	H301 + H311, H318, H330, H334	P264, P280, P301 + P310, P302 + P352, P304 + P340, P305 + P351 + P338, P342 + P311
Isopropanol	  GHS02 GHS07	H225, H319, H336	P210, P233, P305 + P351 + P338
Kanamycin Sulfate	 GHS07	H315, H319, H335	P302 + P352, P305 + P351 + P338, P304 + P340, P312, P280
Methanol	   GHS02 GHS06 GHS08	H225, H301 + H311 + H331, H370	P210, P280, P301 + P310, P303 + P361 + P353, P304 + P340, P405, P501
Paraformaldehyde	   GHS05 GHS07 GHS08	H315, H317, H318, H335, H351	P280, P302 + P352, P304 + P340, P310, P305 + P351 + P338
Penicillin- Streptomycin	  GHS07 GHS08	H317, H361	P201, P202, P261, P272, P280, P302 + P352, P308 + P313, P333 + P313, P362 + P364
Propionic acid	   GHS02 GHS05 GHS07	H226, H314, H335	P210, P233, P240, P280, P303 + P361 + P353, P305 + P351 + P338
Sodium Hydroxide	 GHS05	H290, H314,	P234, P260, P280, P303 + P361 + P353, P304 + P340 + P310, P305 + P351 + P338
Sulfuric acid	 GHS05	H290	
Triton X-100	   GHS05 GHS07 GHS09	H302, H315, H318, H410	P264, P273, P280, P301 + P312, P302 + P352, P305 + P351 + P338

Table 24: List of H statements.

H225	Highly flammable liquid and vapor
H226	Flammable liquid and vapor
H290	May be corrosive to metals
H301 + H311	Toxic if swallowed or in contact with skin
H301 + H311 + H331	Toxic if swallowed, in contact with skin or if inhaled.
H302	Harmful if swallowed
H314	Causes severe skin burns and eye damage
H315	Causes skin irritation
H317	May cause an allergic skin reaction
H318	Causes serious eye damage
H319	Causes serious eye irritation
H330	Fatal if inhaled
H332	Harmful if inhaled
H334	May cause allergy or asthma symptoms or breathing difficulties if inhaled
H335	May cause respiratory irritation
H336	May cause drowsiness or dizziness
H351	Suspected of causing cancer
H361	Suspected of damaging fertility or the unborn child
H370	Causes damage to the central nervous system and the visual organs.
H373	May cause damage to organs (Respiratory Tract) through prolonged or repeated exposure if inhaled
H410	Very toxic to aquatic life with long lasting effects

Table 25: List of P statements.

P201	Obtain special instructions before use.
P202	Do not handle until all safety precautions have been read and understood.
P210	Keep away from heat, hot surfaces, sparks, open flames and other ignition sources. No smoking.
P233	Keep container tightly closed.
P234	Keep only in original packaging.
P240	Ground and bond container and receiving equipment.
P241	Use explosion-proof [electrical/ventilating/lighting] equipment.
P260	Do not breathe dust/fume/gas/mist/vapors/spray.
P261	Avoid breathing dust/fume/gas/mist/vapors/spray.

P264	Wash skin thoroughly after handling.
P271	Use only outdoors or in a well-ventilated area.
P272	Contaminated work clothing should not be allowed out of the workplace.
P273	Avoid release to the environment.
P280	Wear protective gloves/protective clothing/eye protection/face protection/hearing protection.
P301 + P310	IF SWALLOWED: Immediately call a POISON CENTER or doctor/physician.
P301 + P312	IF SWALLOWED: Call a POISON CENTER/ doctor if you feel unwell.
P302 + P352	IF ON SKIN: Wash with plenty of soap and water.
P303 + P361 + P353	IF ON SKIN (or hair): Take off immediately all contaminated clothing. Rinse skin with water [or shower].
P304 + P340	IF INHALED: Remove victim to fresh air and keep at rest in a position comfortable for breathing.
P304 + P340 + P310	IF INHALED: Remove person to fresh air and keep comfortable for breathing. Immediately call a POISON CENTER/ doctor.
P304 + P340 + P312	IF INHALED: Remove person to fresh air and keep comfortable for breathing. Call a POISON CENTER/ doctor if you feel unwell.
P304 + P341	IF INHALED: If breathing is difficult, remove victim to fresh air and keep at rest in a position comfortable for breathing.
P305 + P351 + P338	IF IN EYES: Rinse cautiously with water for several minutes. Remove contact lenses, if present and easy to do. Continue rinsing.
P308 + P313	IF exposed or concerned: Get medical advice/attention.
P310	Immediately call a POISON CENTER or doctor/physician.
P312	Call a POISON CENTER or doctor if you feel unwell.
P314	Get medical advice/ attention if you feel unwell.
P332 + P313	If skin irritation occurs: Get medical advice/attention.
P333 + P313	If skin irritation or rash occurs: Get medical advice/attention.
P337 + P313	If eye irritation persists: Get medical advice/attention.
P342 + P311	If experiencing respiratory symptoms: Call a POISON CENTER or doctor/physician.
P362 + P364	Take off contaminated clothing and wash it before reuse.
P405	Store locked up.
P501	Dispose of contents/container in accordance with local/regional/national/international regulations.

DANKSAGUNG

An dieser Stelle möchte ich all jenen meinen Dank aussprechen, ohne deren Unterstützung und Bereitschaft diese Arbeit nicht möglich gewesen wäre.

Besonders dankbar bin ich Frau Prof. Dr. Maria A. Brehm für die Möglichkeit, als Teil ihrer Forschungsgruppe an einem so interessanten Thema gearbeitet zu haben. Deine Expertise und Deine Erfahrung haben wesentlich zur Weiterentwicklung und Verfeinerung dieser Arbeit beigetragen und die Diskussionen mit Dir haben mich inspiriert und ermutigt. Außerdem möchte ich mich bei Dir für die vielen Gelegenheiten zur Teilnahme an zahlreichen spannenden Kongressen bedanken und für die Ermöglichung des Auslandsaufenthaltes. Vielen Dank auch für die vielen netten Abende und lustigen Gespräche. Ich hätte mir keine bessere Betreuerin wünschen können.

Ich danke Herrn Prof. Dr. med. Stefan W. Schneider dafür, dass er mir die Durchführung meiner Doktorarbeit im Labor des Instituts für Dermatologie und Venerologie am UKE in Hamburg ermöglicht hat. Selbst nach einigen organisatorischen Schwierigkeiten haben Sie mich ohne Zögern in Ihre Arbeitsgruppe aufgenommen. Ich konnte mich immer auf Ihre Unterstützung verlassen.

Vielen Dank auch an Herrn Prof. Dr. rer. nat. Dr. Sc. Christian Betzel für die Betreuung und Begutachtung meiner Arbeit und den fachlichen Austausch.

Besonderer Dank gilt Frau Dr. Cécile Denis von Le Kremlin Bicêtre, die mich freundlich in ihrer Forschungsgruppe willkommen heißen hat, mich während meines Auslandsaufenthaltes betreut und die Arbeit durch interessante Diskussionen angeregt hat. Überdies vielen Dank auch für die praktische Unterstützung bei den Durchführung der Mausexperimente an Dr. Cécile Denis, Dr. Peter Lenting und Eloïse Pascal. Merci an Eloïse und Eric für die schöne Zeit in Paris. Dank euch habe ich mich direkt wohl gefühlt und werde die Zeit nie vergessen.

Ich möchte außerdem allen Patienten und freiwilligen Spendern danken, die durch Ihre Blutspenden den Aufbau der Patientenkohorte und die Durchführung von Experimenten erst ermöglicht haben. Vielen Dank an Herrn Prof. Dr. Dursun Gündüz vom Diakonie Klinikum Jung-Stilling für die Kooperation und die Bereitstellung der Patientenproben.

Danke auch an Herrn Dr. Volker Huck für die Einweisung in die Mikrofluidik und Herrn Christian Meß für die Bereitstellung der Clusterquant Software. Außerdem danke ich besonders Herrn Tobias Obser für seine kompetenten Ratschläge und Hilfe im Labor. Ich möchte dem gesamten Team des Dermatologischen Labors, einschließlich Tobias, Sabine, Ewa, Christian G., Christian M., Alex und Volker, für ihre Offenheit und Unterstützung bedanken. Ich wurde herzlich in Eure Gruppe aufgenommen und habe den morgendlichen Kaffee und das gemeinsame Frühstück mit euch sehr genossen.

Vielen Dank ebenfalls an die ganze AG Brehm in Siegen, an Muhammad, Jakob, Katharina und Barbara für die netten Meetings und Diskussionen. Danke an der Stelle besonders an Katharina Albrecht, Leah Glowacki und Milena Grützmann für Isolation der DNA aus dem Patientenkollektiv und an Nico Remmert für die Unterstützung bei der Untersuchung der Varianten im Rahmen seiner Bachelor-Arbeit.

Vielen Dank auch an Herrn Dr. Reinhard Schneppenheim und Frau Dr. Sonja Schneppenheim für den netten Austausch bei Kongressen und insbesondere an Dr. Sonja Schneppenheim für die Durchführung der VWF-Multimer-Aufnahmen.

Vielen Dank auch an die Kooperationspartner Dr. Camilo Aponte-Santamaría und Dr. Nicholas Michelarakis aus dem HITS für die *in silico* Untersuchungen und Herrn Florian Oyen aus der PHO des UKE für die Durchführung der Sequenzierungen.

Danke an die Deutsche Forschungsgemeinschaft für die Finanzierung dieser Arbeit (DFG-Projekt BR3522/5-1) und an die UKE Microscopy Imaging Facility für die Bereitstellung des Olympus FV3000 Mikroskops (DFG-Forschungsinfrastrukturportals: RI_00489).

Ich möchte mich auch bei meinen Eltern, meinem Bruder Damian, meiner Familie und Freunden für Ihren Beistand in dieser stressigen Zeit bedanken. Mama und Papa, ich danke euch dafür, dass ihr mich immer ermutigt habt, besser zu werden und dass ihr mich gelehrt habt, dass man alles schaffen kann. Für eure unermüdliche Liebe und Unterstützung und dafür, dass ihr mich spüren lasst, wie stolz ihr auf mich seid.

Abschließend bedanke ich mich von ganzem Herzen bei meinem Partner Dominik, der mir in der ganzen Zeit Rückhalt gegeben und mir immer gut zugesprochen hat. In Situationen, in denen ich niedergeschlagen und entmutigt war, hast du mich liebevoll wiederaufgebaut und mir neue Kraft geschenkt. Danke, dass du immer da bist.

EIDESSTÄTLICHE ERKLÄRUNG

Hiermit versichere ich an Eides statt, die vorliegende Dissertationsschrift selbst verfasst und keine anderen als die angegebenen Quellen und Hilfsmittel benutzt zu haben. Sofern im Zuge der Erstellung der vorliegenden Dissertationsschrift generative Künstliche Intelligenz (gKI) basierte elektronische Hilfsmittel verwendet wurden, versichere ich, dass meine eigene Leistung im Vordergrund stand und dass eine vollständige Dokumentation aller verwendeten Hilfsmittel gemäß der Guten wissenschaftlichen Praxis vorliegt. Ich trage die Verantwortung für eventuell durch die gKI generierte fehlerhafte oder verzerrte Inhalte, fehlerhafte Referenzen, Verstöße gegen das Datenschutz- und Urheberrecht oder Plagiate.

Hamburg, 04.12.2024

Ort, Datum

Mojzisch

Unterschrift